

**Mechanistic Investigation of a H_{Au}Cl₄ catalyzed oxidative C-C coupling
reaction**
and Synthesis of new supramolecular Silver(I) and Gold(I) NHC compounds
or
handling of a Mass Spectrometric Challenge
and catching Counterions on Supramolecular Playgrounds

Dissertation

zur

Erlangung des Doktorgrades (Dr. rer. nat.)

der

Mathematisch-Naturwissenschaftlichen Fakultät

der

Rheinischen Friedrich-Wilhelms-Universität Bonn

vorgelegt von

Melanie Tatiana Stefanie Krause

aus

Neuwied

Bonn 2020

Angefertigt mit Genehmigung der Mathematisch-Naturwissenschaftlichen Fakultät der Rheinischen Friedrich-Wilhelms-Universität Bonn

1. Gutachterin: PD. Dr. Marianne Engeser

2. Gutachter: Prof. Dr. Arne Lützen

Tag der Promotion: 16.02.2021

Erscheinungsjahr: 2021

Summary

Reaction monitoring by electrospray (ESI) mass spectrometry is a valuable technique to investigate reaction mechanisms. It allows a glimpse into the reacting solution and the characterization of transient intermediates by tandem mass spectrometry. Herein we studied a captivating gold(III)-catalyzed synthesis of dicoumarin derivatives which consists of a combination of hydroarylation and homo coupling steps. A special challenge lies in the corrosivity of the catalyst HAuCl_4 , which requires the use of inert material for every step. The application of a *fused-silica* capillary eliminated almost all side reactions of the catalyst during the mass spectrometric experiments. Another problem is the necessary switching of the measurement modus while investigating the reacting solutions. Whereas the reactants and products could be detected in positive mode, the negatively charged species, correlating with all proposed transient intermediates, could only be detected in negative mode. Fast reaction rates hampered the monitoring of the interesting species additionally. Therefore the reaction conditions had to be adjusted and improved. The interesting ions were characterized by accurate mass determinations and supporting gas phase fragmentation experiments. The following species could be detected and characterized: $[\text{AuCl}_2]^-$; $[\text{AuCl}_4]^-$; $[\text{A}+\text{AuCl}_4]^- = \text{B}/\text{C}+\text{Cl}^-$; $[\text{A}-\text{H}+\text{AuCl}_3]^- = \text{D}$; $[2\text{A}-\text{H}+\text{AuCl}_3]^- = \text{D}+\text{A}$; $[2\text{A}-2\text{H}+\text{AuCl}_2]^- = \text{E}$, $\text{F} = \text{coumarin}$, $\text{G} = \text{dicoumarin}$ (The nomenclature of the species **A**, **B**, **C**, **D**, **E**, **F** and **G** originated from the postulated mechanism and is listed consecutively with the reaction steps). Thus, the nature and ligand sphere of all reaction intermediates, formerly proposed in the catalytic cycle, were clarified and their evolution over different periods of time were followed. A strong influence of the substrate and catalyst concentrations on the reaction time could be demonstrated.

Furthermore the synthesis and characterization of three consistent series of dinuclear gold(I) *N*-heterocyclic carbene (NHC) complexes in comparison with a previously reported series is presented. Herein the differences of the four compelling series consist in the imidazole or benzimidazole moieties, the lengths of the alkylene linkers (C1-C3), the methyl or ethyl side chains and the counterion Br^- or PF_6^- . Single crystals suitable for x-ray diffraction were obtained as $[\text{M}_2\text{L}_2]^{2+}$ macrocycles from all complexes and from additional two new PO_2F_2^- salts and a NO_3^- salt. Furthermore the crystal structure of a dinuclear gold(I) NHC BF_4^- complex with a notably short intramolecular $\text{Au}\cdots\text{Au}$ distance of 2.999 Å was obtained.

Significant influences of intra- and intermolecular $\pi\cdots\pi$ - and $\text{Au}\cdots\text{Au}$ interactions as well as hydrogen bonding, depending on the varying functionalization, have been found. Gold(I) NHC complexes are known for their intriguing luminescence behaviour. Therefore detailed UV/Vis- and fluorescence spectroscopic experiments were performed, which confirmed the impact of the counterions on the supramolecular interaction. The most outstanding examples are all propylene complexes. They have all shown an intense emission band at $\sim 350\text{-}400\text{ nm}$ (λ_{ex} (imidazolium) = 255 nm , λ_{ex} (benzimidazolium) = 289 nm). The assumed aurophilic interactions could be altered via the addition of an excess of bromide, which leads to the quenching of the emission and the concurrent increase of a new lower energy maximum ($\sim 450\text{-}500\text{ nm}$) and an additional emission band at shorter wavelengths ($\sim 350\text{ nm}$). Those are attributed to association complexes and/or changes of the $\text{Au}\cdots\text{Au}$ bond lengths. The exceptional aggregation behaviour between the cationic complexes and other ions in solution was also investigated by additional NMR spectroscopic measurements. The imidazolium compounds have shown a strong interaction with bromide via hydrogen bonding with the aromatic protons, whereas the interactions with the benzimidazolium complexes have changed the chemical shift of the alkylene bridge protons. The strongest downfield shifts could be found for the methylene compounds. The results are all highly depending on the analytical technique, but all experiments have shown a strong interaction of the complexes with the counterions. The combined investigations illustrate the highly tuneable behaviour of the complexes and provide more information for a better understanding of it.

The last chapter of this thesis deals with larger astounding cage like trinuclear silver(I) and gold(I) NHC complexes. The enlargement of the system from two to three metal centres and a bigger cavity allows the insertion of larger substrates. The backbone of the new host molecules is based on tribenzotriquinacene. Three additional amine substituents were inserted to provide binding sites. Thereby a chiral C_3 symmetry was obtained. The aromatic scaffold could be linked to the imidazolium units by an amidation reaction with DMAP and EDC. The key to an effective reaction was the use of the highly nucleophilic but steric hindered base DIPEA. Unfortunately the reaction was incomplete and lead to a mixture of three different imidazolium compounds, containing one, two or three successful coupled imidazolium units. Nevertheless the obtained main compound is the intended tripodal compound. Tested reactions of the ligand precursor mixture with a gold source did not

yielded the trinuclear complexes, but different side products. Thus, the silver base route was used prior to create Ag cage templates. Silver(I) NHC compounds usually contain weaker M-C bonds than Au(I) NHC complexes and are known as dynamic and reversible in solution. This behaviour allows self driven ligand exchange processes, to sustain different products and correct mismatching. The syntheses of the corresponding gold compounds were realized via transmetallation of the silver cage molecules. The products were investigated by mass spectrometric means. Almost all possible silver and gold complexes could be detected and confirmed through their accurate masses and isotopic pattern. This led to a new library of a variety of fascinating silver and gold TBTQ cage compounds. In the future, possible supramolecular host-guest aggregations could get enabled via hydrogen bonding or $\pi\cdots\pi$ - and Au \cdots Au interactions. Additional binding sites for specific guest molecules are available through the amide substituents. The chiral symmetry could potentially support the separation or differentiation of isomers.

Acknowledgement

Ich möchte mich bei allen bedanken, die mich während meines Studiums und meiner Promotionszeit begleitet und unterstützt haben.

Zuerst möchte ich meiner Doktormutter PD Dr. Marianne Engeser dafür bedanken, dass Sie mir die Möglichkeit gegeben hat in Ihrer Gruppe zu forschen und die vorliegende Arbeit anzufertigen. Sie hat mir die außergewöhnliche Möglichkeit gegeben, mich sowohl analytisch als auch präparativ mit den interessanten Themen beschäftigen zu können. Ich bedanke mich für den Freiraum, den ich bei meiner Ausarbeitung hatte und die stete Unterstützung und Motivation die ich erhalten habe.

Besonders danken möchte ich auch Herrn Prof. Dr. Lützen für die Übernahme des Zweitgutachtens. Er hat es mir ermöglicht alle meine Abschlussarbeiten bei Marianne anzufertigen und mich dabei stets mit fachlichem Rat unterstützt. Ihnen und Ihrer Arbeitsgruppe danke ich für die freundliche und konstruktive Arbeitsatmosphäre in den Gruppenseminaren und den Laboren.

Bei Prof. Dr. Kirchner und Prof. Dr. Manthey möchte ich mich für die Bereitschaft zur Teilnahme in meiner Promotionskommission und die freundliche Zusammenarbeit bedanken.

Prof. Dr. Hermann A. Wegner und Anne-Florence Stoessel danke ich für eine gute Zusammenarbeit und ihre hilfreichen Ratschläge zur Durchführung der Gold-katalysierten Reaktionen.

Ich bedanke mich bei meinen lieben Kollegen aus der Arbeitsgruppe für die schöne Zeit, die gegenseitige Unterstützung und freundschaftliche Zusammenarbeit. Martin Schmidt und Alejandro Paz Schmidt danke ich dafür, dass sie mich damals so freundlich in den Arbeitskreis aufgenommen haben. Ich danke Stefanie Becker dafür, dass sie mich in die Welt der NHCs eingeführt hat und mir im Labor mit Rat und Tat zur Seite stand. Ich danke Yvonne Lorenz, die mich bei der Arbeit an den Massenspektrometern unterstützt hat und Alexander Willms auf

dessen Hilfe ich mich stets verlassen konnte. Weiterhin danke ich Janina Heider, die mein Projekt durch ihre Bachelorarbeit sehr unterstützt hat und mit der ich eine unvergessliche Zeit im Labor verbracht habe. Ich möchte mich auch bei Frau Peters-Pflaumbaum, aus der Abteilung Massenspektrometrie, für die gute Kooperation bedanken.

Den Mitarbeitern des Einkristallröntgenbeugungsservices und besonders Charlotte Rödde danke ich für die Vermessung meiner Proben und die gute Zusammenarbeit.

Der Jürgen Manchot Stiftung danke ich für mein Promotionsstipendium und auch der Deutschen Forschungsgemeinschaft (SFB 813 und 624) für die finanzielle Unterstützung. Ich möchte mich besonders dafür bedanken, dass ich bei der Women in Science Initiative teilnehmen konnte (unterstützt durch den SFB 813). Es waren sehr anregende und schöne Konferenzen sowie Vortragsabende, bei denen ich einiges lernen und interessante Wissenschaftlerinnen kennen lernen durfte.

Ich danke vor allem meiner Familie, die mich während meiner Studienzeit unterstützt, motiviert und an mich geglaubt hat. Ich danke besonders meinen Eltern und Großeltern für ihre finanzielle Unterstützung. Großer Dank gilt meinem Mann René Krause, der mir die Kraft und den Rückhalt gegeben hat, die ich brauchte um mich zu verwirklichen.

Vielen Dank!

Table of contents

1 Introduction	1
2 Mechanistic Investigation of a H ₂ AuCl ₄ catalyzed oxidative C-C coupling reaction	5
2.1 Introduction	5
2.2 Synthesis of the substrates.....	8
2.3 Mass Spectrometry Experiments.....	8
2.4 Preparation of Reaction Mixtures	8
2.5 Results and discussion	9
2.6 Conclusion.....	26
2.7 Appendix.....	28
3 A conformational and spectroscopic investigation of Auophilicity and Hydrogen bonding in Dinuclear Gold(I) NHC complexes.....	33
3.1 Introduction	33
3.2 Synthesis and general characterization of Au(I) NHC complexes	37
3.3 NMR spectroscopy experiments.....	38
3.4 X-ray crystal structures	48
3.5 Photophysical measurements.	90
3.6 Conclusion.....	100
3.7 Experimental section	103
3.8 Appendix.....	107
4 Synthesis and characterization of trinuclear Ag(I) NHC-tribenzotriquinacene and Au(I) NHC tribenzotriquinacene cages as supramolecular host molecules	115
4.1 Introduction	115
4.2 Mass Spectrometry Experiments.....	120
4.3 Synthesis of the ligand precursor	121
4.4 Synthesis of the metal TBTQ NHC complexes	154
4.5 Conclusion.....	194

4.6 Experimental section	195
4.7 Appendix.....	197
5 Summarizing conclusion and brief outlook	213
6 Abbrevations.....	221
7 References	223

1 Introduction

The central theme in this work is gold and its compounds with their intriguing miscellaneous features. Numerous successful uses of the noble metal are known in the literature and they still play an important role in chemical research. The applications are versatile and amongst other things range from catalysis, nanotechnology and medical implementations to luminescence chemosensing. The number of gold related publications is high and still rising. Gold as catalyst in organic reactions and total synthesis is one of the important and interesting research tasks. Particularly the interplay of Au(I)/ Au(III) catalysts is fascinating and sometimes requires further investigation for a better understanding of the reaction mechanisms. In 2008 *Wegner et al.* described an intriguing gold(III) catalyzed domino cyclization and oxidative coupling reaction of phenylpropionic esters which yield dicoumarin derivatives.^[1] Different conditions were tested, which lead to the combination of H₂AuCl₄ as catalyst, *tert*-butylhydroperoxide (*tert*-BuOOH) as oxidant and 2-dichloroethane (DCE) as solvent. The catalyst coordinates to the alkyne, and activates a ring closure reaction via an electrophilic substitution. Rearomatization could lead to the monomeric species or be followed by another cyclization process and eventually yield the dimer via a reductive elimination. Even though most of the mechanism steps have already been described, the exact composition of the catalyst during the reaction stays unclear. A possible role of the oxidant or other compounds in the solution could not directly be excluded. Next to the thirst for knowledge, the potential antitumor activity of the products emphasizes the importance of deeper and more detailed researches. The first goal of this work is to use mass spectrometric means for a further insight into the reaction mechanism and a concrete identification of the ligand sphere of the catalyst. Electrospray (ESI) mass spectrometry is a great tool for the investigation of reaction mechanisms in the gas phase. The used catalyst H₂AuCl₄ is an acid, which gets deprotonated fast in solution. Therefore the anion of the species should be easily detectable in the negative ESI modus as [AuCl₄]⁻ and allow the planned analysis. Potential transient species could also bear negative charges. Next to the structural, the temporal evolution of all species should be investigated (substrate, product and intermediates) for a better understanding of the reaction cycle.

N-heterocyclic carbenes (NHC) are an intriguing class of molecules. These compounds and their corresponding metal complexes are known for decades.^[2] The range of applications for these valuable ligands and complexes is wide. Some of the most common uses are as

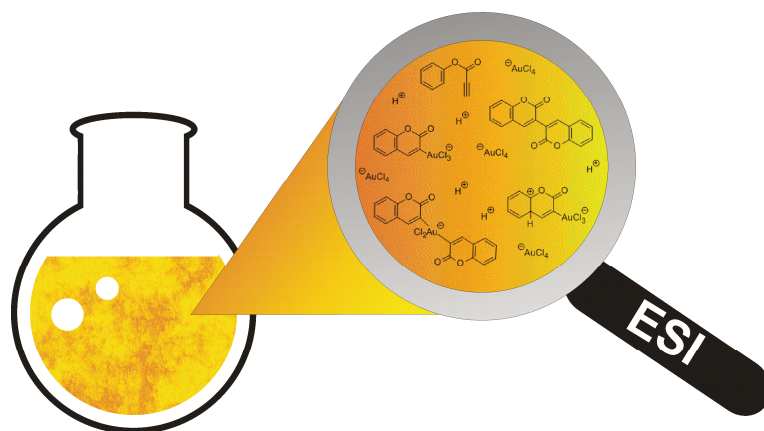
catalysts^[3], in medical research or as luminescent material^[4]. The last example leads to a fascinating feature of gold compounds in general, the occurrence of aurophilic interactions. They are often combined with an interesting spectroscopical behaviour. The name was introduced by *Schmidt* in 1988.^[5] This remarkable bonding type is provoked by brief intermetallic distances. The strength of the weak supramolecular interactions is comparable to hydrogen bonds. The accumulations of these aggregates are often associated with extraordinary photophysical properties. The visible emission can be perturbed by anion/solvent aggregations. Intrinsic designed sensor molecules could act as a host for supramolecular interactions. Inter- or intramolecular aurophilic interactions can be triggered or interrupted by the penetration of a substrate molecule inside the specific cavity. These interactions are weakly bonded and therefore reversible. Accordingly the potential supramolecular host-guest system would be reusable. Another criterion for a long life receptor molecule is the stability of the host structure itself. Gold(I) NHC complexes are pretty stable in solution and in the solid state. Therefore they are used with good prospects for the intended purpose. Next to the Au...Au interactions, the complexes could provide other weak interactions due to their substituents. Possible aggregations could be promoted by hydrogen bonding, ion...ion-, cation... π -, anion... π - as well as π ... π interactions. Thus the intended host-guest aggregations could be stabilized in deliberately drafted systems.

A previous research project in our group, mainly operated and controlled by *Kobialka*, included the synthesis and characterization of four consistent series of dinuclear gold(I) *N*-heterocyclic carbene (NHC) complexes.^[4f,6] The differences of the compounds consist in the imidazole or benzimidazole moieties, the lengths of the alkylene linkers (C1-C6), the methyl or ethyl side chains and the counterion Br⁻ or PF₆⁻. The homoleptic [M₂L₂]²⁺ cations bear a cavity between the two metal centres, which could probably be occupied by small molecules or ions. Potential aurophilic interactions in these systems should be detected in the solid state via x-ray diffraction and in solution by UV/Vis- and fluorescence spectroscopic experiments. The extensive investigations suggest a huge influence of the counterions to the properties of the complexes. This interesting behaviour was also found and published by other research groups.^[7] The biggest impact was detected for the complexes with short alkylene linkers (C1-C3). Foregoing comparison mainly contained only one of the series at a time, e.g. all relations of the imidazole ethylene complexes (C1-C6). The now presented work should compare all four series to each other. The anion exchange with hexafluorophosphate

was only performed for the imidazolium compounds before. Accordingly the benzimidazolium complexes should be synthesized for the overall comparison. Hitherto single crystals suitable for x-ray diffraction could not yet be obtained for all compounds. For the intended complete overview, all missing compounds of the 24 complexes have to be crystallized. Further investigations in solution could clarify the influence of the counterions and detect potential substrates for supramolecular sensor systems. On that account detailed NMR-, UV/Vis- and fluorescence spectroscopic experiments are planned with all interesting complexes and counterions. The scheduled project should enhance our understanding of the highly tuneable behaviour of the gold(I) NHC compounds and their intriguing ability to build supramolecular aggregates with small ions.

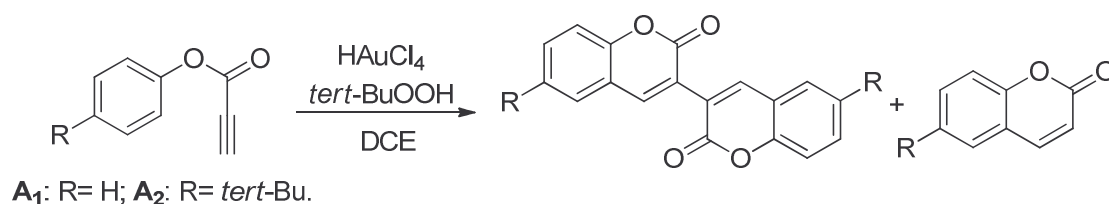
The up to now in our group investigated compounds are limited to mono- and mainly dinuclear homoleptic and heteroleptic silver and gold complexes. As the cooperative effect explains, simultaneous execution of numerous interactions encourages the stability of a host-guest system.^[8] The integration of more binding sites could improve the aggregation behaviour, for the purpose of a supramolecular receptor molecule. On that consideration, a more complex cage like structure with three metal centres is aimed. This motif is also chosen because of the better preorganisation of the cavity structure. The rigid structure of macrobicyclic compounds is often beneficial for supramolecular interactions, due to small rearrangement energies.^[9] Due to the already predetermined bowl shaped scaffold tribenzotriquinacene (TBTQ) is chosen as potential backbone of the cage. The cup like molecule was found by *Kuck et al.*^[9d,10] and seems promising as template for a capsule structured host compound. Due to the versatile options to introduce substituents, the NHC moieties could probably be linked to them and additional binding sites could be created. Another benefit is expected by a C_3 symmetrical configuration, arising from the substitution design. This could provide the ability to distinguish racemate mixtures and separate the containing compounds. For this project a suitable synthesis route for the coupling of the imidazolium ligand precursors to the TBTQ backbone has to be established. The planned compounds should then be transferred to the corresponding gold(I) NHC complexes. The best case scenario includes additional experiments of possible host-guest systems.

2 Mechanistic Investigation of a HAuCl₄ catalyzed oxidative C-C coupling reaction



2.1 Introduction

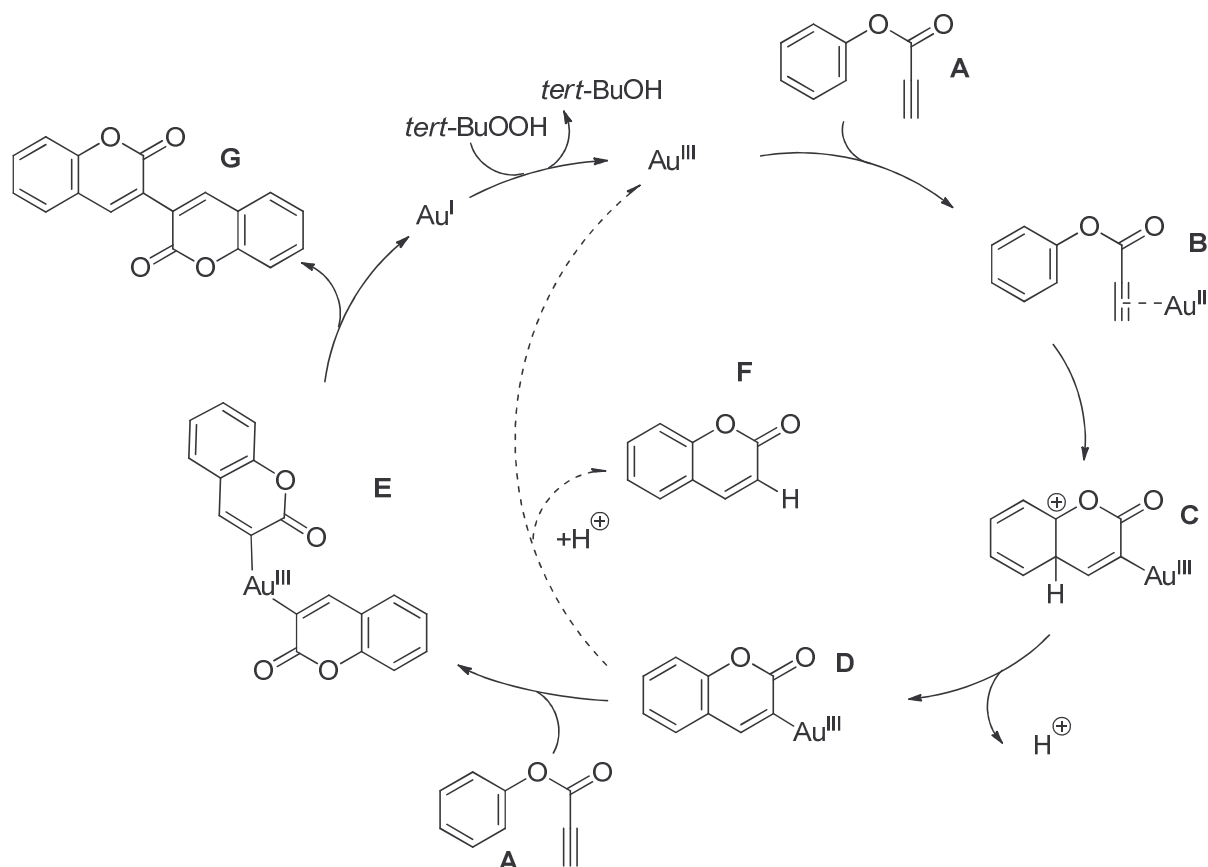
The discovery of the reactivity of gold compounds started a so-called gold rush in chemical research.^[2d,3a,11] Since then the application of gold in organic catalysis increased rapidly. Gold-catalyzed reactions are suitable for total synthesis^[12] of numerous natural products like the synthesis of Reticulol^[13] from the Hashmi group, Echavarren's synthesis of (\pm)-laurokamurene B^[14] or Fürstner's use of a typical [3,3]-sigmatropic rearrangement of a propargyl acetate for the total synthesis of Enigmazole A.^[15] An important part of current organometallic research aims at versatile and selective gold-catalyzed reactions.^[16] Special interest recently is laid on gold(III)-catalysts which can be used in C-C coupling reactions.^[17]



Scheme 1: Investigated gold(III)-catalyzed domino cyclization and oxidative coupling reaction.

Herein, we focus on the mechanism of an intriguing gold(III)-catalyzed domino cyclization and oxidative coupling reaction for the synthesis of dicoumarin derivatives, first reported by Wegner *et al.* in 2008.^[1] Dicoumarins are an interesting class of natural products with potential anti-tumour activity.^[18] Different gold compounds and oxidants were tested, to catalyze the reaction. HAuCl₄ in combination with anhydrous *tert*-butylhydroperoxide (*tert*-

BuOOH) and the solvent 2-dichloroethane (DCE) gives the best yields. The reaction scope could also be extended to bisbenzofurans.^[19] The group of *Stratakis* used Au/TiO₂ as catalyst for a similar reaction.^[20] *Tang et al.* contributed with density-functional theory calculations on the mechanism of a related reaction catalyzed by gold-clusters.^[21]



Scheme 2: Proposed reaction mechanism^[1] for the Au(III)-catalyzed dicoumarin formation. The actual composition/ligand sphere at the Au centre remained unclear.

Some mechanistic information is available concerning the first step of the reaction.^[1] The proposed catalytic cycle^[1] (Scheme 2) starts with coordination of the gold catalyst to the alkyne which allows ring closure via electrophilic substitution. Rearomatization leads to a σ -complex **D** which either directly forms the monomeric product **F** via protodeauration or catalyzes another cyclization process in a second reactant molecule **A**. The final step is the reductive elimination of the dicoumarin product **G**, overall resulting in an oxidative coupling reaction. An alternative mechanism via C-H activation^[1] was already ruled out by mixing coumarin **F** and the catalyst as no reaction could be observed under these conditions.^[1] The mechanism depicted in Scheme 2 proposes Au(III) species for both the cyclization and coupling steps. However, a combination of Au(I)- and Au(III)-catalyzed processes could also

be involved.^[1,2d,12a,17,22] Further, the actual composition and ligand shell of the catalyst and the transient Au complexes are still unknown. The aim of the present work is the experimental detection and characterization of the intermediate species **B - E** using mass spectrometric means.

Electrospray ionization mass spectrometry (ESI-MS)^[23] is a powerful tool for the investigation of reaction mechanisms and reaction monitoring.^[24] The technique transfers molecules from the reacting solution directly into the gas phase of a mass spectrometer. Thereby, it gives an overview of the species present in the reacting solution containing substrates, transient intermediates as well as products. High-resolving mass analyzers allow the determination of elemental compositions via accurate mass measurements. The combination with fragmentation experiments like collision induced dissociation (CID) gives access to structural information.^[25] Beautiful studies have been published about mass spectrometric mechanistic investigations of homogeneous reactions catalyzed by metal complexes or organocatalysts.^[24,26] The group of *McIndoe* developed a very useful technique to transfer a reacting solution directly from the flask into the mass spectrometer by pressurized sample infusion.^[27] Short-lived reactive species can be detected with a micro reactor setup.^[24b,28] *Roithová et al.* recently presented an intriguing method to investigate the kinetics of reactive intermediates of diaurated complexes.^[24e] There are numerous more examples of charged gold species detected by ESI-MS.^[26a,26c,29] Furthermore, the key transmetallation step during a Sonogashira reaction was successfully investigated in the gas phase.^[30] Several interesting publications deal with negatively charged reactive species^[31] including palladate(II) complexes as intermediates in a cross coupling reaction.^[31a,32] Yet there are some challenges and limitations for the investigation of reaction mechanisms by mass spectrometric means.^[26k,28d] In particular, the structure elucidation, identification and differentiation of isomers is sometimes difficult. The study presented herein was complicated by a series of technical problems due to the extreme corrosivity of H₂AuCl₄, the unusual solvent DCE, and the need to observe negatively as well as positively charged ions of interest. E.g. the relative intensities of the detected species do not necessarily correlate with the real concentration in the solution. They vary by their so called *ESI response*^[33] depending on the charge, the molecular structure, the mass spectrometer and the measuring parameters. Additional signals resulting from impurities, side products or background noises are possible. Exotic artefacts can also be generated during the ionization process and have to be excluded by

further experiments. However ESI-MS is an effective method to detect charged gold species.^[26k,34]

2.2 Synthesis of the substrates

The used phenylpropionic esters were synthesized via a Steglich esterification according to the literature.^[1,22] For a better handling, we used solid $\text{HAuCl}_4 \cdot 3\text{H}_2\text{O}$ for our investigation. Gold(III) chloride trihydrate, 1,2-dichloroethane, *tert*-butylhydroperoxide (5.5 M in decane), propiolic acid, phenol, and 4-*tert*-butylphenol were used as received from commercial sources. The solvents were dried and stored under argon according to standard procedures.

2.3 Mass Spectrometry Experiments

If not mentioned otherwise, experiments were performed on a Fisher Scientific LTQ-Orbitrap XLTM hybrid Ion Trap with an ESI/APCI Ion Max Source. Spectra for the reaction monitoring and CID experiments were recorded in the He-filled ion trap (accuracy of one decimal place in the given spectra). High resolution spectra for accurate masses were recorded with the Orbitrap analyzer (spectra shown with three or four decimal places). Additional measurements carried out with a commercial quadrupole/time of flight (Q/TOF) hybrid mass spectrometer (Bruker micrOTOF-Q) equipped with an Apollo ESI source show similar results. Investigation of aggressive compounds like oxidants and inorganic acids via ESI-MS is complicated by corrosion of stainless steel material. Thus, we used ESI needles and capillaries made of inert *fused-silica* and strictly avoided all metal containing syringes and connectors. Acetonitrile (HPLC grade) from VWR was used for MS-measurements. Trifluoroacetic acid from Roth was added when appropriate to enhance signal intensities of protonated molecules for the measurement of pure substances (not reaction mixtures). Relative intensities are normalized to the sum of all depicted ions. ESI-Low Concentration Tuning Mix from Agilent was used as internal standard in some monitoring experiments.

2.4 Preparation of Reaction Mixtures

Reactions were performed in 2 – 10 ml of dry 1,2-dichloroethane as solvent under argon atmosphere using standard Schlenk technique. The amount of the catalyst was varied from 5 mol% to 20 mol% and the substrate was used in concentrations from 20 mmol/L up to 110

mmol/L. Small samples were taken after different reaction time intervals and diluted 1:100 up to 1:50 in 1 mL acetonitrile. High concentrated solutions could not be measured due to blocking of the capillaries. This prevents the application of the method introduced by *McIndoe*.^[27]

2.5 Results and discussion

All investigations were performed with the two substrates **A₁** and **A₂** (Scheme 1). The nomenclature of species in the following text is based on the labels in Scheme 2, the index indicates the respective starting compound.

The substrates and products of the reaction in pure isolated form are well detected as $[M+H]^+$ or $[M+Na]^+$ ions with ESI- or atmospheric-pressure chemical ionization (APCI)-MS. Unfortunately the monomer product **F₁** and the substrate **A₁** are isomers with equal m/z values. They can nevertheless be distinguished by mass spectrometric means using CID. While the main fragmentation of $[F_1+H]^+$ is the loss of CO_2 , this elimination is absent during the fragmentation of $[A_1+H]^+$. For **A₂** and the respective products **F₂** and **G₂** with *tert*-butyl substituent, additional loss of C_4H_8 is dominating the fragmentation (see Figure 2 and Figure 3).

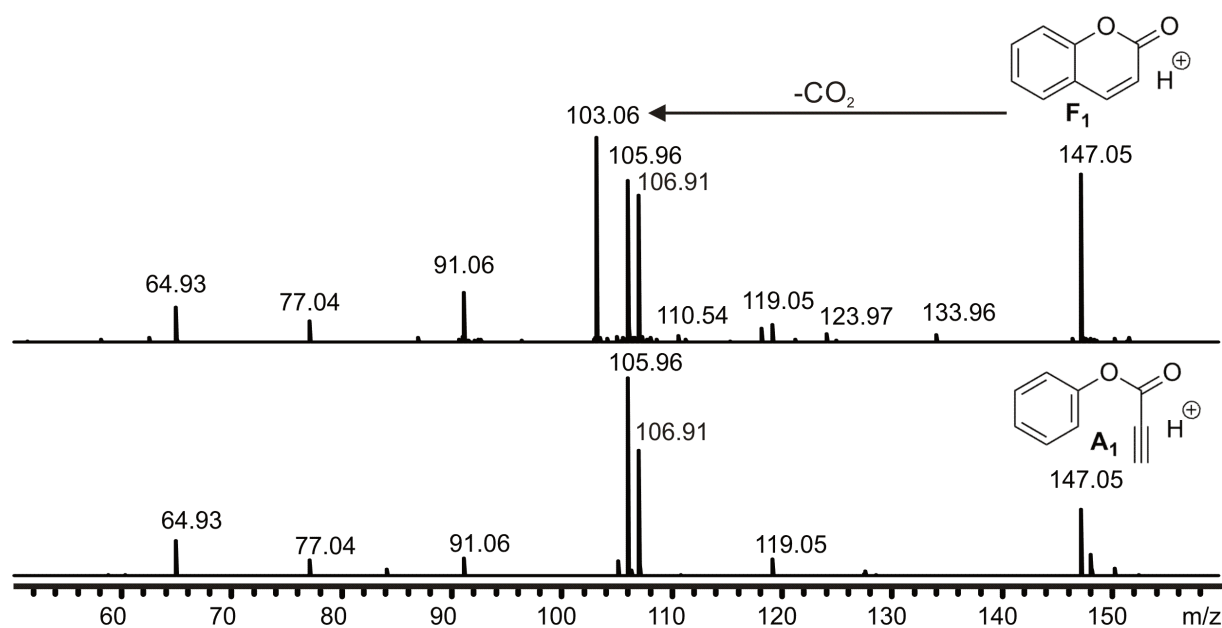


Figure 1: ESI(+)-CID spectrum of the mass-selected cations $[F_1+H]^+$ and $[A_1+H]^+$ recorded with the Q/TOF mass spectrometer.

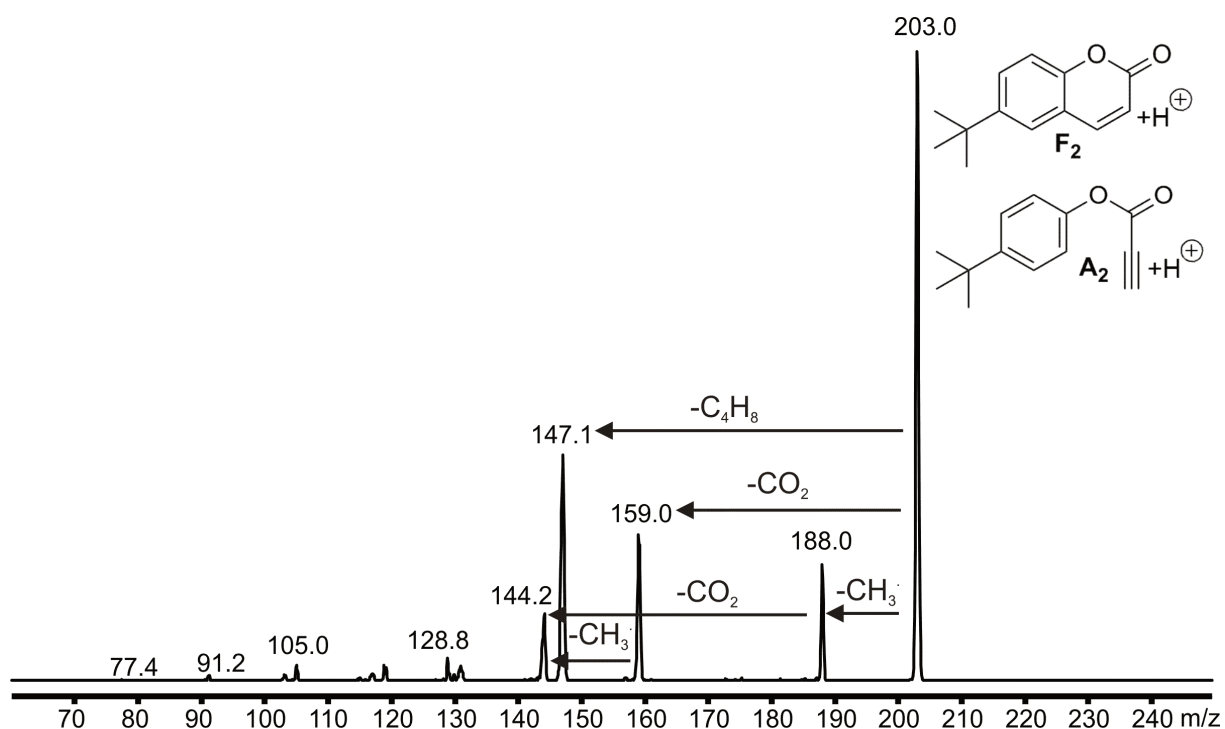


Figure 2: ESI(+)-CID spectrum of a mixture of mass-selected protonated molecules F_2 and A_2 .

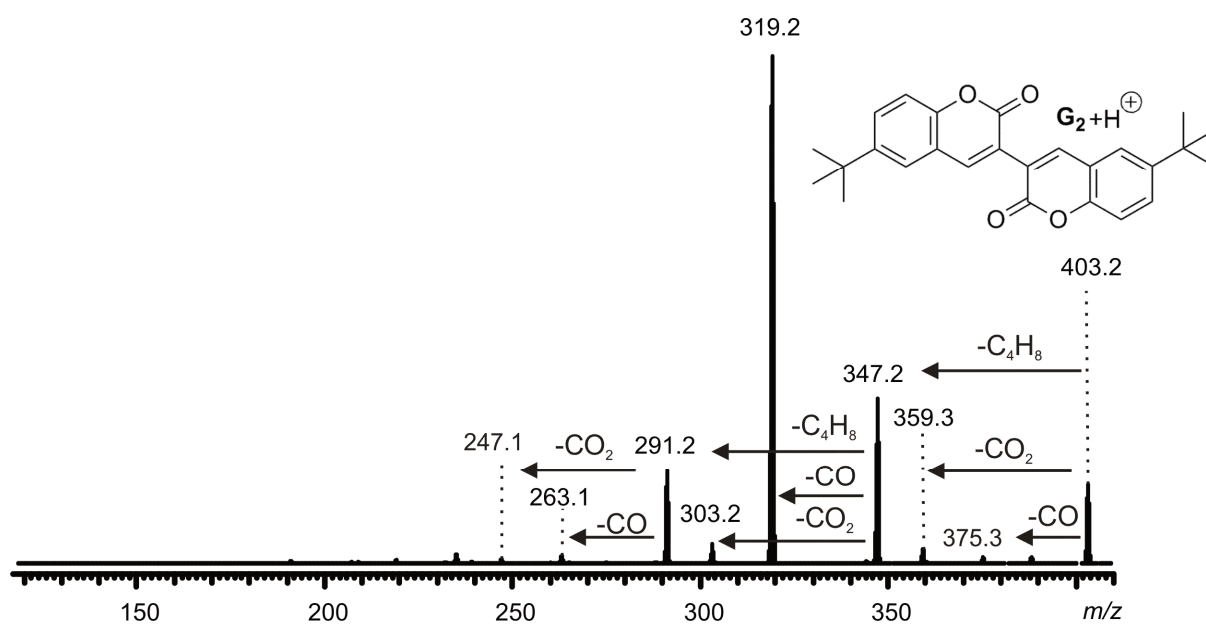


Figure 3: ESI(+)-CID spectrum of the mass-selected protonated molecule G_2 .

As expected the catalyst $HAuCl_4$ is not visible in ESI or APCI spectra in positive mode. Its deprotonated form $[AuCl_4]^-$ however has a very good ESI response.^[33] ESI(-) spectra of catalyst-containing solutions show high intensities of the ion. Yet, it is also very prone to fragmentation. Reductive elimination of Cl_2 leads to the Au(I) species $[AuCl_2]^-$,^[35] which we unfortunately could not avoid even under mild ESI tuning conditions. Reduction processes during ESI in negative mode are expected.^[36]

To gain access to reaction intermediates, we obtained best results when performing the reaction offline in a flask. Small samples with a defined volume were taken from the solution, diluted and immediately measured at varying reaction times. Mass spectra recorded in ESI(+) mode only showed the substrate and both products, but no gold containing intermediates. However, ESI(-) spectra of reacting solutions showed several negatively charged species (Figure 4).

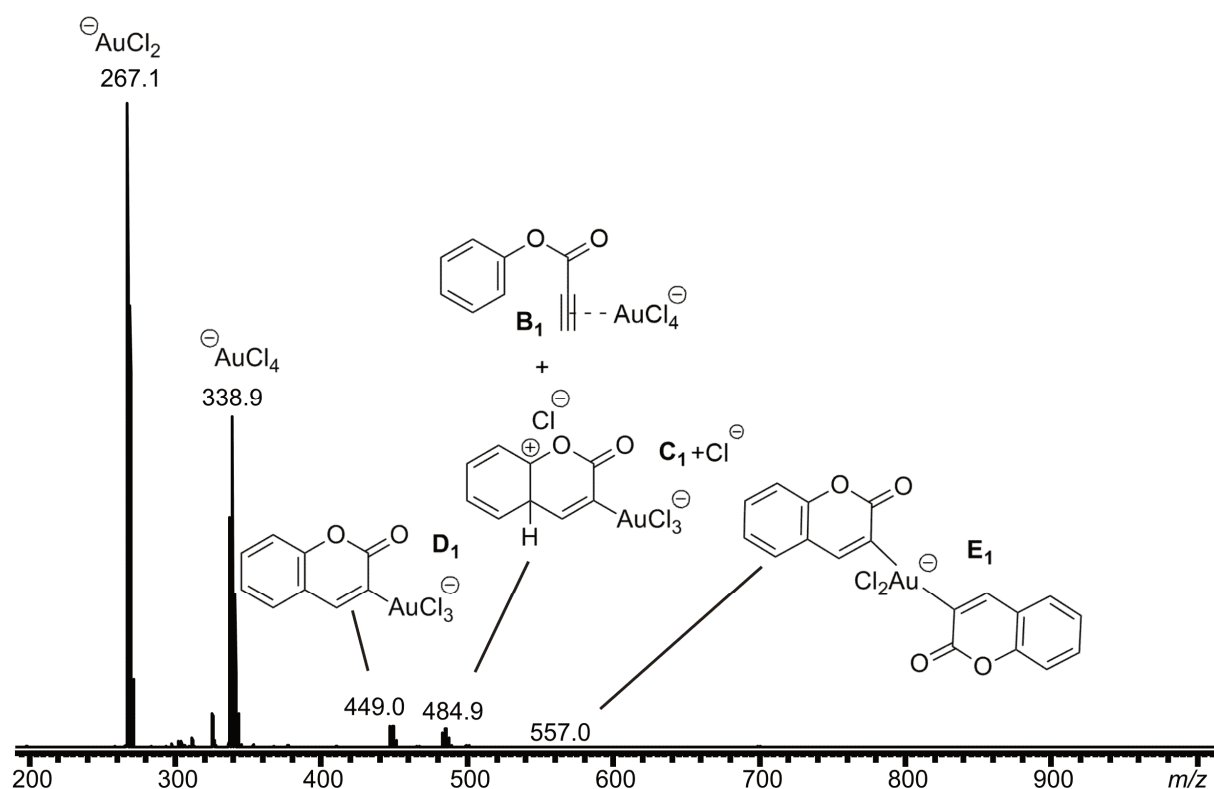


Figure 4: ESI(-) mass spectrum of a reacting solution containing 20 mol% of HAuCl_4 and a concentration of substrate A_1 of 12 mmol/L in DCE at room temperature. Sample taken after 37 minutes and diluted 1:100 with acetonitrile.

The signal with a monoisotopic m/z value of 482.9 (max. 484.9) shows the characteristic isotope pattern of four Cl atoms and an accurate mass indicating the elemental composition $[\text{C}_9\text{H}_6\text{AuCl}_4\text{O}_2]^-$ (Figure 4). This composition fits to a putative coordination complex between substrate A_1 and $[\text{AuCl}_4]^-$, i.e. the first intermediate B_1 in the mechanism proposed in Scheme 2. Yet, it is likely that a species with five ligands at one gold centre is only loosely bound and thus probably fragments during ESI. Another potential assignment of this signal is intermediate C_1 with three chloride ligands binding to gold and an additional chloride as

counter anion for the carbocation (Figure 4). Intermediate **C** without the additional chloride anion is zwitterionic. These kinds of compounds are hard to detect by ESI-MS and they are likely to bind other ions to form a species with only one charge. Hence the ions **B**₁ and [**C**₁+Cl]⁻ are isomers they cannot be distinguished by simple mass spectrometry. Different structures can however result in a different fragmentation behaviour which can be probed by tandem mass spectrometry. In species **B**₁, the weak interaction between the two stable subcomponents should be broken preferably yielding the ion [AuCl₄]⁻ via loss of neutral **A**₁. In intermediate **C**₁, the covalent bond between the gold centre and the substrate is stronger which should open other fragmentation routes. Mass selection and fragmentation of the species $m/z = 483.0$ [**C**₁+Cl]⁻ by CID results mainly in the reduced form of the catalyst [AuCl₂]⁻ which unfortunately is not helpful for structural assignments. Two other fragments could be detected with an intensity of only 1 % from the mass selected signal, but still more than 5 times higher than the baseline noise (Figure 5). These two fragments are indicative for the presence of intermediate [**C**₁+Cl]⁻ with a covalent Au-C bond. The ion with $m/z = 301.8$ corresponds to AuCl₃⁻ with an unusual formal oxidation state Au(II). Its formation by homolytical cleavage of an Au-C bond in a minor gas phase fragmentation pathway is plausible. The ion with $m/z = 446.9$ is formed via loss of HCl – which is exactly the next step in the proposed catalytic cycle: rearomatization of the substrate by deprotonation of **C** leads to intermediate **D** (Scheme 2, since species **D**₁ does not bear a positive charge like species **C**₁, the additional chloride anion also gets separated from the transient species. Therefore the deprotonation step from Scheme 2 is replaced by the loss of HCl).

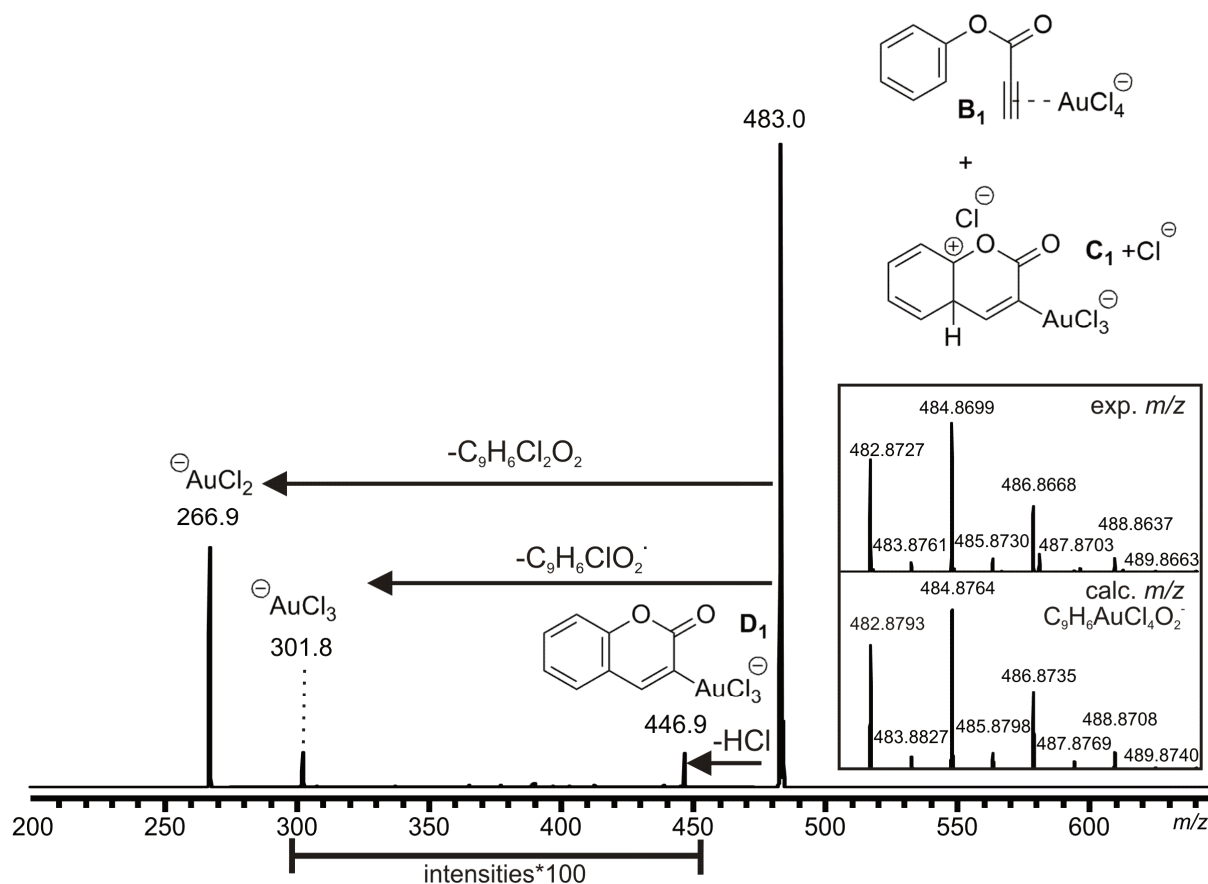


Figure 5: ESI(-) CID spectrum of the mass-selected ion with $m/z = 482.9$ corresponding to intermediates **B1** and/or $[C_1+Cl]^-$, The intensities in the mass range $m/z = 300 - 450$ are enlarged by a factor of 100.

The formation of **D1** cannot only be provoked by CID in the gas phase. The intermediate is also present in the reacting solution: It is visible in the respective spectra (Figure 4) in remarkable intensity at $m/z = 446.9$ with the expected isotope pattern of three Cl atoms and the correct accurate mass for $[C_9H_5AuCl_3O_2]^-$ (Figure 4). Fragmentation of the mass selected ion again yields the reduced ion $[AuCl_2]^-$. Although we cannot strictly exclude that the observed ion **D1** is produced from $[C_1+Cl]^-$ via loss of HCl during the ionization process, the relative abundances of **B1** and $[C_1+Cl]^-$ in the ESI spectra (Figure 4) and the very low efficiency of HCl abstraction in the CID spectra of **B1** (Figure 5) lead us to the conclusion that the observed signal for **D1** mainly is due to its presence in solution.

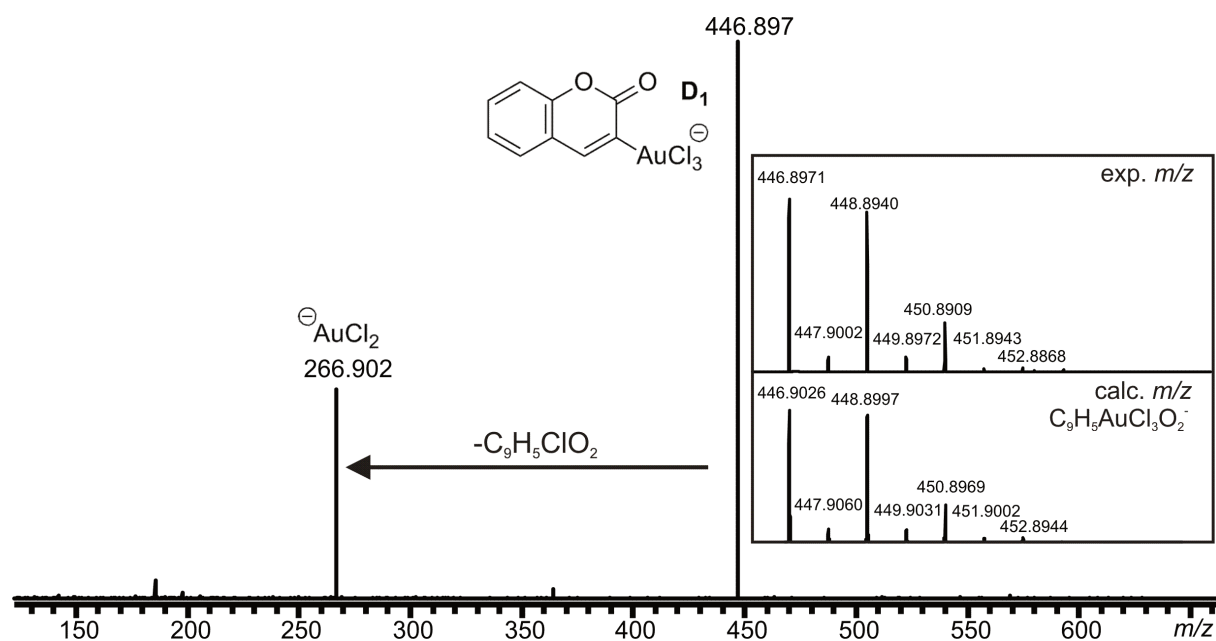


Figure 6: ESI(-) CID spectrum of the mass-selected ion with $m/z = 446.9$ corresponding to intermediate \mathbf{D}_1 .

According to the proposed mechanism, the σ -complex \mathbf{D}_1 undergoes two possible reaction pathways. Addition of a proton leads to the monomer \mathbf{F}_1 and releases the Au(III) catalyst. Alternatively, the reaction with an additional substrate molecule \mathbf{A}_1 results in a second ring closure and the final oxidative coupling to the dimer. ESI(-) spectra of the reacting solution show very small amounts of a negatively charged ion with the isotope pattern of three chloride anions and a monoisotopic mass of 592.9 (Figure 7). This ion fits to a new species resulting from the coordination of \mathbf{D}_1 to an additional substrate \mathbf{A}_1 . CID experiments of this aggregate unfortunately were not successful due to low signal intensity.

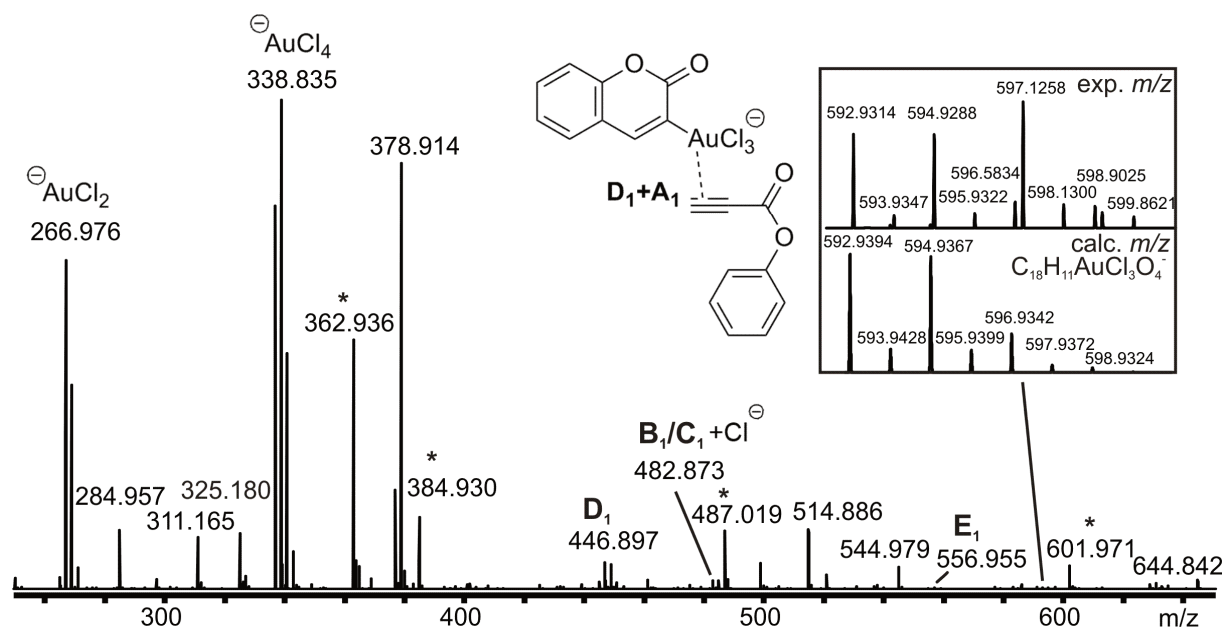


Figure 7: ESI(-) mass spectrum of a reacting solution containing 20 mol% of HAuCl_4 and a concentration of substrate A_1 of 100 mmol/L in DCE at room temperature. Sample taken after 22 minutes and diluted 1:50 with acetonitrile (* = internal standard, for full spectrum see Figure 22).

Further, a species with the isotope pattern of two chlorine atoms and an accurate mass in accordance with $[\text{C}_{18}\text{H}_{10}\text{AuCl}_2\text{O}_4]^-$ was found in small abundance consistent with intermediate E_1 . Mass selection and CID yields the Au(I) fragment at $m/z = 377.0$ (Figure 8) which indicates that the two coumarin subunits are still separated in the mass-selected ion. The additional formation of $[\text{AuCl}_2]^-$ in this case is revealing as it represents the next step in the catalytic cycle, the reductive elimination of the desired dicoumarin product.

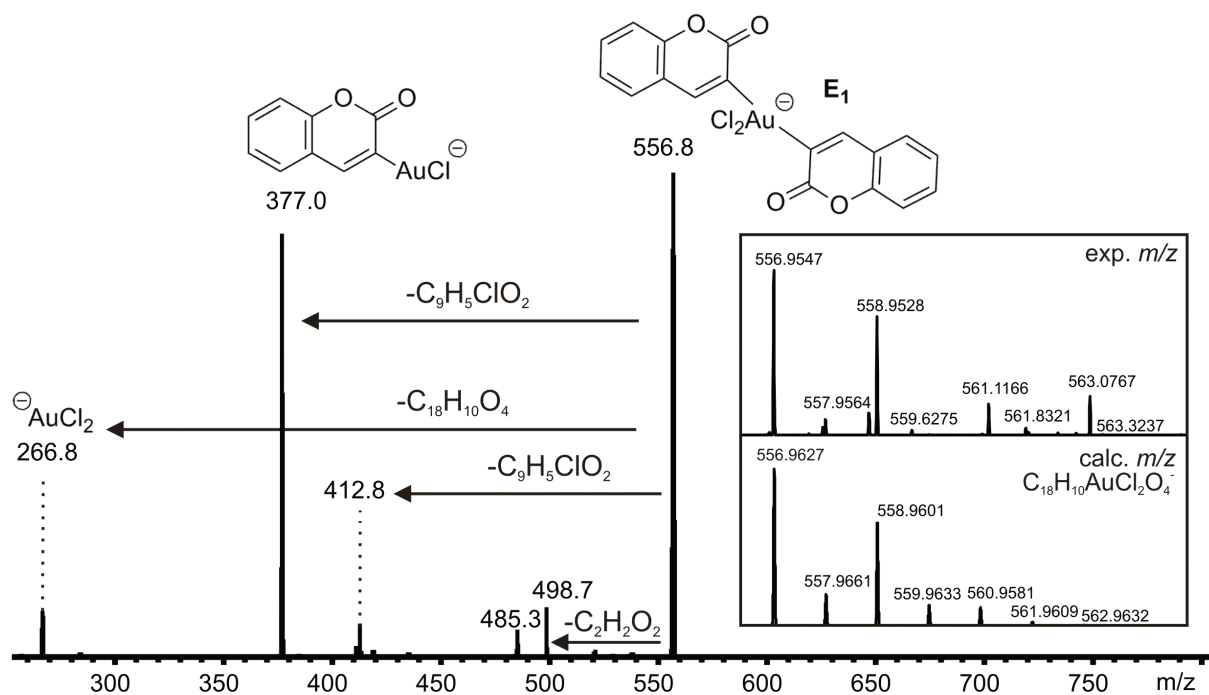


Figure 8: ESI(-) CID spectrum of the mass-selected ion with $m/z = 556.8$ corresponding to intermediate E_1 .

In analogy to the results obtained with substrate A_1 , all the anionic species $B_2/[C_2+Cl]^-$, D_2 , E_2 and the aggregate D_2+A_2 could also be detected for the reaction with substrate A_2 (see Figure 18, Figure 19, Figure 20 and Figure 21).

Thus, we successfully detected all species proposed as reaction intermediates of the reacting solutions by ESI MS. The spectra also clarify that the previously undefined coordination sites at the gold centre are continuously possessed by chloride ligands. As a consequence, the gold-containing intermediates are negatively charged. In addition, their reactivity could also be addressed: two of the single steps along the catalytic cycle could indeed be mirrored in the gas-phase reactivity of $[C_1+Cl]^-$ and E_1 provoked by CID.

Some diaurated species are reported as catalysts for similar reactions.^[24e,26k,37] However, we did not find any indications for intermediates with several gold atoms or gold dimers. We further aimed to monitor relative signal intensities during the course of the reaction. Reactant and products are only detected in the positive mode, whereas the negative mode is needed for the anionic intermediates and catalyst. Observing all relevant species in one spectrum is thus impossible. We therefore chose to measure mass spectra in the ion trap part of our instrument which allows fast switching between positive and negative mode and thus achieved a quasi-simultaneous monitoring of reacting solutions in both modes. In

absence of *tert*-BuOOH, ESI(-) shows the disappearance of Au(III) in the course of approx. 2 h (Figure 9) in good accordance with the time for the respective synthetic procedure under stoichiometric conditions.^[22]

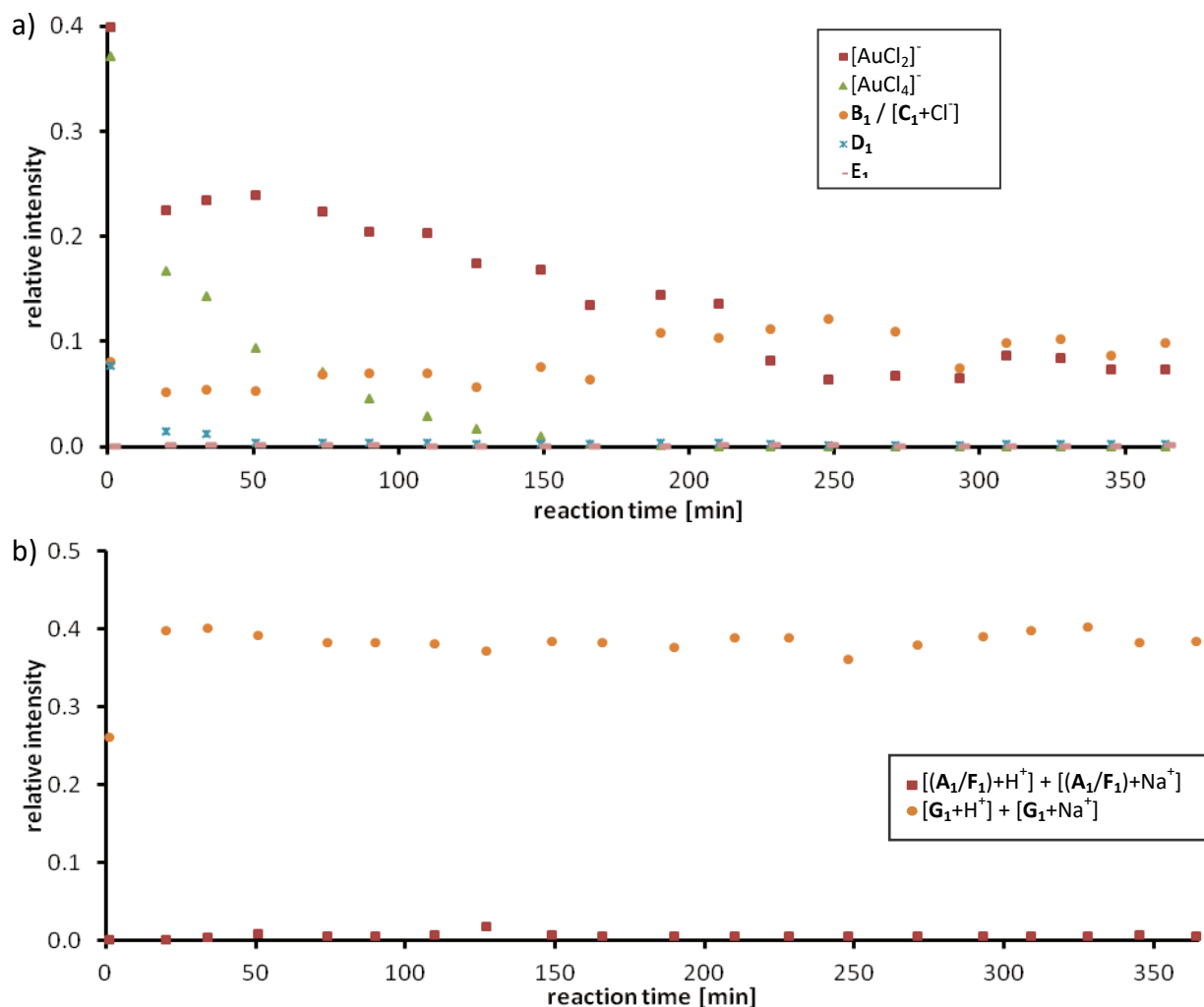


Figure 9: Temporal evolution of ionic species recorded with ESI from a solution containing 7 mol% HAuCl_4 and a substrate concentration (A_1) of 110 mmol/L in DCE reacting at 60 °C. Samples are diluted with acetonitrile before measurement.

Signal intensities are normalized relative to an internal standard. (a) negative mode; (b) positive mode.

Note that Au(I) is the major fragmentation product of all negative compounds in the catalytic cycle. Some undefined proportion of its abundance thus is due to fragmentation in the ESI source. The reaction can be slowed down by reducing the temperature (Figure 10). The abundances of ions D_1 and E_1 are rather low, but in accordance with their presence as reaction intermediates.

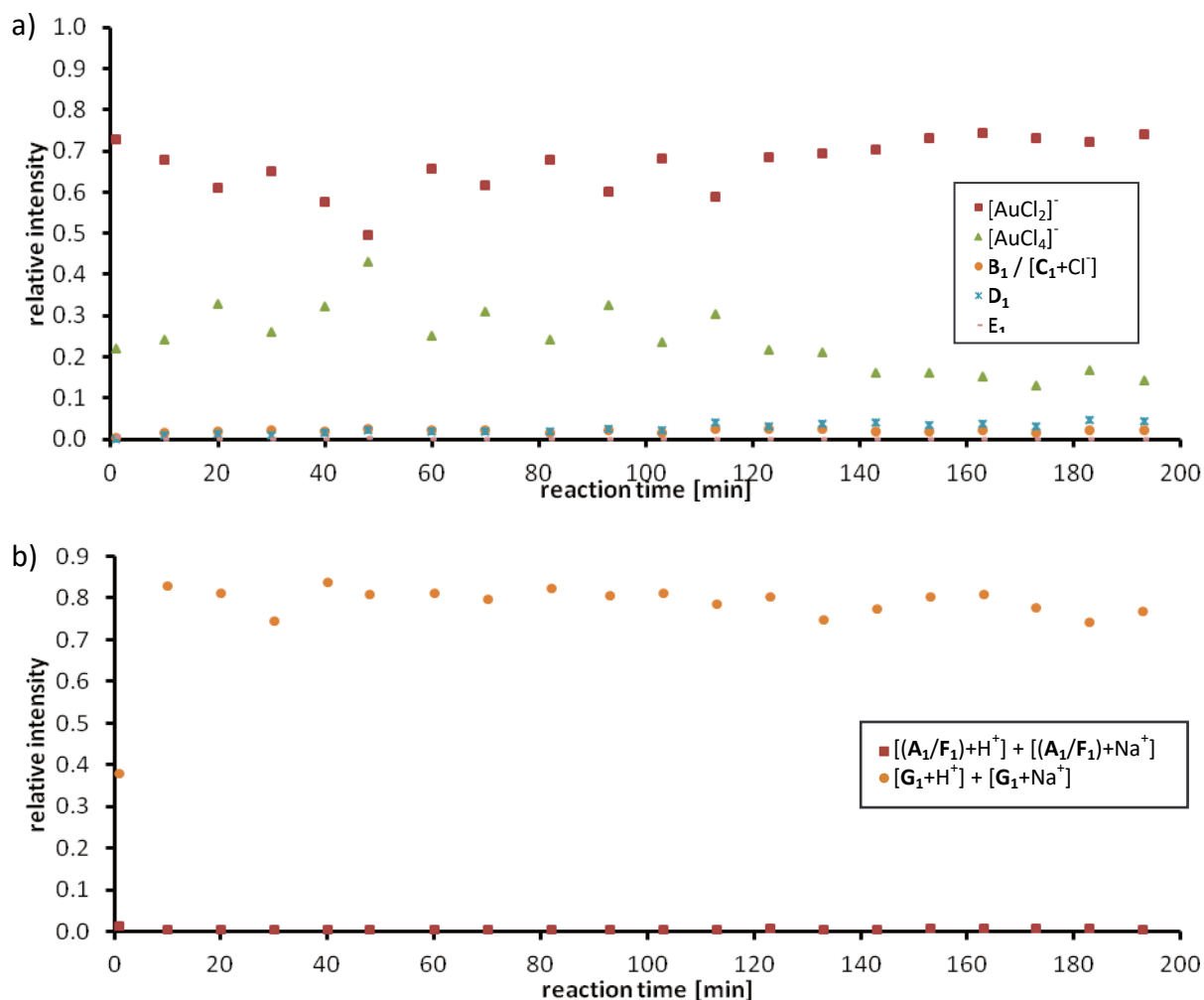


Figure 10: Temporal evolution of ionic species recorded with ESI from a solution containing 5 mol% HAuCl_4 and a substrate concentration (A_1) of 50 mmol/L in DCE reacting at 40 °C. Samples are diluted with acetonitrile before measurement. Signal intensities are normalized relative to an internal standard. (a) negative mode; (b) positive mode.

An unexpected increase for the ions assigned to the intermediates $\text{B}_1 / [\text{C}_1 + \text{Cl}]^-$ at late reaction times is shown in Figure 10. Based on this behaviour, we considered the presence of a third isomer $[\text{F}_1 + \text{AuCl}_4]^-$, i.e. an unspecific adduct of the catalyst with the monomeric reaction product. Such a species can easily be generated independently by mixing pure coumarin F_1 with HAuCl_4 and recording a mass spectrum in negative mode. This spectrum indeed shows the three expected species: $[\text{AuCl}_2]^-$, $[\text{AuCl}_4]^-$ and $[\text{F}_1 + \text{AuCl}_4]^-$. Mass-selection and CID of the latter ion mainly yielded $[\text{AuCl}_2]^-$ and small amounts of $[\text{AuCl}_4]^-$. In good accordance with earlier results,^[12b] we could not detect the dimeric product G_1 after addition of $[\text{AuCl}_4]^-$ to a solution of monomeric product F_1 .

ESI(+) spectra are more difficult to rationalize. First, reactant **A** and monomeric product **F** are isomers and therefore isobaric. We had hoped to distinguish both species by CID of protonated molecules as described above for the spectra of pure compounds. However, it turned out that ESI of reaction mixtures mostly yielded $[M+Na]^+$ instead of $[M+H]^+$, and we could not obtain reasonable fragmentation spectra of the sodiated ions probably due to charge loss by elimination of Na^+ .^[38] Therefore, we could only follow the sum of **A** and **F**. Second, there is a tremendous difference in ESI response of **A** and **G**, **G** is detected much better. In Figure 11 a spectrum measured from a 10:1 mixture of **A**₂ and **G**₂ is shown.

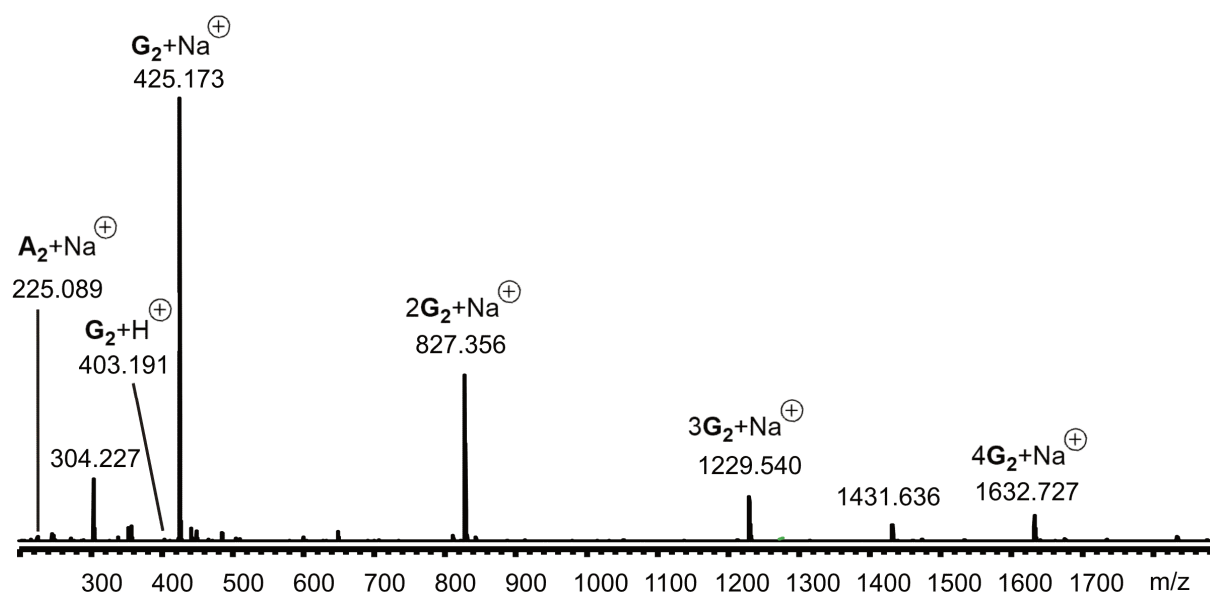


Figure 11: ESI(+) mass spectrum of a 10:1 mixture of **A**₂ and **G**₂. Irrespective of its presence in large excess, **A**₂ is suppressed.

Irrespective of its presence in tenfold excess, **A**₂ is visible only in traces, whereas **G**₂ is detected in very high intensity in monomeric and aggregated form. As a result, ESI(+) spectra are dominated by signals of **G** as soon as this product is present even in very small percentages. Accordingly, Figure 9 shows the presence of **A**₁ only at the very beginning of the reaction. Already after 10 min, signals for **G**₁ prevail in the ESI(+) spectra even though **A**₁ was added in twenty-fold excess. Figure 12 shows an ESI(+) spectrum of a reacting solution after 40 minutes. Due to the ESI response factor of the positive species the signal to noise ratio is worse than for the negative species.

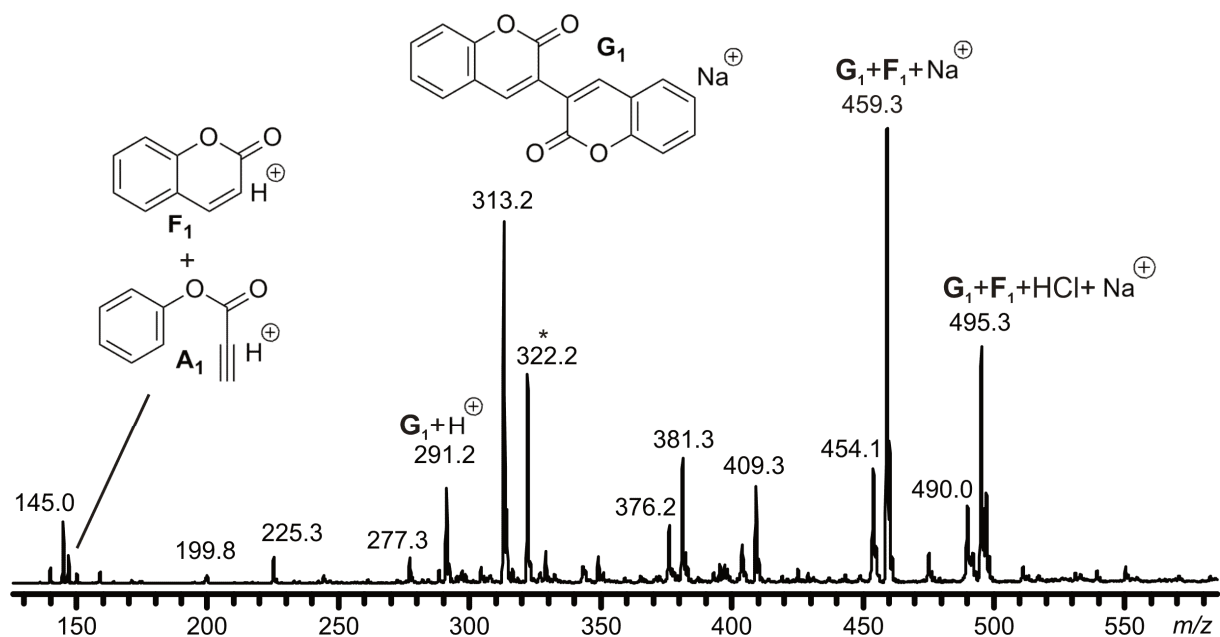


Figure 12: ESI(+)-mass spectrum of a reacting solution containing 20 mol% of H_{AuCl₄} and a substrate concentration (A₁) of 100 mmol/L in DCE at room temperature. Sample taken after 40 minutes and diluted 1:50 in acetonitrile (* = internal standard).

Similar results were obtained for the reaction with **A₂** leading to **F₂/G₂**. Nevertheless performing the reaction at room temperature significantly slows down the reaction and therefore the temporal evolution of the positive species could be followed. The initial increase of **G₂** and decrease of **A₂** is then nicely monitored (Figure 13). Please bear in mind that the chart only depicts the measured signal intensities which do not mirror the correct relative concentration ratios due to the strong difference in ESI response of **A₂** and **G₂**. The spectra clearly show that **A₂** has a higher affinity for Na⁺ instead of H⁺, whereas the preference is vice versa for **G₂** (Figure 13).

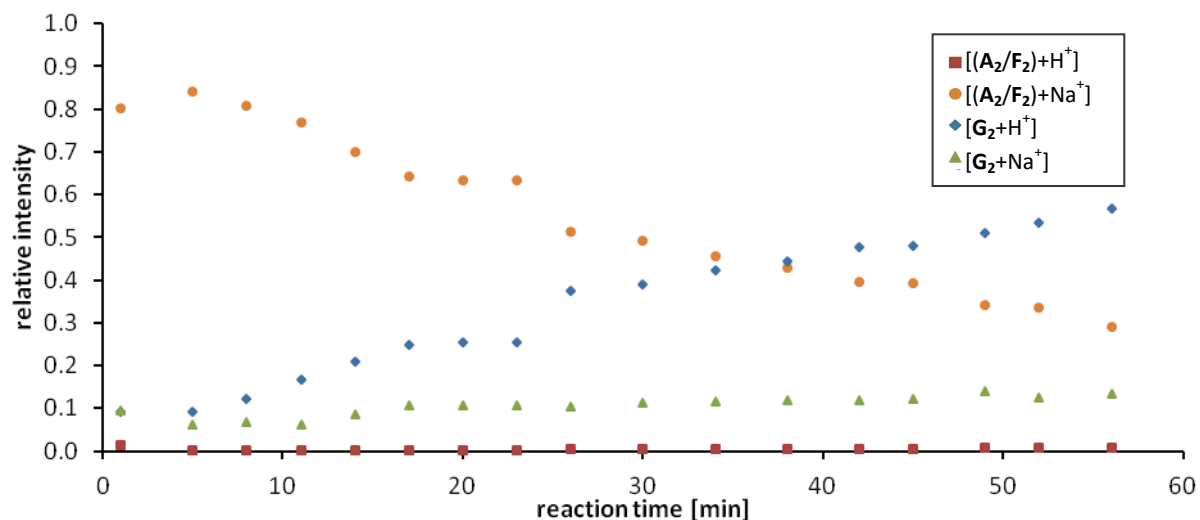


Figure 13: Temporal evolution of ionic species recorded with ESI from a solution containing 20 mol% HAuCl₄ and a substrate concentration (A₂) of 20 mmol/L in DCE reacting at room temperature. Samples are diluted with acetonitrile before measurement. Relative intensities are normalized to the sum of all depicted ions.

The described intricacy hampers a quantitative modelling of the time-dependent ion abundances. However, the qualitative behaviour fully supports the proposed mechanism. Consistent with the already published results^{[22] [1]} we found a faster reaction at higher ratios of the catalyst (Figure 14, Figure 15, Figure 16 and Figure 17). We concluded that by comparing the time when the intensity of product **G**₂ got higher than the signal of substrate **A**₂ in the reacting solution. For an easier evaluation we combined the intensities of the Na⁺ and H⁺ species. Changing the substrate concentration from 50 mmolL⁻¹ to 20 mmolL⁻¹ lengthened the time just a few minutes or seconds, while increasing the amount of the catalyst from 5 mol% to 20 mol% fastened the reaction essentially. The curves are already crossing after 5 min instead of 30 min. Even though this does not reflect the real concentrations, it still illustrates the course of the evolution.

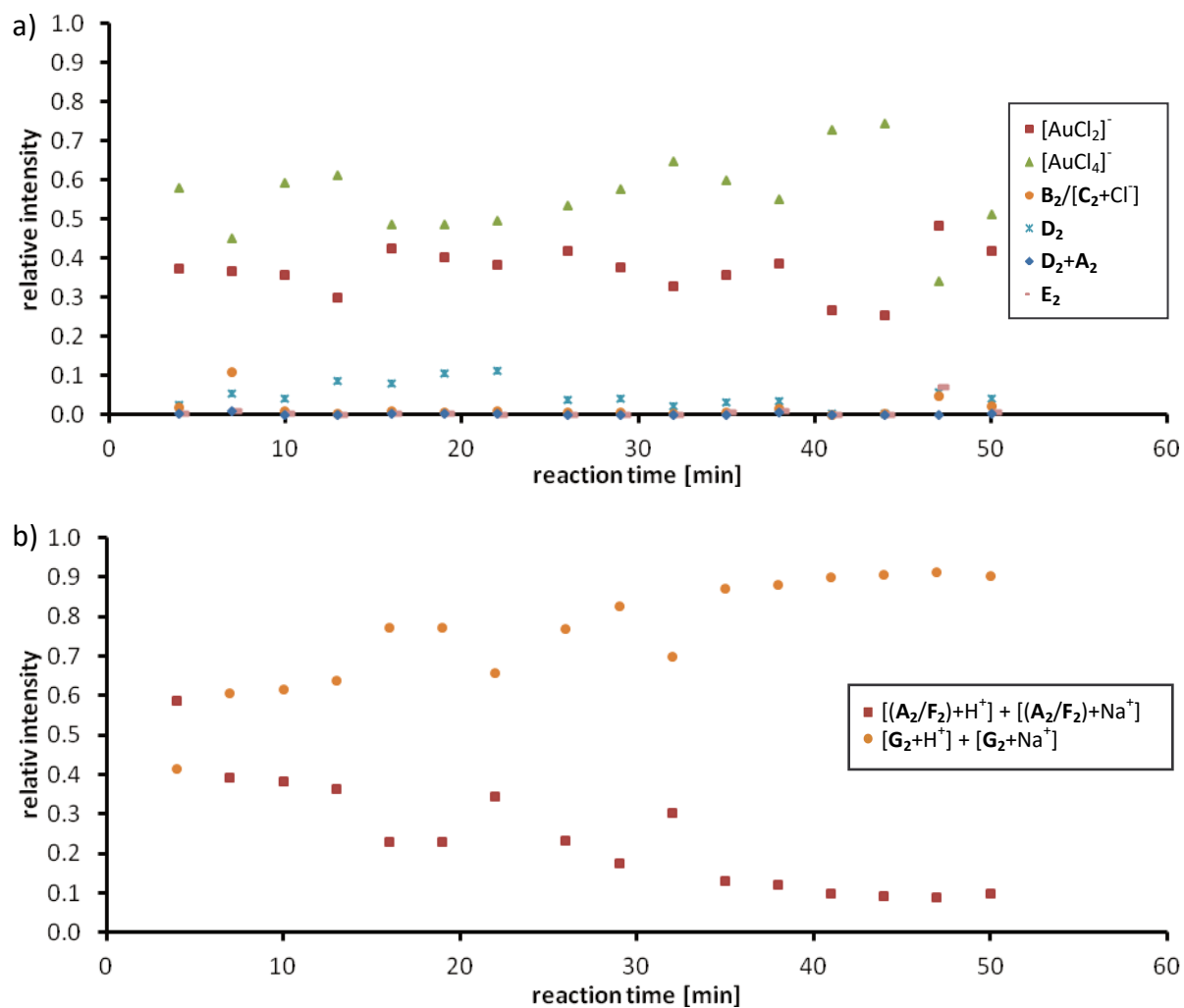


Figure 14: Temporal evolution of ionic species recorded with ESI from a solution containing 20 mol% HAuCl_4 and a substrate concentration (A_2) of 50 mmol/L in DCE reacting at room temperature. Samples are diluted with acetonitrile before measurement. Relative intensities are normalized to the sum of all depicted ions. (a) negative mode; (b) positive mode.

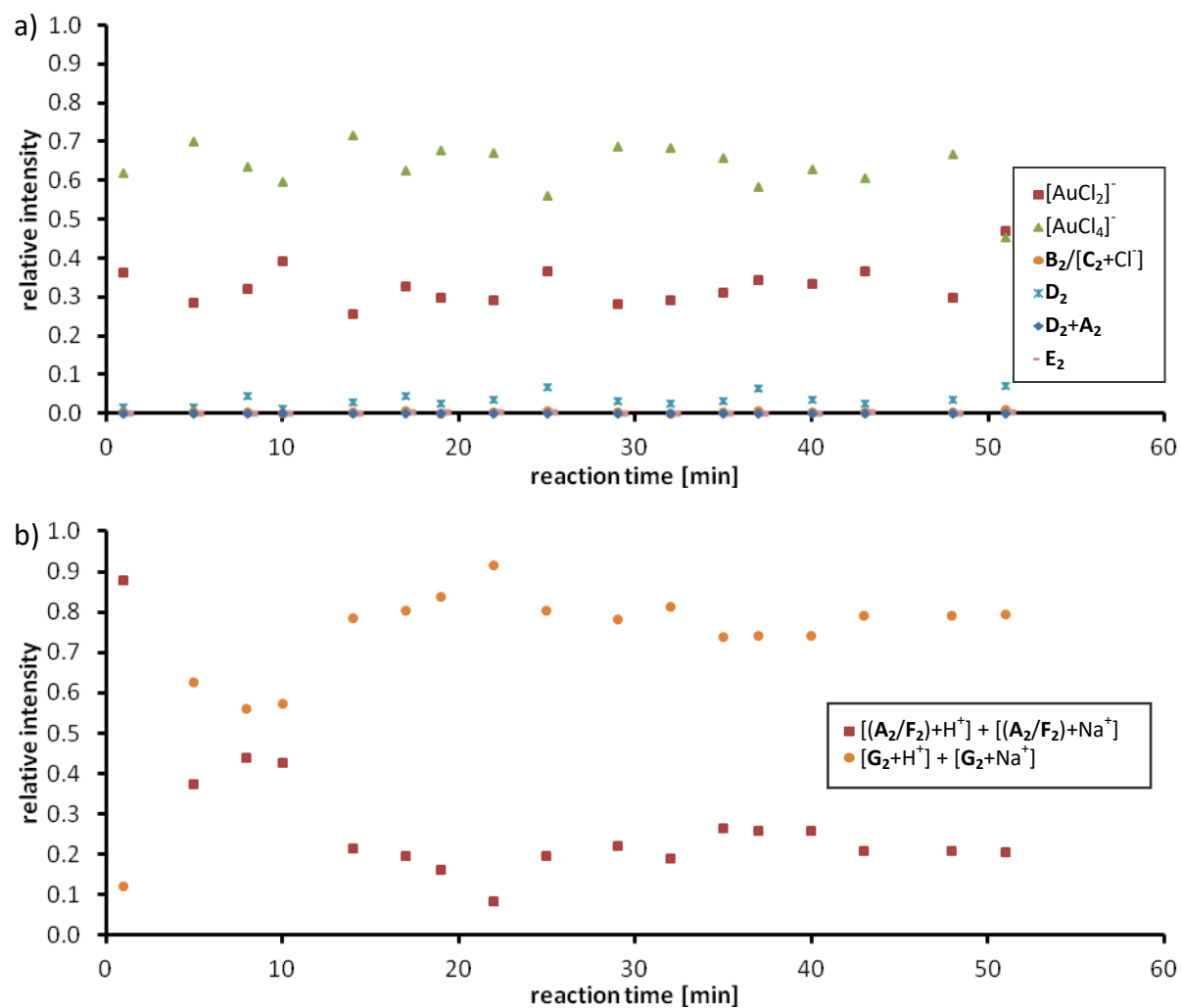


Figure 15: Temporal evolution of ionic species recorded with ESI from a solution containing 20 mol% HAuCl_4 and a substrate concentration (A_2) of 20 mmol/L in DCE reacting at room temperature. Samples are diluted with acetonitrile before measurement. Relative intensities are normalized to the sum of all depicted ions. (a) negative mode; (b) positive mode, the same data as shown in Figure 13; depicted without separation for protonated and sodium-coordinated molecules.

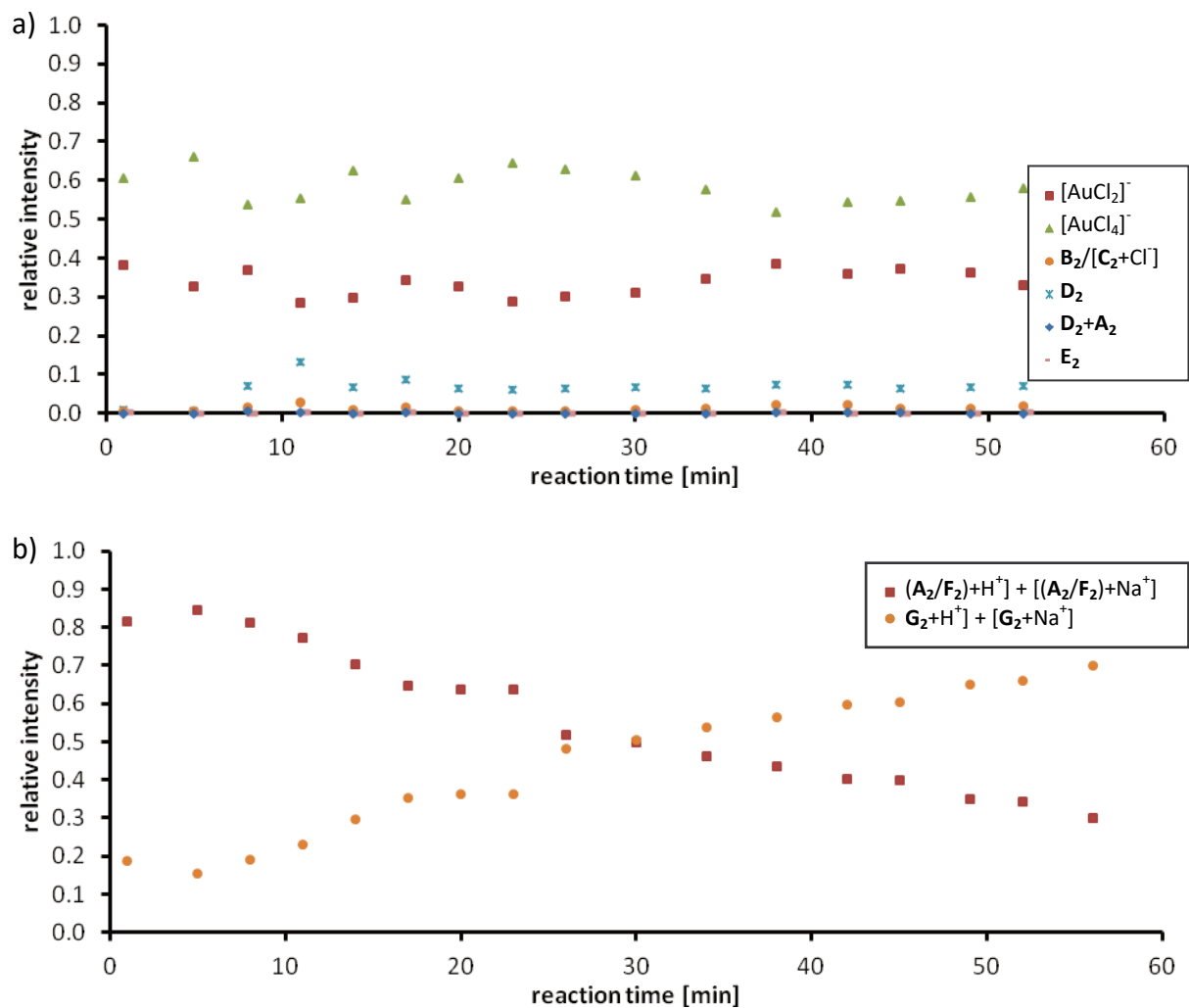


Figure 16: Temporal evolution of ionic species recorded with ESI from a solution containing 5 mol% HAuCl_4 and a substrate concentration (A_2) of 50 mmol/L in DCE reacting at room temperature. Samples are diluted with acetonitrile before measurement. Relative intensities are normalized to the sum of all depicted ions. (a) negative mode; (b) positive mode.

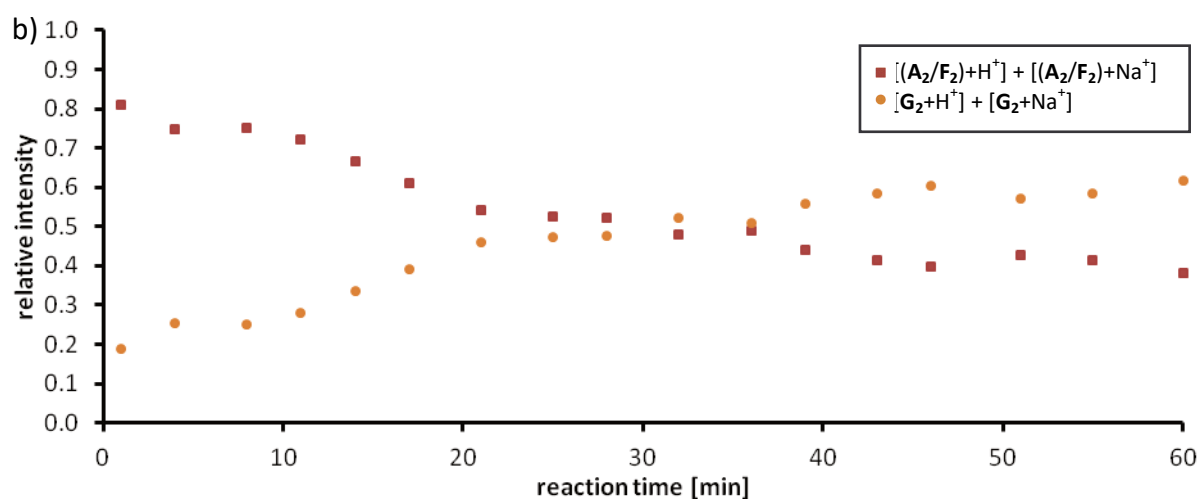
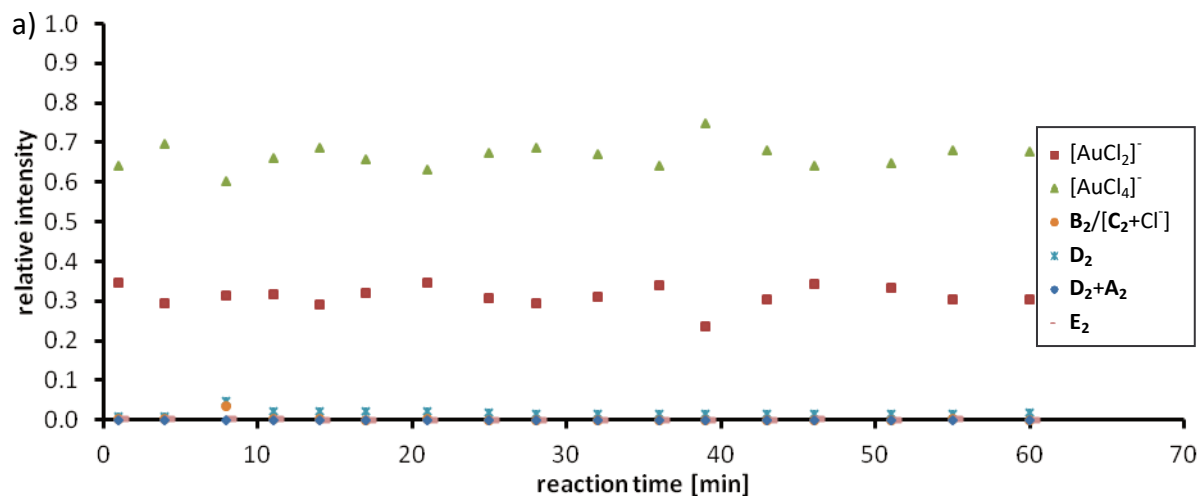
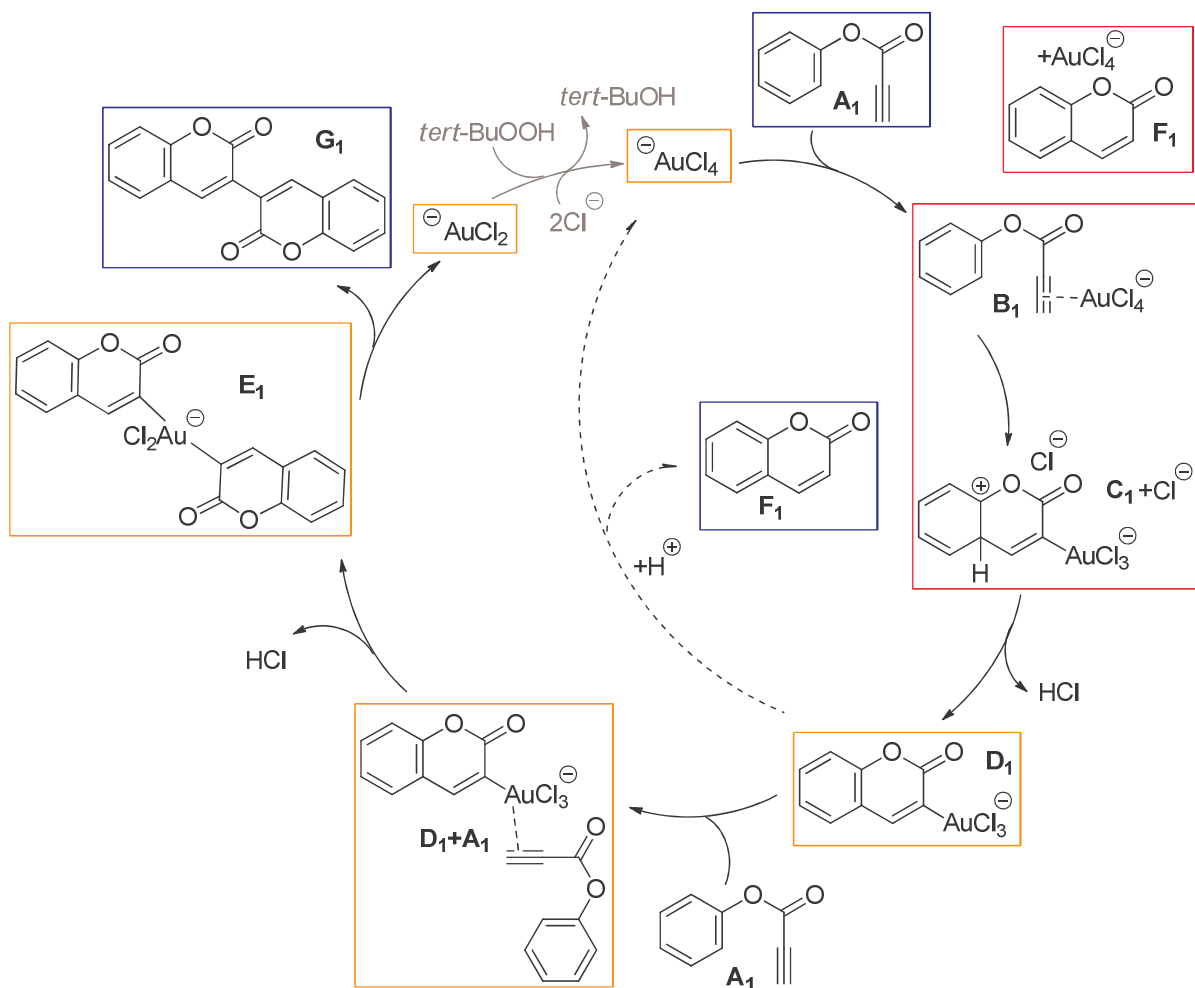


Figure 17: Temporal evolution of ionic species recorded with ESI from a solution containing 5 mol% HAuCl_4 and a substrate concentration (A_2) of 20 mmol/L in DCE reacting at room temperature. Samples are diluted with acetonitrile before measurement. Relative intensities are normalized to the sum of all depicted ions. (a) negative mode; (b) positive mode.

2.6 Conclusion

We present an ESI-MS investigation of an interesting tandem cyclization and oxidative coupling reaction catalyzed by HAuCl_4 . All postulated intermediates of the catalytic cycle could be detected and characterized by accurate mass determinations and collision induced dissociation. All involved ions bearing organic ligands are found as Au(III) complexes. In all cases, the remaining ligand sphere at the Au centre is filled with chloride ligands resulting in negatively charged intermediates (**A** = substrate, **F** = coumarin, **G** = dicoumarin; all found species are $[\text{AuCl}_2]^-$; $[\text{AuCl}_4]^-$; $[\text{A}+\text{AuCl}_4]^- = \text{B}/ \text{C}+\text{Cl}^-$; $[\text{A}-\text{H}+\text{AuCl}_3]^- = \text{D}$; $[2\text{A}-\text{H}+\text{AuCl}_3]^- = \text{D}+\text{A}$; $[2\text{A}-2\text{H}+\text{AuCl}_2]^- = \text{E}$ (The nomenclature of the species **A**, **B**, **C**, **D**, **E**, **F** and **G** originated from the postulated mechanism and is listed consecutively with the reaction steps). While all gold containing species bear a negative charge, the organic substrates and products are only detectable as $[\text{M}+\text{H}]^+$ and $[\text{M}+\text{Na}]^+$ in the positive ESI modus. Monitoring the temporal evolution of the reacting solution was unfortunately hampered due to fragmentation during the ionization process, strong ESI suppression effects, currently indistinguishable isobaric species and several interesting species with different charges which could not be followed in one measurement modus (ESI(-) or ESI(+)). However, after some alterations to slow down the reaction conditions, the progress of all species (positive and negative) could be monitored over an hour. The results were pretty helpful for a better insight of the reaction mechanism. Two of the proposed steps along the catalytic cycle, including the key C-C coupling step by reductive elimination, could be proven to be viable by provoking them in mass-selected ions in the gas-phase. We could not find evidence for diaurated species or gold clusters involved in this reaction. We very much hope to contribute to a better understanding of Au(III)-catalyzed oxidative coupling reactions which paves the way for further optimization and the development of new reactions.



Scheme 3: Proposed reaction mechanism with all detected positive (blue boxes) and negative (orange boxes) species. The red boxes show the three different possible isobaric species which currently cannot be distinguished.

2.7 Appendix

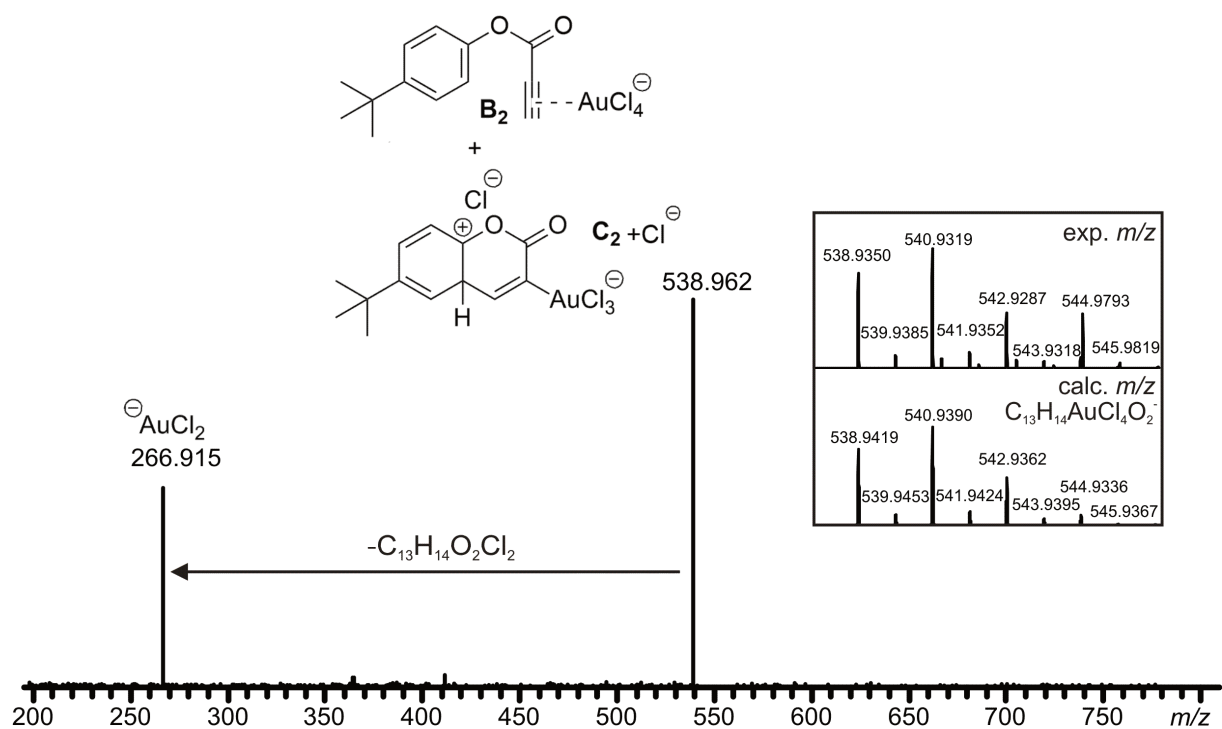


Figure 18: ESI(-) CID spectrum of mass-selected ions with $m/z = 539$ corresponding to intermediates B_2/C_2 .

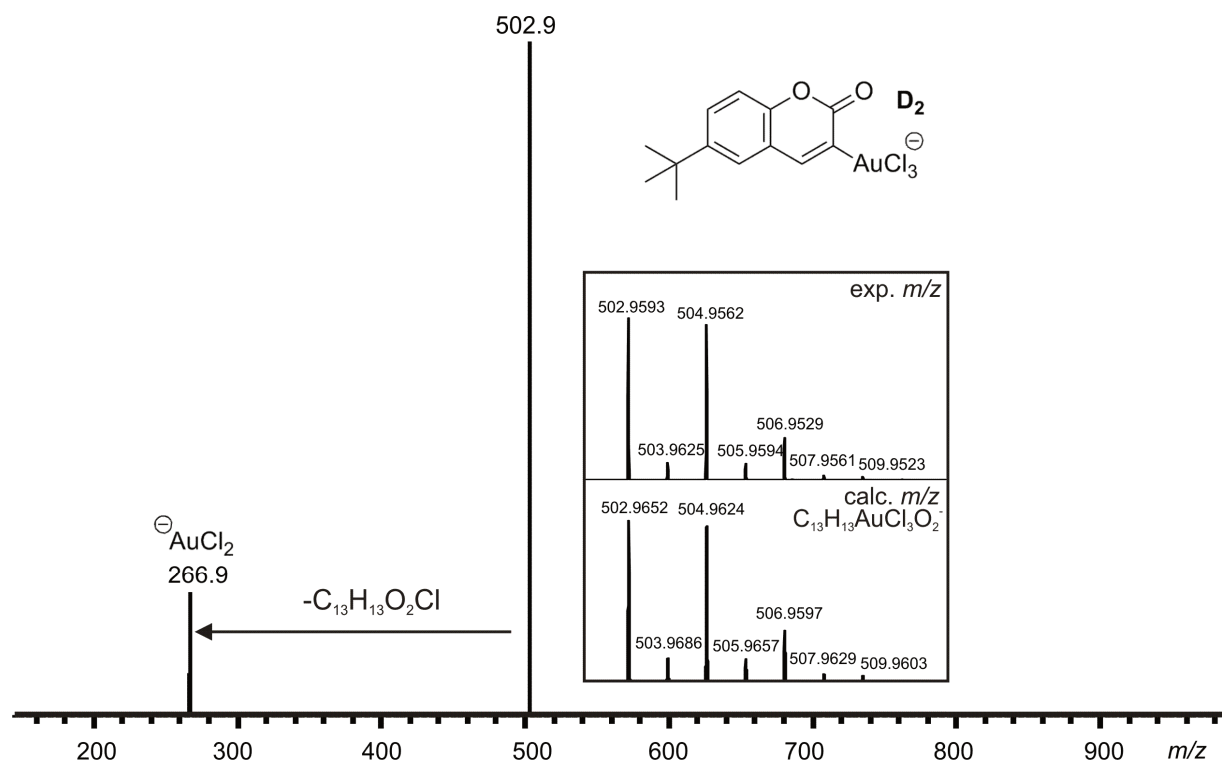


Figure 19: ESI(-)CID spectrum of mass-selected ions with $m/z = 502.9$ corresponding to intermediate D_2 .

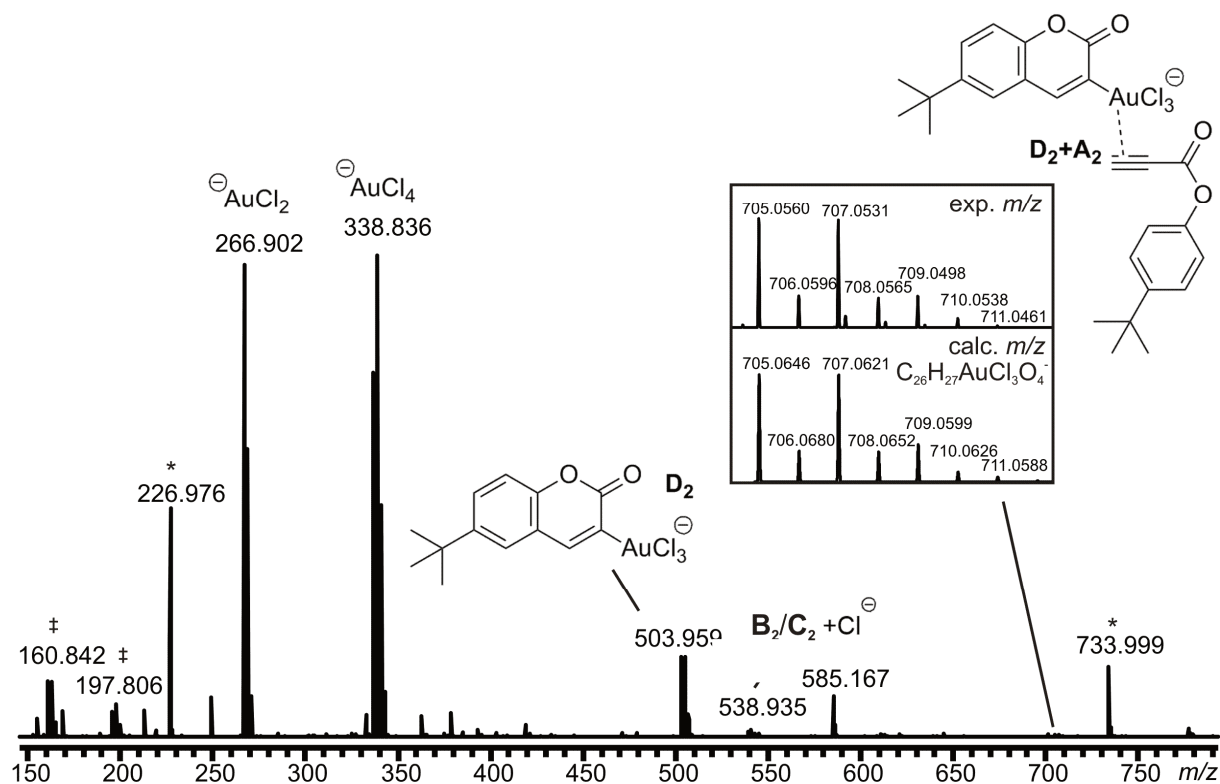


Figure 20: ESI(-) mass spectrum of a reacting solution containing 20 mol% of HAuCl_4 and a substrate concentration (A_2) of 45 mmol/L in DCE at room temperature. Sample taken after 71 minutes and diluted 1:50 in acetonitrile (* = internal standard; ‡ = FeCl_3 ($m/z = 158.8$ (max. 160.8)), FeCl_4 ($m/z = 193.8$ (max. 197.8))); iron-containing signals stem from corrosion of steel equipment).

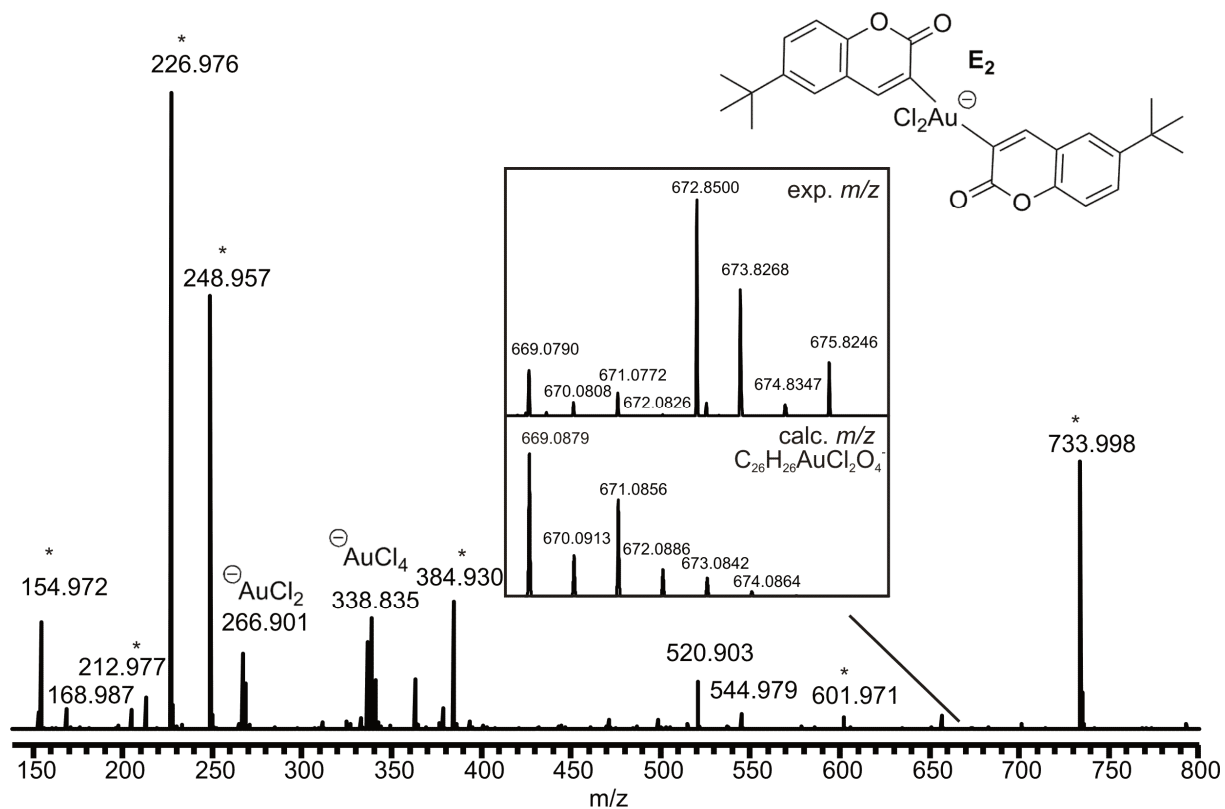


Figure 21: ESI(-) mass spectrum of a reacting solution containing 20 mol% of $HAuCl_4$ and a substrate concentration (A_2) of 45 mmol/L in DCE at room temperature. Sample taken after 7 minutes and diluted 1:50 with acetonitrile (* = internal standard).

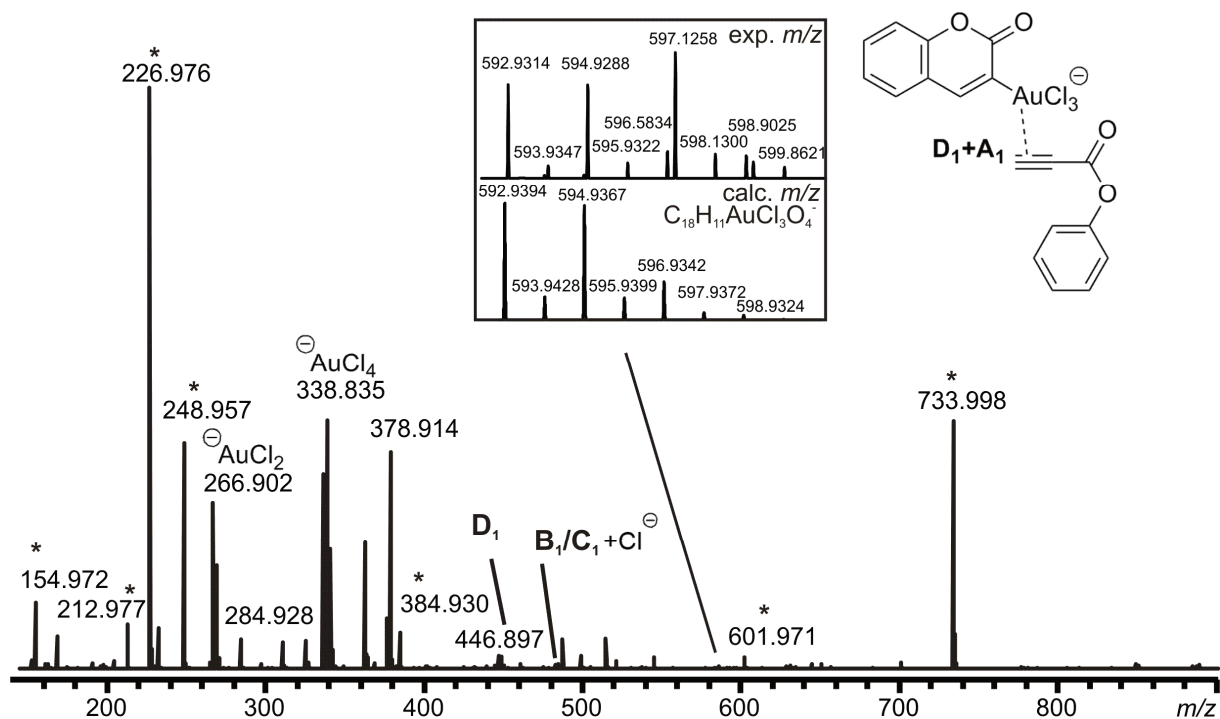


Figure 22: Full ESI(-) mass spectrum of a reacting solution containing 20 mol% of $HAuCl_4$ and a substrate concentration (A_1) of 100 mmol/L in DCE at room temperature. Sample taken after 22 minutes and diluted 1:50 with acetonitrile (* = internal standard).

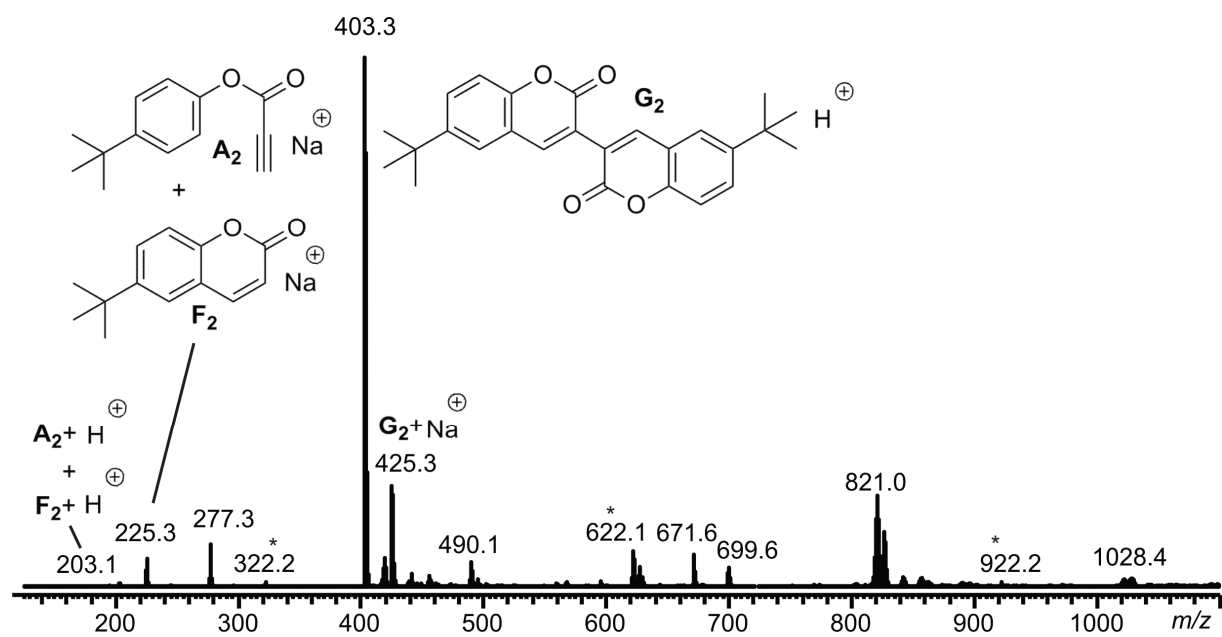
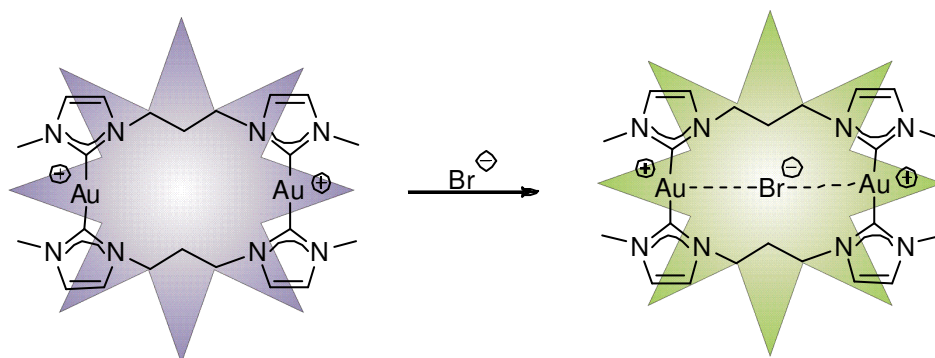


Figure 23: ESI(+)-mass spectrum of a reacting solution containing 20 mol% of $HAuCl_4$ and a substrate concentration (A_2) of 45 mmol/L in DCE at room temperature. Sample taken after 71 minutes and diluted 1:50 in acetonitrile (* = internal standard).

3 A conformational and spectroscopic investigation of Auophilicity and Hydrogen bonding in Dinuclear Gold(I) NHC complexes



3.1 Introduction

The initial mention of NHC compounds was done by *Öfele*^[2a] and *Wanzlick*^[2b] in 1968 but the first isolation of a free carbene was accomplished by *Arduengo* and his co-workers not before over 20 years later in 1991.^[39] This pioneering work however led to crystals of [1,3-bis(1-adamantyl)imidazol-2-ylidene], bearing two adamantyl substituents. Since then NHC compounds and their corresponding metal complexes have gained strong attention, due to a huge variety of promising applications^[40], which still provide an interesting and growing research field. Their coinage metal complexes are often used in catalysis,^[3a-m] as luminescent compounds^[4] or other materials^[41]. The group of *Hashmi* recently published a study of highly active asymmetrically substituted NHC gold(I) catalysts.^[3n] There are also many medical applications^[42] known for gold(I) or silver(I) NHC complexes, based on their cytotoxicity^[43], cell imaging properties^[44] and anti-tumour activity^[45]. Coinage metal complexes with NHC ligands are also well established due to their intriguing and highly tuneable spectroscopic properties,^[4a,4b,46] which are often based on exceptional d^{10} - d^{10} interactions. These aurophilic interactions were first introduced by *Schmidtbaur* in 1988.^[5] They belong to weak supramolecular interactions with the bonding energy of 5-10 kcal/mol and a typical bonding length smaller than the sum of the van der Waals radii ($\leq 3.5 \text{ \AA}$). Over the past decades, aurophilic interactions were mainly known in solid state. More recently some intriguing reversible supramolecular systems were found in solution and since then significantly changed the possible fields of application.^[47]

Cationic gold(I) and silver(I) NHC complexes usually feature linear structures with two heteroleptic or homoleptic ligands. The aromatic carbene moieties can be modified and bear different kinds of substituents, which leads to a wide array of electronic and steric parameters. Lots of varying examples are known in the literature with imidazole or benzimidazole units. Some examples are given below. Hence NHCs provide strong σ -donor abilities, they are often used as option instead of phosphine complexes. Especially gold(I) NHC complexes are also air and moisture stable and offer a great alternative. This type of complexes often provides several different binding sites on the ligands and the metal centres and therefore could be used as chemosensors for small molecules^[48], ions^[4d,7c,49] and even solvents.^[4f,50] Metal complexes with NHC ligands can therefore be part of metallosupramolecular aggregates^[51], cages^[52], macro molecules^[53], helicates^[54], pincers^[49b,55], clusters^[56] and other 3d structures^[7b,7d,57]. Aggregation processes are realized by weak interactions like hydrogen bonding, ion pairing, $\pi\cdots\pi$ - as well as metallophilic interactions and sometimes even $\text{Au}\cdots\text{H}$ bonds^[58]. Exceptional host-guest interactions are often accompanied by a change of the photophysical behaviour,^[59] which is usually based on metallophilic^[60] interactions. Due to the weak interaction most of the supramolecular systems are reversible and could provide fascinating switchable^[48a] systems. Initiation of the aggregation can be triggered through numerous simple or special techniques like mixing, grinding (mechanochromic) and even exposure to vapours (vapochromic).^[4f,7c,61] This utmost interesting behaviour provides a convenient yet versatile colour adjustability of metal NHC compounds. The counterions and their affinity to the cations also play an important role for the reactivity of catalysts or other properties like solubility, crystal structures or the aggregation behaviour of host-guest compounds. Therefore their influence should not be neglected while creating new systems or during investigations of known compounds. Due to their highly tuneable properties and different features, which are often triggered by small alterations, coinage metal NHC complexes provide the entry to an attractive research field and have a huge impact in organometallic chemistry.

Numerous homoleptic dinuclear gold(I) NHC complexes with varying captivating properties have already been reported before.^[2c,4a,44a,46b,46c,53,61a,62] Next to the alkyl substituents other functional groups can be attached at the ligand.^[63] Derivatives with differences at the linker,^[4e,4i,62g,62s,64] the side chains,^[4g,62f,62m,65] and the imidazolium moieties^[62q] are possible. All of these parameters are highly affecting the characteristic parameters of the compounds.

Crystal structures of gold(I) NHC complexes are highly depending on all functional groups inside the molecule as well as the choice of the solvent used during the crystallization. Simple modifications at the side chain^[66] or variation of the counterion^[7b] could change the whole structure. The exchange of the anions^[62f,67] has an additional huge impact on other properties^[7a] like their photophysical behaviour^[68] or their catalytical performance^[69].

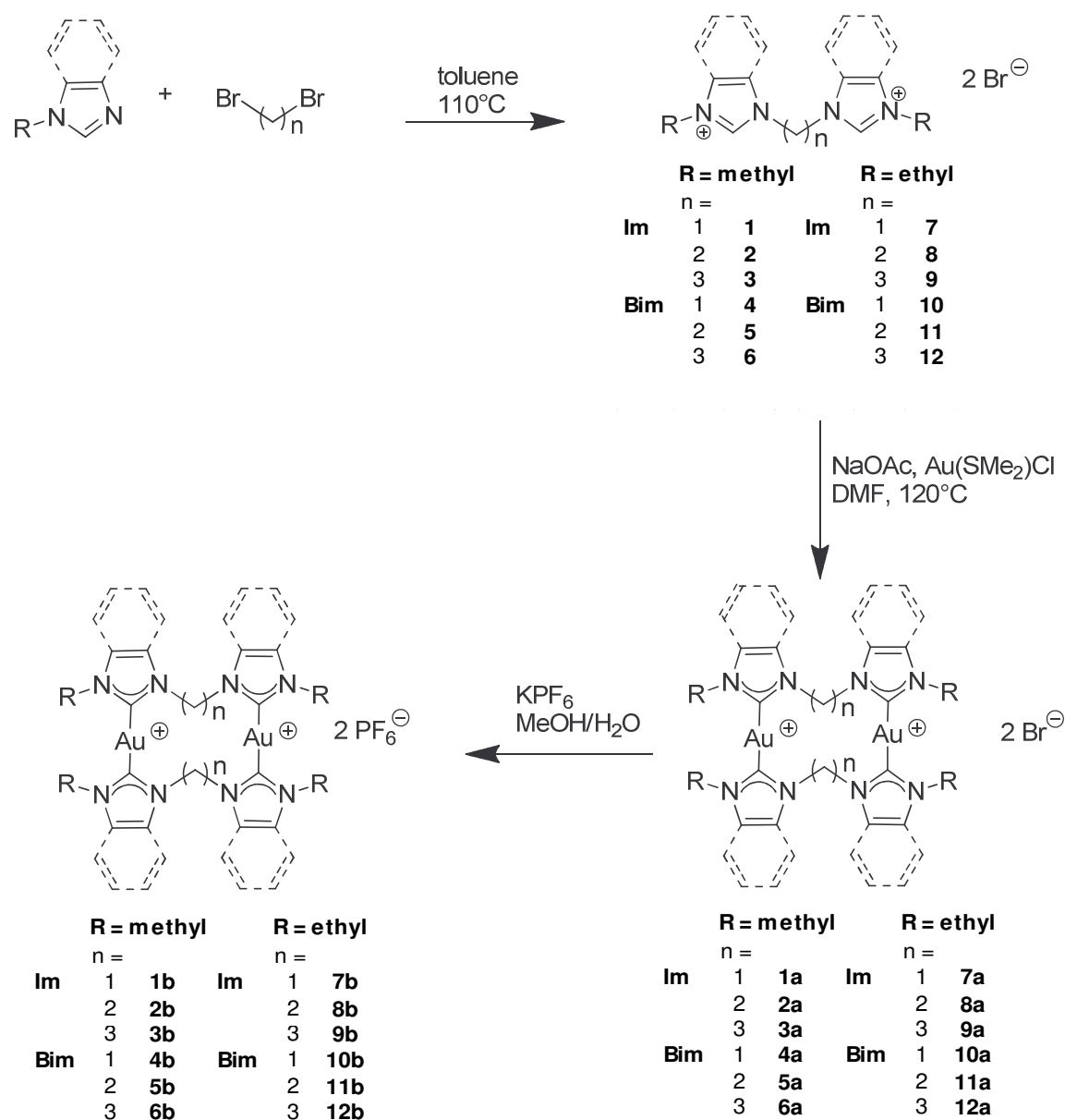
Former investigations in our group have shown the correlation between different counterions and the properties of a series of gold(I) NHC complexes with ethyl side chains and imidazolium moieties.^[4f] Varying crystal structures and a change in the fluorescence behaviour could be connected to different lengths of the flexible alkyl chains between two NHC units. The main focus of that study lies in the investigation of aurophilic^[5a,5c,5d,70] interactions. Nearly at the same time *Pelle et al.* presented a $[\text{Ag}_2(\text{bis-NHC})_2]^{2+}$ complex as an outstanding example for an Ag^+ sensor supported by argentophilic interactions.^[71] In addition to our results, *Penney et al.* confirmed the interactions between similar homoleptic gold(I) NHC complexes with benzimidazole moieties and bromide as counterion, by fluorescence- and NMR titration experiments.^[72] They have shown reversible aurophilic interactions triggered by the counterion or the solvent methanol. However the connection between the bromide concentration and the fluorescence of dinuclear NHC complexes accompanied with a red shift of the emission band was first mentioned by *Wedlock et al.*^[73] Another interesting selective halogen receptor was found by *Baron et al.*^[74] The supramolecular host-guest interactions of the square planar gold(III) NHC complexes with the anions are based on hydrogen bonding, which derive from the wingtip groups of the ligands.

Overall the research of this type of compounds bears a lot of interesting features and is not utilized yet. Thus, we now report the synthesis and characterization of three systematic series of dinuclear gold(I) NHC complexes with hexafluorophosphate and bromide counterions and compare them with our previously reported results. The choice of the counterions is not arbitrarily. The bromide salts are deriving from the starting materials of the synthesis (see Scheme 4) and PF_6^- was chosen for the anion exchange, because crystallization of those compounds often results in crystal structures free of additional solvent molecules. Pure substances are important for a clear investigation of the properties. For additional binding sites the aromatic systems were expanded from imidazole to the

bigger benzimidazole derivatives. To examine the role of the side chains and linkers, we synthesized the methyl and ethyl derivatives and complexes with different alkylene bridges (C1-C3). Crystal structures of all complexes from the series and four new salts with other counterions ($[\text{Au}_2(\text{bisEt}_2\text{MeIm})_2](\text{NO}_3)_2$, $[\text{Au}_2(\text{bisMe}_2\text{PrIm})_2](\text{BF}_4)_2$, $[\text{Au}_2(\text{bisEt}_2\text{MeBIm})_2](\text{PO}_2\text{F}_2)_2$ and $[\text{Au}_2(\text{bisEt}_2\text{EtBIm})_2](\text{PO}_2\text{F}_2)_2$) were obtained. A subsequently consistent study of all structural parameters in correlation with the derivatization has been performed. Supplementary UV/Vis-, fluorescence- and NMR spectroscopic experiments were performed to analyze the qualification of the complexes as receptor for small substrates, including the counterions.

3.2 Synthesis and general characterization of Au(I) NHC complexes

The homoleptic gold(I) NHC complexes **1a** – **12a** were prepared according to a modified synthesis adapted from *Baker et al.*^{12a,25b} The corresponding imidazolium salts were synthesized via a nucleophilic substitution and then dissolved in DMF, in the presence of sodium acetate and Au(SMe₂)Cl. Anion exchanges were forced by adding an excess of KPF₆ in H₂O to a solution of the complexes^[4f,62f] in methanol (**1a** – **3a**, **7a** - **9a**) or a mixture of methanol/dichloromethane (**4a** – **6a**, **10a** - **12a**).

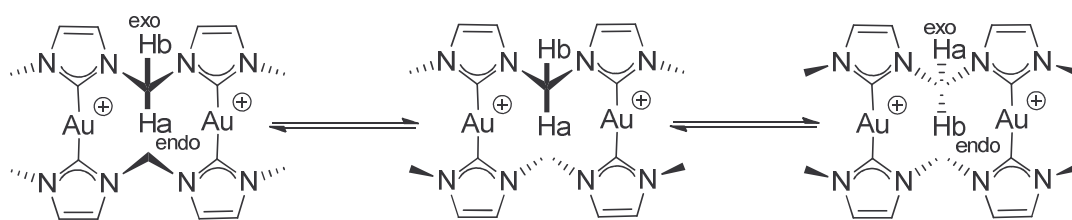


Scheme 4: Syntheses of the NHC precursors 1–12 and the dinuclear gold(I) NHC complexes 1a,b–12a,b.

Purification was achieved by slow diffusion of diethyl ether into a concentrated solution of the complexes. The characterizations of all complexes were performed by NMR spectroscopy and electrospray mass spectrometry (ESI-MS). The cations were detected as $[M-2X]^{2+}$ and $[M-X]^+$ species in the positive ESI-MS modus and the separated anions in the negative modus. Complete conversions of the imidazolium salts were proven by the shifting of some resonances and/or the absence of the resulting respective signals in the ^1H - and ^{13}C -NMR spectra. The synthesized gold(I) NHC complexes can easily be distinguished from the corresponding imidazolium compounds by a different shifting of the belonging resonances. The synthesis of the highly symmetrical homoleptic compounds **1a** – **12a** involves the disappearance of the resonance from the acidic proton H4 at $\delta \approx 9.5$ ppm. Additionally the signal from the $\text{C}_{\text{carbene}}$ atom shifts from approximately 140 ppm up to > 180 ppm.^[75] The change from bromide to hexafluorophosphate could be confirmed by ^{31}P - and ^{19}F -NMR spectroscopy.

3.3 NMR spectroscopy experiments

Gold(I) NHC complexes show an interesting ring inversion dynamic in solution, which can be investigated by means of NMR spectroscopy. This effect is especially pronounced for methylene compounds. The two resonances of the linker (**Ha** and **Hb**) are not isochronic, in consequence of their different chemical environment. Due to their flexibility in solution they are constantly changing from the exo to the endo position, converting the conformation from twisted to folded (see Scheme 5).^[46b]



Scheme 5: Ring inversion of dinuclear gold(I) NHC complexes with methylene linkers.^[46b]

The ring inversion can be simply promoted by heating the solution, resulting in a single resonance for both protons at their coalescence temperature. Yet at room temperature the molecule is rigid on the NMR timescale and the signals appear as two well distinguishable doublets.^[4e] Similar ethylene complexes are indeed less rigid and show an enhanced

flexibility in solution, resulting in a much lower coalescence temperature. Therefore they cannot be separated, in a spectrum measured at temperatures cooler than ambient conditions.^[6,76] $^1\text{H-NMR}$ spectra of complexes with longer alkylene chains did show a much faster dynamic in solution, which could ultimately not be frozen on the NMR time scale. Hence, a splitting of the signals could not be reached by lowering the temperature down to -80°C . All NMR experiments in the now presented work were performed at 298 K. Since the temperature should not have an influence on the mobility of the complexes in solution, which is important for the comparability of the compounds and their behaviour. The chemical shift of the signals is not only influenced by the conformation of the complexes but also by their interactions with the counterions. The interplay of the cations and the anions is often accompanied with a significant shift of some of the proton resonances caused by the aggregation, and more precisely by the resulting hydrogen bonding and shielding processes. The interaction depends on the nature of both of the components, the anions and the cations, which means that other substrates interact differently with the potential binding sites of the receptor molecules. Therefore several hydrogen bonds are possible, which will result in the shifting of the respective resonance or resonances. E.g. *Biz et al.* found a gold metallo-tweezer molecule which is able to bind polycyclic aromatic hydrocarbons. The NHC moiety bears butyl wingtip substituents. Amongst other signals the N-CH_2 resonances of the alkylene chain undergo a significantly downfield shift.^[77] *Penney et al.* examined a shifting of the signals for dinuclear gold(I) NHC complexes with benzyl side chains and varying alkylene bridges (C1-C3).^[72] They found a significant downfield shift for the endo methylene proton resonance for bromide complexes in comparison with hexafluorophosphate complexes. Small shifts of the CH_2 -benzyl resonances and the signals of the aromatic side chain substituents were also visible. Adding excess TBAB intensifies the effects. The ethylene and propylene complexes show a similar behaviour and small downfield shifts for the CH_2 -benzyl signals, the N-CH_2 resonances of the alkylene bridges and some of the aromatic resonances. The strongest changes are however detected for the endo protons of the complexes with methylene bridges. Another fascinating halogen sensor was found by *Basato et al.* as a gold(III) tetra NHC PF_6^- complex. The ligand precursors are the same as in compound **1** in this work (bisMe₂Melm), but they are linked to only one gold centre with a higher oxidation state (Au(III)). Thus, the complex bears two methylene groups and four methyl side chains. The resonances of the methyl substituents undergo a small downfield shift after the addition of

halides, while the H_{endo} signal shows a much stronger shift. This effect is attributed to hydrogen bonding with the halides.^[74]

All these aggregation phenomena are highly depending on the concentration of the receptors and substrates. High concentrations in solution support the aggregation, due to higher possibilities of an encounter of the compounds. The mixture will always contain unbounded cations and anions, due to the reversibility of the weak interactions. High concentrations change the chemical equilibrium. Most of the host compounds bear several binding sites. Hence they are able to interact with more than just one potential guest.^[74] On the basis of this experience, the supramolecular interactions in combination with the visible changes in the spectra are therefore influenced by the stoichiometry of the compounds in solution.

In addition to the counterions, solvent molecules can also associate with the NHC complexes.^[72,78] Some of these interactions are also activated by solvent vapours.^[4f,7c,61] Comparing experiments of different complexes should therefore be performed in the same (preferably purified) solvent. Otherwise a change of the NMR-signals could not be exclusively connected to the addition of the counterions and the resulting interactions with them.

The counterions also have essential effects on the solubility and the resulting $^1\text{H-NMR}$ spectra of the complexes. While the bromide salts dissolve completely in methanol-*d*4 the preferred solvent for most hexafluorophosphate salts is acetonitrile-*d*3 (the solubility of benzimidazole complexes could be improved by adding dichloromethane-*d*2). Changing the solvents involves a crucial decrease of the solubility for most complexes. In contrast to other solvents all complexes show an adequate but limited solubility in DMSO-*d*6. Therefore this solvent was chosen to compare all compounds in Table 1, Table 2 and Table 3. Some of these solutions could also be used to perform $^{13}\text{C-NMR}$ experiments, but some were not concentrated enough for that purpose. Therefore the overall comparison is limited to the proton resonances. The C_{carbene} atoms are directly bonded to the gold centres and the resonances would probably shift visibly triggered by an aggregation process to the metal.^[79] Even though these data would also be pretty interesting, we were not able to find a good solvent to compare all these spectra homogenous.

Table 1: $^1\text{H-NMR}$ data of the alkylene linker protons in $\text{DMSO-}d_6$, for the complexes 1a,b – 12a,b in ppm.

	$-\text{CH}_2-$ endo/exo	$-\text{CH}_2-\text{CH}_2-$	$-\text{CH}_2-\text{CH}_2-\text{CH}_2-$
ImMe*Br $^-$	7.19/ 6.34	4.81	4.16/ 2.59
ImMe*PF $_6^-$	7.18/ 6.33	4.79	4.17/ 2.59
ImEt*Br $^-$	7.18/ 6.38	4.82	4.23/ 2.62
ImEt*PF $_6^-$	7.14/ 6.35	4.81	4.22/ 2.62
BImMe*Br $^-$	7.86/ 7.53	5.39	4.95/ 3.05
BImMe*PF $_6^-$	7.53/ 7.47	5.37	4.93/ 3.05
BImEt*Br $^-$	7.81/7.47	5.39	4.97/ 3.00
BImEt*PF $_6^-$	7.54/ 7.44	5.36	4.97/ 3.01

Table 2: $^1\text{H-NMR}$ data of the aromatic protons in $\text{DMSO-}d_6$, for the complexes 1a,b – 12a,b in ppm.

	C1	C2	C3
ImMe*Br $^-$	7.91/7.60	7.89/7.59	7.73/7.60
ImMe*PF $_6^-$	7.42/7.38	7.73/7.60	7.70/7.57
ImEt*Br $^-$	7.93/ 7.71	7.52/ 7.45	7.67/ 7.63
ImEt*PF $_6^-$	7.90/ 7.70	7.51/ 7.38	7.65/ 7.61
BImMe*Br $^-$	8.15/ 7.92/ 7.62	7.71/ 7.64/ 7.44/ 7.33	7.71/ 7.60/ 7.32/ 7.22
BImMe*PF $_6^-$	8.10/ 7.93/ 7.64	7.71/ 7.62/ 7.48/ 7.34	7.68/ 7.58/ 7.31/ 7.21
BImEt*Br $^-$	8.12/ 8.01/ 7.63	7.78/ 7.58/ 7.44/ 7.31	7.77/ 7.69/ 7.34/ 7.29
BImEt*PF $_6^-$	8.10/ 8.02/ 7.64	7.77/ 7.55/ 7.45/ 7.32	7.75/ 7.68/ 7.34/ 7.28

Table 3: $^1\text{H-NMR}$ data of the side chain protons in $\text{DMSO-}d_6$, for the complexes 1a,b – 12a,b in ppm.

	C1	C2	C3
ImMe*Br $^-$	3.88	3.78	3.50
ImMe*PF $_6^-$	3.88	3.78	3.49
ImEt*Br $^-$	m/ 1.39	4.14/ 1.33	3.87/ 1.27
ImEt*PF $_6^-$	m/ 1.39	4.13/ 1.33	3.87/ 1.27
BImMe*Br $^-$	4.13	4.00	3.99
BImMe*PF $_6^-$	4.13	4.00	3.98
BImEt*Br $^-$	4.63/ 1.44	4.49/ 1.16	4.52/ 1.38
BImEt*PF $_6^-$	4.64/ 1.45	4.48/ 1.17	4.52/ 1.39

The proton resonances of the wingtip substituents are not shifting after the anion exchange. Some small alterations are found by investigating the second position after the decimal point, which is rather negligible. A strong interaction of the counterions with the alkyl chains (as $\text{H}\cdots\text{Br}$ bonds) are therefore excluded. The experiments yield also just small shifting for

the linker resonances of the imidazolium complexes **1a,b** – **3a,b** and **7a,b** – **9a,b**. However the corresponding aromatic signals show strong shifting. The major differences were observed for the methylene complexes. The complexes with the longer ethylene linker cause smaller shifting of the signals, while the differences in the spectra of the propylene complexes are rather subtle and almost not observable. This could presumptively be linked to another dynamic in solution. While the signals of the aromatic protons of the imidazole complexes are changing visibly, the spectra of the benzimidazole complexes do not show significant differences in this area, after anion exchange. The protons are farther from the gold centres and therefore apparently not strongly affected by the aggregation process. The more pronounced differences for the complexes **4a,b** – **6a,b** and **10a,b** – **12a,b** are visible in the shifting of the resonances of the linker. The strongest examples are again the methylene compounds, while the propylene resonances are almost unaffected by the anion exchange. Nonetheless the bigger benzimidazole moiety should provide an additional binding site in the first place and so support the interaction of the cation with the counterion. This could lead to different bonding motifs for these compounds. The anion could be either interacting with the big π system or lying between the two gold centres (stabilized by Au...Br and/or H...Br interactions). The aggregation of cations and anions could be achieved by either one of these motifs or a combination of them. Due to the accessibility of several different bonding sites, the NHC compounds could potentially interact with more than just one anion (For a better overview the following NMR spectra will only show the aggregation between the gold centres (see Figure 24, b), even though other motifs or a combination are probably present in solution). Those interactions could activate a folding process of the complexes and therefore promote the intended aurophilic interactions, due to short Au...Au distances. The supramolecular interplay does not necessarily include the penetration of the cation by a counterion. The negative charged substrates could also interact with the complex, by coordination on the outside of a cavity or interfolded structure.

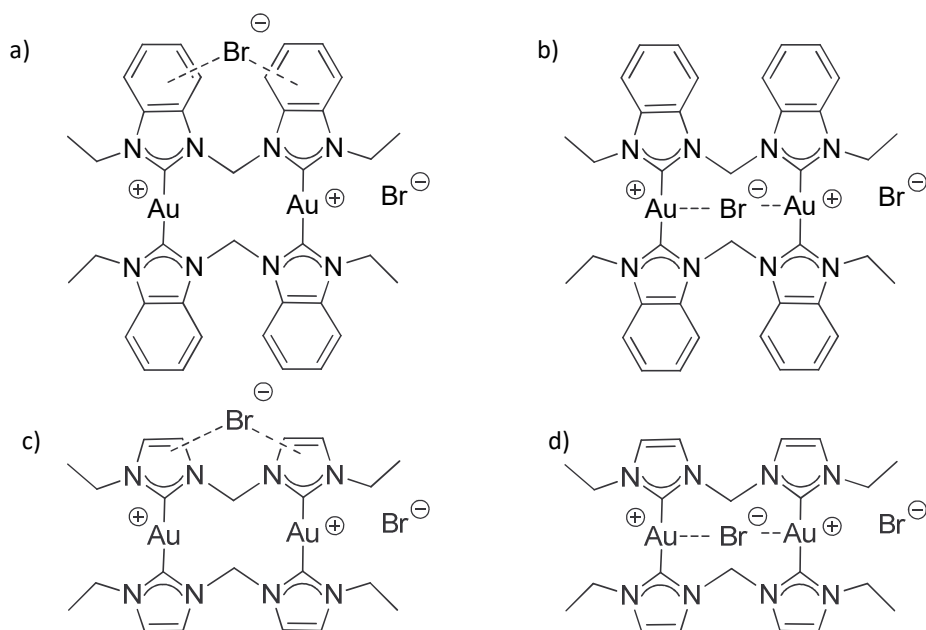


Figure 24: Potential binding motifs of the cation-anion aggregates, a) anion- π aggregation in benzimidazolium complexes, b) Au...Br and/or H...Br aggregation in benzimidazolium complexes, c) anion - π aggregation in imidazolium complexes, d) Au...Br and/or H...Br aggregation in imidazolium complexes.

Even though the aggregation behaviour and changes of the dynamic in solution are different for imidazolium and benzimidazolium complexes, both derivatives seem to interact with the counterions, resulting in visible changes in the respective spectra. The herein presented benzimidazolium complexes demonstrate a comparable ion pairing interaction, as seen in the work of *Penney et al.*^[72], but without the additional benzyl function. These additional aromatic systems seem to support the aggregation behaviour but can be ruled out as essential for the binding process. The smaller complexes used in our work do provide several binding sites which are, depending on the results, able to interact with the counterions.

The connection between a bromide - complex interaction and the downfield shift could be proven by adding tetrabutylammonium bromide (TBAB) to the solution of the PF_6^- complexes. Switching from the bromide complex **10a** ($\mathbf{10} = [\text{Au}_2(\text{bisEt}_2\text{MeBim})_2]^{2+}$) to the corresponding hexafluorophosphate complex **10b** shows the abovementioned strong downfield shift of the two signals from the endo/exo protons. Yet adding TBAB to the solution of **10b** causes the reverse downfield shift of the examined signals, proving the influence of the counterion. The shifting was therefore attributed to an aggregation of the anion into the cavity of the cation in solution.

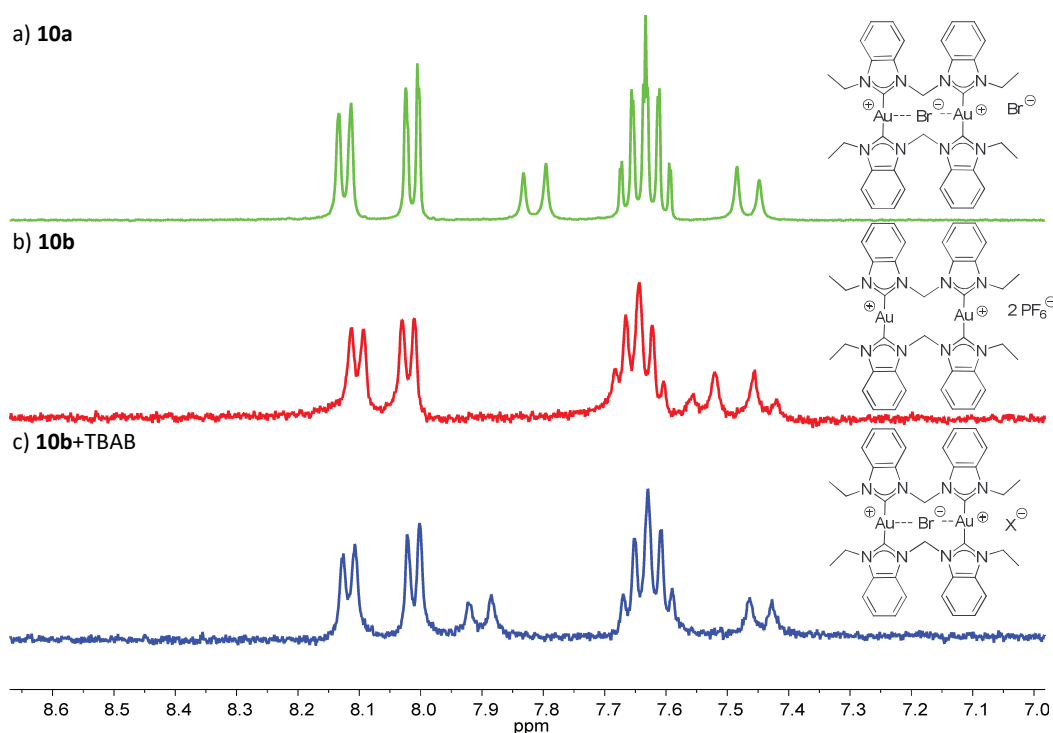


Figure 25: $^1\text{H-NMR}$ spectra of a) **10a**, b) **10b** and c) **10b+TBAB** in $\text{DMSO-}d_6$.

Measurements in other solvents than $\text{DMSO-}d_6$, though obtain stronger shifting of the signals of the bridging protons (see Figure 26, Figure 27, Figure 28 and Figure 29). These spectra are recorded from solutions in $\text{ACN-}d_3$. Only some of the complexes show a good solubility in this solvent and can therefore be used for experiments, in an adequate concentration. DMSO is not a good solvent for UV/Vis measurements, due to the limited measurement range. Acetonitrile however is a good solvent for the investigation in the interesting wavelength area. Thus the NMR experiments in both solvents are interesting and constructive.

Hexafluorophosphate and bromide are not the only possible counterions for gold(I) NHC complexes. Even though we are mainly working with these two derivatives, others are also possible and the investigation of their behaviour is just as interesting. Several examples of compounds with other anions are known to the literature.^[2c,4b,4d,4h,7b,7d,80] According to *Viji et al.* the addition of AgNO_3 in acetonitrile shows a similar impact on the proton resonance of a dinuclear silver(I) NHC complex.^[7c] These changes could be confirmed for the benzimidazolium complex **10b** after the addition of AgNO_3 in acetonitrile. The both doublets of the endo and exo protons undergo the shifting process. In accordance with our previously found results, the signals of the aromatic benzimidazole systems undergo only small but still visible shifting after the addition of TBAB (Figure 25) or AgNO_3 (Figure 26).

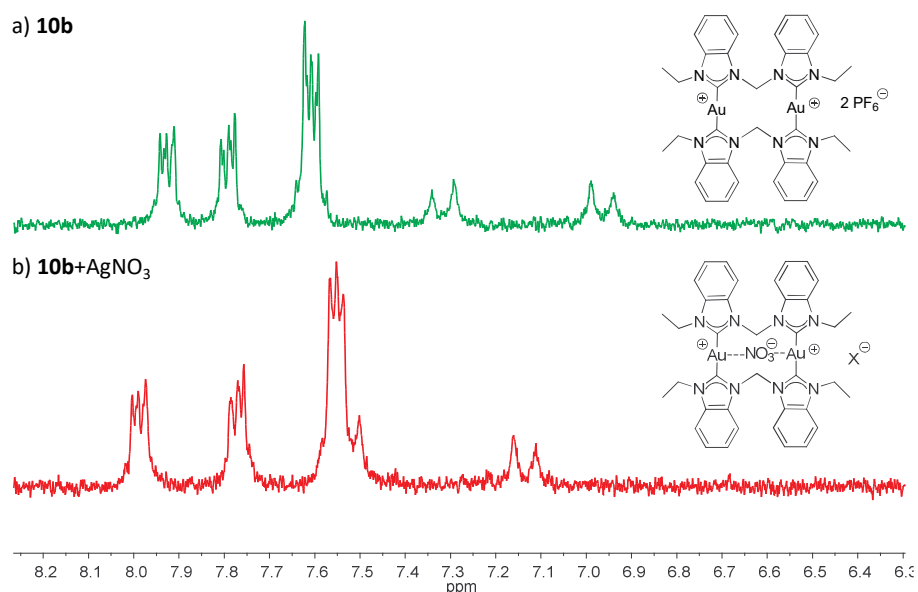


Figure 26: $^1\text{H-NMR}$ spectra of a) **10b** and b) **10b+AgNO₃** in $\text{ACN-}d_3$.

In contrast to these results, adding AgPF_6 to the solutions causes no changes in the NMR spectra. This silver salt, with the non coordinating counterion, was chosen to reduce cation anion interplay and to force an $\text{Au}\cdots\text{Ag}$ interaction, but resulted in none observable effects at all. The experiment indicates that the examined complex was not able to form aggregates with silver ions but rather with nitrate, after the addition of AgNO_3 to the solution of the complexes (Figure 26). Interestingly the resonances of the aromatic systems are also slightly shifting. This could be an indication for an aggregation of counterions to several binding sides of the complex, inside the cavity as well as between the benzimidazolium moieties.

Next to the counterions the solvents are also important for the dynamic and interaction in solution. The spectra in Figure 25 b) and Figure 26 a) are both recorded with a solution of complex **10b**, but one in $\text{DMSO-}d_6$ and the other in $\text{ACN-}d_3$. The shifted signals could be attributed to different solvation behaviour with containing moisture and interactions of the solvent itself with the complexes. *Penney et al.* were able to confirm phosphorescence arising from exciplexes formed between the excited state of the cation and methanol.^[72]

Using complexes with imidazolium moieties for these aggregation experiments shows stronger shifts of the aromatic resonances as already mentioned. The two signals of the ring

protons are strongly shifted after the addition of different silver salts. Figure 27 shows the $^1\text{H-NMR}$ spectra of the two imidazolium complexes **7a** and **7b** as well as the three spectra of the solutions of **7b** after the addition of an excess AgNO_3 , AgOTf and AgBF_4 respectively (**7** = $[\text{Au}_2(\text{bisEt}_2\text{Melm})_2]^{2+}$). The anion exchange from bromide to hexafluorophosphate results in a difference of the proton resonance of the methylene linker (small shift) and the imidazolium ring (strong shift). Adding a huge excess of the silver salts leads to a comparable downfield shift of the respective resonances depending on the counterion. The intensity of this effect is highly influenced by the counterion. The strongest impact was achieved by adding the nitrate compound. This improved anion cation aggregation is probably supported by additional hydrogen bonds. The oxygen atoms in NO_3^- are good acceptors for these bonding interactions. Keep in mind, that all experiments are showing differences in relation to the PF_6^- complexes in acetonitrile. Hexafluorophosphate has the weakest interaction of all anions with the complexes, under the given conditions. This was already investigated by adding AgPF_6 to the complex solutions, resulting in NMR spectra with no recognizable shifting of the resonances. The new results are highly recommending cation (dinuclear gold compound) anion interactions, independently of the cation in the added salt (here silver).

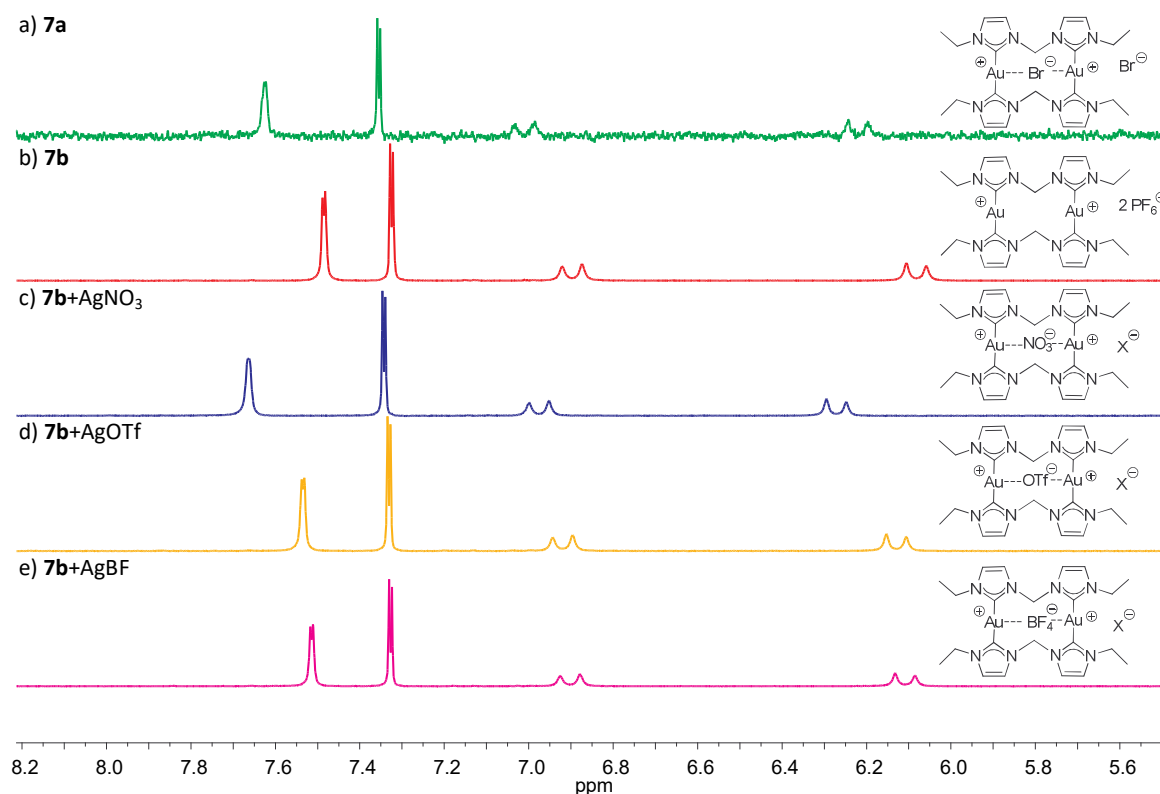


Figure 27: $^1\text{H-NMR}$ spectra of a) **7a**, b) **7b**, c) **7b+AgNO₃**, d) **7b+AgOTf**, e) **7b+AgBF₄** in $\text{ACN-}d_3$.

Due to the fact that this impact is similar to the changes caused by bromide, more detailed investigations of the anions of the corresponding silver salts were performed. The two compounds with the strongest (NO_3^-) and the weakest (BF_4^-) impact (in comparison with the PF_6^- complexes) were chosen for further experiments. An excess of the corresponding tetrabutylammonium (TBA^+) salts was added to a solution of **7b** in acetonitrile and the resulting spectra compared to the former results. The achieved spectra show a comparable effect. An excess of the NO_3^- salts (Ag^+ or TBA^+) causes a strong downfield shift of the signals, while adding BF_4^- (Ag^+ or TBA^+) causes only a small but still recognizable difference. Therefore we concluded that the shifting of the proton resonances is based on the aggregation of the anions to the cation. This result is supported by the absence of these processes after adding AgPF_6 and the obvious shifting in the spectra of the complexes with different counterions. The anions PF_6^- and BF_4^- are known as non-coordinating. The aggregation with the NHC compounds could be forced by several possible weak $\text{H}\cdots\text{F}$ hydrogen bonds. The bigger hexafluorophosphate is probably more steric hindered and therefore the interactions with the smaller tetrafluoroborate seem stronger, based on the shifting process of the aromatic resonances. The aggregation of NO_3^- however results in the strongest changes in the ^1H -NMR spectrum. This behaviour could be explained by stronger hydrogen bonding with the oxygen atoms ($\text{O}\cdots\text{H}$). While the cation does not significantly influence the aggregation with BF_4^- the interactions of the NO_3^- salts are different. They likely derive from additional interactions of the anion with TBA^+ . Nevertheless both nitrate containing mixtures show the strongest shift of the proton resonances, in comparison with the other tested anions. Based on the given results, an attractive interaction of the added cations (Ag^+ and TBA^+) with the dicationic gold compounds was again excluded. Even though $\text{Au}\cdots\text{Ag}$ interactions are possible, metallophilic attractions are not strong enough to overcompensate the coulomb repulsion. An interplay of the compounds, would obtain three positive metal centres next to each other, which is often unstable and therefore unusual.

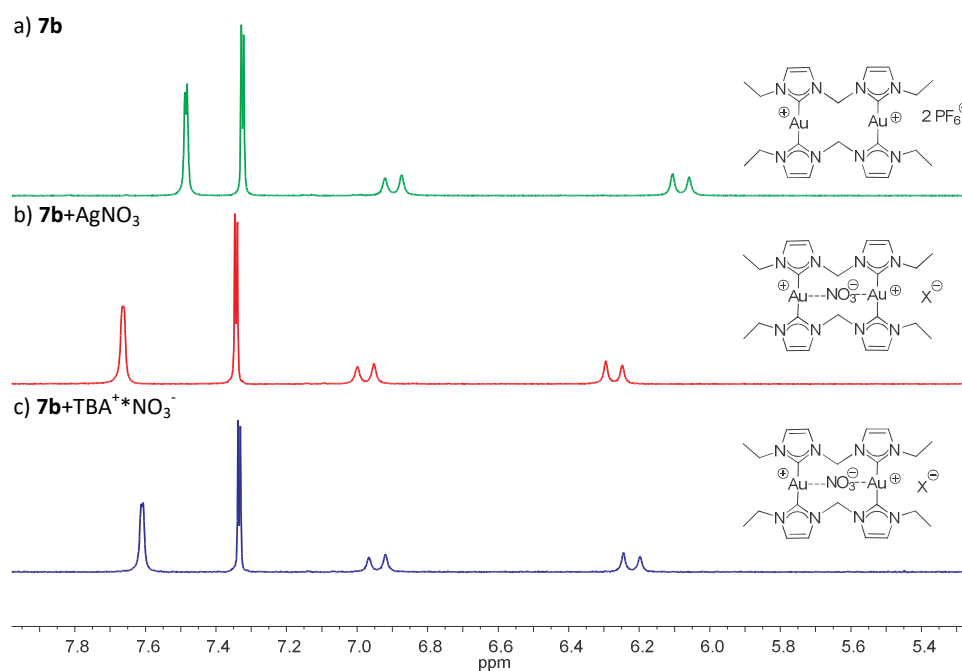


Figure 28: ¹H-NMR spectra of a) **7b**, b) **7b+AgNO₃**, c) **7b+TBA⁺*NO₃⁻** in ACN-*d*3.

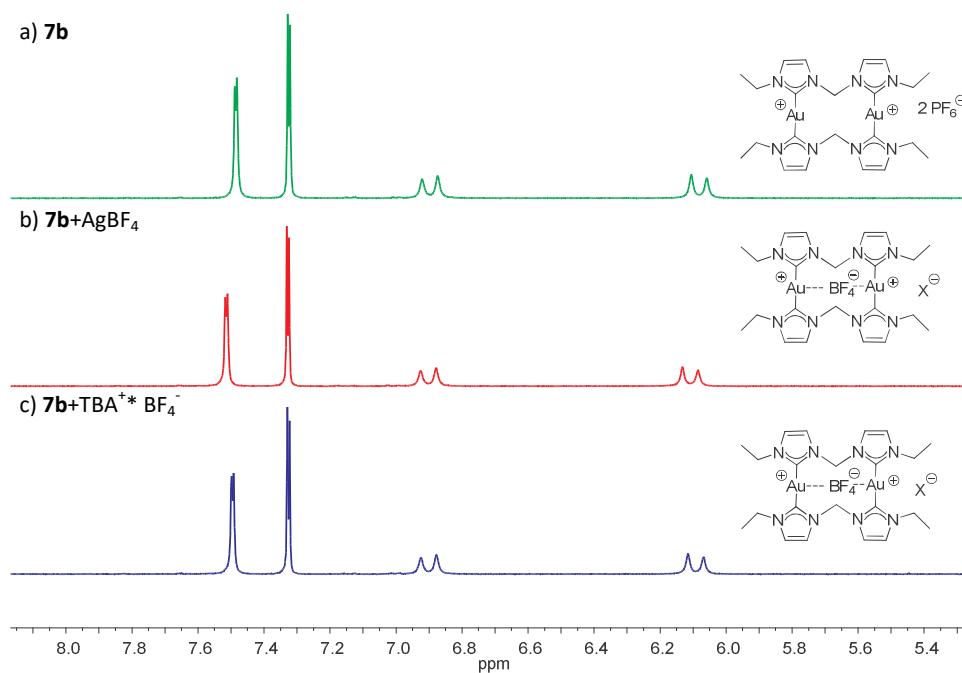


Figure 29: ¹H-NMR spectra of a) **7b**, b) **7b+AgBF₄**, c) **7b+TBA⁺*BF₄⁻** in ACN-*d*3.

3.4 X-ray crystal structures

Single crystals suitable for x-ray diffraction were obtained by slow diffusion of diethyl ether in a solution of methanol for the bromide complexes (**1a** – **12a**) or acetonitrile for the

hexafluorophosphate complexes (**1b** – **12b**). Thus we compared those 24 crystal structures including 15 not yet known to the literature. Supplemental aggregation experiments with different silver and ammonium salts were performed in solution. During these investigations four additional single crystals with other counterions could be obtained (**3c** = $[\text{Au}_2(\text{bisMe}_2\text{PrIm})_2]^{2+} \cdot 2\text{NO}_3^-$, **7c** = $[\text{Au}_2(\text{bisEt}_2\text{MeIm})_2]^{2+} \cdot 2\text{BF}_4^-$, **10c** = $[\text{Au}_2(\text{bisEt}_2\text{MeBim})_2]^{2+} \cdot 2\text{PO}_2\text{F}_2^-$, **11c** = $[\text{Au}_2(\text{bisEt}_2\text{EtBim})_2]^{2+} \cdot 2\text{PO}_2\text{F}_2^-$). All relevant structural parameters are summarized in Table 4. The structures are typically consisting of layers of dinuclear gold(I) NHC cations with two surrounding anions. The two coordinated gold centres with mostly coplanar NHC moieties show almost linear C-Au-C axes with an expected length of approximately 2.0 Å for the Au-C bonds. ^[4a,4e,4f,4i,46c,62f,63b,71-72,81]

Table 4: Selected data of the crystal structures for the complexes 1a,b – 12a,b and 3c, 7c, 10c, 11c.

	n	<i>i</i> moieties	Au-C/ Å	C-Au-C/ °	Au...Au/ Å Intra- molecular	Au...Au/ Å Inter- molecular	π-π/ Å inter- molecular	ⁱ H-X/ Å linker	ⁱ H-X/ Å side- chain	ⁱ H-X/ Å ring
1a^g	1	Im methyl	2.021(8) 2.022(8) 2.023(9) 2.024(8)	169.3(3) 172.3(3)	3.4671(4)	4.4997(5)	3.2132(4) 3.5205(4) 3.5313(4)	2.715 2.730	2.713 2.757 2.970 2.986	2.682 2.722 2.865 2.895 2.915
1b^g	1	Im methyl	2.013(4) 2.019(4)	177.9(2) 170.5(2)	3.8842(1)	3.7236(1)	3.59184(9) 3.76566(10) 3.95247(11)	2.400 2.458 2.608	2.396 2.527 2.588	2.255 2.404 2.478 2.557 2.591
2a^d	2	Im methyl	2.051(11) 2.009(11) 2.028(11) 2.027(11)	177.1(5) 174.0(4)	4.6320(3)	6.8465(3)	3.2815(2) 3.4522(2) 3.7038(2)	2.646 2.926 2.985	2.799 2.849 2.912 3.033	2.698 2.707 2.739 2.896 2.900 2.970
2b^d	2	Im methyl	2.035(5)	177.11(19)	5.5492(3)	4.6992(2)	3.4034(2) 3.5177(2)	2.494 2.654	2.384 2.631	2.493 2.547 2.563
3a^{e,h}	3	Im methyl	2.007(15) 2.045(12)	177.2(5)	3.1153(2)	3.9286(3)	3.1556(2) 3.3809(2) ^b	3.030	3.044	2.895
3b^e	3	Im methyl	2.024(6) 2.009(6)	177.6(2)	3.2283(4)	3.7036(1)	3.29060(6) ^b 3.55873(7)	2.456 2.470 2.473 2.618 2.650	2.428 2.578	2.357 2.520
3c^f	3	Im methyl	2.023(8) 2.031(9)	178.7(4)	2.9990(6)	3.7469(3)	3.4272(3)	2.348 2.503 2.558 2.562 2.584	2.331 2.337 2.376 2.529 2.601	2.490 2.505 2.637

4a^{f,g,h}	1	Bim methyl	1.993(15) 2.016(14) 2.024(15) 2.024(15)	174.8(6) 175.3(6)	3.0469(10)	9.010	3.3964(7) 3.5091(7) 3.4023(8) 3.4672(5)	2.779 2.895	2.837 3.019	2.757 2.854 2.958 2.961 2.995
4b^{f,g}	1	Bim methyl	2.027(10) 2.032(10)	169.6(4)	3.0744(8)	8.664	3.66132(19) 3.46569(17)	2.315	2.395 2.521 2.530 2.589 2.598	2.433 2.507 2.544 2.619
5a^{e,h}	2	Bim methyl	2.027(13) 2.045(13) 2.046(13) 2.070(14)	178.4(6) 178.6(7)	3.43670(19)	9.416	3.46978(19) 3.39365(16) 3.46485(19) 3.44875(18)	2.673 2.747	-	2.951 2.953 2.988 2.992 3.034
5b^e	2	Bim methyl	2.020(15) 2.030(15) 2.019(19) 2.064(17)	177.8(6) 176.6(7)	3.2359(10)	8.680	3.3398(4) 3.2739(3) 3.4139(4) 3.3043(4)	2.340 2.395 2.562 2.584 2.660	2.454 2.538 2.554 2.617 2.618 2.629	2.441 2.514 2.526 2.535 2.569 2.581 2.635 2.644 2.645 2.659 2.664
6a^{f,h}	3	Bim methyl	1.993(17) 2.029(15)	175.0(6)	4.7375(6)	7.4740(1)	3.4097(3) 3.4625(4)	2.845 2.933	2.788 2.829	2.904 2.976 3.027
6b^d	3	Bim methyl	2.009(10) 2.008(9)	175.6(4)	6.3844(5)	6.903	3.3427(3)	-	2.591 2.494	2.401 2.391 2.630 2.670
7a^{g,h}	1	Im ethyl	2.015(12) 2.018(13) 2.026(12) 2.031(12)	170.0(5) 174.5(5)	3.6627(13)	3.57866(16)	3.4598(16) 3.48532(15)	2.750 2.855 2.905	2.869 2.956	2.677 2.786 2.814 2.846 3.024

7b^g	1	Im	2.017(5)	172.6(3)	3.6475(5)	5.2346(8)	3.4790(5)	2.311	2.515	2.287
		ethyl	2.022(5)	174.3(2)			4.6784(6)	2.422	2.539	2.353
								2.588	2.518	
								2.589	2.612	
								2.611	2.646	
7c^{g,h}	1	Im	2.025(4)	172.39(15)	3.69346(10)	3.580	3.30811(7)	2.265 ^c	2.447 ^c	2.232 ^c
		ethyl	2.015(4)	173.45(15)			3.39609(10)	2.541 ^c	2.475 ^c	2.272 ^c
			2.029(4)					2.647 ^c	2.536 ^c	2.290 ^c
			2.026(4)					2.714 ^c	2.669 ^c	2.324 ^c
									2.680 ^c	2.368 ^c
								2.720 ^c	2.379 ^c	
									2.470 ^c	
									2.546 ^c	
									2.619 ^c	
8a^{e,h}	2	Im	2.018(5)	173.8(2)	3.3988(1)	7.2397(3)	3.28064(12)	-	2.675	2.836
		ethyl	2.021(5)	177.4(2)						2.884
			2.023(5)							2.921
			2.025(5)							2.978
8b^e	2	Im	2.025(3)	175.29(11)	3.2328(2)	6.2975(2)	3.22013(14)	2.332	2.437	2.372
		ethyl	2.027(3)	176.22(11)			3.28141(15)	2.511	2.499	2.469
			2.032(3)					2.590	2.582	2.492
			2.032(3)					2.644	2.598	2.514
								2.659	2.657	2.552
								2.670		2.566
								2.625		
								2.531		
								2.592		
9a^d	3	Im	2.012(5)	178.6(2)	6.7918(3)	7.1092(4)	3.4334(2)	-	3.036	3.016
		ethyl								3.041
9b^{d,h}	3	Im	2.0069(3)	175.6(4)	6.4190(9)	3.2916(4)	3.4283(5)	2.440	2.386	2.325
		ethyl	2.0151(3)	176.6(4)			3.5103(4)	2.480	2.458	2.344
			2.0261(3)					2.536	2.547	2.410
			2.0333(3)					2.593	2.566	2.435
								2.619	2.574	2.593
								2.640	2.584	2.604
								2.654	2.600	2.611
									2.601	
									2.625	
							2.644			

10a^{f, g, h}	1	Bim ethyl	2.032(5) 2.017(5) 2.017(5) 2.022(5)	174.45(18) 175.86(19)	3.1700(3)	7.8570(2)	3.19075(8) 3.28623(7) 3.38093(7) 3.50901(9)	2.591 2.759 2.808 2.966	3.022 3.027	2.815 2.865 2.928 2.949 2.979 3.006
10b^{f, g}	1	Bim ethyl	2.031(6) 2.027(5)	172.2(2)	3.1635(5)	6.108	3.44976(5)	2.553 2.664 2.649	2.552 2.569 2.669	2.510 2.523 2.525
10c^{f, g}	1	Bim ethyl	1.981(17) 2.065(17)	172.8(6)	3.2241(11)	6.119	3.43696(10)	2.246	2.592 ^c 2.660 ^c 2.423 ^c	2.515 2.466 2.667
11a^{e, h}	2	Bim ethyl	2.023(9) 2.011(9)	175.6(4)	3.5194(2)	8.1412(4)	3.31395(13) 3.4894(2)	2.948	2.300 2.630 2.758 2.786 2.827 2.926 2.992 3.033	2.498 2.501 2.937 2.973 3.006 3.009
11b^{e, h}	2	Bim ethyl	2.032(4) 2.030(4) 2.013(4) 2.019(4)	179.71(18) 178.26(18)	3.3937(2)	8.497	3.33847(17) 3.37197(18) 3.40200(17) 3.5317(2)	2.526 2.542 2.587	2.374 2.426 2.534 2.647	2.340 2.386 2.431 2.447 2.466 2.797 2.508 2.529 2.593 2.657
11c^e	2	Bim ethyl	1.997(15) 2.000(15) 2.008(18) 2.010(15) 2.011(13) 2.011(13) 2.011(14) 2.021(15) 2.040(13)	174.3(6) 174.8(6) 175.5(6) 175.7(6)	3.54335(14) 3.54575(15) 3.63054(15)	8.006	3.29492(9) 3.30034(9) 3.38703(12) 3.49989(13)	2.649 2.480 ^c 2.575 ^c 2.630 ^c	2.331 2.543 2.133 ^c 2.616 ^c 2.688 ^c 2.689 ^c 2.708 ^c	2.430 2.522 2.544 2.548 2.581 2.616 2.621 2.405 ^c 2.468 ^c 2.562 ^c 2.678 ^c 2.718 ^c

12a^d	3	Bim ethyl	2.021(4) 2.018(4)	175.32(13)	6.6437(2)	7.1395(2)	3.29403(10) 3.47269(11)	2.800 2.924 2.953	2.953 3.042	2.980 3.043
12b^d	3	Bim ethyl	2.10(5)	172(3)	6.669(5)	7.259	2.7651(15) 4.102(2)	2.362	-	2.483 2.600

^aThe value NHC plane centre to centre is given; ^b intramolecular π - π distances; ^c O-H bond distances; Geometrie of the cations: ^d stretched, ^e folded, ^f twisted, ^g U shaped, ^h additional solvent molecules in the structure; ⁱ aromatic moiety: im = imidazole, Bim = benzimidazole; ^j X represents F or Br.

In accordance with the NMR experiments, silver salts of NO_3^- , BF_4^- , OTf^- and PF_6^- were added to the solutions. All realized attempts to crystallize a silver containing system just resulted in the exchange of the counterion and the formation of bright yellow silver nanoparticles. These results are not depending on the counterion of the complexes, which were used for the crystallization experiments. Adding an excess of AgNO_3 to a solution of the PF_6^- complexes simply produces the nitrate complexes. The corresponding crystal suitable for x-ray crystallography was exclusively obtained from the imidazolium complex **7c** (Figure 1; **7** = $[\text{Au}_2(\text{bisEt}_2\text{MeIm})_2]^{2+}$). Even though the NMR experiments have shown the strongest interactions between the cations and nitrate, this counterion does not support the growth of monocrystals. Changing the solvent or the crystallization technique could overcome this problem, but was not further tested in the given work. The crystal structures of the other ethyl compounds **7a,b** – **9a,b** have already been discussed in detail.^[4f] The previous work is limited to the comparison of the complexes of this series and will now be expanded with the new complexes.



Scheme 6: Anion exchange of the complex **7b** with AgNO_3 .

The new structure of **7c** is comparable to the structure of the equivalent bromide salt **7a**.^[4f] The preferred and more stable conformation of the cation is U shaped.^[71] All imidazole complexes with methylene linker (**1a,b** and **7a,b,c**) have these folded structures in common.

They consist of a network build of π stacked layers of cations with surrounding anions (and solvent molecules) which are connected via hydrogen bonding. Therefore the cations take up different orientations in the crystal which allows face to face interactions of the aromatic systems. Sometimes the two imidazolium moieties linked by a gold atom are lying above a pair of two imidazolium moieties which are also linked by a gold centre, allowing intermolecular $\text{Au}\cdots\text{Au}$ distances slightly above the range for aurophilic interactions. This structure motif is not continuous in the whole crystal. Several aromatic systems linked by the same Au atom are interacting with the π systems of different cations. This arrangement connects the cation arrays.

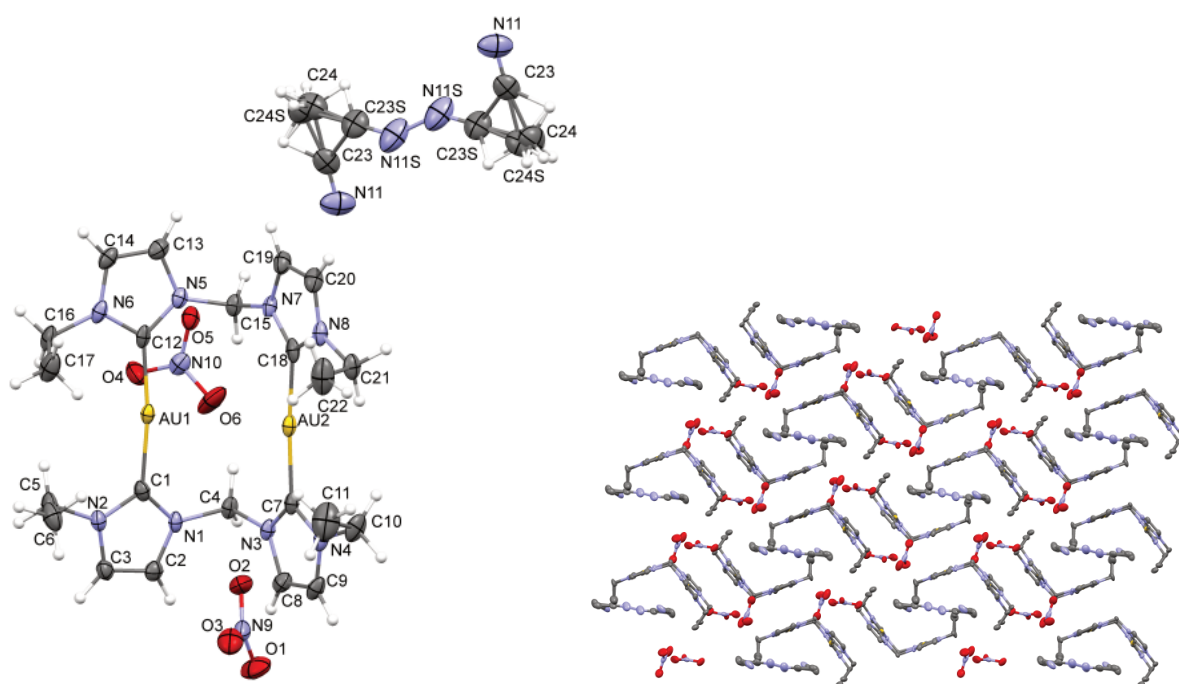


Figure 30: ORTEP drawing and crystal packing of complex 7c (50% probability level for the thermal ellipsoids). Hydrogen atoms have been omitted for clarity.

The influence of the counterions on the structure seems small and the conformation of the linker terminates the arrangement. All C-Au-C axes are slightly bent and the gold atoms are pointing inwards to each other, resulting in intramolecular $\text{Au}\cdots\text{Au}$ distances just a little longer than the range of aurophilic interactions. They are strongly determined by the N-C-N angles of the tetrahedral methylene bridges with the two connected nitrogen atoms. All ethyl wingtip groups are pointing to the cavity of the U shaped cations as seen in the bromide complex **7a**. In contrast, two of the side chains of the PF_6^- complex **7b** are pointing

to the outside of the cavity. This in out conformation indicates the influence of the counterion to the conformation of the side chains, based on different interactions with the cocrystallized solvents and the anions. The NO_3^- counterions are interacting with the imidazolium cations and the acetonitrile molecules via several hydrogen bonds. One counterion is arranged near a gold centre with a $\text{Au}\cdots\text{O}$ distance of 3,363 Å. According to the work of *Bondl*^[82] these distances are larger than the sum of the van der Waals radii of the atoms (3.18 Å). But there are newer findings of *Batsanov*^[83] which provide larger radii for gold and result in a $\text{Au}\cdots\text{O}$ distance of 3.65 Å. Weak interactions between the counterion and the gold atom could not be excluded. Keep in mind, that packing effects and other different bonding types (like hydrogen bonds) could promote the position of the counterion and be the driving force for the given geometry.

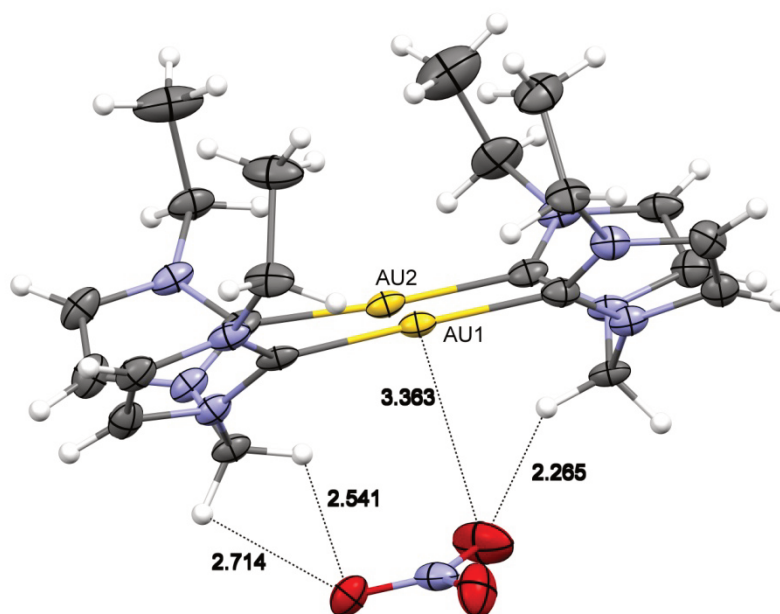


Figure 31: OR ORTEP drawings of complexes 7c showing short $\text{Au}\cdots\text{O}$ and $\text{H}\cdots\text{O}$ distances in the crystal (50% probability level for the thermal ellipsoids).

The bromide complex **1a** is the only imidazole methylene complex with an $\text{Au}\cdots\text{Au}$ distance shorter than 3.5 Å (**1** = $[\text{Au}_2(\text{bisMe}_2\text{Melm})_2]^{2+}$). Bigger counterions lead to longer distances between two cations, in account of steric effects. Additional $\text{H}\cdots\text{F}/\text{H}\cdots\text{O}$ bonding between the cations and the counterions support a more linear conformation. Interactions between the hydrogen atoms of the complexes and halides are common for this type of compounds.^[57b,58a,62r,74,84] This type of counterions are unusual, but actually good hydrogen bond acceptors^[85] and therefore able to interact with the cations. The NHC compounds for

their part do bear several CH, CH₂ and CH₃ groups which can all act as donors and provide hydrogen bonds with bromide (C-H...Br) and the rather non-coordinating hexafluorophosphate (C-H...F-P).

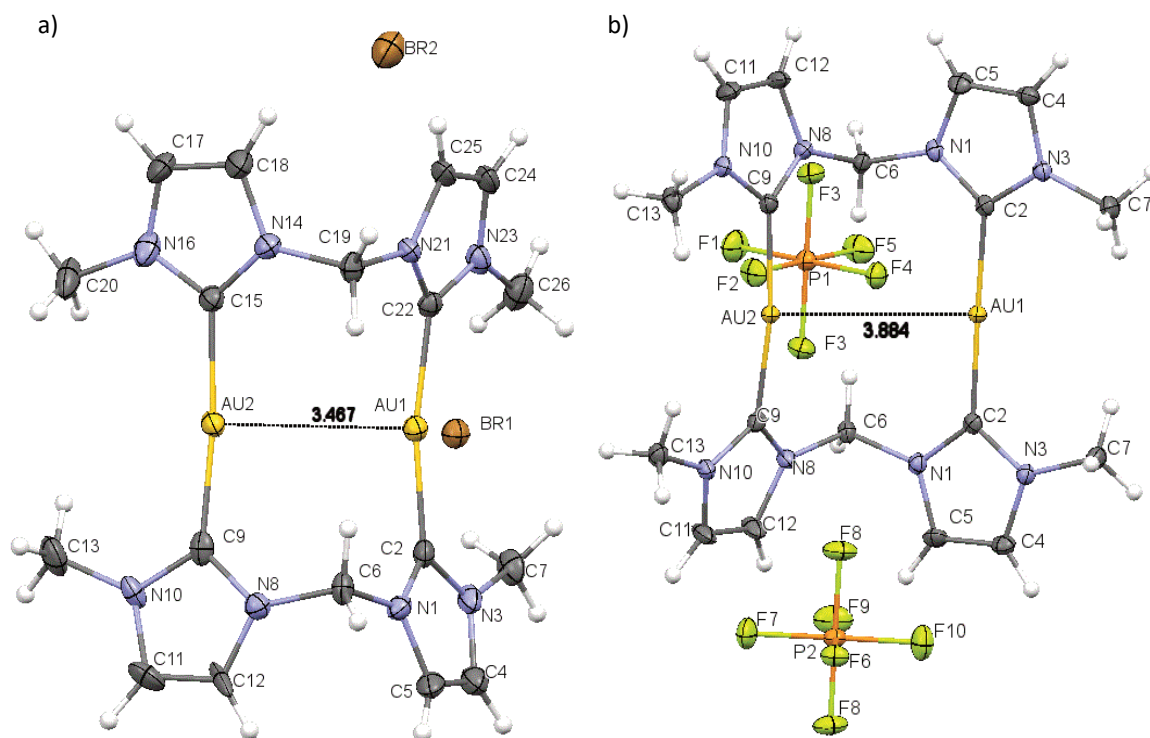


Figure 32: ORTEP drawings of complexes a) **1a** and b) **1b** (50% probability level for the thermal ellipsoids).

The crystal structures of the complexes **1a** and **1b** (see Figure 32) are quite similar to **7a** - **7c** (**7** = [Au₂(bisEt₂MeIm)₂]²⁺). The longer ethyl side chain enables the cocrystallization of solvent molecules in **7a** and **7c**. Using the bulky PF₆⁻ ion prevents this phenomenon in the structure of **7b**.^[4f] There are two different positions of the anions in the structure of **1a**. The bromide (Br₂) in the structure of **1a** is mainly interacting with the aromatic hydrogen atoms of one cation and the methyl substituents of another cation.

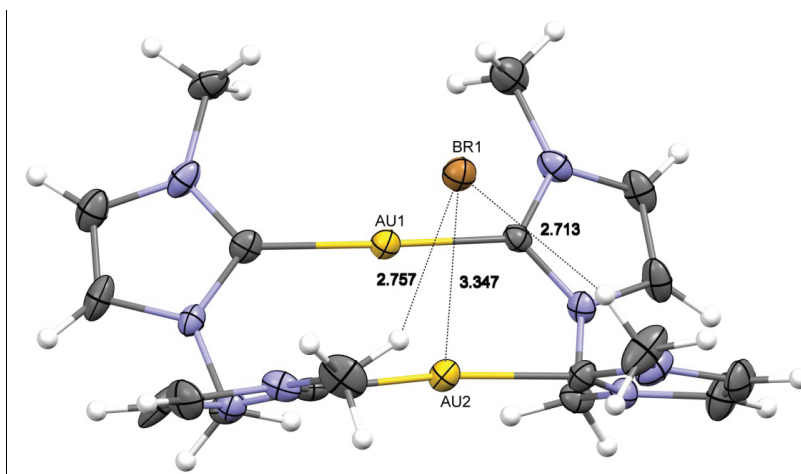


Figure 33: ORTEP drawings of complexes 1a showing short Au...Br and H...Br distances in the crystal (50% probability level for the thermal ellipsoids).

The other counterion (Br1) however lies between two methyl groups next to a metal centre of one complex and two methylene bridges of another cation. This configuration provides short Au...Br distances of 3.347 Å, next to the H...Br bonds. Based on the results of *Bondi*^[82] the van der Waals radii of Au...Br are 3.51 Å. Therefore the interactions could probably be classified as attractive. They could also be forced by packing effects or in contrast be another driving force for the give crystal structure.

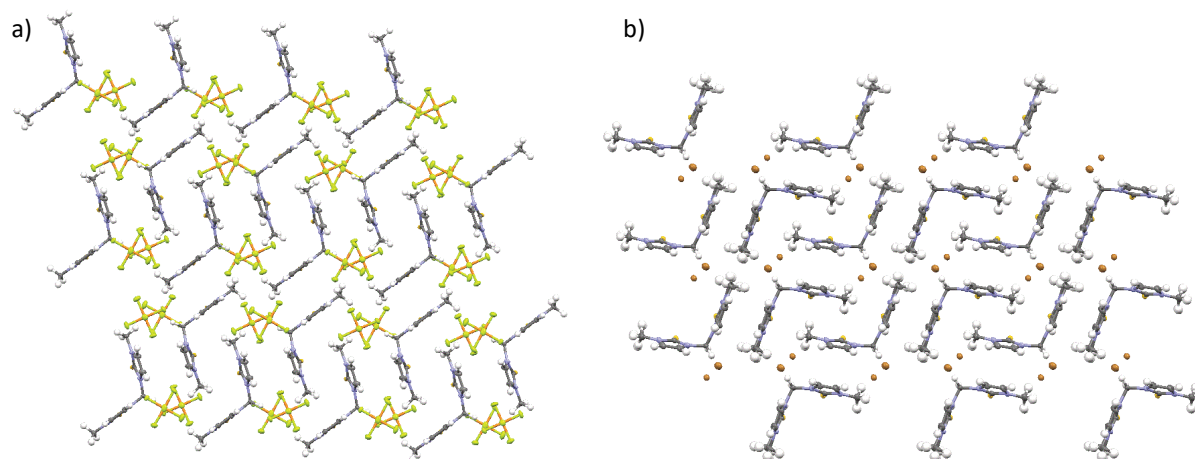


Figure 34: ORTEP drawing of complex a) 1a and b) 1b (50% probability level for the thermal ellipsoids). Hydrogen atoms have been omitted for clarity.

The PF₆⁻ counterion also provides two different positions of the anions in the structure. One (with P1) is centrally arranged above the cavity and is stabilized by H...F bonds to the methylene bridges and the other one (with P2) lies next to the aromatic moieties of the

cation. Both counterions also build hydrogen bonds to the methyl wing tip substituents of the neighbouring cations. According to *Bondi*, the van der Waals radii of Au...F are 3.13 Å.^[82] In contrast to that *Batsanov* reports van der Waals radii of gold, which can reach 2.1 Å.^[83] With this data the Au...F distances could reach 3.6 Å (and 4.0 Å for Au...Br). Following these results, shows one short Au...F distance of 3.478 Å and one long distance of 3.626 Å which is slightly above those values. The interaction of the metal centres with the counterion is not as clear as in compound **1a** and therefore at the utmost described as weak.

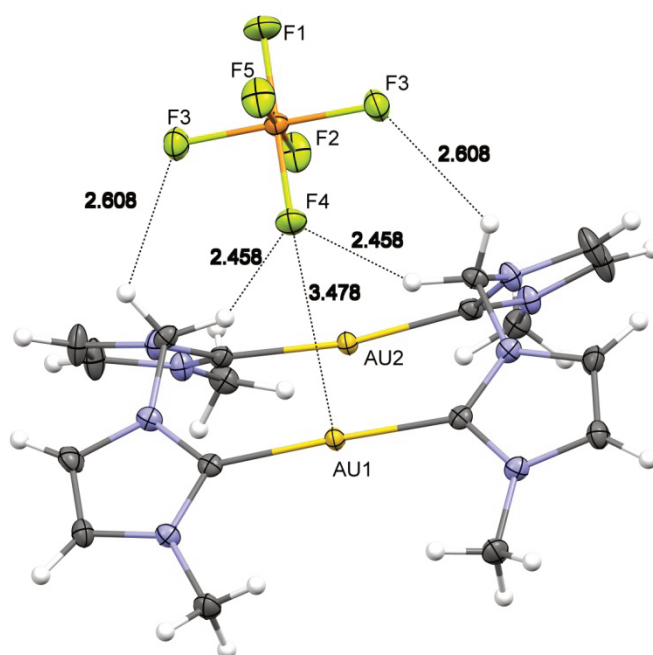


Figure 35: ORTEP drawings of complexes **1b** showing short Au...F and H...F distances in the crystal (50% probability level for the thermal ellipsoids).

Changing the counterion to iodide has similar effects on the structure, shown by *Barnard et al.*^[46b] The cations are also U shaped and stabilized by π stacking, but the Au...Au distances are longer in comparison with complex **1a**. The described 3.5425(6) Å are slightly above the range for aurophilic interactions.

The structure of **7b** ($\mathbf{7} = [\text{Au}_2(\text{bisEt}_2\text{Melm})_2]^{2+}$) should not be discussed in detail in this work, but is still providing some interesting interactions. As seen before for the compound **1b**, the hexafluorophosphate ion is centrally arranged above the cavity. This geometry allows short $\text{Au}\cdots\text{F}$ distances of 3.405 Å. This is shorter than the sum of the van der Waals radii and therefore considered carefully as a weak attractive interaction.

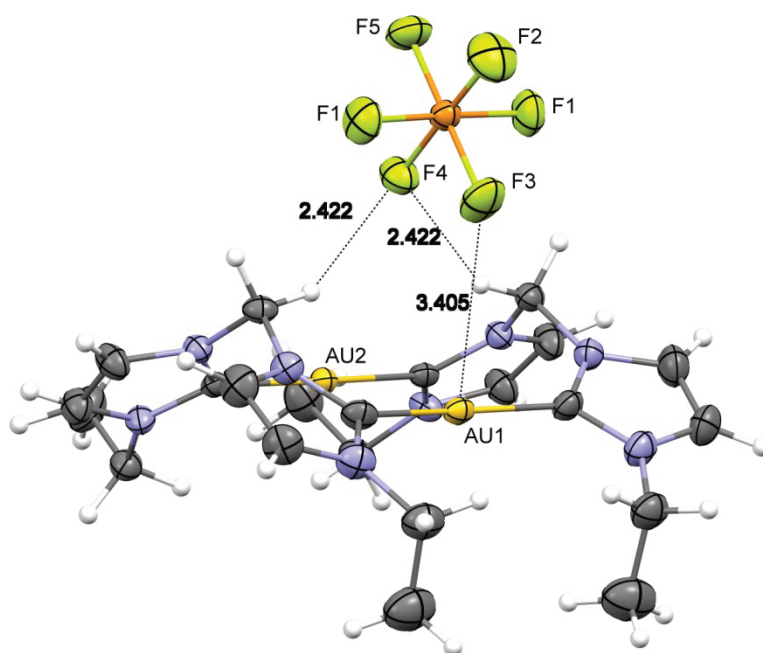


Figure 36: ORTEP drawings of complexes **7b** showing short $\text{Au}\cdots\text{F}$ and $\text{H}\cdots\text{F}$ distances in the crystal (50% probability level for the thermal ellipsoids).

Contrary to the first examples the structures of imidazole complexes with ethylene bridges are highly depending on the counterion and the wingtip groups. While both complexes with ethyl side chains (**8a,b**) build folded pocked shaped cations with short metallophilic distances, the corresponding methyl derivatives (**2a,b**) are stretched out without $\text{Au}\cdots\text{Au}$ interactions ($\mathbf{8} = [\text{Au}_2(\text{bisEt}_2\text{EtIm})_2]^{2+}$; $\mathbf{2} = [\text{Au}_2(\text{bisMe}_2\text{EtIm})_2]^{2+}$).

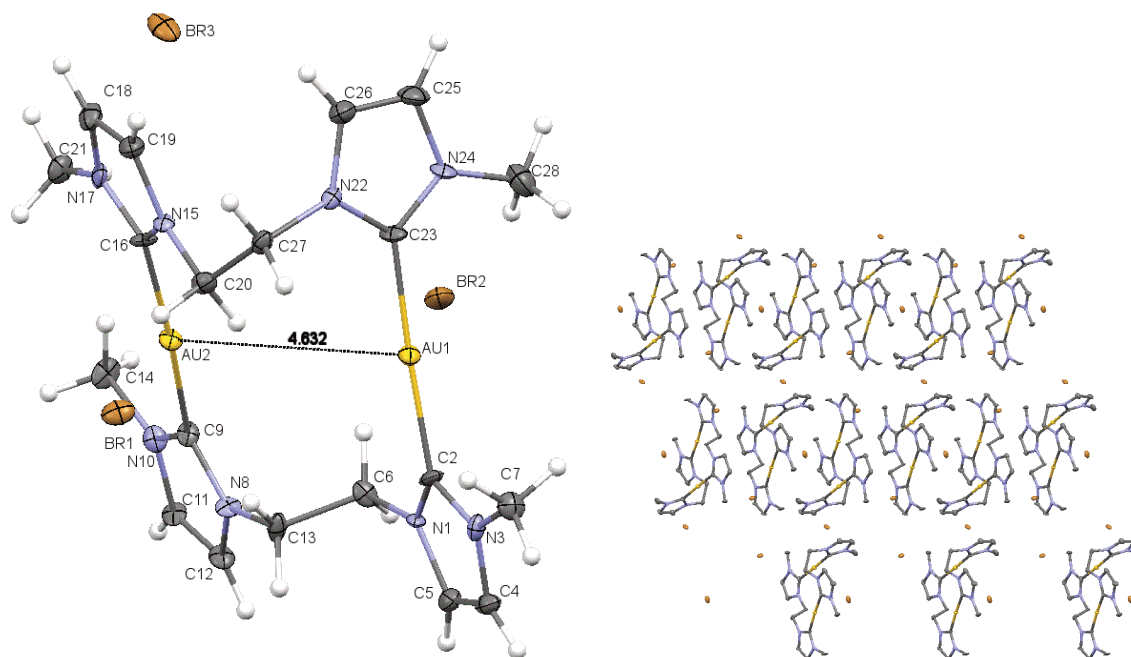


Figure 37: ORTEP drawing and crystal packing of complex 2a (50% probability level for the thermal ellipsoids). Hydrogen atoms have been omitted for clarity.

Two cations of the bromide salt **2a** show a capsule like conformation, surrounding one anion and leading to short H...Br distances. Therefore one linker has a trans and one a gauche conformation. This creates long Au...Br distances of 3.735 and 4.496 Å, which cannot mainly be explained by aurophilic interactions but packing effects in combination with hydrogen bonding and π stacking. The smaller Au...Br distance does fit to the van der Waals radii found by *Batsanov*^[83] but they are at best a weak support for the hydrogen bonds. The bromide (Br2) is the one inside the cavity of two cations. This counterion has mainly short distances to the ethylene bridges and methyl side chains, but also to the aromatic protons of a cation next to the aggregates. The both other counterions (Br1 and Br3) are arranged in the space around the cationic dimers. They show short H...Br distances to all possible protons (methyl-H, ethylene-H and imidazolium-H).

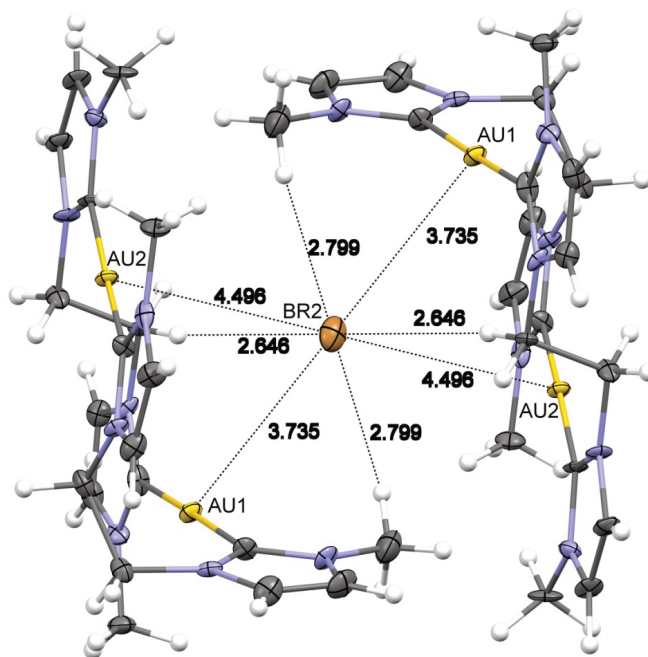


Figure 38: O ORTEP drawings of complexes **2a** showing short Au...Br and H...Br distances in the crystal (50% probability level for the thermal ellipsoids).

The corresponding PF_6^- derivative **2b** has an all trans conformation (see Figure 39). The S-shaped cations are stretched with a long intramolecular Au...Au distance of 5.5492 Å. The cations are highly symmetrical and form layers, stabilized by π stacking. The PF_6^- ions are lying on top of the zigzag cations. The conformation is stabilized by multiple short H...F bonds. They arrive from the ethylene bridges of the cations above and beneath the counterions but also from the imidazolium moieties and the methyl substituents of the surrounding complexes. This crystal structure was previously published by *Baron et al.* in 2016.^[86]

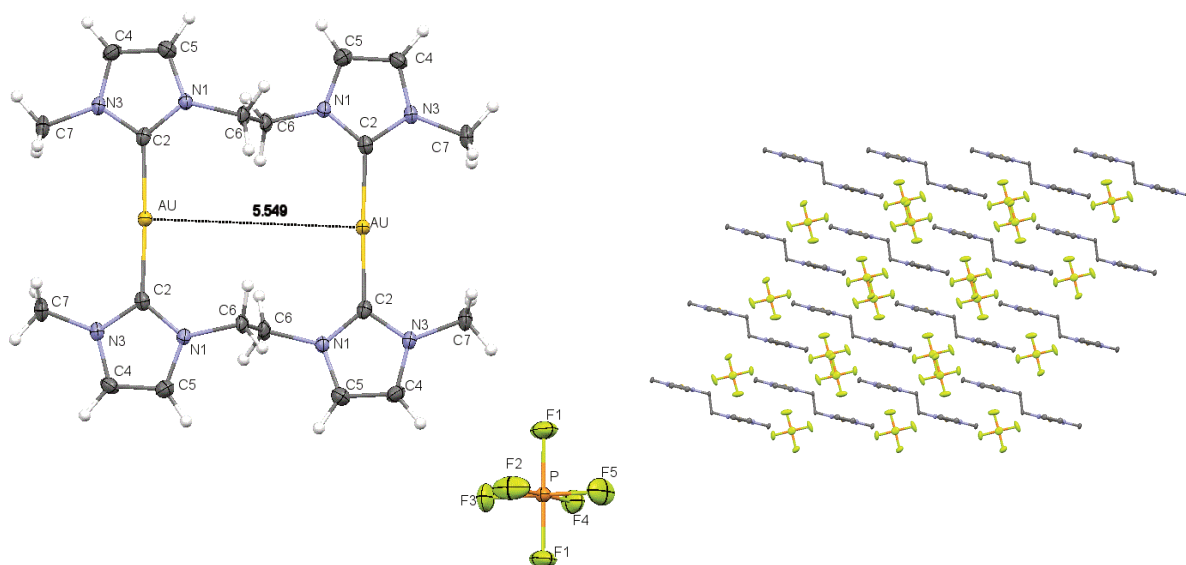


Figure 39: ORTEP drawing and crystal packing of complex 2b (50% probability level for the thermal ellipsoids). Hydrogen atoms have been omitted for clarity.

The geometry of the counterions allow one shorter Au...F distance of 3.162 Å, which could be considered as weak attractive interaction. Again the H...F interactions are more clearly pronounced.

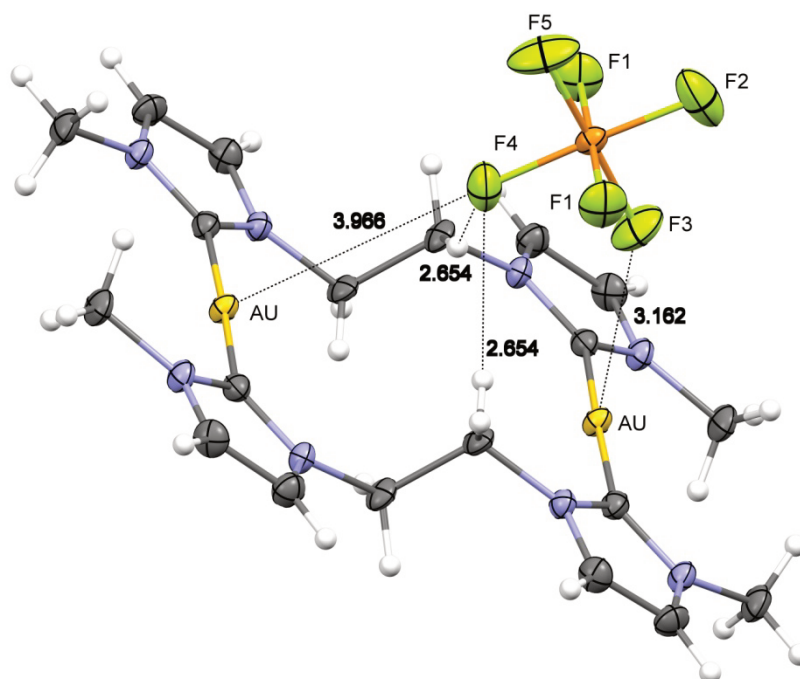


Figure 40: ORTEP drawings of complexes 2b showing short Au...F and H...F distances in the crystal (50% probability level for the thermal ellipsoids).

Even though the structures of **8a** and **8b** were described in detail before^[4f,6], some of the shorter interactions are still worth mentioning. As seen in Figure 41 the bromide has a distance of 3.733 Å to Au2, which is shorter than the sum of their van der Waals radii according to *Batsanov*.^[83] There are no H...Br interactions marked in the figure, because the counterion does only form hydrogen bonds to other cations. This means, that the Au...Br interaction is the only connection of this counterion and the cation.

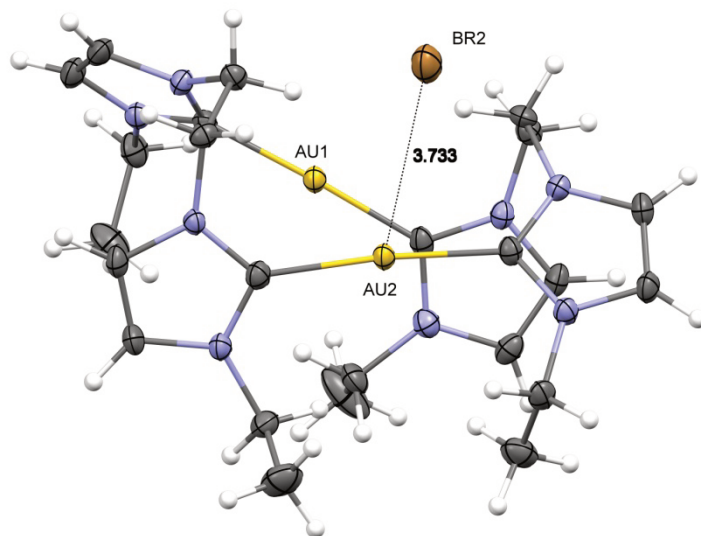


Figure 41: ORTEP drawings of complexes **8a** showing short Au...Br distances in the crystal (50% probability level for the thermal ellipsoids).

The crystal structure of **8b** shows another bonding type, which has not been seen and discussed before in this work. The counterions are lying next to aromatic moieties, providing anion... π interactions. They are realized by short distances between the NHC planes and the respective fluorine atoms (F4: 2.98231(10) Å, F5: 3.51648(12) Å, F6: 3.16659(10) Å for one moiety and F8: 3.22091(11) Å, F11: 3.04657(11) Å, F12: 3.19695(11) Å for the other moiety).

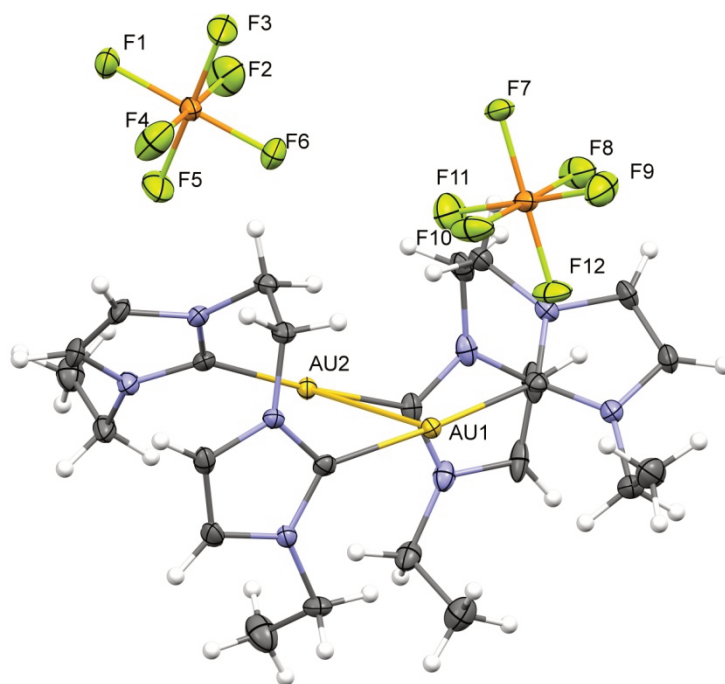


Figure 42: ORTEP drawing of complex **8b** (50% probability level for the thermal ellipsoids).

The imidazole propylene structures are as well highly affected by the wingtip groups. Reverse to the ethylene derivatives the methyl complexes (**3a,b**) build sandwich analogue cations with short Au...Au distances and the ethyl derivatives (**9a,b**) are stretched out (**3** = $[\text{Au}_2(\text{bisMe}_2\text{PrIm})_2]^{2+}$; **9** = $[\text{Au}_2(\text{bisEt}_2\text{PrIm})_2]^{2+}$).

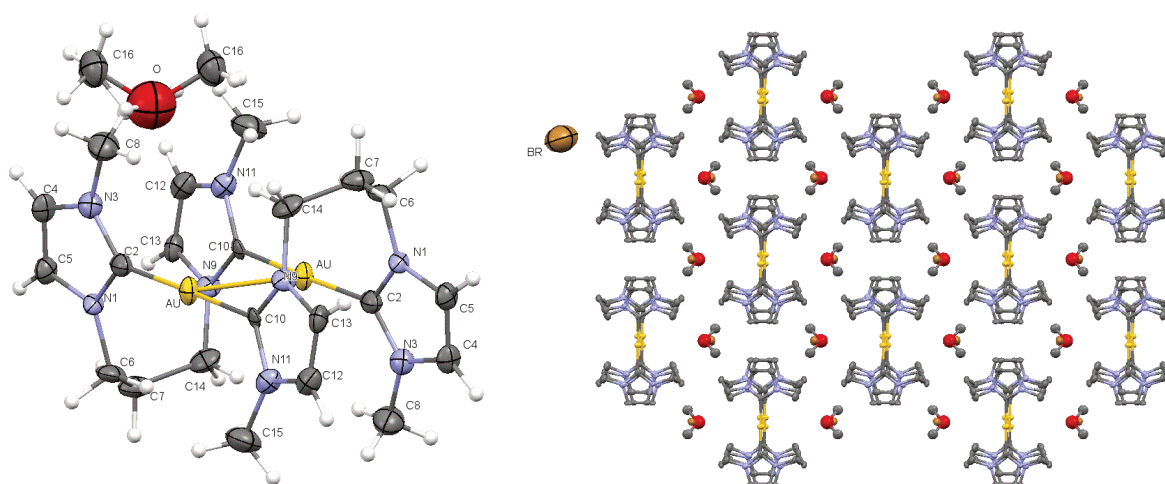


Figure 43: ORTEP drawing and crystal packing of complex **3a** (50% probability level for the thermal ellipsoids). Hydrogen atoms have been omitted for clarity.

The structure of complex **3a** consists of alternating layers of the folded π stacked cations. The C-Au-C axes are parallel arranged providing short aurophilic interactions of 3.1153(2) Å. The linkers are pointing in different directions from these axes, building a chair conformation. The solvent molecules and counterions are arranged in layers connected to the side chains and linkers by attractive hydrogen bonding. All bromide anions in the structure of **3a** show short H...Br distances to four protons which are always the same for every layer. They are interacting with three cations (one methyl-H8, one propylene-H6 and one aromatic H13) and the hydroxyl proton of the here distorted methanol molecule. All other protons do not provide any short distances to bromide. The hydrogen bonds in this structure are exceptionally long for these kind of complexes (2.895 Å, 3.030 Å and 3.044 Å) and therefore only moderate. The distances of the H...Br bonds with the solvent are depending on the arrangement in the structure. The distorted position could provide distances of 2.327 Å or long 3.033 Å. The driving force in this structure seems to be the π stacking and the metallophilic interactions.

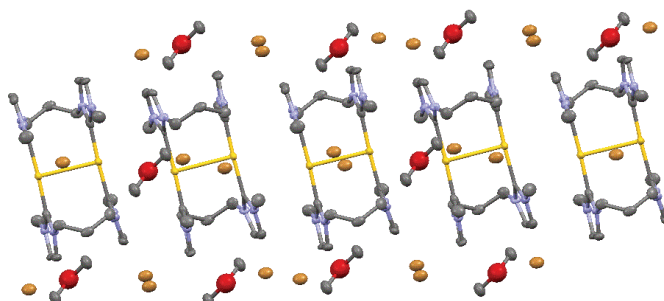


Figure 44: Crystal packing of complex **3a** (50% probability level for the thermal ellipsoids). Hydrogen atoms have been omitted for clarity.

The cations of **3b** show three different rotated U shaped arrangements in the crystal (see Figure 45). They form horizontal layers with the cations pointing in the same direction and vertical layers with the different orientations. The view along the Au...Au axes looks like triangles formed by the C-Au-C axes and an overall structure similar to a picture from a kaleidoscope. Interestingly the three intramolecular and respective intermolecular Au...Au

distances are identical (3.2293(4) Å intramolecular and 3.7036(1) Å intermolecular). The structure found here is in good agreement with the already published results of *Baron et al.*^[4a] The bigger counterion fills out the space between the cations and renders the additional solvent molecules unnecessary. Due to the alternating overall structure the counterions are surrounded by several cations, providing versatile short H...F bonds to all of them. Even though the arrangement of the cations and counterions is pretty different in the structures of **3a** and **3b**, both structures have the sandwich like configuration of the cation with aurophilic interactions in common. The key for that favourable geometry is the long and dynamic propylene linker.

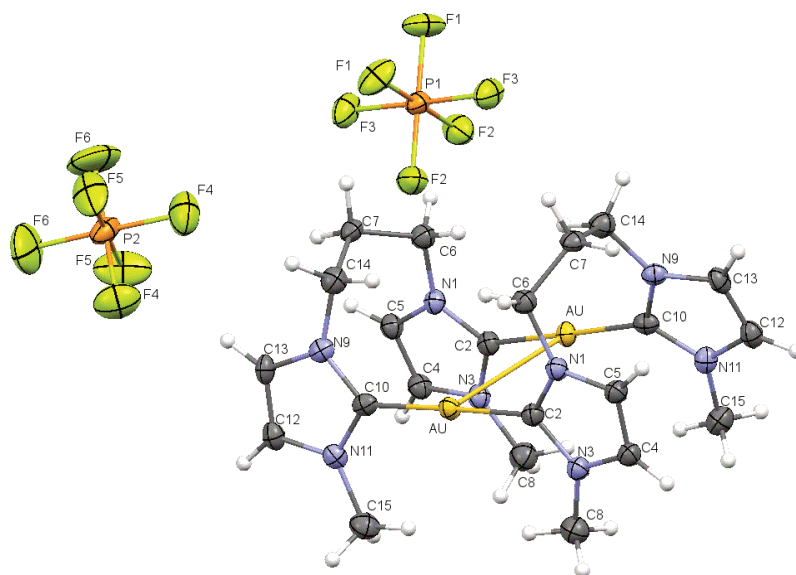


Figure 45: ORTEP drawing of complex **3b** (50% probability level for the thermal ellipsoids).

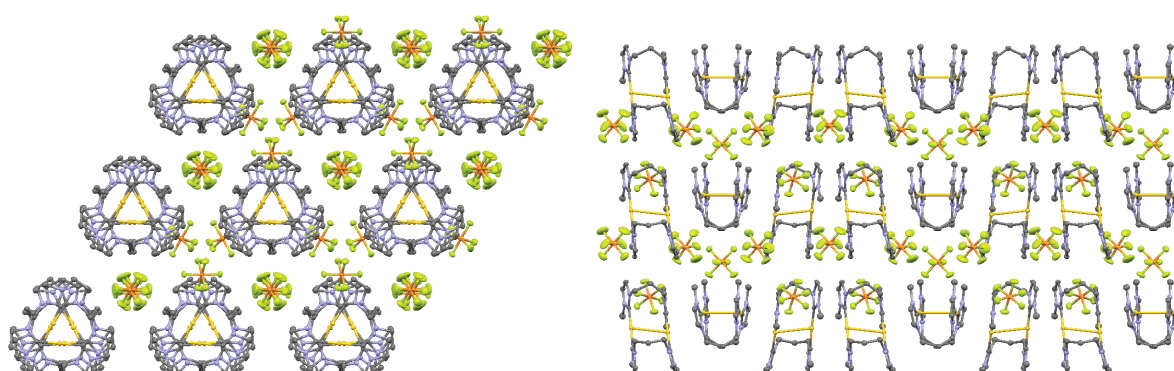
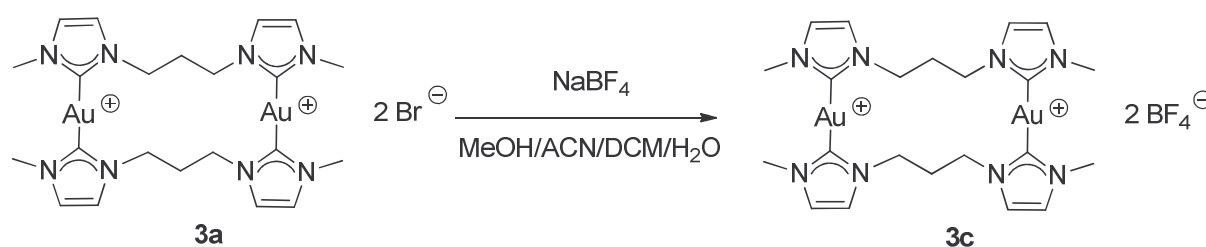


Figure 46: Crystal packing of complex **3b** (50% probability level for the thermal ellipsoids). Hydrogen atoms have been omitted for clarity.

The previously reported structures of **9a** and **9b** are W shaped^[4f] and their overall structure is rather similar with the structures found for the methylene complexes **1a,b** and **7a,b,c**. While the arrangement of the cations in **9a** does not allow aurophilic interaction, the structure of **9b** provides short intermolecular aurophilic interactions. This is a unique feature of this structure and could not be detected for any other complex, even though the distances in **7a** and **7c** are only slightly above 3.5 Å.

Adding AgBF₄ to the crystallizing solutions always yielded in crystals of [Ag(CH₃CN)₄](BF₄). Therefore an anion exchange was performed before the crystallization process. The complex was dissolved in a mixture of methanol, acetonitrile, dichloromethane and then a saturated solution of NaBF₄ in water was added. Removing the organic solvent led to the new compound **3c**. Single crystals were obtained by slow diffusion of diethyl ether in a saturated acetonitrile solution of the pure complex.



Scheme 7: Anion exchange of the complex **3a** with NaBF₄.

The structure of this peculiar new complex contains the shortest Au...Au distance (2.9990(6) Å) of all investigated complexes. This strong aurophilic bond is fulfilled by a distorted conformation of the cation. The two C-Au-C axes are not parallel but almost vertically arranged.

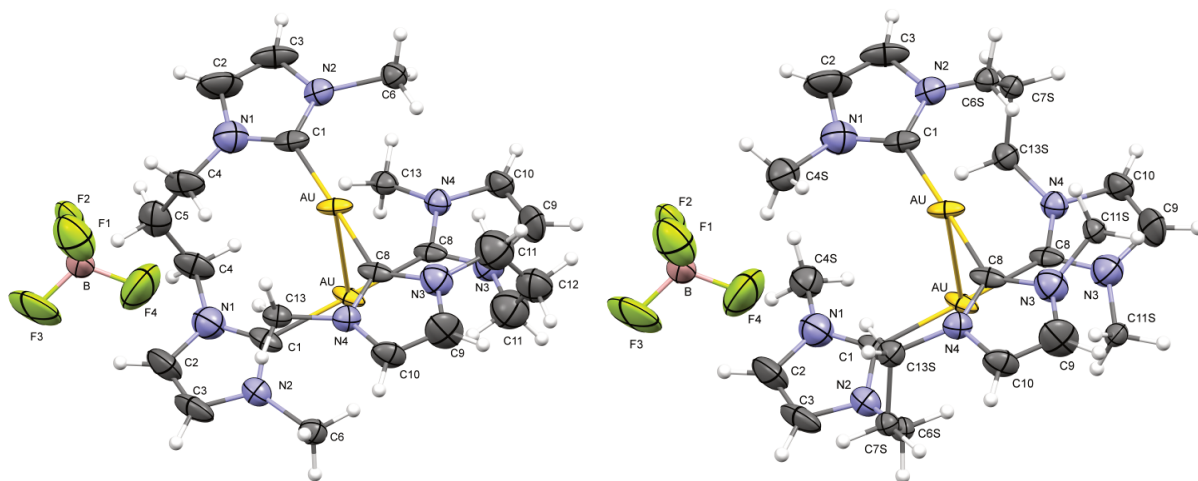


Figure 47: ORTEP drawing of the distorted cations of complex 3c (50% probability level for the thermal ellipsoids).

The arrangement of the cations is slightly disordered, resulting in two almost identical but rotated molecules. The methyl carbon atoms C6 and C13 are part of the propylene-linker in the other conformation and the loss of C5 and C12 leads to the new methyl side chains (see Figure 47).

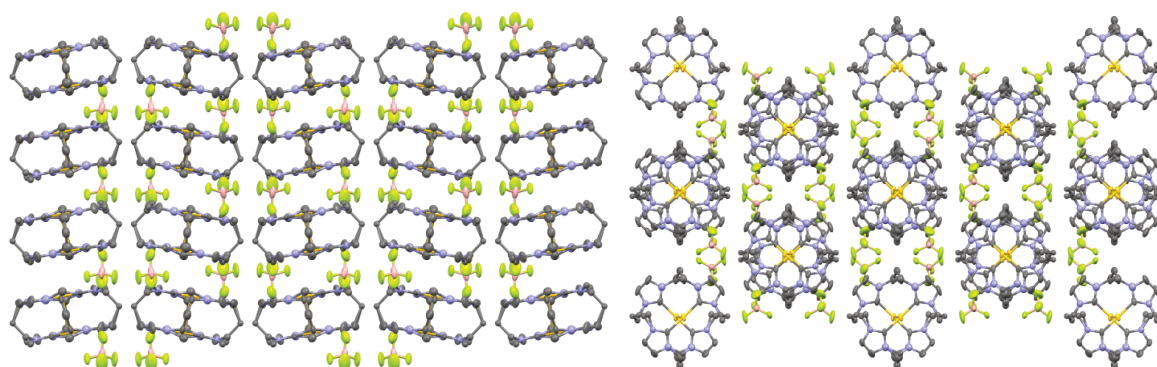


Figure 48: Crystal packing of complex 3c (different cation conformation, 50% probability level for the thermal ellipsoids). Hydrogen atoms have been omitted for clarity.

The counterions are stabilized via H...F bonds and form separated sections between the cations. While the complexes **3a** and **3b** contain the already mentioned sandwich like cations with intramolecular $\pi\cdots\pi$ interactions, in complex **3c** only intermolecular π stacking is possible. Therefore the complexes are stacked with parallel C-Au-C axes of the two neighbouring cations. Thus the next cation above is turned to achieve the same parallel orientation to the other C-Au-C axis. This leads to long alternating chains of the gold compounds. Another example of an imidazole propylene complex with a methyl side chain was found by *Gil-Rubio et al.* in 2013.^[62n] The given structure was crystallized with triflate

counterions. The bulky anion promotes a stacked arrangement with twisted cations similar to **3c**. Even though the Au...Au distances in that structure are slightly longer than in the crystal of the here presented BF_4^- complex.

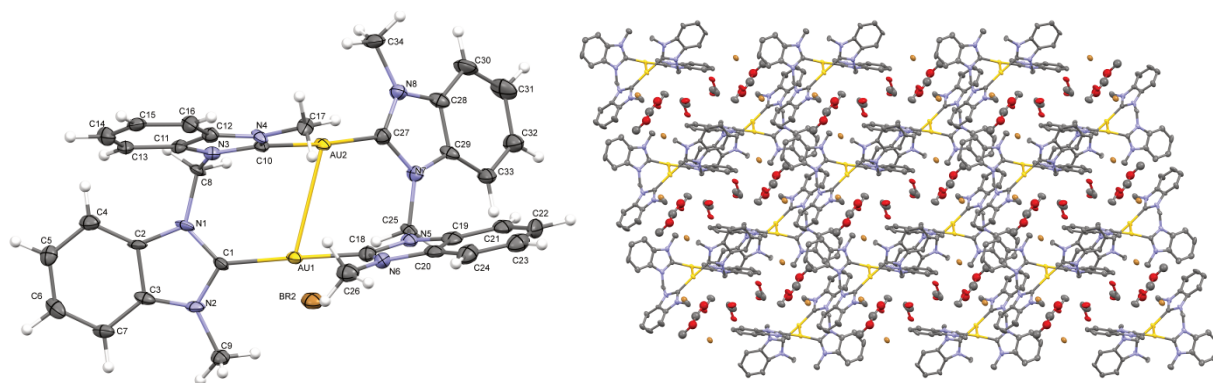


Figure 49: ORTEP drawing and crystal packing of complex 4a (50% probability level for the thermal ellipsoids). Hydrogen atoms have been omitted for clarity.

Changing the imidazole scaffold to benzimidazole creates a bigger π -system with a higher ability for π stacking and additional binding sites. The methylene complexes **4a,b** and **10a,b** were crystallized to compare them with their imidazolium derivatives (**4** = $[\text{Au}_2(\text{bisMe}_2\text{MeBim})_2]^{2+}$; **10** = $[\text{Au}_2(\text{bisEt}_2\text{MeBim})_2]^{2+}$). They cannot create the same U shaped conformation like the imidazolium complexes, due to repulsive interactions of the interfering bigger benzimidazole backbones. The bulky ligands support an even more complex arrangement. The aromatic systems are not coplanar but twisted, resulting in slightly crosswise arranged C-Au-C axes. While most of the methylene imidazolium complexes do not show short Au...Au distances, the different geometry of the benzimidazole complexes enables aurophilic interactions in all investigated compounds. Two of the benzimidazole moieties are leant to each other and the other two ring systems are turned away from the pocket shaped occurring cavity. The cations are interacting with other cations by π stacking. All benzimidazole containing complexes with methylene linker got this structural motif in common, with small changes of the angles. But the different wingtip groups and counterions are changing the overall arrangement of the neighbouring cations, due to their sizes and interactions. Using bromide requires the cocrystallization of methanol, independent from the length of the side chains (see Figure 53).

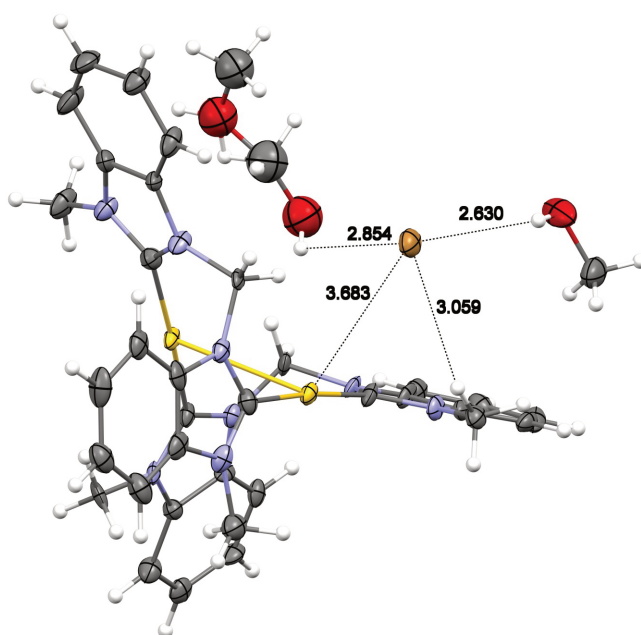


Figure 50: ORTEP drawings of complexes **4a** showing short Au...Br, O...H and H...Br distances in the crystal (50% probability level for the thermal ellipsoids).

The position of the counterion in the structure of **4a** provides several hydrogen bonds to the solvent and the cation. Another interesting weak interaction could also be found between the counterion and one of the gold centres (see Figure 50). The counterions and solvent molecules in the bromide complexes are stabilized via several H...Br and O...H bonds with the cations. The Au...Br distances are smaller than the sum of their corresponding van der Waals radii.

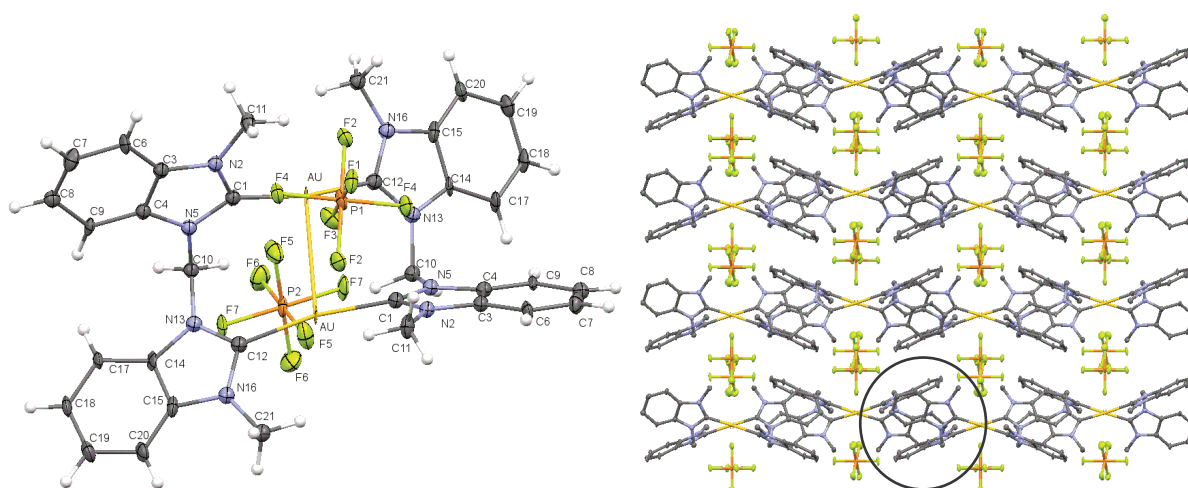


Figure 51: ORTEP drawing and crystal packing of complex **4b** (50% probability level for the thermal ellipsoids). Hydrogen atoms have been omitted for clarity. Intramolecular π -stacking indicated by the black circle, the four benzimidazole units are building a box like arrangement.

The corresponding PF_6^- containing structures of **4b** and **10b** do not require additional solvent molecules. Interestingly the smaller methyl complexes **4a** and **4b** also have smaller Au...Au distances of 3.0469(10) Å and 3.0744(8) Å compared to the complexes **10a**, **10b** and **10c** with distances of 3.1700(3) Å, 3.1635(5) Å and 3.2241(11) Å respectively. The ethyl substituents are sufficient to open the folded structure a bit due to varying attractive interactions with the counterions.

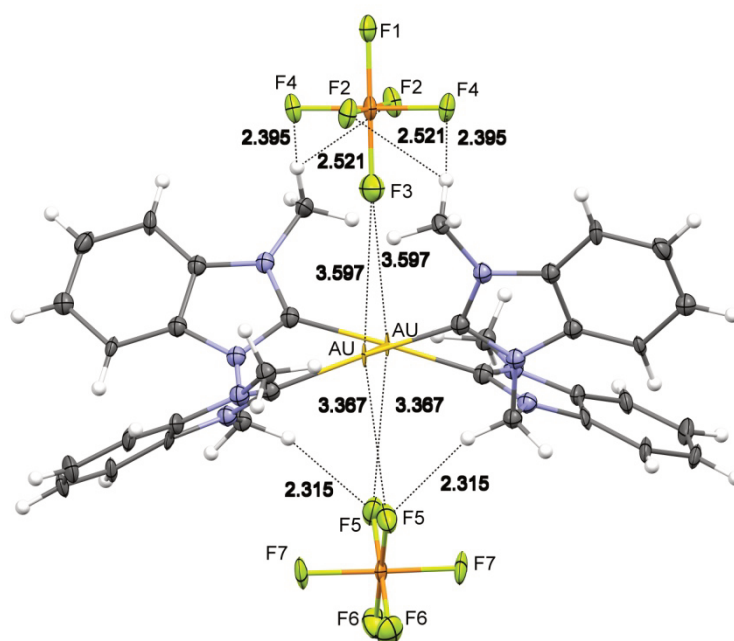


Figure 52: Crystal packing of complex **4b** (50% probability level for the thermal ellipsoids). Au...F distances in the crystal.

Due to the stacked arrangement the counterions and cations in the crystal structure of **4b** are lying centric above and below the cavity of the gold(I) NHC compound. The two differently ordered anions are stabilized via various hydrogen bonds to the side chains of the cation. This geometry is additionally stabilized by weak Au...F interactions, which are seen as short distances between the atoms.

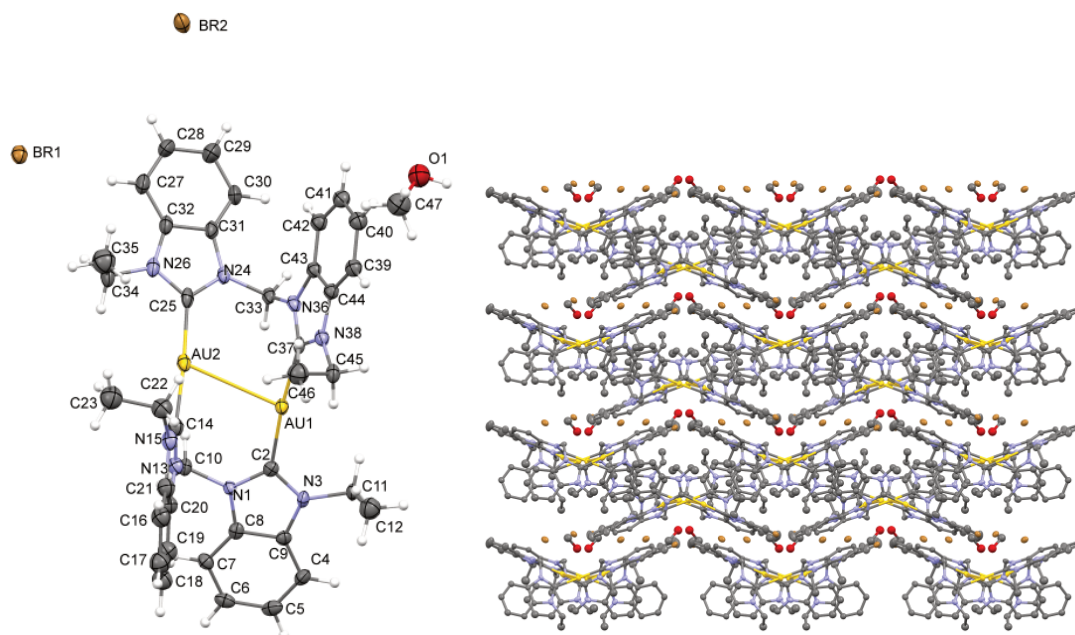


Figure 53: ORTEP drawing and crystal packing of complex **10a** (50% probability level for the thermal ellipsoids). Hydrogen atoms have been omitted for clarity.

Similar to the crystal packing of **4a**, the structure of **10a** contains Au...Br distances shorter than the sum of their van der Waals radii. Due to the longer ethyl wingtips, the counterions have the ability to build additional H...Br bonds to the side chain protons. This leads to a more centric position of the bromide above the metal centre and a slightly shorter Au...Br distance than found in the structure of **4a**.

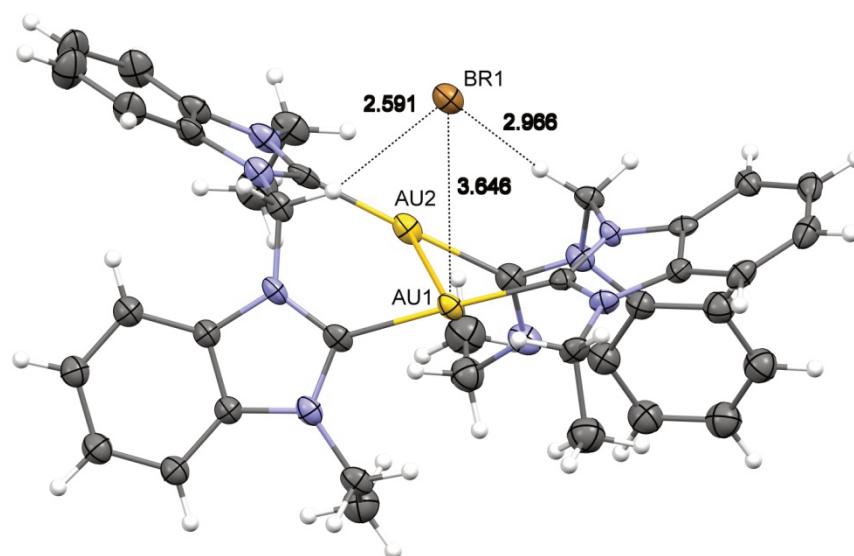


Figure 54: ORTEP drawings of complexes **10a** showing short Au...F and H...F distances in the crystal (50% probability level for the thermal ellipsoids).

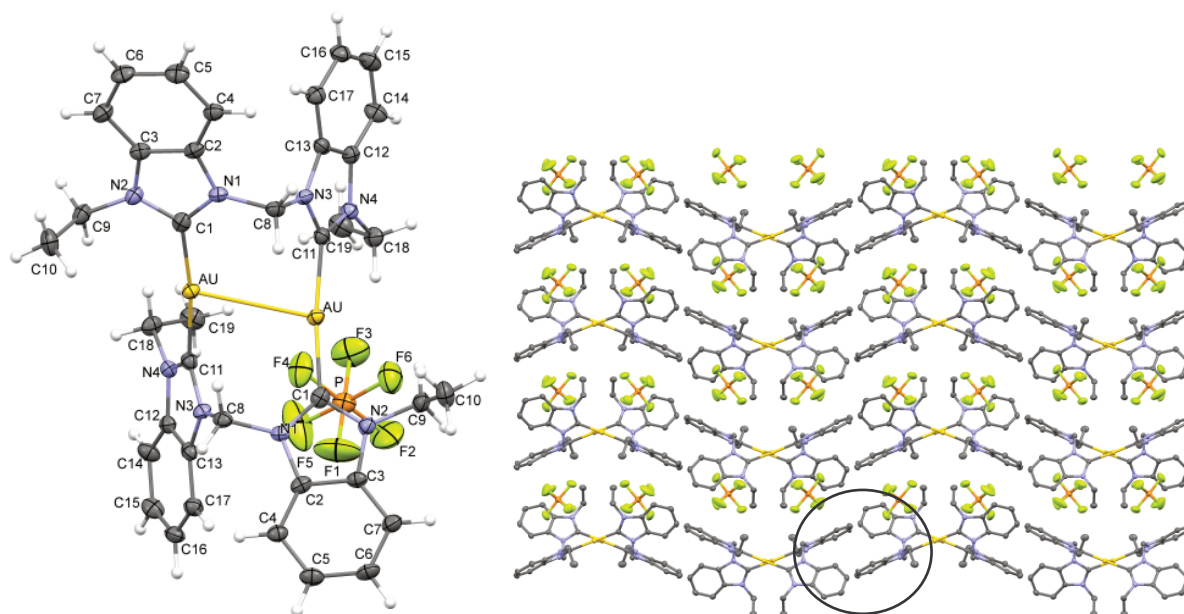


Figure 55: ORTEP drawing and crystal packing of complex 10b (50% probability level for the thermal ellipsoids). Hydrogen atoms have been omitted for clarity. Intramolecular π -stacking indicated by the black circle.

Comparing the overall structures of **4b** and **10b** demonstrates the impact of the longer wingtip groups. Both structures contain layers of alternating cations. The distances between these cations and the locations of the counterions are determined by the size of the alkyl substituents. The cations of the ethyl containing structure of **10b** are farther away from each other, while in **4b** the cations are nearer and therefore creating a box like arrangement consisting of four benzimidazole moieties. In **10b** the distances of the cations are longer, creating a larger “box” (consisting of the NHC planes). The structures bear alternating layers of the cations where one layer is turned upside down in contrast to the next layer. While these rows are stacked on top of each other in the structure of **10a**, they lay next to each other in the structure of **10b**. As seen in Figure 55, one cation does always enclose two counterions between two aromatic moieties respectively. The interactions of one PF_6^- ion and the cation are shown in Figure 56. The aggregation is mainly based on the particular hydrogen bonds with the counterion (here only shown with the side chains, the other $\text{H}\cdots\text{F}$ interactions are formed with neighbouring cations and not shown for clarity). But there is also a short distance of 3.074 Å between one Au centre and F4, hinting for utmost interesting $\text{Au}\cdots\text{F}$ interactions. The picture does only contain one counterion for a better view, but the given distances are the same for the other anion. The position of the counterion between two aromatic moieties provides the possibility of another bonding type

which has not seen in the other structures. A connection of the PF_6^- anions with the benzimidazolium ring system by anion $\cdots\pi$ interaction is assumed, due to the short distances of the NHC planes and one of the respective fluorine atoms (F1: 3.14133(14) Å and F4: 3.12561(14) Å) of the counterion.

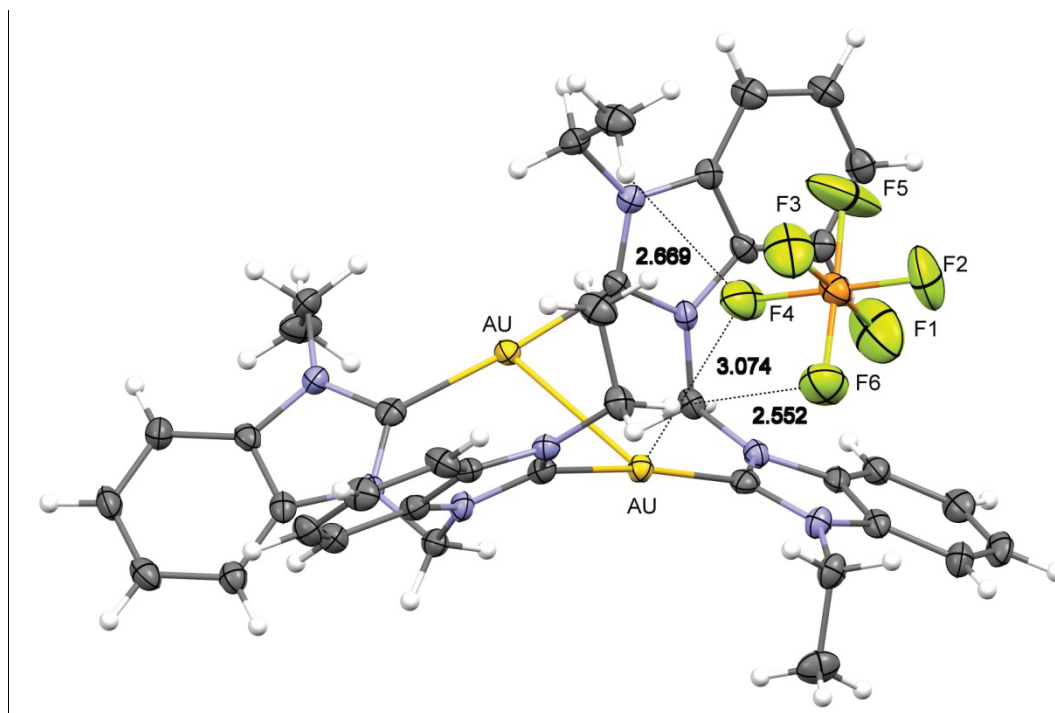


Figure 56: Crystal packing of complex 10b (50% probability level for the thermal ellipsoids). Au \cdots F and H \cdots F distances in the crystal, hydrogen atoms have been omitted for clarity.

To avoid exchange processes of the counterions and force Ag \cdots Au interactions while adding silver salts, AgPF_6 was added to solutions of all PF_6^- containing complexes. The reaction of AgPF_6 with even minimal amounts of water results in a hydrolysis process and yields the anion PO_2F_2^- .^[87] By adding the silver salt to solutions of the complexes and letting them rest for several days, this counterion was build unintentionally.

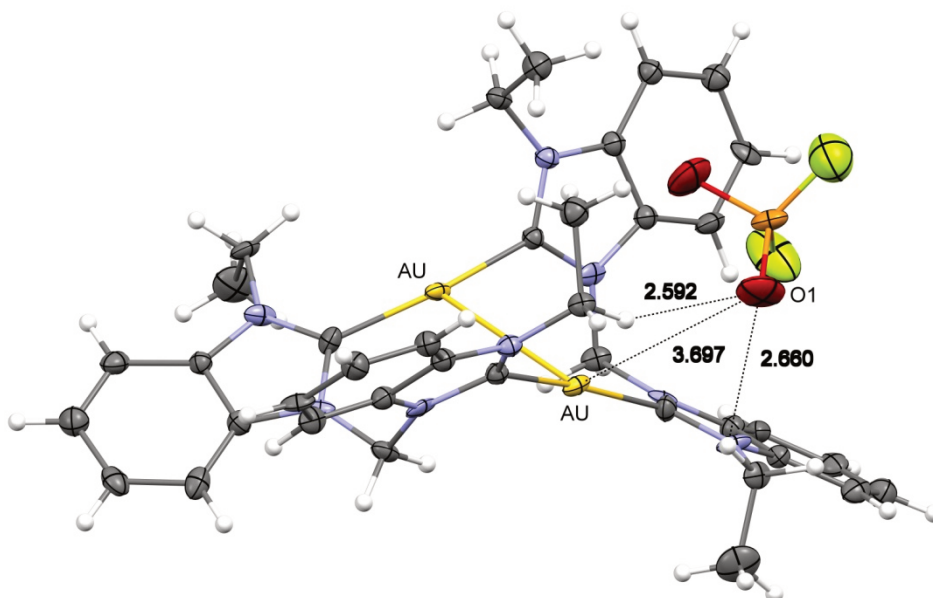


Figure 58: Crystal packing of complex **10c** (50% probability level for the thermal ellipsoids). Au...O and H...O distances in the crystal.

The anion aggregation via hydrogen bonds in **10c** is similar as seen for the PF_6^- compound. Two of the wingtip substituents are part of the O...H interactions. The Au...O distances however are too long to be considered as real interactions. The fluorine atoms are pointing away from the metal centres and form the special H...F bonds with the neighbouring cations. As already seen for compounds **10b**, the counterions are stabilized by anion... π interactions. They are seen as short distances between the NHC planes and one oxygen atom of the anion (O1) (3.52809(12) Å and 3.10905(9) Å).

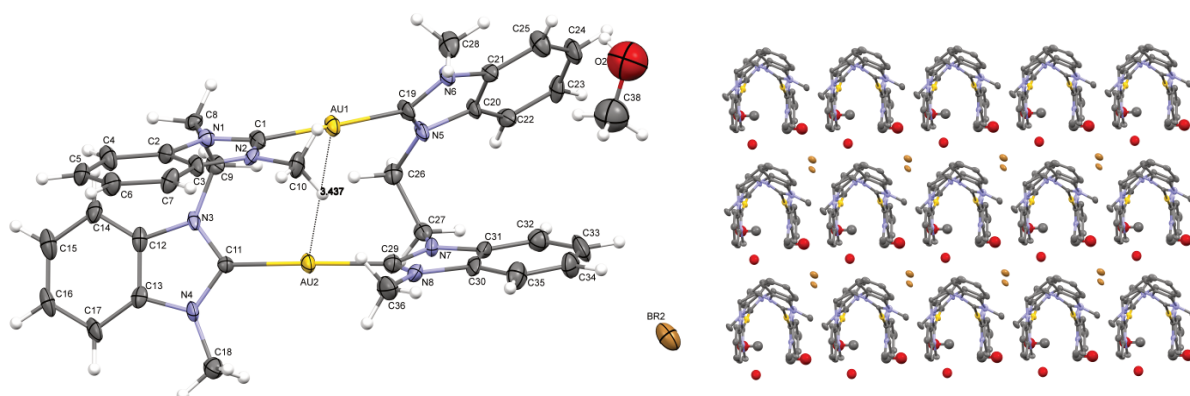


Figure 59: ORTEP drawing and crystal packing of complex **5a** (50% probability level for the thermal ellipsoids). Hydrogen atoms have been omitted for clarity.

The benzimidazolium ethylene compounds do all crystallize with a folded geometry. The folded structures provide small Au...Au distances for some of the complexes (**5a**: 3.43670(19) Å, **5b**: 3.2359(10) Å, **11b**: 3.3937(2) Å), while **11a** and **11c** have distances slightly above 3.5 Å (**5** = [Au₂(bisMe₂EtBim)₂]²⁺; **11** = [Au₂(bisEt₂EtBim)₂]²⁺). The wingtip groups and counterions are providing different arrangement of the cations in the crystal packing. All of these structures contain four different π...π distances, resulting from the interaction from one cation with four other cations. While the crystal structure of the methyl complex **5a** requires additional methanol molecules, the voids between the different cations of complex **5b** are exclusively occupied by the bigger hexafluorophosphate anions.

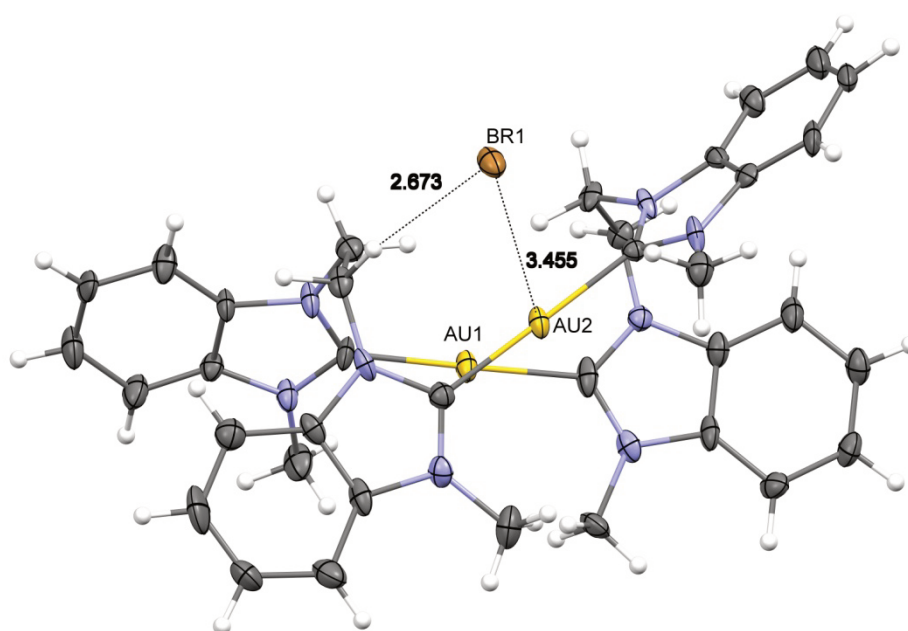


Figure 60: Crystal packing of complex 5a (50% probability level for the thermal ellipsoids). Au...Br distances in the crystal, hydrogen atoms have been omitted for clarity.

The counterion Br1 is centrally lying above the cavity of compound **5a**. This arrangement does again support short interactions between the anion and the metal centre. The Au...Br distances are 3.455 Å and therefore considered as attractive interactions.

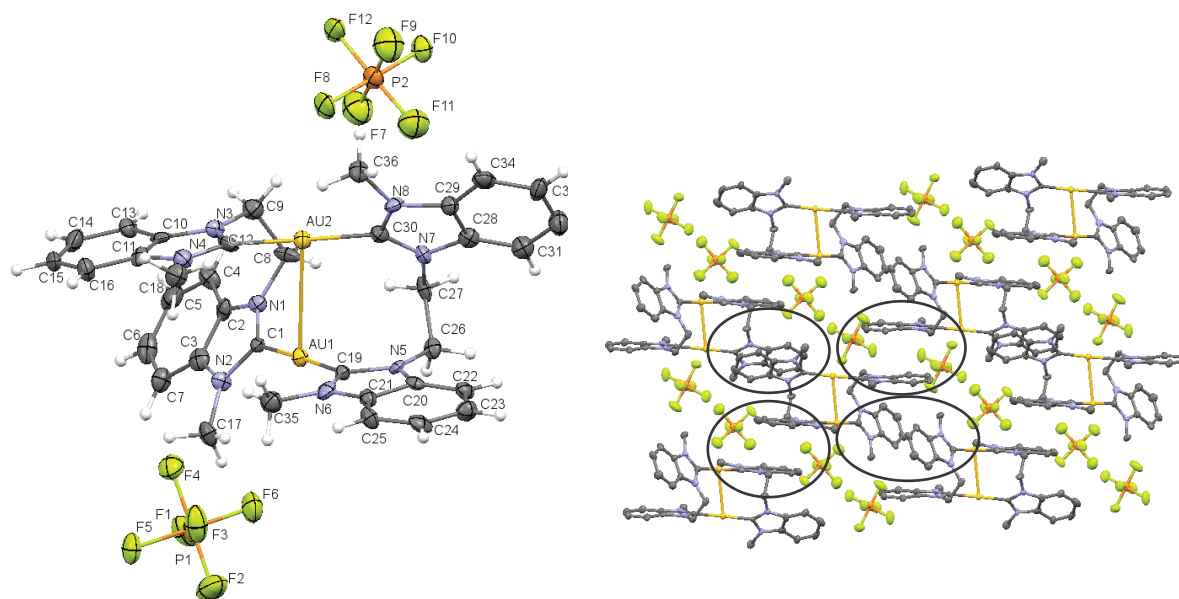


Figure 61: ORTEP drawing and crystal packing of complex 5b (50% probability level for the thermal ellipsoids). Hydrogen atoms have been omitted for clarity. Intramolecular π stacking is indicated by the black circles.

The conformation of the cations of the benzimidazole complexes with ethylene linkers are not depending on the side chains or counterions. Similar to the methylene complexes they form U shaped cavities. Due to the longer linker the two inwards turned aromatic systems are almost parallel. The two others are pointing outwards. Similar to complex **10b** ($\mathbf{10} = [\text{Au}_2(\text{bisEt}_2\text{MeBim})_2]^{2+}$) the geometry of the counterion provides short distances to one of the benzimidazolium moieties. The distances of the anion $\cdots\pi$ interactions in this compound are 2.8929(3) Å. In contrast to the methylene complex **10b** the interactions in **5b** are limited to one of the aromatic systems, due to the different folding and arrangement of the cations.

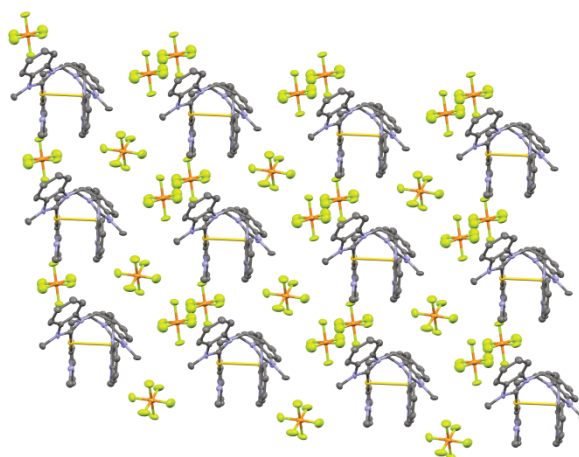


Figure 62: Crystal packing of complex 5b (50% probability level for the thermal ellipsoids). Hydrogen atoms have been omitted for clarity.

The hexafluorophosphate anion in the structure of **5b** is lying above one aromatic moiety. This arrangement provides short Au...F distances of 3.397 Å. The stabilization of the counterion in that position is supported by anion... π interactions, leading to pretty small distances between the counterion and the NHC plane (F11: 2.8929(3) Å).

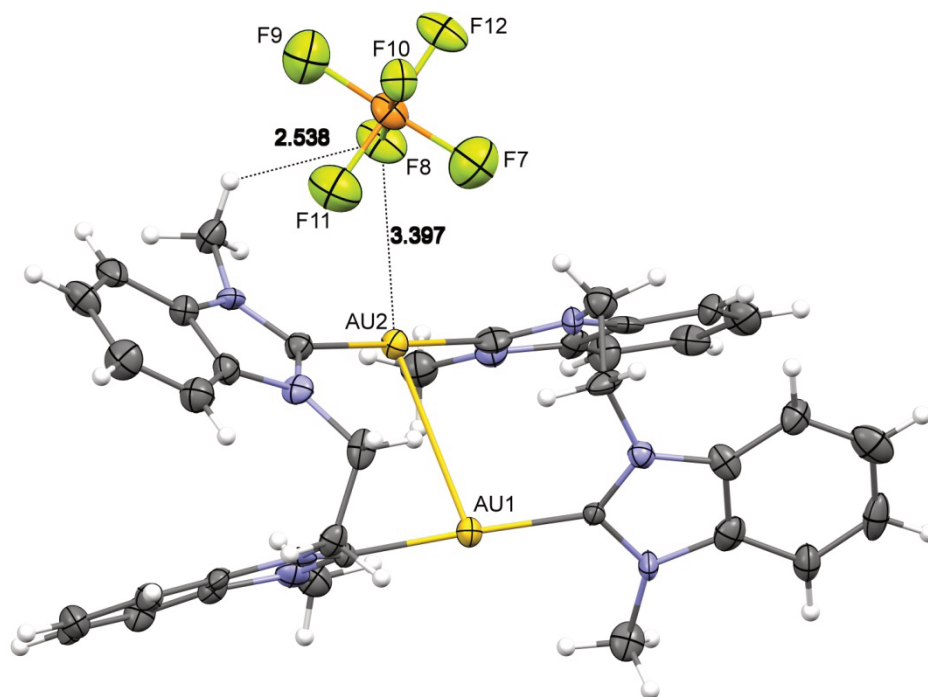


Figure 63: ORTEP drawings of complexes **5b** showing short Au...F and H...F distances in the crystal (50% probability level for the thermal ellipsoids).

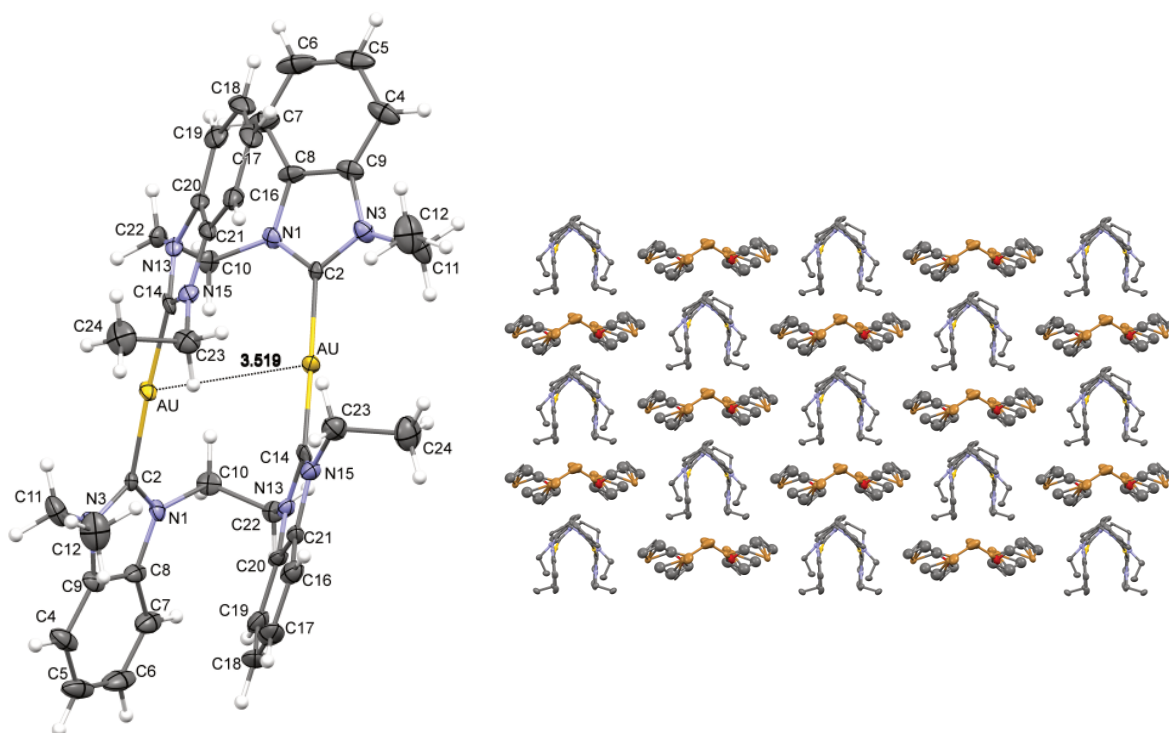


Figure 64: ORTEP drawing and crystal packing of complex 11a (50% probability level for the thermal ellipsoids). Hydrogen atoms have been omitted for clarity.

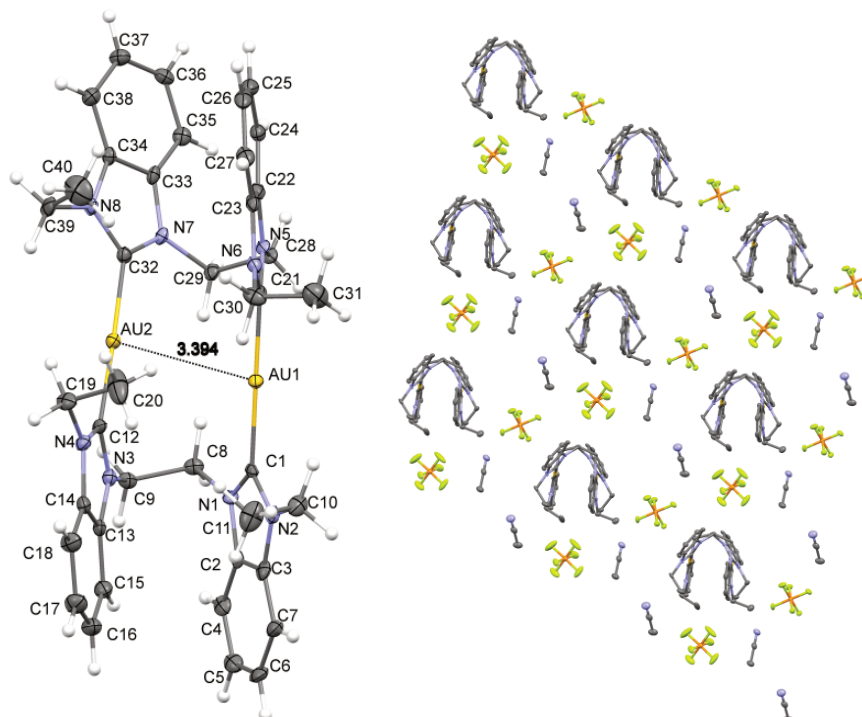


Figure 65: ORTEP drawing and crystal packing of complex 11b (50% probability level for the thermal ellipsoids). Hydrogen atoms have been omitted for clarity.

Even though the ethyl derivatives **11a,b,c** have similar conformations of the cations as the methyl complexes, only the PF_6^- complex **11b** provides $\text{Au}\cdots\text{Au}$ distances in the range of aurophilic interactions. Depending on the anion, the ethyl side chains point inwards or outwards. In the Br^- and the PO_2F_2^- complexes **11a** and **11c** the two alkyl substituents of the same ligand are pointing in the same direction (two inwards and two outwards). Contrary to that in the structure of **11b** three ethyl substituents are pointing inwards. The cations and methanol molecules are stacked and form alternating layers in the structure of **11a**. The row next to one layer is shifted, so they are also alternating in this direction. While it is a common arrangement of bromide complexes, the remarkable structure of **11b** is the only example of a benzimidazole PF_6^- complex with cocrystallized solvent molecules. The big counterions in combination with the ethyl side chains provide the different arrangement of the molecules.

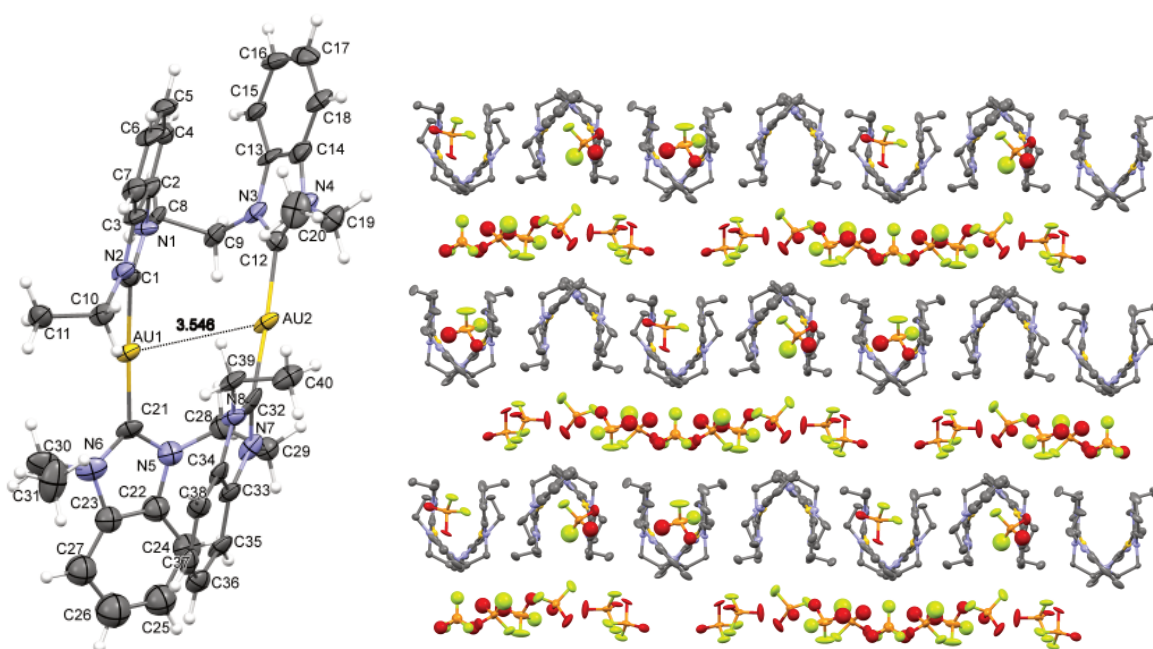


Figure 66: ORTEP drawing and crystal packing of complex **11c** (50% probability level for the thermal ellipsoids). Hydrogen atoms have been omitted for clarity.

The structure of **11c** is an interesting example of an overall structure with three similar geometries of the cation, leading to three $\text{Au}\cdots\text{Au}$ distances slightly longer than aurophilic interactions. This is the only structure with more than only one geometry of the cations. The unusual PO_2F_2^- counterions surround layers of the cations, which originate from π stacking. Each aromatic ring interacts with one benzimidazole unit of another cation, resulting in interactions with four different cations (like **5a,b** and **11a,b**). This arrangement provides long

strings of cations and anions. These strings are ordered like chessboards, stabilized by O...H and H...F bonds (Figure 66).

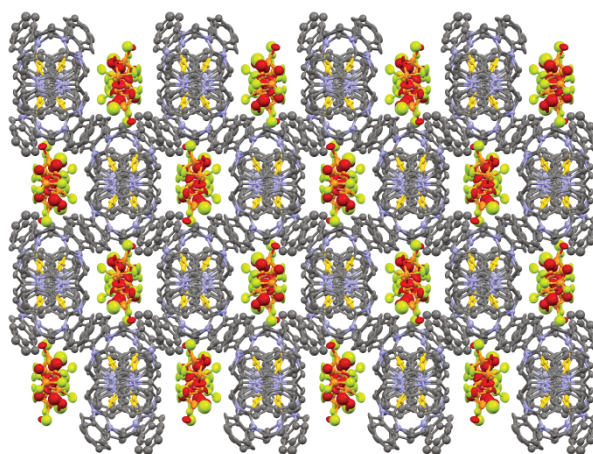


Figure 67: Crystal packing of complex 11c (50% probability level for the thermal ellipsoids). Hydrogen atoms have been omitted for clarity.

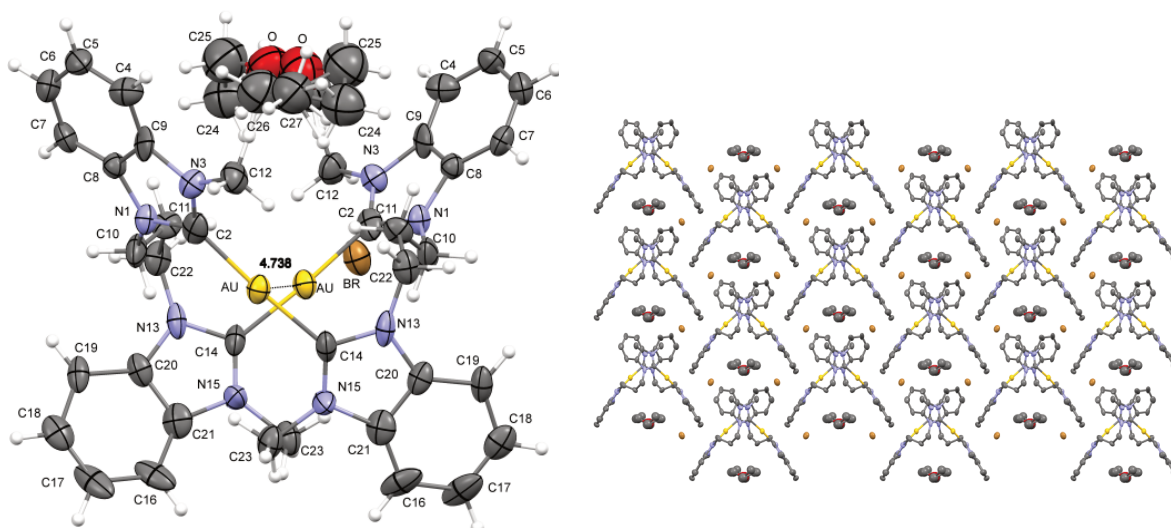


Figure 68: ORTEP drawing and crystal packing of complex 6a (50% probability level for the thermal ellipsoids). Hydrogen atoms have been omitted for clarity.

Analogue to the imidazolium complex **3c** the benzimidazolium complex **6a** has a folded conformation with crossing C-Au-C axes (**3** = $[\text{Au}_2(\text{bisMe}_2\text{PrIm})_2]^{2+}$; **6** = $[\text{Au}_2(\text{bisMe}_2\text{PrBim})_2]^{2+}$). Nevertheless while **3c** consists of two coplanar pairs of NHCs, the cations of **6a** are more distorted. The conformation results in a cup like cavity including an additional methanol guest molecule encircled by two benzimidazole moieties. The bromide ions are outside of the cavity connected via hydrogen bonding with the NHCs and the

solvent molecules. Unlike the other twisted conformations the structure does not include intramolecular aurophilic interactions.

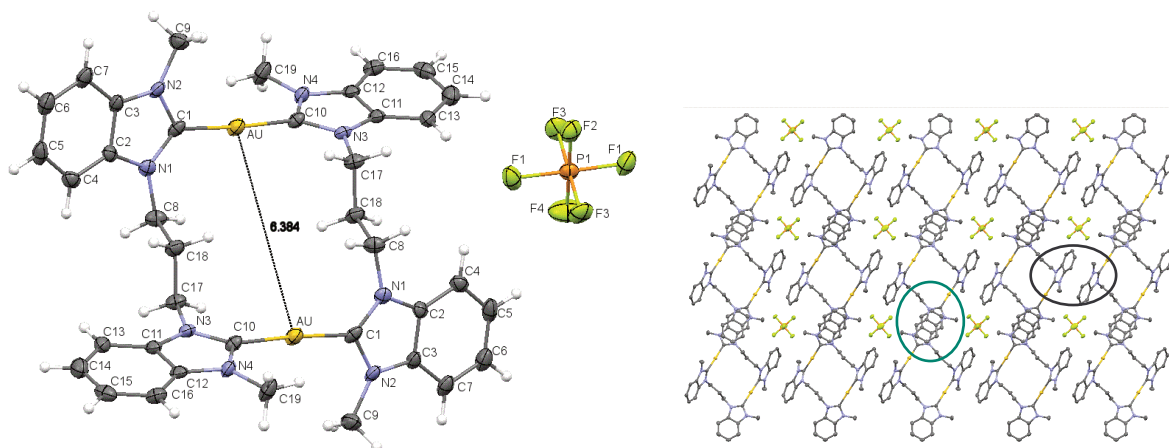


Figure 69: ORTEP drawing and crystal packing of complex **6b** (50% probability level for the thermal ellipsoids). Hydrogen atoms have been omitted for clarity.

The PF_6^- derivative **6b** has a stretched and all trans geometry. The aromatic systems linked by the gold atoms are not coplanar but $73.380(4)^\circ$ rotated, resulting in a Z conformation of the complex. The overall conformation consists of two face to face and two edge to face π interactions per cation (see Figure 69 and Figure 70). The flat structure involves pretty long Au...Au distances of $6.3844(5)\text{\AA}$. Unlike the example shown here the structure of $[\text{Au}_2(\text{bisMe}_2\text{PrBlm})_2](\text{PF}_6)_2$ previously found by *Tubaro et al.* is different, although they were using the same crystallization technique.^[61a] The cations in the crystal structure show a flattened conformation and almost coplanar NHC moieties. These cations show a stacked W like arrangement, stabilized by π interactions.

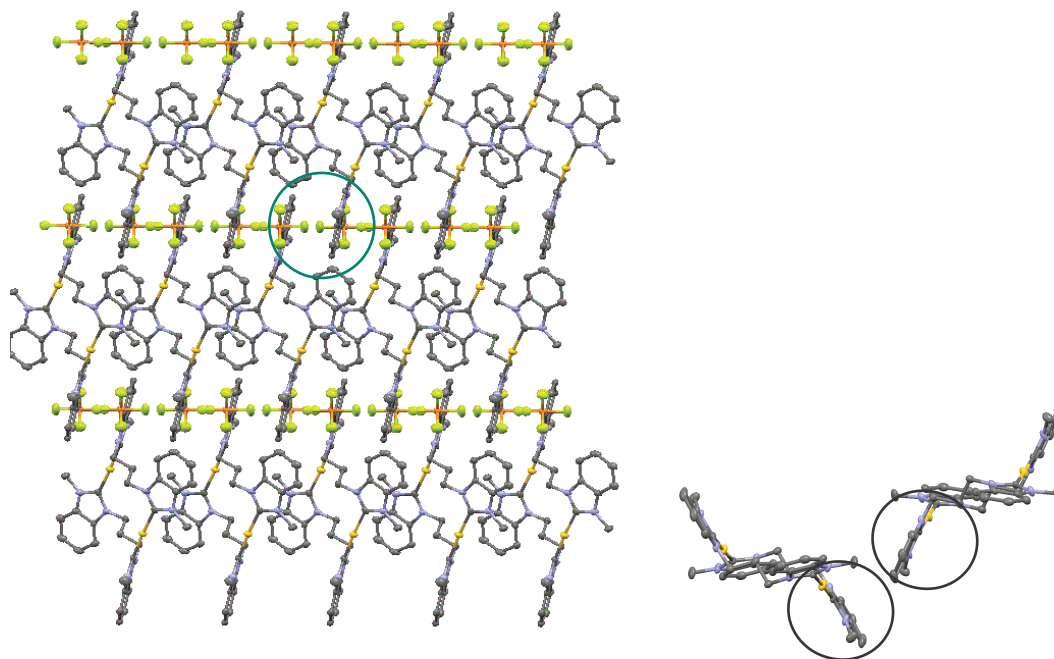


Figure 70: Crystal packing of complex **6b** (50% probability level for the thermal ellipsoids). Hydrogen atoms have been omitted for clarity. Intramolecular π -stacking indicated by the black (edge to face) and green (face to face) circle (for different view see the supporting information).

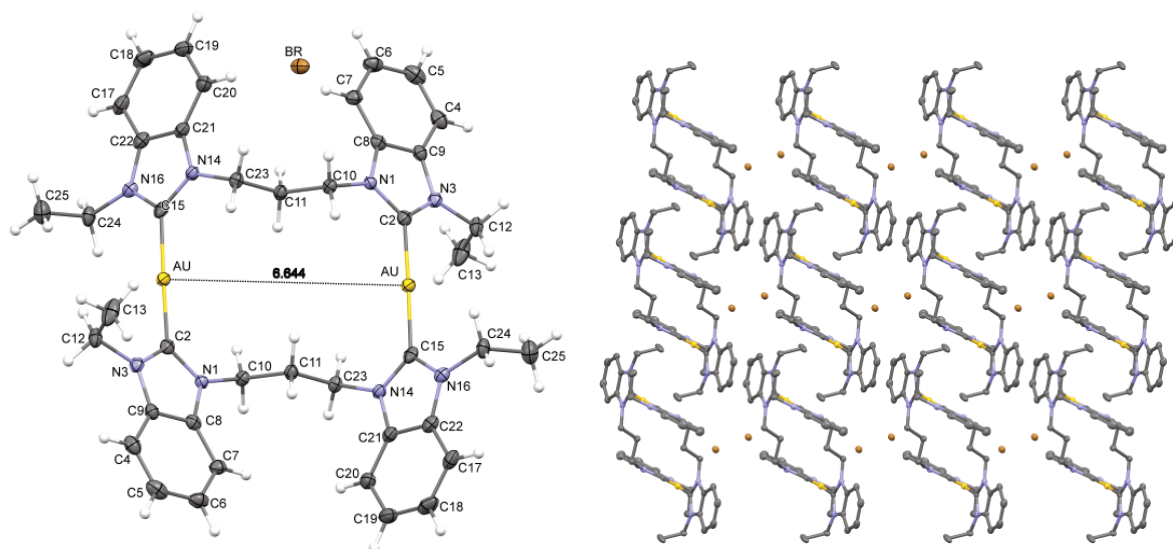


Figure 71: ORTEP drawing and crystal packing of complex **12a** (50% probability level for the thermal ellipsoids). Hydrogen atoms have been omitted for clarity.

The structure of **12a** is another example of a stretched structure without aurophilic interactions, similar to **6b** (**12** = $[\text{Au}_2(\text{bisEt}_2\text{PrBim})_2]^{2+}$; **6** = $[\text{Au}_2(\text{bisMe}_2\text{PrBim})_2]^{2+}$). The complex shown here also has a big torsion angle between the aromatic rings and an all trans

propylene linker. The resulting stretched conformation and stacked arrangement of the cations are sufficient for a crystal structure without cocrystallized solvent molecules. This is the only example of the benzimidazole bromide complexes without additional methanol. The side chains in that conformation seem big enough to fill the existing free spaces in the crystal.

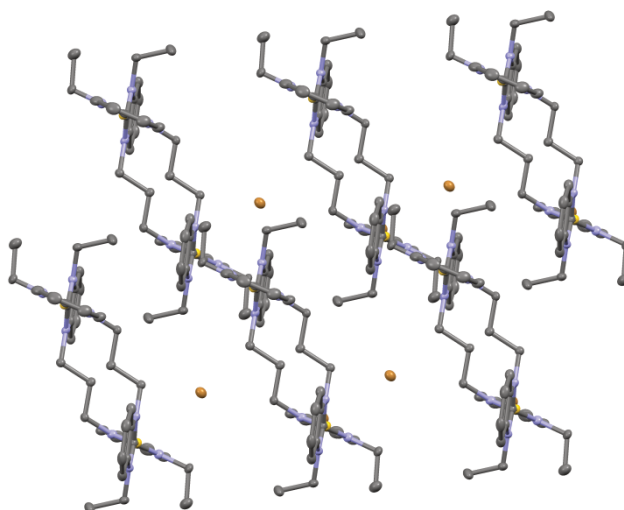


Figure 72: Crystal packing of complex 12a (50% probability level for the thermal ellipsoids). Hydrogen atoms have been omitted for clarity.

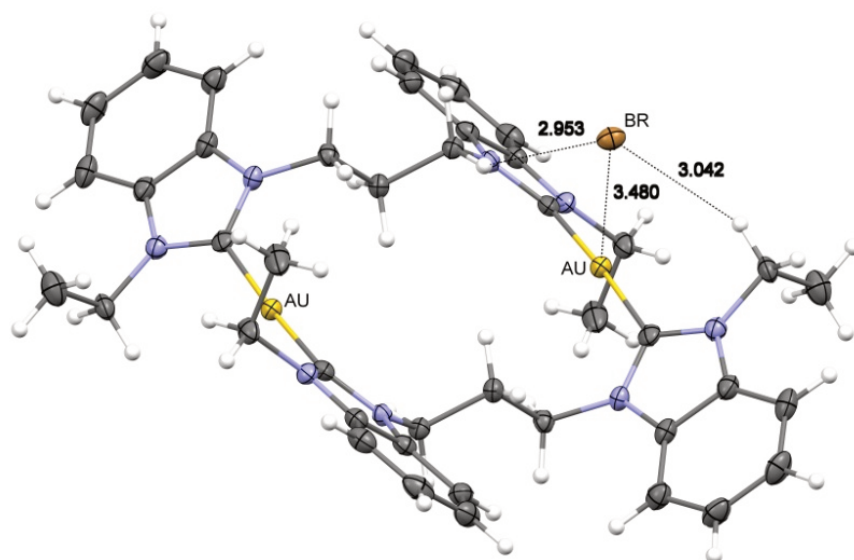


Figure 73: Crystal packing of complex 12a (50% probability level for the thermal ellipsoids). Au...Br distances in the crystal.

The bromide counterion in the structure of **12a** is not centrally arranged above the cavity of the counterion. It is positioned nearby one gold centre, providing small Au...Br distances of 3.480 Å. This attractive interplay is supported by some hydrogen bonds of the bromide with the cation.

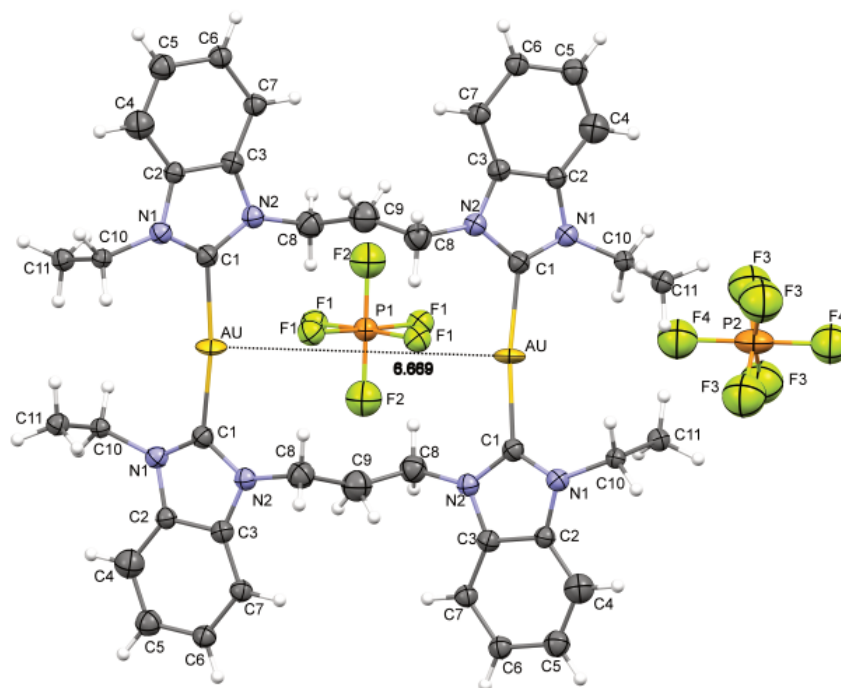


Figure 74: ORTEP drawing of complex 12b (50% probability level for the thermal ellipsoids). Hydrogen atoms have been omitted for clarity.

The cations of **12b** are highly symmetrical and show a stacked conformation stabilized by π interactions. The gold(I) NHCs are staggered arranged surrounded by the anions. While half of the PF₆⁻ ions are connected to the wingtip groups the other anions lie directly above the cavity provided by the open conformation of the cations. This arrangement is realized by short H...F distances between the linker and the PF₆⁻ anions. The given structure provides only Au...Au distances longer than 6 Å, which could not be considered as attractive interactions.

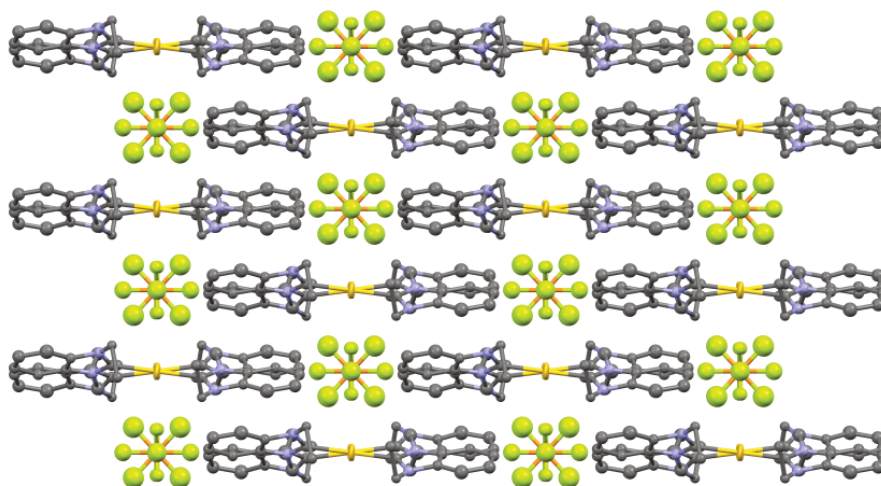


Figure 75: Crystal packing of complex 12b (50% probability level for the thermal ellipsoids). Hydrogen atoms have been omitted for clarity.

As seen in Figure 76 the distances between fluoride and gold are 3.433 Å. In agreement with *Batsanov*^[83] these could be considered as smaller than the sum of their van der Waals radii. The arrangement of the counterion in between two cations is therefore stabilized via several bonding types.

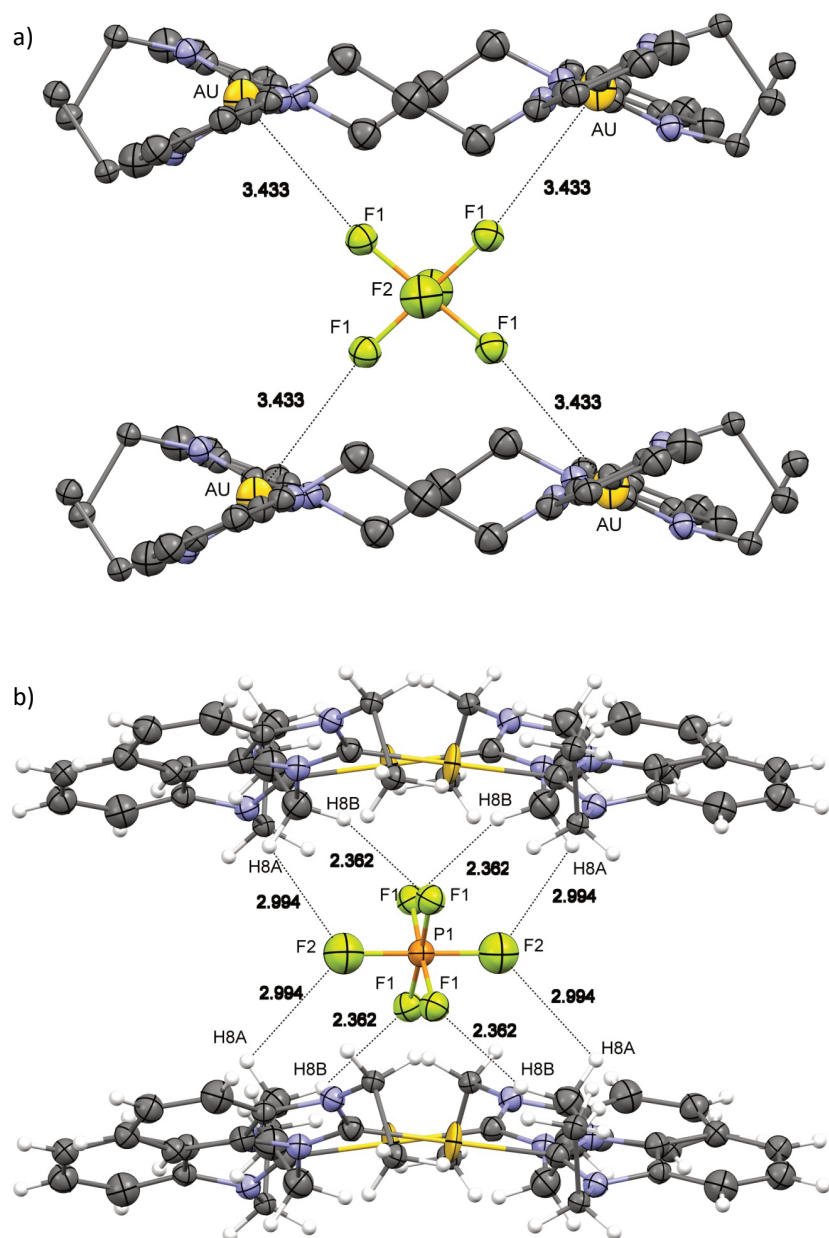


Figure 76: Crystal packing of complex 2b (50% probability level for the thermal ellipsoids). a) Au...F distances in the crystal, hydrogen atoms have been omitted for clarity; b) H...F distances in the crystal.

3.5 Photophysical measurements.

Gold(I) NHC complexes usually feature strong absorbance - and emission bands. They can change when host-guest interactions are induced. For an investigation of the photophysical effects, all bromide and hexafluorophosphate complexes were diluted in acetonitrile. Measurements in DMSO would be interesting to match the results with the NMR experiments. Unfortunately the solvent could not be used for investigations in the interesting wavelength range, due to absorption provoked by the solvent itself. Using acetonitrile overcomes this problem. The poor solubility of some compounds does not apply for those experiments, because the concentration is much lower (10^{-5} M) than for NMR measurements.

As an example the absorption spectra of the imidazolium ligand precursors **1 - 3** and **7 - 9** are given. We were using only the bromide compounds and therefore are not able to compare them to the hexafluorophosphate compounds. However the given spectra do only show high energy absorptions.

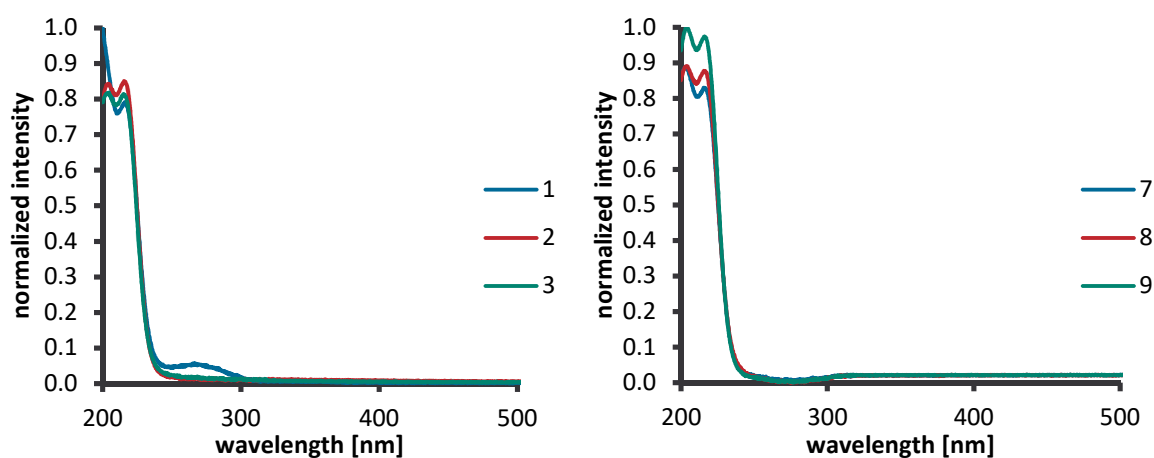


Figure 77: UV/Vis spectra of the ligand precursors a) **1 - 3** and b) **7 - 9**; measured in acetonitrile at room temperature.

Meanwhile the UV/Vis spectra of the imidazole complexes **1a,b - 3a,b** and **7a,b - 9a,b** show absorption maxima between 255 and 265 nm, the λ_{max} on the corresponding benzimidazole complexes **4a,b - 6a,b** and **10a,b - 12a,b** undergo a red shift to 282 - 289 nm (see Figure 72 and Figure 78). These high energy bands are attributed to π - π^* ligand centred transition processes.^[79a,89] The changes of the emission bands^[79a,89] in comparison with the ligand precursors are lead back to the associated metal perturbed transition.^[72] Switching the counterions does not strongly affect these unremarkable spectra. There are several changes in the

intensity of the absorption maxima or additional shoulders in the curve, but they are not continuous systematically. Most hexafluorophosphate compounds show a more intense curve, but the methylene complexes **7a,b** and **10a,b** do not follow this trend. While all of the absorption maxima of the propylene imidazolium complexes are shifted to longer wavelengths, the methylene complexes show this trend for benzimidazolium compounds (both in comparison to the other gold(I) NHC compounds of the series). There are already visible variations between the different series, but they are mostly small.

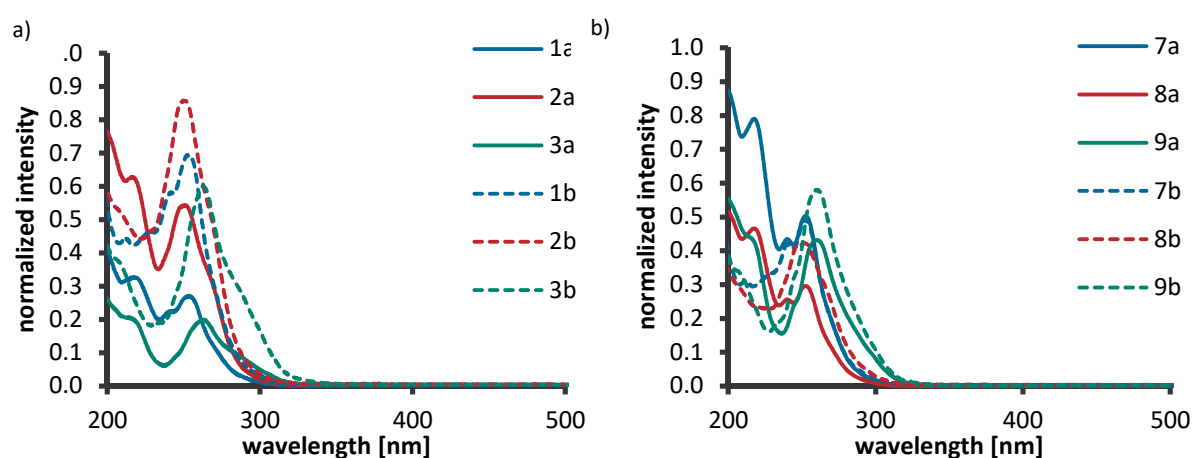


Figure 78: UV/Vis spectra of the complexes a) 1a,b – 3a,b and b) 7a,b – 9a,b; measured in acetonitrile at room temperature.

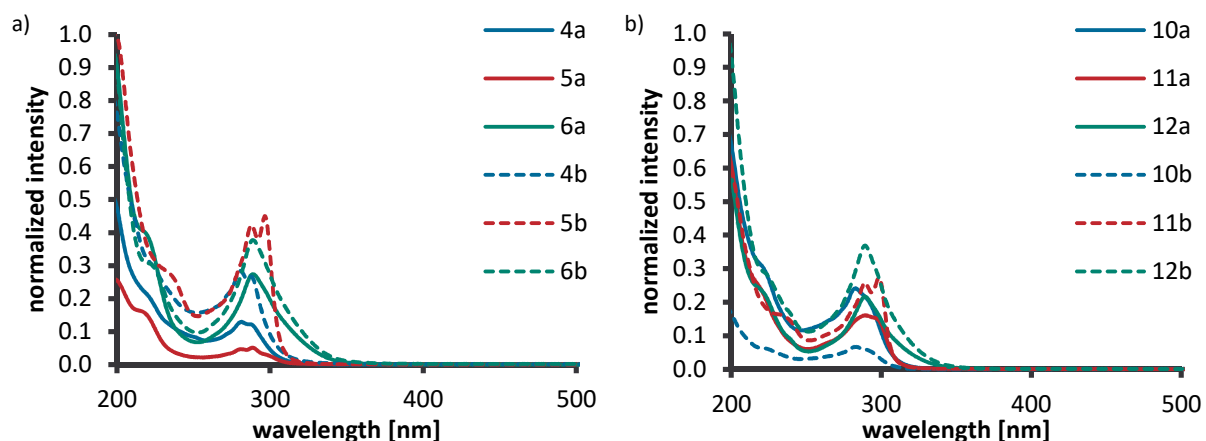


Figure 79: UV/Vis spectra of the complexes a) 4a,b – 6a,b and b) 10a,b – 12a,b; measured in acetonitrile at room temperature.

Excitation at the described wavelengths indeed leads to the intriguing emission spectra. For a better understanding of the following data, some emission spectra of the ligand precursors are given first. Both examples show strong emission bands at ~ 330 nm, which are mainly found for the methylene salts **1** and **7**. The other imidazolium compounds do show only minor emission maxima after excitation. Due to the fact, that we exclusively used bromide compounds the respective spectra for hexafluorophosphate are not available. Therefore the interaction with the counterions and the resulting influence to the fluorescence could not be evaluated. Comparing the fluorescence spectra of the imidazolium salts with the spectra of the corresponding complexes illustrates the impact of the metal centres (see Figure 80 as example for the imidazolium compounds, a detailed investigation of the ligand precursors was done before^[6] and is not part of this work).

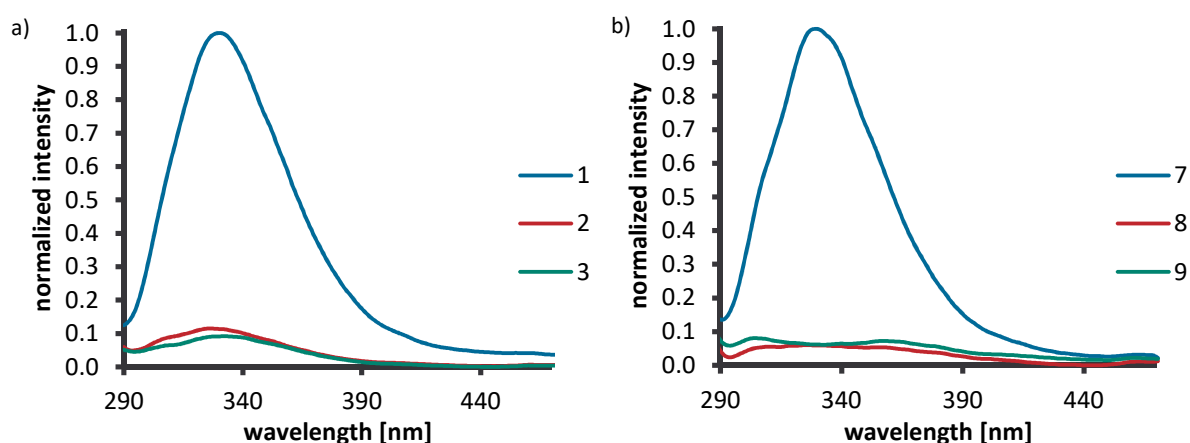


Figure 80: Fluorescence spectra of the ligand precursors a) **1** – **3** and b) **7** – **9**; measured in acetonitrile at room temperature after excitation at 255 nm.

Some of the fluorescence spectra of the complexes show a strong maximum between 350 and 400 nm after the excitation at 255 nm (imidazole) or 289 nm (benzimidazole) respectively, measured in acetonitrile. These were not visible in the spectra of the imidazolium compounds. Those emission bands are attributed to stable exciplexes ($^3[\text{do}^*\text{p}\sigma]$ excited state).^[4f,6,72-73,90] All complexes with a propylene linker have these strong emission maxima in common. Interestingly the maxima are also visible in the spectra of the ethylene imidazole complexes, while the benzimidazole derivatives are not emissive at the given

excitation (see Figure 81 and Figure 82). This behaviour implicates different transition processes inside the compounds. The herein demonstrated photophysical behaviour is attributed to the formation of aurophilic interactions. The formation of Au...Au interactions in these compounds could be explained by the flexibility of the propylene compounds and the resulting possibility of sandwich-like structures. This folding process of the complexes can be supported by the formation of hydrogen bonds with the counterions.^[7a] The ethylene complexes with an imidazolium moiety are also able to form similar exciplexes, but the sterically hindered benzimidazolium compounds are unlikely to promote this type of bonds. Even though the methylene complexes do show a demonstrative interplay with the counterions in solution (in the ¹H-NMR spectra), the attractive interactions of the gold centres seem hampered. This is probably determined by the more rigid N-(CH₂)-N angles and the resulting distances of the alkylene bridges. The emission band of the hexafluorophosphate compounds is always more intense than for the corresponding bromide complexes. Those differences occur via another aggregation behaviour of the counterions. This suggests a strong interaction of bromide with the complexes, that probably changes the Au...Au bonds. One possibility could be the penetration of the cavity by bromide, which would interrupt the aurophilic interactions.

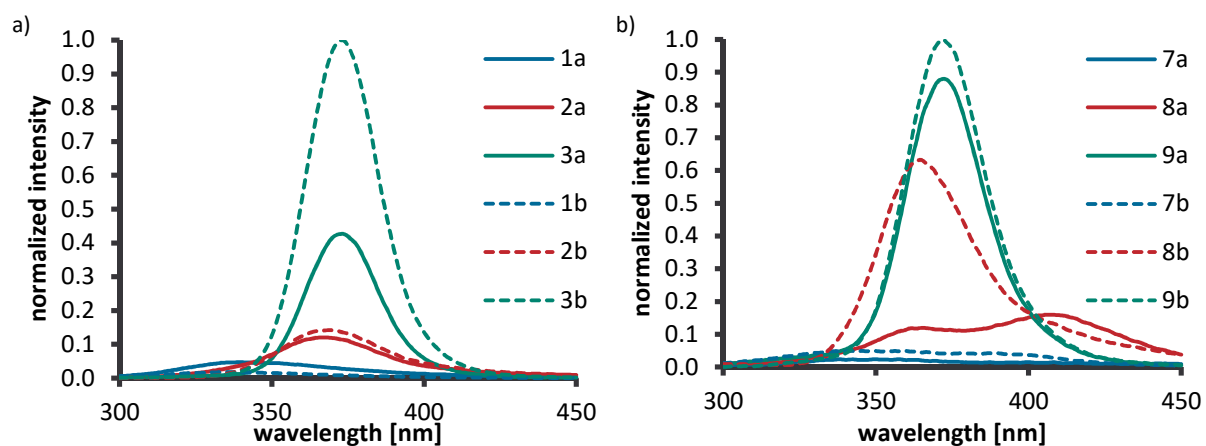


Figure 81: Fluorescence spectra of the complexes a) 1a,b – 3a,b and b) 7a,b – 9a,b; measured in acetonitrile at room temperature after excitation at 255 nm.

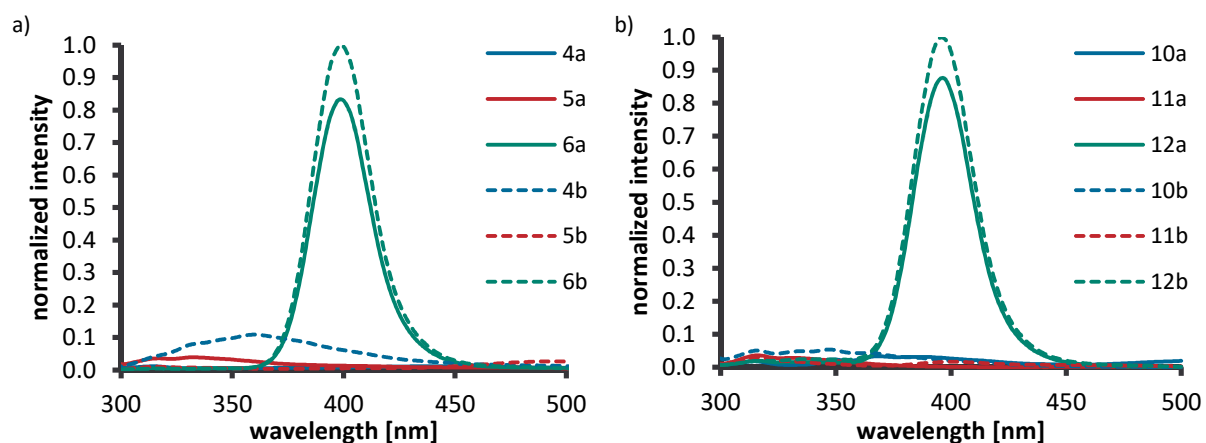


Figure 82: Fluorescence spectra of the complexes a) 4a,b – 6a,b and b) 10a,b – 12a,b; measured in acetonitrile at room temperature after excitation at 289 nm.

Regardless of that, similar emission maxima as seen for the ligand precursors at $\sim 330\text{-}360\text{ nm}$ are found in all spectra of the gold compounds **1a,b** – **12a,b** with moderate intensities. The intensity is the strongest for the methylene compounds **1a,b**; **4a,b**; **7a,b** and **10a,b**. The other curves tend to form shoulders at the given wavelength, which hints to the occurrence of different charge transfer processes at the same time. The simultaneous presence of ligand centred and metal perturbed transitions are already known for this type of compounds.^[4a,62f] The intensities of the curves for the bromide and hexafluorophosphate compounds are also varying, although without the clear correlation, which could be seen for the lower energy bands. The similarity of the emission bands in the spectra of the complexes and ligand precursors, suggest the occurrence of ligand centred transition processes.

As the next step, the correlation between the emission and the counterion should be further investigated. If the intensity changes are clearly assigned to the varying interaction with bromide and hexafluorophosphate, they should be controllable by adding those anions. A supposed reversibility of the effects should be examined by adding a huge excess of bromide to the solutions of both, the bromide and the hexafluorophosphate compounds. The interactions between the anions and the metal centres could affect the $\text{Au}\cdots\text{Au}$ bonds and therefore will probably have an impact on the fluorescence. Bromide is known to form association complexes with the cations and therefore quench the high energy emission.^[73] This leads to the formation of lower energy emission bands.^[12a,90d,90e] As expected the addition of 300 eq TBAB quenches this high energy emission (as seen before in Figure 81 and

Figure 82 for stoichiometric amounts), while a new maxima at ~ 460 nm for the complexes **1a,b** – **3a,b** (see Figure 83) and **7a,b** – **9a,b** (see Figure 84) is detectable. The maxima for the benzimidazole complexes **4a,b** – **6a,b** (see Figure 82) and **10a,b** – **12a,b** (see Figure 86) appear at ~ 540 nm. In the emission spectra are additional shoulders visible at roundly 350 nm. Those are comparable to the high energy emission of the ligand precursors, but the curves do not have a single maximum. Instead the emission shows several shoulders. This indicates different transfer processes at the same time, which are not necessarily the same as in the ligand precursors. This thesis is supported by the rising of the maxima for all compounds after adding bromide. This behaviour could possibly explained by an alteration of the Au...Au interaction by the aggregation of bromide. E.g. shortening of the bond distances, provoked by an interaction with the counterion alters the emission^[49a,91]. This is also an explanation for the already existing high energy emission bands of the methylene complexes. They are not as flexible as the complexes with longer alkylene chains for which reason the Au...Au distances could only be a little modified.

Similar to the complexes described by *Wedlock et al.*^[73], the complexes **1a,b** – **12a,b** do not show the strong emission at wavelengths over 400 nm without the addition of bromide. The fluorescence quenching performance is comparable to the effects observed in the NMR spectra of the complexes. The shifting of the proton resonances induced by the different counterions is reversible as expected and a stronger effect was again provoked by adding more of the better coordinating bromide, even though the intensity of the results are stronger for different chain lengths. While the shifting of the resonances in the NMR spectra is stronger for the methylene complexes, the fluorescence spectra of the propylene complexes show the most intense emission bands and changes of them. The quenching process after the addition of TBAB is more pronounced for the benzimidazolium complexes **4a,b** - **6a,b** and **10a,b** - **12a,b**. This interesting effect could be explained by additional H...Br bonds or anion... π interactions. Those attractive interactions support the aggregation of the counterions to the complexes.

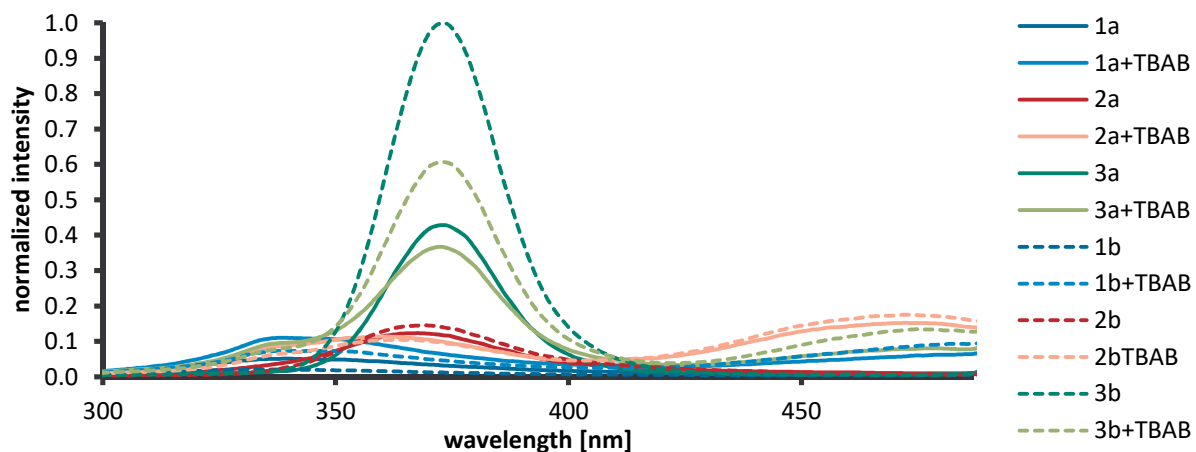


Figure 83: Fluorescence spectra of the complexes 1a,b – 3a,b (with TMAB addition); measured in acetonitrile at room temperature after excitation at 255 nm.

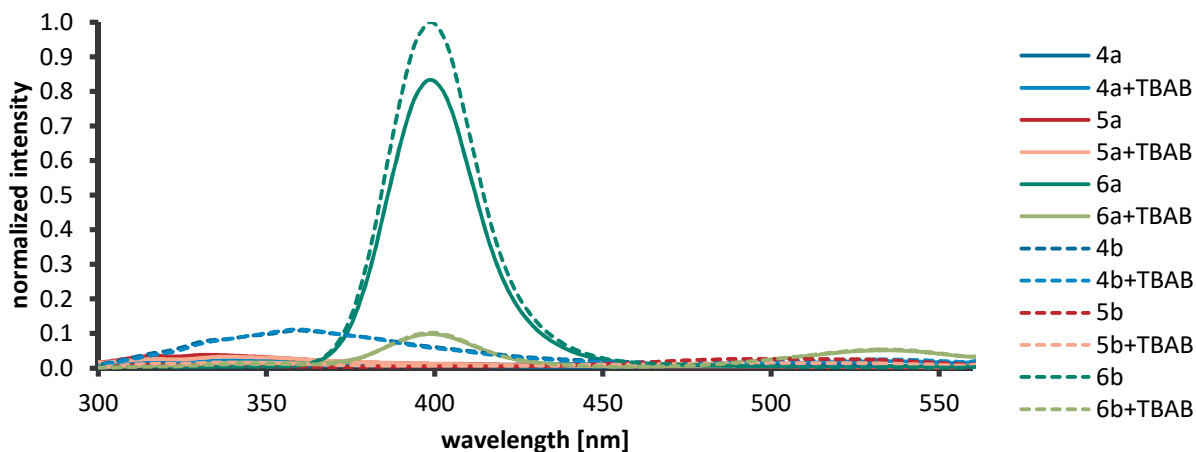


Figure 84: Fluorescence spectra of the complexes 4a,b – 6a,b (with TMAB addition); measured in acetonitrile at room temperature after excitation at 289 nm.

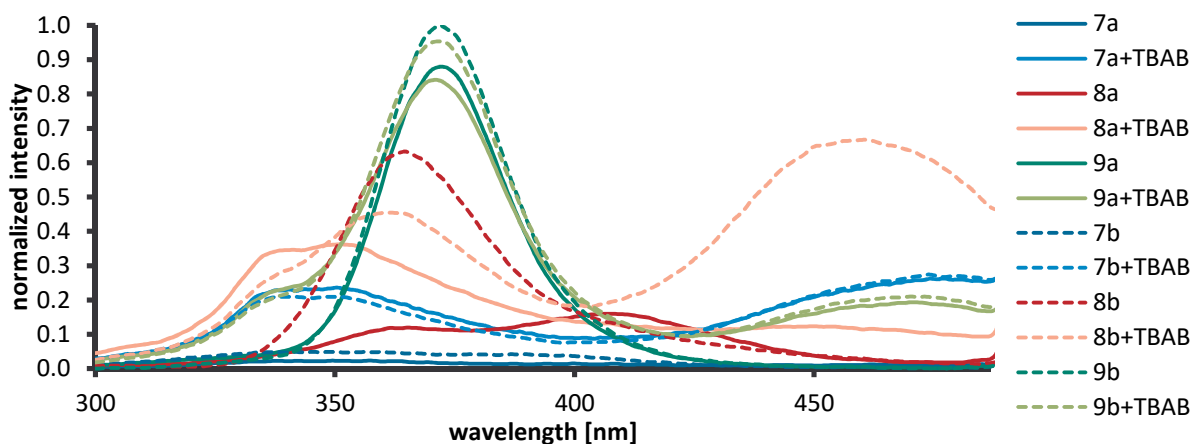


Figure 85: Fluorescence spectra of the complexes 7a,b – 9a,b (with TMAB addition); measured in acetonitrile at room temperature after excitation at 255 nm.

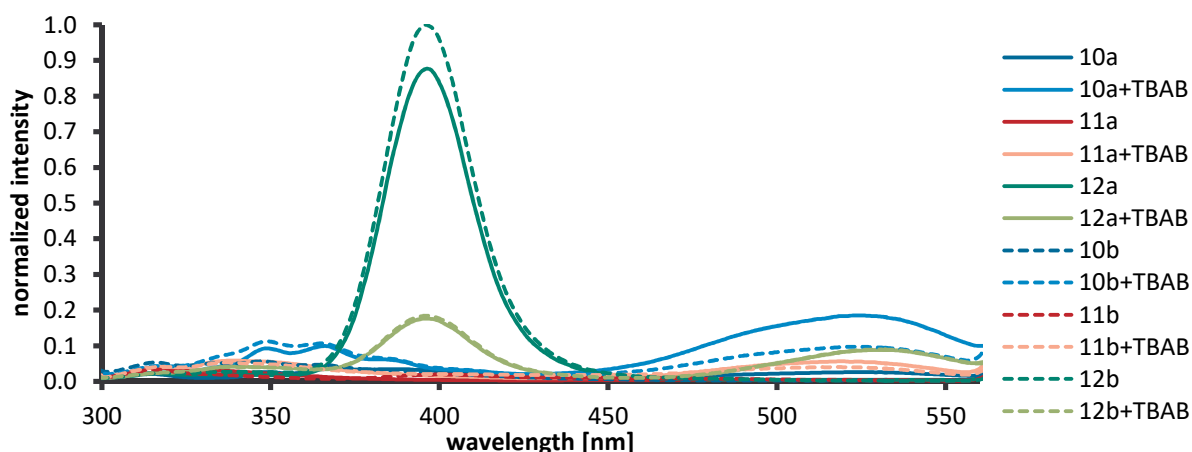


Figure 86: Fluorescence spectra of the complexes **10a,b** – **12a,b** (with TBAB addition); measured in acetonitrile at room temperature after excitation at 289 nm.

Adding silver salts to the solutions in acetonitrile did not yield evidence for Au...Ag interactions. In general a new absorption maximum was found at ~ 400 nm and the excitation at the given wavelength resulted in an emission band at ~ 560 nm. This behaviour was attributed to the formation of silver nano particles^[92] in the mixture.

The influence of the solvent was further investigated. Therefore additional absorption and emission spectra of the benzimidazole complexes **10a,b** – **12a,b** in methanol were measured. The alteration of the solvent did not change the location of the absorption bands but some intensities switched.

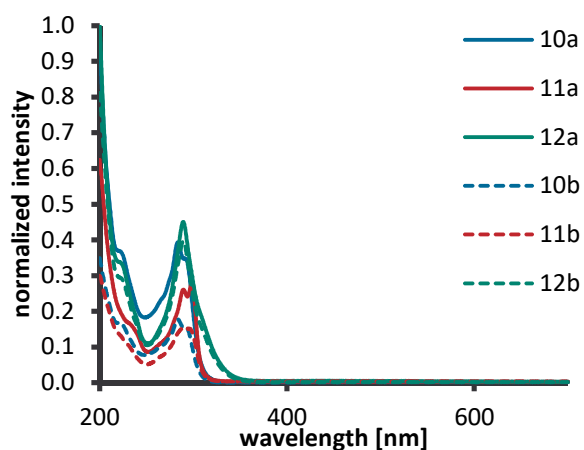


Figure 87: UV/Vis spectra of the complexes **10a,b** – **12a,b**; measured in methanol at room temperature.

The propylene complexes are also the strongest emitters in methanol. Interestingly the intensities of the bromide and hexafluorophosphate complexes are almost the same. This behaviour implies the interaction of methanol with the $^3[d\sigma^*p\sigma]$ excited state in a similar way as seen for bromide. Another possibility could be the solvation of either the counterion or the cations by methanol. This could hamper the folding of the complexes and therefore reduce the aurophilic interactions. A methanol molecule could also potentially lie inside the cavity and prevent the gold atoms from interacting. The luminescence of some gold(I) NHC compounds is known to be highly depending on the solvent, because the solvent molecules are aggregating to the complexes and could change the geometry. Sometime those interactions lead to shorter metallophilic bonds and those are reflected by an other emission behaviour.^[50]

Adding an excess of TBAB to the solutions of the complexes **10a,b** and **12a,b** (> 100 eq) causes a strong increase of the intensities of the shoulders at 350 nm (**10** = $[Au_2(\text{bisEt}_2\text{MeBim})_2]^{2+}$; **12** = $[Au_2(\text{bisEt}_2\text{PrBim})_2]^{2+}$). The excess of bromide also lead to the familiar maxima at 510 nm for the methylene (**10a,b**) and propylene (**12a,b**) complexes. This is in good agreement with the results of the complexes in acetonitrile. The corresponding ethylene complexes **11a,b** do only show weak luminescence (**11** = $[Au_2(\text{bisEt}_2\text{EtBim})_2]^{2+}$). These findings are similar to the published benzyl derivatives in methanol.^[72] Contrary to the bigger aromatic complexes in the literature, the here investigated complexes necessarily need the addition of a huge excess of bromide to be emissive at wavelengths over 500 nm. Even though the intensity of the maxima at 400 nm are not as high as seen for the measurements in acetonitrile, the maxima at 510 nm are more intense (in comparison with the lower energy emission).

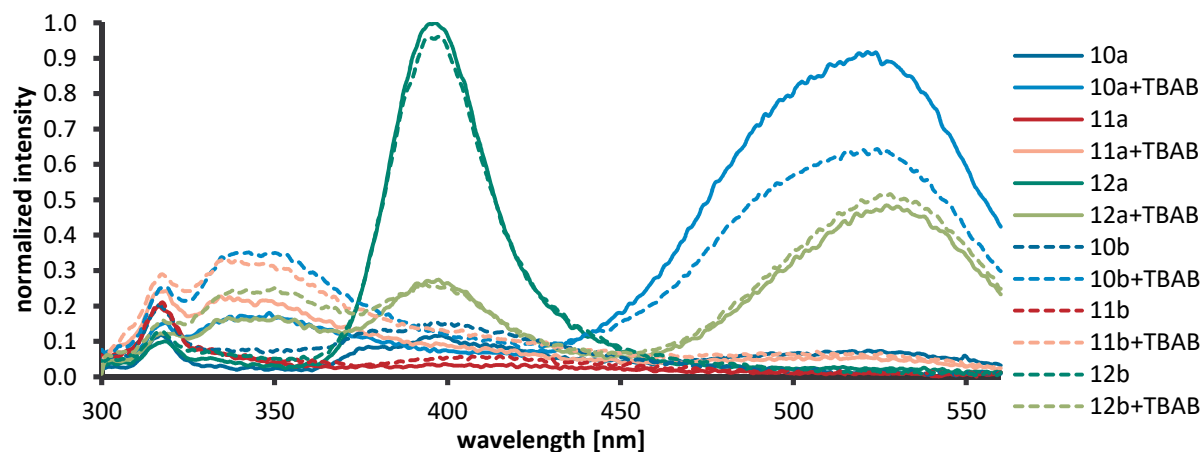


Figure 88: Fluorescence spectra of 10a,b - 12a,b (with TBAB addition); measured in methanol at room temperature after excitation at 290 nm.

Aggregation experiments in methanol are also different because the solvent itself can interact with the complexes and induce or change the phosphorescence.^[72,90d] Even though the investigated complexes do not contain the additional aromatic moieties, similar aggregation processes could be demonstrated. Therefore the herein presented Au(I) NHC compounds could provide interesting applications in the future. There are also several interesting examples of compounds with aggregated methanol or acetonitrile molecules in the literature.^[43b,50b,71]

3.6 Conclusion

The here presented work shows a clear connection between the counterions and the behaviour of the NHC complexes in solution and in solid state. Interactions with silver ions (and TBA⁺) could be excluded for the hereby used complexes.

Shifting of the proton resonances were observed by changing the counterions. All investigated counterions induced a downfield shift of some signals in comparison with the shifting of the corresponding signals of the complexes with the non coordinating PF₆⁻ anion (the anion affinity was ranked: PF₆⁻ < BF₄⁻ < OTf⁻ << NO₃⁻ ~ Br⁻). While the counterions provoked a notably shifting of the aromatic resonances of the imidazolium complexes, the shifting of the alkylene bridging protons were stronger for the benzimidazolium complexes. The wingtip substituents were almost not affected by this behaviour. This performance could be explained by different binding motifs. The bigger aromatic benzimidazolium units provide additional binding sites for anion••• π interactions but they also offer more steric hindered moieties. Additionally the protons are farther away from the metal centre and therefore less affected by an Au•••Au interaction. The effect of anion exchanges observed in the ¹H-NMR spectra is highly depending on the length of the linking alkylene chain and the NHC moiety. The methylene complexes show the strongest impact and shifting. This is attributed to the different flexibility of the compounds in solution.

The crystal structures of the investigated compounds provided a good overview of the dominating interacting between the cations and anions and even solvent molecules. Even though, the stabilisation is mainly based on hydrogen bonding between the cations and anions (and cocrystallized solvent molecules) as well as dominating intra- and intermolecular π stacking, we were able to find some examples with short distances between the Au centres and the counterions. The interactions of the gold atoms with other compounds like the counterions does usually weaken the Au-C bond or existing Au•••Au bonds, but we were not able to find such a trend inside the series. The structures are influenced by several interactions and packing effects. Those often hamper clear and simple correlation of a single bonding interaction in the crystal back to the configuration or conformation of the compounds. Aurophilic interactions in general play a minor part of most of the overall structures and they are mainly limited to the cations. The conformations of the cations with small linkers are often independent from the corresponding counterion, while longer linkers

provide different possible arrangements. Crystals including small anions as bromide often require additional solvent molecules in the structure. In contrast hexafluorophosphate complexes tend to grow in more clearly arranged structures. The NHC units of imidazolium complexes are often coplanar while the benzimidazolium derivatives show a bigger torsion angle, due to steric effects. However all analyzed differences including linker length, side chains, aromatic backbones and the anion types do change the structures. Some trends caused by the derivatization could be shown but there are also a few examples with unique properties. This is another evidence for the highly tuneable properties of the NHC complexes. Auophilic interactions are not limited to particular building blocks of the molecules, but originate from an interplay of the whole set of cations, anions and even the solvent.

UV/Vis experiments have shown strong absorption bands for the gold(I) NHC complexes which are attributed to metal perturbed π - π^* ligand centred transition processes. The corresponding emission spectra are more interesting. Excitation leads to the emission maxima between 350 and 400 nm for all propylene compounds and the imidazolium ethylene complexes (λ_{ex} (imidazolium)= 255 nm, λ_{ex} (benzimidazolium)= 289 nm). The corresponding benzimidazolium ethylene compounds are probably steric hindered and therefore not able to form the analogous auophilic interactions. The methylene compounds show a weak maximum at higher energies (~340-350 nm). The emission is explained by the formation of auophilic interactions ($^3[d\sigma^*p\sigma]$ excited state). Changing the counterion from bromide to hexafluorophosphate increases the intensity, due to different interactions with the counterions. The intense emission could also be quenched after the addition of a huge excess of bromide and new red shifted emission maxima occurred. This behaviour is attributed to the formation of an association aggregate with differing auophilic interactions. Further increases of the curves (including several maxima and shoulders) are seen at shorter wavelengths ~350 nm, as seen for the methylene complexes. Those emissions could be explained by the formation of auophilic interactions with different distances. The emission spectra of gold(I) NHC compounds are known to change with different Au...Au distances (e.g. forced by aggregation of additional molecules or temperature changes). The different bond lengths could be achieved by folding of the complexes. The propylene linker provides more flexibility than the methylene bridge. Therefore they are able to build sandwich like geometries. The ethylene compounds are also able to achieve folded or stretched

conformations. But they are not as flexible as the propylene compounds. Changing the solvent from acetonitrile to methanol slightly alters the emission behaviour of the complexes. Methanol does also form aggregates with the complexes and therefore quenches the emission provoked by Au...Au and Au...Br interactions. Hence methanol is not a good choice for aggregation experiments with the given gold(I) NHC complexes. In summary a strong interaction between the cations and anions (as well as the solvent) was proven by photophysical measurements.

Hence the intriguing aurophilic interactions could also be triggered in solution and not exclusively as short distances in the solid state. They are supported by the plausible NMR- and fluorescence experiments. Specific configurations of the complexes providing suitable host molecules seem promising. In view of the application as receptor molecule the best match depends also on the used analysis technique. While ^1H -NMR experiments provide stronger shifting of resonances from methylene complexes with bromide, the corresponding propylene compounds show distinct changes of the photophysical behaviour. In comparison with the NMR experiments those results are astonishing. While the emission behaviour of the propylene compounds changes visibly with the counterions, the proton resonances show only neglectable differences. The interaction of stoichiometric amounts of bromide with the complexes is therefore not strong enough to be observed in the NMR experiments. Investigations with higher bromide concentrations are interesting and planned for the future.

3.7 Experimental section

If not mentioned otherwise, all operations were performed under argon atmosphere using standard schlenk techniques with conventional glassware and dried solvents. Most solvents were dried, distilled, and stored under argon according to standard procedures. All starting materials were used as received from commercial sources. NMR data were recorded on a Bruker Avance 300 or 400 spectrometer at 25°C. The references for NMR spectra are as follows: ^1H (MeOD (3.31 ppm), DMSO-*d*₆ (2.50 ppm), CD₃CN (1.94 ppm)), $^{13}\text{C}\{^1\text{H}\}$ (MeOD (49.0 ppm), DMSO-*d*₆ (39.52 ppm), CD₃CN (118.26 ppm)).^[93] The spectroscopic characterization matches the reported data.^[10b-h] X-ray crystallographic data were collected on a Nonius Kappa CCD diffractometer at 123 K using graphite monochromated Mo- $K\alpha$ radiation ($\lambda = 0.71073 \text{ \AA}$) (**1a**, **2a**, **2b**, **3a**, **3b**, **10a**, **11a**, **12a**), a STOE IPDS2T diffractometer at 123 K (**5a**, **6a**), a Bruker D8-Venture at 100 K (**3c**, **4a**, **4b**, **5b**, **6b**, **7c**, **10b**, **10c**, **11b**), and a Bruker X8- KappaApexII diffractometer at 100 K (**1b**, **11c**, **12b**). Intensities were measured by fine-slicing ϕ - and ω -scans and corrected for background, polarization and Lorentz effects. A semi-empirical absorption correction was applied for the data sets following Blessing's method.^[94] The structures were solved by direct methods and refined anisotropically by the least squares procedure implemented in the ShelX program system.^[95] The hydrogen atoms were included isotropically using the riding model on the bound atoms.^[96] UV/Vis and fluorescence spectra were measured with 10^{-5} M solutions in ACN in precision cuvettes (SUPRASIL®) with 10 mm thickness. For UV/Vis measurements a Perkin Elmer Lambda 18 was used, for fluorescence a Perkin LS50B. Scan rate was 120 nm/s (200 nm - 700 nm).

The imidazolium/ benzimidazolium salts^[97] and the corresponding complexes **1a,b-3a,b**; **4a-6a**; **7a,b-9a,b** and **10a-12a** were synthesized according to the literature. The spectroscopic data agree with the previously reported.^[4f,6]

3c. 3a (19.0 mg, 1.97 μmol) was dissolved in a mixture of methanol, dichloromethane and acetonitrile (5 mL). A solution of NaBF₄ (10.8 mg, 9.80 μmol) in water (4 mL) was added to precipitate the corresponding complex. The white powder was filtered, washed with water and methanol and dried in vacuo. The complex was purified by crystallization (slow diffusion of diethyl ether into a solution in acetonitrile). Yield 55%. $^1\text{H-NMR}$ (500 MHz, DMSO-*d*₆, 298 K): δ =7.72 (d, $^3J(\text{H,H})=1.8 \text{ Hz}$, 4H; H-4), 7.59 (d, $^3J(\text{H,H})=1.8 \text{ Hz}$, 4H; H-5), 4.16 (m, 8H; H-6),

3.49 (s, 12H; H-8), 2.58 (m, 4H; H-7); $^{13}\text{C-NMR}$ (125 MHz, DMSO-*d*₆, 298 K): δ =181.9 (C-2), 124.3 (C-5), 121.2 (C-4), 46.3 (C-6), 36.7 (C-8), 30.7 (C-7); HR-ESI-MS(+) m/z : 401.1044 [M-2BF₄]²⁺, calc. for C₂₂H₃₂Au₂N₈²⁺: 401.1035; ESI-MS(-) m/z : 86.8 [BF₄].

4b. 4a (106.2 mg, 96.0 μmol) was dissolved in a mixture of methanol and dichloromethane (15 mL). A solution of KPF₆ (88.3 mg, 480 μmol) in water (3 mL) was added to precipitate the corresponding complex. The white powder was filtered, washed with water and methanol and dried in vacuo. The complex was purified by crystallization (slow diffusion of diethyl ether into a solution in acetonitrile). Yield 40%. $^1\text{H-NMR}$ (500 MHz, DMSO-*d*₆, 298 K): δ =8.10 (m, 4H; H-4), 7.93 (m, 4H; H7), 7.64 (m, 8H; H-5/6), 7.53 (m, 2H; H10a), 7.47 (m, 2H; H10b), 4.13 (s, 12H; H-11); $^{13}\text{C-NMR}$ (125 MHz, DMSO-*d*₆, 298 K): δ =190.2 (C-2), 133.6 (C-8 or C-9), 132.2 (C-8 or C-9), 125.8 (C-5 or C-6), 125.6 (C-5 or C-6), 113.2 (C-4 or C-7), 111.9 (C-4 or C-7), 66.0 (C-10), 35.8 (C-11); $^{19}\text{F-NMR}$ (470 MHz, DMSO-*d*₆, 298 K): δ =-70.1 (d); $^{31}\text{P-NMR}$ (202 MHz, DMSO-*d*₆, 298 K): δ =-144.2 (sept); HR-ESI-MS(+) m/z : 473.1012 calc. for C₃₄H₃₂Au₂N₈⁺: 473.1035 [M-2PF₆]⁺; ESI-MS(-) m/z : 144.1 [PF₆].

5b. 5a (55.9 mg, 49.2 μmol) was dissolved in mixture of methanol and dichloromethane (15 mL). A solution of KPF₆ (45.3 mg, 246 μmol) in water (2 mL) was added to precipitate the corresponding complex. The white powder was filtered, washed with water and methanol and dried in vacuo. The complex was purified by crystallization (slow diffusion of diethyl ether into a solution in acetonitrile). Yield 40%. $^1\text{H-NMR}$ (300 MHz, DMSO-*d*₆, 298 K): δ =7.71 (d, $^3J(\text{H,H})=8.1$ Hz, 4H; H-4 or H-7), 7.62 (d, $^3J(\text{H,H})=8.1$ Hz, 4H; H-4 or H-7), 7.46 (m, 8H; H-5 or H-6), 7.34 (m, 8H; H-5 or H-6), 5.37 (s, 8H; H-10), 4.00 (s, 12H; H-11); $^{13}\text{C-NMR}$ (125 MHz, DMSO-*d*₆, 298 K): δ =189.7 (C-2), 133.3 (C-8 or C-9), 132.7 (C-8 or C-9), 124.8 (C-5 or C-6), 124.6 (C-5 or C-6), 112.3 (C-4 or C-7), 111.5 (C-4 or C-7), 35.2 (C-10), 34.0 (C-11); $^{19}\text{F-NMR}$ (470 MHz, DMSO-*d*₆, 298 K): δ =-70.1 (d); $^{31}\text{P-NMR}$ (202 MHz, DMSO-*d*₆, 298 K): δ =-144.2 (sept); HR-ESI-MS(+) m/z : 487.1179 calc. for C₃₆H₃₆Au₂N₈⁺: 487.1192 [M-2PF₆]⁺; ESI-MS(-) m/z : 144.1 [PF₆].

6b. 6a (211 mg, 181 μmol) was dissolved in mixture of methanol and dichloromethane (15 mL). A solution of KPF₆ (167 mg, 905 μmol) in water (5 mL) was added to precipitate the corresponding complex. The white powder was filtered, washed with water and methanol and dried in vacuo. The complex was purified by crystallization (slow diffusion of diethyl ether into a solution in acetonitrile). Yield 26%. $^1\text{H-NMR}$ (500 MHz, DMSO-*d*₆, 298 K): δ =7.68

(d, $^3J(\text{H,H})=8.2$ Hz, 4H; H-4 or H-7), 7.58 (d, $^3J(\text{H,H})=8.2$ Hz, 4H; H-4 or H-7), 7.31 (dd, $^3J(\text{H,H})=7.8$ Hz, 8H; H-5 or H-6), 7.21 (dd, $^3J(\text{H,H})=7.8$ Hz, 8H; H-5 or H-6), 4.93 (t, 8H; H-10), 3.98 (s, 12H; H-12), 3.05 (m, 4H; H-11); $^{13}\text{C-NMR}$ (125 MHz, DMSO-*d*₆, 298 K): $\delta=189.1$ (C-2), 133.3 (C-9), 131.9 (C-8), 124.5 (C-5), 124.3 (C-6), 112.5 (C-4 or C-7), 111.7 (C-4 or C-7), 48.0 (C-10), 34.7 (C-12), 25.7 (C-11); $^{19}\text{F-NMR}$ (470 MHz, DMSO-*d*₆, 298 K): $\delta=-70.1$ (d); $^{31}\text{P-NMR}$ (202 MHz, DMSO-*d*₆, 298 K): $\delta=-144.2$ (sept); HR-ESI-MS(+) *m/z*: 501.1325 calc. for $\text{C}_{38}\text{H}_{40}\text{Au}_2\text{N}_8^+$: 501.1348 [M-2PF₆]⁺; ESI-MS(-) *m/z*: 144.1 [PF₆]⁻.

10b. 10a (35.7 mg, 30.7 μmol) was dissolved in mixture of methanol and dichloromethane (15 mL). A solution of KPF₆ (28.3 mg, 154 μmol) in water (2 mL) was added to precipitate the corresponding complex. The white powder was filtered, washed with water and methanol and dried in vacuo. The complex was purified by crystallization (slow diffusion of diethyl ether into a solution in acetonitrile). Yield 71%. $^1\text{H-NMR}$ (400 MHz, DMSO-*d*₆, 298 K): $\delta=8.10$ (d, $^3J(\text{H,H})=8$ Hz, 4H; H-4), 8.02 (d, $^3J(\text{H,H})=8$ Hz, 4H; H-7), 7.64 (m, 8H; H-5, H-6), 7.54 (d, $^2J(\text{H,H})=13.8$ Hz 2H; H10a), 7.44 (d, $^2J(\text{H,H})=13.8$ Hz, 2H; H-10b), 4.64 (q, $^3J(\text{H,H})=7$ Hz 8H; H-11), 1.45 (t, $^3J(\text{H,H})=7$ Hz, 12H; H-12); $^{13}\text{C-NMR}$ (175 MHz, DMSO-*d*₆, 298 K): $\delta=190.2$ (C-2), 132.9 (C-8 or C-9), 132.8 (C-8 or C-9), 126.3 (C-5 or C-6), 126.2 (C-5 or C-6), 113.4 (C-4 or C-7), 112.3 (C-4 or C-7), 58.8 (C-10), 44.8 (C-11), 16.1 (C-12); $^{19}\text{F-NMR}$ (202 MHz, DMSO-*d*₆, 298 K): $\delta=-70.1$ (d); $^{31}\text{P-NMR}$ (470 MHz, DMSO-*d*₆, 298 K): $\delta=-144.3$ (sept); HR-ESI-MS(+) *m/z*: 501.1316 calc. for $\text{C}_{38}\text{H}_{40}\text{Au}_2\text{N}_8^{2+}$: 501.1348 [M-2PF₆]⁺; ESI-MS(-) *m/z*: 144.9 [PF₆]⁻.

11b. 11a (152 mg, 128 μmol) was dissolved in mixture of methanol and dichloromethane (15 mL). A solution of KPF₆ (118 mg, 638 μmol) in water (4 mL) was added to precipitate the corresponding complex. The white powder was filtered, washed with water and methanol and dried in vacuo. The complex was purified by crystallization (slow diffusion of diethyl ether into a solution in acetonitrile). Yield 43%. $^1\text{H-NMR}$ (500 MHz, DMSO-*d*₆, 298 K): $\delta=7.77$ (d, $^3J(\text{H,H})=8.3$ Hz, 4H; H-4 or H-7), 7.55 (d, $^3J(\text{H,H})=8.3$ Hz, 4H; H-4 or H-7) 7.32 (m, 4H; H-5 or H-6), 7.45 (m, 4H; H-5 or H-6), 5.36 (bs, 8H; H-10), 4.48 (q, $^3J(\text{H,H})=7.2$ Hz, 8H; H-11), 1.17 (t, $^3J(\text{H,H})=7.2$ Hz, 12H; H-12); $^{13}\text{C-NMR}$ (125 MHz, DMSO-*d*₆, 298 K): $\delta=189.2$ (C-2), 132.7 (C-8 or C-9), 132.1 (C-8 or C-9), 124.9 (C-5 or C-6), 124.6 (C-5 or C-6), 112.1 (C-4 or C-7), 111.7 (C-4 or C-7), 46.6 (C-10), 43.4 (C-11), 30.7 (C-12); $^{19}\text{F-NMR}$ (470 MHz, DMSO-*d*₆, 298 K): $\delta=-70.1$ (d); $^{31}\text{P-NMR}$ (202 MHz, DMSO-*d*₆, 298 K): $\delta=-144.2$ (sept); HR-ESI-MS(+) *m/z*: 515.1749 calc. for $\text{C}_{40}\text{H}_{44}\text{Au}_2\text{N}_8^{2+}$: 515.1505 [M-2PF₆]⁺; ESI-MS(-) *m/z*: 145.0 [PF₆]⁻.

12b. 12a (197 mg, 162 μmol) was dissolved in mixture of methanol and dichloromethane (15 mL). A solution of KPF_6 (149 mg, 810 μmol) in water (8 mL) was added to precipitate the corresponding complex. The white powder was filtered, washed with water and methanol and dried in vacuo. The complex was purified by crystallization (slow diffusion of diethyl ether into a solution in acetonitrile). Yield 36%. $^1\text{H-NMR}$ (500 MHz, $\text{DMSO-}d_6$, 298 K): $\delta=7.75$ (d, $^3J(\text{H,H})=8.15$ Hz, 4H; H-7), 7.68 (d, $^3J(\text{H,H})=8.15$ Hz, 4H; H-4), 7.34 (m, 4H; H-5, H-6), 7.28 (m, 4H; H-5, H-6), 4.97 (t, $^3J(\text{H,H})=6.30$ Hz, 8H; H-10), 4.52 (q, $^3J(\text{H,H})=6.70$ Hz, 8H; H-12), 3.01 (m, 4H; H-11), 1.39 (t, $^3J(\text{H,H})=7.15$ Hz, 12H; H-13); $^{13}\text{C-NMR}$ (125 MHz, $\text{DMSO-}d_6$, 298 K): $\delta=189.1$ (C-2), 132.2 (C-8), 132.2 (C-9), 124.7 (C-5), 124.5 (C-6), 112.6 (C-7), 111.7 (C-4), 48.0 (C-10), 43.3 (C-12), 27.0 (C-11), 15.8 (C-13); $^{19}\text{F-NMR}$ (470 MHz, $\text{DMSO-}d_6$, 298 K): $\delta=-70.1$ (d); $^{31}\text{P-NMR}$ (202 MHz, $\text{DMSO-}d_6$, 298 K): $\delta=-144.2$ (sept); HR-ESI-MS(+) m/z : 529.1618 calc. for $\text{C}_{42}\text{H}_{48}\text{Au}_2\text{N}_8^{2+}$: 529.1661 [M-2PF_6] $^+$; ESI-MS(-) m/z : 144.1 [PF_6] $^-$.

3.8 Appendix

Table 5: Crystallographic Data.

	1a	2a	3a
formula	$C_{18}H_{24}Au_2Br_2N_8$	$C_{20}H_{28}Au_2Br_2N_8$	$C_{23}H_{36}Au_2Br_2N_8$
cryst size [mm ³]	0.25 x 0.08 x 0.06	0.34 x 0.20 x 0.04	0.21 x 0.10 x 0.06
cryst syst	triclinic	triclinic	monoclinic
space group	$P\bar{1}$	$P\bar{1}$	$C2/c$
<i>a</i> [Å]	7.5549(9)	9.7703(7)	13.1421(11)
<i>b</i> [Å]	12.2807(14)	11.2794(8)	17.5172(16)
<i>c</i> [Å]	13.3725(17)	12.7721(9)	13.8320(11)
α [°]	70.942(4)	71.643(2)	90
β [°]	82.744(4)	69.989(2)	117.786(2)
γ [°]	88.960(4)	82.087(3)	90
<i>V</i> [Å ³]	1162.9(2)	1254.54(15)	2817.1(4)
<i>Z</i>	2	2	4
ρ_{calc} [mg m ³]	2.588	2.473	2.344
<i>F</i> ₀₀₀	832	864	1864
μ [mm ⁻¹]	16.059	14.891	13.273
θ range [°]	2.75 - 27.48	2.20 - 28.00	2.11 - 28.00
reflns collected	48844	39576	31616
reflns unique	5280	6001	3418
<i>R</i> _{int}	0.0608	0.0764	0.0780
GOF	1.052	1.054	1.024
refined params	275	296	171
<i>R</i> 1 [<i>I</i> > 2 σ (<i>I</i>)]	0.0368	0.0556	0.0684
w <i>R</i> 2 (all data)	0.0943	0.1658	0.1770
largest diff peak [e Å ⁻³]	2.866/ -1.995	4.633/ -5.692	6.610/ -3.738

	1b	2b	3b
formula	$C_{18}H_{24}Au_2F_{12}N_8P_2$	$C_{20}H_{28}Au_2F_{12}N_8P_2$	$C_{22}H_{32}Au_2F_{12}N_8P_2$
cryst size [mm ³]	0.12 x 0.06 x 0.05	0.40 x 0.34 x 0.15	0.20 x 0.16 x 0.08
cryst syst	monoclinic	monoclinic	hexagonal
space group	<i>C2/m</i>	<i>C2/m</i>	<i>P3₁12</i>
<i>a</i> [Å]	17.0766(5)	14.2284(8)	11.9420(2)
<i>b</i> [Å]	13.3831(4)	13.1742(5)	11.9420(2)
<i>c</i> [Å]	12.7710(4)	8.6638(5)	18.9955(4)
α [°]	90	90	90
β [°]	105.0990(10)	116.197(2)	90
γ [°]	90	90	120
<i>V</i> [Å ³]	2817.90(15)	1457.19(13)	2346.04(7)
<i>Z</i>	4	2	3
ρ_{calc} [mg m ³]	2.443	2.426	2.320
<i>F</i> ₀₀₀	1936	1000	1548
μ [mm ⁻¹]	10.620	10.272	9.574
θ range [°]	3.04 - 27.99	2.62 - 27.00	1.07 - 28.00
reflns collected	3534	4940	30574
reflns unique	3536	1653	3780
<i>R</i> _{int}	0.0449	0.0512	0.0676
GOF	1.218	1.061	1.029
refined params	211	110	212
<i>R</i> 1 [<i>I</i> >2 σ (<i>I</i>)]	0.0187	0.0287	0.0246
w <i>R</i> 2 (all data)	0.0540	0.0645	0.0522
largest diff peak [e Å ⁻³]	1.243/ -0.914	1.959/ -2.517	0.756/ -0.934

	4a	5a	6a
formula	$2\text{C}_{34}\text{H}_{32}\text{Au}_2\text{Br}_2\text{N}_8$	* $\text{C}_{36}\text{H}_{36}\text{Au}_2\text{Br}_2\text{N}_8$ * $2\text{CH}_3\text{OH}$	$\text{C}_{38}\text{H}_{40}\text{Au}_2\text{Br}_2\text{N}_8$ * Et_2O
cryst size [mm^3]	$0.15 \times 0.08 \times 0.07$	$0.24 \times 0.12 \times 0.1$	$0.06 \times 0.03 \times 0.02$
cryst syst	triclinic	triclinic	monoclinic
space group	$\text{P}\bar{1}$	$\text{P}\bar{1}$	C2/c
a [\AA]	10.195(2)	9.4157(5)	26.092(3)
b [\AA]	13.426(3)	9.3416(5)	11.4454(14)
c [\AA]	17.046(3)	22.4692(11)	18.010(3)
α [$^\circ$]	74.219(10)	94.007(4)	90
β [$^\circ$]	73.143(11)	97.240(4)	128.499(9)
γ [$^\circ$]	71.246(8)	95.609(4)	90
V [\AA^3]	2072.9(7)	1944.42(18)	4209.2(11)
Z	1	2	4
ρ_{calc} [mg m^{-3}]	2.004	2.047	1.951
F_{000}	1202.0	1144.0	2376
μ [mm^{-1}]	9.048	9.636	8.905
θ range [$^\circ$]	4.328 – 55.996	5.328 - 55.996	2.84 - 28.00
reflns collected	76152	18344	21810
reflns unique	10019	9283	5072
R_{int}	0.1191	0.1179	0.2344
GOF	1.374	1.143	0.897
refined params	516	473	273
R1 [$I > 2\sigma(I)$]	0.1129	0.1029	0.0747
wR2 (all data)	0.3318	0.2701	0.1859
largest diff peak [$e \text{\AA}^{-3}$]	14.98/ -11.42	7.78/ -6.91	1.750/ -3.004

	4b	5b	6b
formula	$C_{34}H_{32}Au_2F_{12}N_8P_2$	$C_{36}H_{36}Au_2F_{12}N_8P_2$	$C_{38}H_{40}Au_2F_{12}N_8P_2$
cryst size [mm ³]	0.09 × 0.05 × 0.03	0.05 × 0.04 × 0.02	0.1 × 0.09 × 0.06
cryst syst	monoclinic	triclinic	monoclinic
space group	<i>C2/c</i>	$P\bar{1}$	<i>C2/c</i>
<i>a</i> [Å]	13.0173(8)	10.4218(11)	24.049(3)
<i>b</i> [Å]	15.8980(10)	11.8946(13)	6.9030(7)
<i>c</i> [Å]	18.0103(10)	17.3704(18)	23.604(2)
α [°]	90	90.032(7)	90
β [°]	92.878(3)	94.993(7)	92.519(3)
γ [°]	90	108.372(6)	90
<i>V</i> [Å ³]	3722.5(4)	2034.9(4)	3914.7(7)
<i>Z</i>	4	2	4
ρ_{calc} [mg m ³]	2.206	2.064	1.947
<i>F</i> ₀₀₀	2352.0	1208.0	2204.0
μ [mm ⁻¹]	16.333	14.957	7.596
θ range [°]	8.786 - 135.462	7.836 - 144.754	4.734 - 55.998
reflns collected	22110	53646	53362
reflns unique	3381	7913	4713
<i>R</i> _{int}	0.0638	0.0886	0.0684
GOF	1.033	1.134	1.173
refined params	266	545	252
<i>R</i> 1 [<i>I</i> > 2 σ (<i>I</i>)]	0.0768	0.0899	0.0668
w <i>R</i> 2 (all data)	0.2055	0.2171	0.1520
largest diff peak [e Å ⁻³]	6.42/ -4.60	6.30/ -3.38	6.90/ -3.34

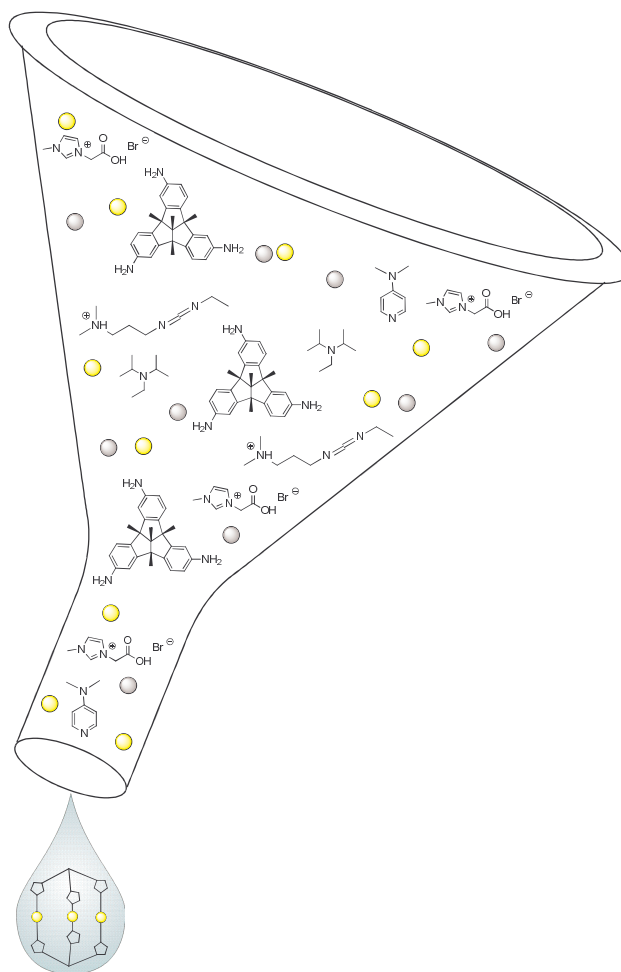
	10a	11a	12a
formula	$C_{38}H_{40}Au_2Br_2N_8 \cdot CH_3OH$	$C_{40}H_{44}Au_2Br_2N_8 \cdot CH_3OH$	$C_{42}H_{48}Au_2Br_2N_8$
cryst size [mm ³]	0.28 x 0.07 x 0.06	0.38 x 0.18 x 0.06	0.41 x 0.11 x 0.10
cryst syst	monoclinic	monoclinic	triclinic
space group	<i>C2/c</i>	<i>C2/c</i>	$P\bar{1}$
<i>a</i> [Å]	26.1417(6)	22.3983(13)	9.0687(3)
<i>b</i> [Å]	19.0405(6)	12.5583(6)	9.3648(3)
<i>c</i> [Å]	19.1794(5)	17.8798(10)	12.6898(3)
α [°]	90	90	105.1110(18)
β [°]	120.9390(14)	120.889(2)	91.103(2)
γ [°]	90	90	95.9969(18)
<i>V</i> [Å ³]	8188.2(4)	4316.0(4)	1033.53(5)
<i>Z</i>	8	4	1
ρ_{calc} [mg m ³]	1.938	1.946	1.958
<i>F</i> ₀₀₀	4560	2440	584
μ [mm ⁻¹]	9.151	8.687	9.063
θ range [°]	2.41 - 27.00	2.65 - 27.00	3.02 - 28.00
reflns collected	26370	13633	14553
reflns unique	8849	4633	4855
<i>R</i> _{int}	0.0659	0.0518	0.0682
GOF	0.955	1.082	1.002
refined params	475	315	247
<i>R</i> 1 [<i>I</i> > 2 σ (<i>I</i>)]	0.0334	0.0524	0.0296
w <i>R</i> 2 (all data)	0.0786	0.1318	0.0639
largest diff peak [e Å ⁻³]	1.058/ -2.106	2.249/ -2.964	1.324/ -3.329

	10b	11b	12b
formula	$C_{38}H_{40}Au_2F_{12}N_8P_2$	$C_{40}H_{44}Au_2F_{12}N_8P_2 \cdot CH_3CN$	$C_{42}H_{48}Au_2F_{12}N_8P_2$
cryst size [mm ³]	0.16 × 0.08 × 0.04	0.18 × 0.09 × 0.02	0.2 × 0.05 × 0.02
cryst syst	orthorhombic	triclinic	orthorhombic
space group	Pccn	$P\bar{1}$	C222
<i>a</i> [Å]	26.4253(14)	13.0703(7)	7.459(5)
<i>b</i> [Å]	9.1729(5)	13.1182(8)	17.896(14)
<i>c</i> [Å]	16.7495(9)	16.8388(10)	17.359(12)
α [°]	90	68.526(3)	90
β [°]	90	89.683(3)	90
γ [°]	90	67.738(3)	90
<i>V</i> [Å ³]	4060.0(4)	2456.6(3)	2317(3)
Z	4	2	2
ρ_{calc} [mg m ³]	2.115	1.896	1.933
<i>F</i> ₀₀₀	2480.0	1360.0	1304.0
μ [mm ⁻¹]	15.011	6.120	6.482
θ range [°]	6.69 - 135.49	4.616 - 61.192	4.552 - 50.488
reflns collected	117466	116270	1154
reflns unique	3673	15060	1154
<i>R</i> _{int}	0.0769	0.1529	0.2668
GOF	1.100	1.011	1.714
refined params	282	637	143
R1 [<i>I</i> > 2 σ (<i>I</i>)]	0.0386	0.0416	0.1839
wR2 (all data)	0.0997	0.0900	0.4476
largest diff peak [e Å ⁻³]	4.84/ -1.87	2.35/ -2.68	8.96/ -5.81

	3c	4c	5c
formula	$C_{22}H_{32}Au_2B_2F_8N_8$	$C_{38}H_{40}Au_2F_4N_8O_4P_2$	$C_{40}H_{44}Au_2F_4N_8O_4P_2$
cryst size [mm ³]	0.21 x 0.04 x 0.03	0.11 × 0.09 × 0.04	0.12 × 0.08 × 0.06
cryst syst	Pbcn	Pccn	C2/c
space group	orthorhombic	orthorhombic	monoclinic
<i>a</i> [Å]	19.5638(16)	26.4711(12)	40.2611(15)
<i>b</i> [Å]	11.3981(11)	9.2158(4)	25.4128(10)
<i>c</i> [Å]	13.1715(10)	16.1720(6)	18.4631(8)
α [°]	90	90	90
β [°]	90	90	108.480(2)
γ [°]	90	90	90
<i>V</i> [Å ³]	2937.1(4)	3945.2(3)	17916.4(13)
<i>Z</i>	4	4	2
ρ_{calc} [mg m ³]	2.207	2.028	1.828
<i>F</i> ₀₀₀	1840.0	2320.0	9536.0
μ [mm ⁻¹]	10.058	15.167	13.376
θ range [°]	5.164 - 54	10.164 - 134.986	4.176 - 135.488
reflns collected	24390	11539	202505
reflns unique	3210	3242	16236
<i>R</i> _{int}	0.0595	0.2768	0.1630
GOF	1.093	1.019	1.038
refined params	241	264	1162
<i>R</i> 1 [<i>I</i> > 2 σ (<i>I</i>)]	0.0416	0.1033	0.0815
w <i>R</i> 2 (all data)	0.0861	0.2969	0.2196
largest diff peak [e Å ⁻³]	1.67/ -2.73	4.81/ -7.52	3.52/ -6.96

	7c
formula	C₂₂H₃₂Au₂N₉O₆ * CH₃CN
cryst size [mm ³]	0.25 × 0.2 × 0.13
cryst syst	monoclinic
space group	<i>P2₁/n</i>
<i>a</i> [Å]	9.4523(3)
<i>b</i> [Å]	13.2133(4)
<i>c</i> [Å]	24.8558(7)
α [°]	90
β [°]	96.8367(11)
γ [°]	90
<i>V</i> [Å ³]	3082.32(16)
<i>Z</i>	4
ρ_{calc} [mg m ³]	2.085
<i>F</i> ₀₀₀	1848.0
μ [mm ⁻¹]	9.565
θ range [°]	5.324 - 55.99
reflns collected	60952
reflns unique	7431
<i>R</i> _{int}	0.0660
GOF	1.042
refined params	422
<i>R</i> 1 [<i>I</i> > 2 σ (<i>I</i>)]	0.0253
w <i>R</i> 2 (all data)	0.0595
largest diff peak [e Å ⁻³]	1.25/ -1.31

4 Synthesis and characterization of trinuclear Ag(I) NHC-tribenzotriquinacene and Au(I) NHC tribenzotriquinacene cages as supramolecular host molecules



4.1 Introduction

The main goal of this work is the synthesis of a homoleptic metal organic assembly with three gold(I) atoms and several additional secondary binding sites. The metal centres should be linked by NHC ligands. The planned cage structure could potentially act as a host for small guest molecules or ions. Imidazolium compounds as ligand precursors can bear multiple substituents and therefore provide a couple of different interesting binding sites. Supramolecular interactions can involve several diverse non covalent bonding types. Next to hydrogen bonding, ion \cdots ion -, cation \cdots π -, anion \cdots π - and $\pi\cdots\pi$ - interactions some others are possible.^[98] The containing gold atoms are also possible donor atoms for intriguing

aurophilic interactions.^[5] In a previous work, vanadium and titanium were tested as a second metal centre for a bimetallic cage molecule.^[99] Both of the metals provide interesting properties and applications fields.^[100] Different routes for the synthesis of these host molecules have been tested. Promising ligand precursors were obtained from 1-methylimidazole and 2-bromoethanol. The tested reactions of these imidazolium salts with the metal compounds lead to air and moisture sensitive species. Those products could only be handled in an argon atmosphere with extra dry solvents. These conditions are unhandy for the intended application as sensor. Analytical experiments would be hindered and the dissociation of the compounds would lead to misinterpretation. Therefore the concept of a bimetallic receptor was dropped and a more stable structure was aimed. More simple and less labile organometallic NHC compounds only based on coinage metals could overcome this stability problem.

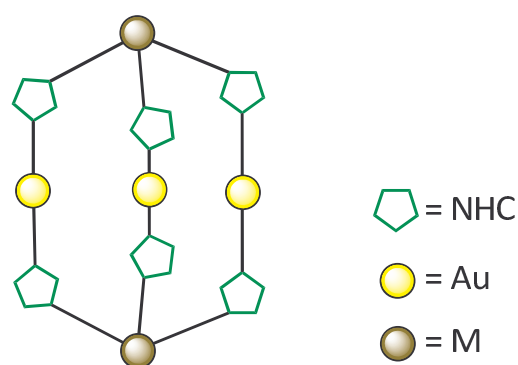


Figure 89: Former planned design of the trinuclear gold(I) NHC cage structure with two additional metal atoms for a bimetallic sensor molecule (M = V, Ti).

The potential application as supramolecular sensor is often combined with an intriguing spectroscopical behaviour. The complexation of a guest inside the intrinsic designed cavity could trigger fluorescence or fluorescence quenching, occurring from metallophilic $d^{10} - d^{10}$ interactions. Therefore the aggregation becomes visible. The high stability of Au(I) NHC complexes assures long term applications and the fascinating host-guest interactions based on supramolecular interaction are reversible, which provides reusable receptor molecules.

There are two possible pathways for the visible recognition of a guest molecule by aurophilic interactions, which are often joined by significant changes of the geometry:

- If the distances between the gold atoms inside the cavity of the host molecules are small enough to generate Au...Au interactions they could be interrupted by a guest molecule.
- If the Au...Au distances inside the cage are too long for aurophilic interactions, the aggregation of a guest molecule could lead to interactions with the gold atoms.

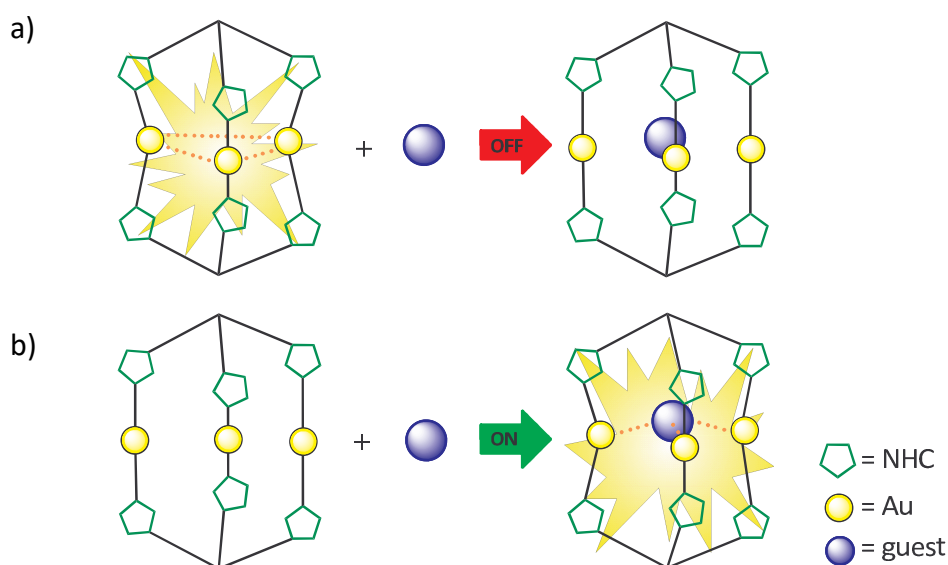
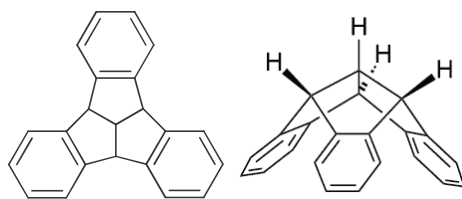


Figure 90: Recognition of a guest molecule inside the host cage accompanied with a) luminescence quenching or b) activation of aurophilic interaction and luminescence.

A multitude of examples for both types of sensor host-guest assemblies are known to the literature. E.g. *Yam et al.* developed a chemosensor for silver ions, based on a calix[4]arene structure.^[101] Beside them, some more specific cation binding host molecules are discovered.^[102] *Pöthig et al.* designed a new tube shaped cage molecule containing gold and macrocyclic ligands.^[4h] Due to the similarity to pillar[*n*]arenes and the metal complex structure they called them pillarplexes. These metallocavitands work highly selective as receptor for linear organic molecules.^[103] The penetration of the cavity goes in with a luminescence quenching. Several examples of C_3 symmetrical structures with different atoms or moieties as linker are well documented in the literature. Boron^[104], carbon^[105] or nitrogen^[106] as well as aromatic systems^[107] are possible as centre piece of the ligands. Some of these molecules are rigid and not able to change the structure. Therefore they are

not able to form short Au...Au distances and to enable aurophilic interactions. So next to the described functional sensor complexes are some examples of non luminescent compounds known. E.g. *Meyer et al.* synthesized a trinuclear metal complex with two tripod ligands resulting in a windmill analogue structure.^[108] The short alkyl chains promote the rigid configuration with long Au...Au distances over 5 Å. Therefore the metal centres cannot induce aurophilic interactions. Fascinating cone shaped NHC compounds as tetrakis(methylimidazolium) calix[4]arenes are also able to bind small molecules as anions.^[109] *Bullough et al.* have shown the successful binding of several anions such as bromide, chloride, nitrate, acetate and dihydrogen phosphate. The aggregation is accompanied by significant shifting of some signals in the ¹H-NMR spectra and permit job plot analysis by NMR titration. Host-guest interactions of metal free imidazolium compounds are also possible but do not provide the interesting fluorescence behaviour, due to the lack of metallophilic interactions. However these investigations and other examples in the literature^[84b,110] prove that NHC compounds are able to provide additional binding sites and encourage aggregation processes.

The purpose of this work was the generation of a tripodal imidazolium compound and the subsequent conversion to a trinuclear gold(I) NHC complex. The backbone of the ligand precursors should be completely organic and preferably rigid with additional flexible NHC units. A not too flexible structure provides a better preorganisation and prevents the formation of more complex structures. The planned host structure should be similar to the complexes found by *Meyer et al.*^[108], but a little more adjustable. Short alkyl chains tolerate rearrangements to obtain the most stable structure and assist supramolecular aggregation. A dynamic behaviour in solution and slight modifications of the molecular structure could also support the insertion of potential guests. A well known organic supramolecular compound is tribenzotriquinacene (TBTQ). *Kuck et al.* have found this mesmerizing cup like molecule in 1992.^[111] The TBTQ structure with the bowl shaped scaffold provides a good template for capsule molecules.



Scheme 9: Tribenzotriquinacene backbone showing the cup like form.^[10e,111]

The addition of a substituent at one C atom of each of the three aromatic systems of the TBTQ, results in a C_3 symmetric chiral conformation. Hence the recognition of specific chiral substrates is possible and the differentiation between two enantiomers could be enabled. Stable host-guest systems are realized through several beneficial binding sites. Simultaneous execution of numerous interactions encourages the stability of the system. The cooperative effect describes this principle.^[8c] Combination of the NHC moieties with different substituents as alkyl chains, amino acids, amines, and hydroxids are imaginable. Some of them have already been synthesized in our group.^[4f,5b,99,112] Thus next to the aurophilic interactions, various binding sites are possible for the planned structure.

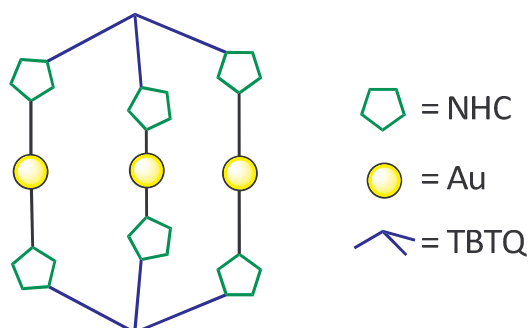


Figure 91: Planned design of the trinuclear gold(I) cage molecule with tribenzotriquinacene NHC ligands.

Hitherto only one successful combination of the TBTQ structure and NHCs was already published by *Segarra et al.* in 2013.^[113] But herein the NHC moieties are integrated into the TBTQ backbone. The carbon atoms C4 and C5 are also part of the aromatic system of the TBTQ. Thus the carbene carbon atoms are pointing outwards and do not support the building of a cage molecule with two of these ligands. Au(I) NHC complexes usually contain linear C-Au-C axes^[2c,4f,45b,63b,114] and would lead to different and probably more complicated structures with these ligands. For the best of our knowledge the now presented work shows the promising synthesis of a C_3 symmetrical ligand precursor with a connection between the

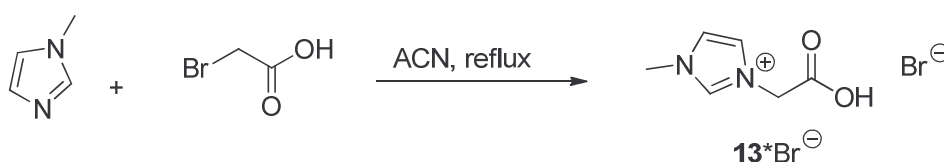
aromatic system of the TBTQ backbone and the nitrogen atom of the imidazolium moiety for the first time. A reaction procedure to obtain the ligand precursor was developed over an amidation reaction between a carboxylic acid and a primary amine. The complexation of the obtained imidazolium salts with silver could be realized via the silver base route. The corresponding gold cage molecules have been prepared by transmetallation of the Ag template compounds.

4.2 Mass Spectrometry Experiments

The intended NHC metal complexes and the ligand precursors bear three permanent positive charges. Therefore the success of the reactions could be verified by mass spectrometric means. The compounds are detected as cations, after the separation of the counterions, and the anions by separation of the metal compounds. Most electrospray ionization mass spectrometry (ESI MS) experiments were performed on a Fisher Scientific LTQ-Orbitrap XLTM hybrid Ion Trap with an ESI/APCI Ion Max Source. High resolution spectra for accurate masses were recorded with the Orbitrap analyzer (spectra shown with three decimal places). The mass spectrometer was calibrated for a broad mass range (mostly $m/z = 100-1000$ for an overview of the whole solution), therefore some accurate masses and isotopic pattern are not as precise as preferred. Additional measurements carried out with a commercial quadrupole/time of flight (Q/TOF) hybrid mass spectrometer (Bruker micrOTOF-Q) equipped with an Apollo ESI source show similar results (spectra shown with two decimal places). Fine tuning of several measurement parameters on this spectrometer allows the suppression of all signals with a smaller m/z value than 240. Acetonitrile and methanol (HPLC grade) from VWR were used for MS-measurements. All detected interesting species were marked in the spectra if their intensities were >1% of the intensity of the base peak. Smaller signals have been omitted for clarity. Some of these small but interesting signals will be mentioned under the schemes, if they are assumed as important.

4.3 Synthesis of the ligand precursor

The connection of the TBTQ framework and the imidazolium moieties should be realized via amide bonds. Hence a carboxylic acid function should be added to the secondary nitrogen atom of the 1-methyl imidazole. The synthesis of this salt was adapted from the literature.^[115] For the nucleophilic substitution, the imidazolium compound and bromo acetic acid were mixed in acetonitrile and refluxed. Evaporation of the solvent lead to a colourless oil, which acts as ionic liquid.^[115] However washing with concentrated hydrochloric acid turns the product to white crystals of compound **13***Br⁻.



Scheme 10: Synthesis of the imidazolium salt **13***Br⁻.

During mass spectrometric investigations of the product, several side products were detected. The ESI MS spectrum (see Figure 92) shows the intended cationic main product **13** ([M⁺] at $m/z = 141.10$) with the highest intensity and some adducts at $m/z = 281.13$ [2M-H]⁺ and $m/z = 421.19$ [3M-2H]⁺. Those aggregated species occur from the ESI process and cannot be avoided even by measuring low concentrated probes. The species at $m/z = 123.09$ and 95.09 originate from fragmentations of the product, which are also common for this technique. The species $m/z = 83.10$ could be attributed to a residue of the starting material 1-methyl imidazole. They also appear by using soft ionization parameters. Next to those simply explainable species, are several signals detectable with a Δm of 58.00. They can be attributed to the addition of one or up to four CH₂CO₂ groups to the product. These side products were generated by unintentional oligomerisation processes of the bromo acetic acid. These could be mostly eliminated by using another fresh load of the reactant.

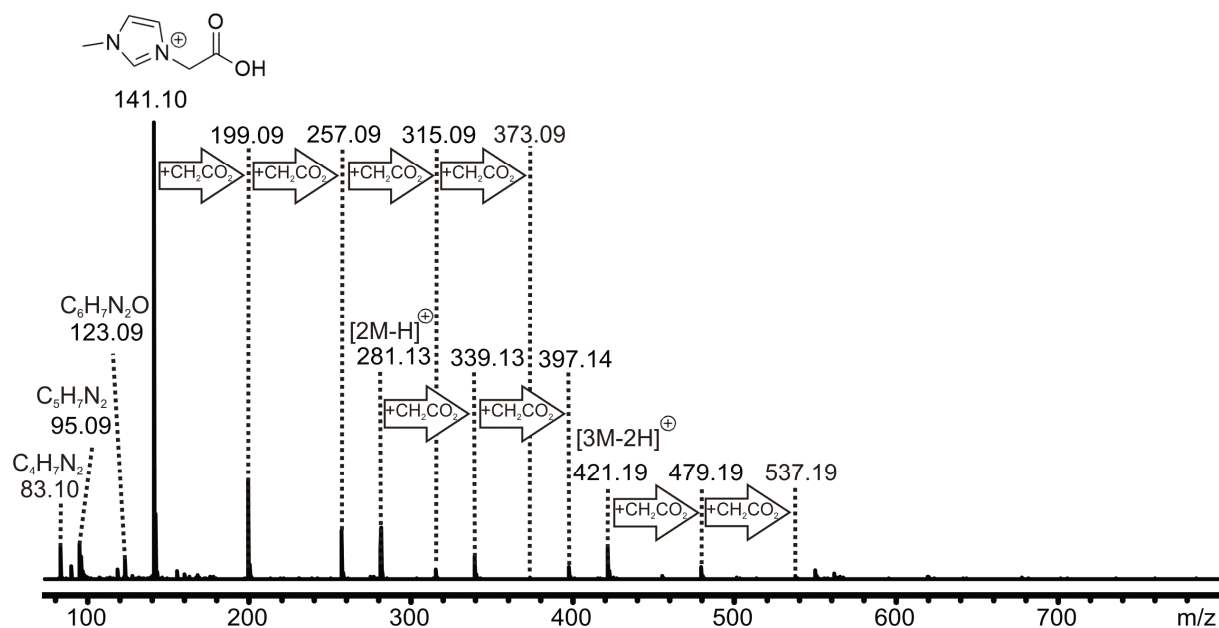


Figure 92: ESI(+) mass spectrum of 13^*Br^- diluted with acetonitrile ($M = 13$).

A different side product could be detected at $m/z = 155.08$. This species was linked to an ester imidazolium compound **14** with an additional methyl group. All side products could be removed by crystallization. However some of the following experiments were performed with the mixture including these side products. Therefore they are visible in the following spectra.

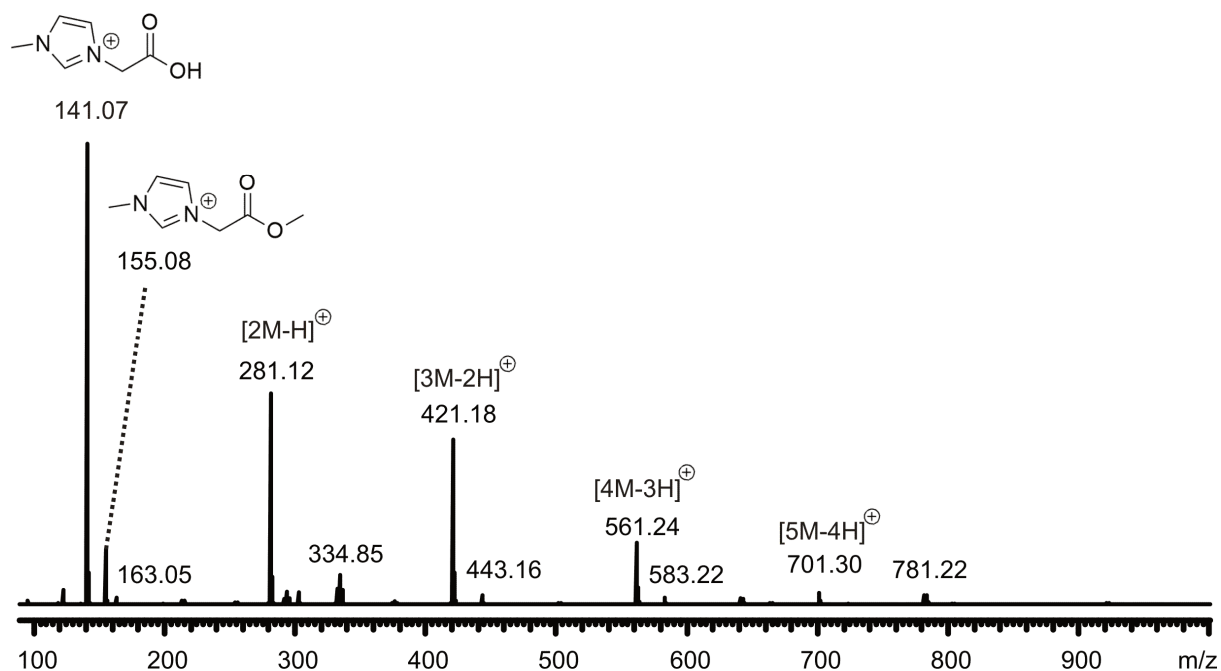


Figure 93: ESI(+) mass spectrum of 13^*Br^- diluted with acetonitrile (product without the additional CH_2CO_2 groups, $M = 13$).

Single crystals suitable for x-ray diffraction were grown slowly from a saturated solution of the imidazolium salt **13**⁺Br⁻ in acetonitrile at 3°C. The crystallographic data are summarized in Table 9. The found bond lengths and angles are comparable with similar compounds in the literature.^[100c,116]

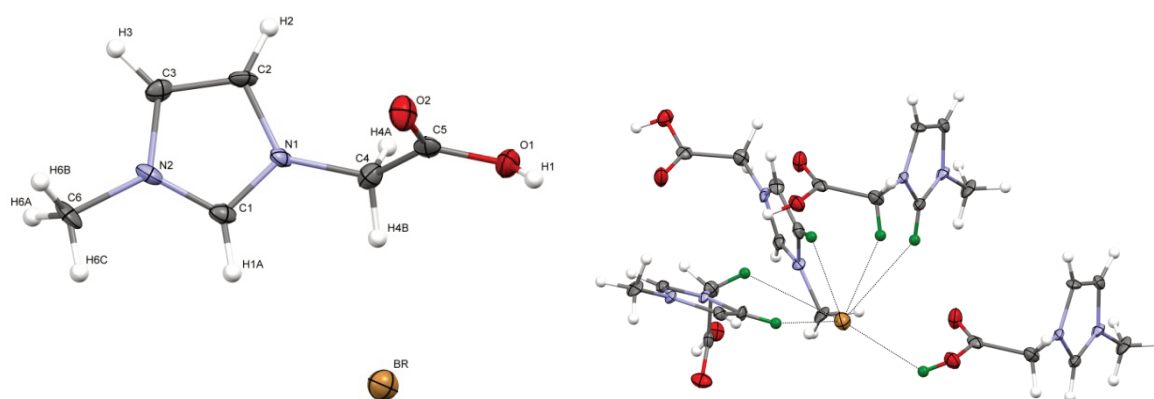


Figure 94: ORTEP drawing and partial crystal packing of the imidazolium salt **13**⁺Br⁻ (50% probability level for the thermal ellipsoids). The right picture illustrates the short H...Br bonds (all involved hydrogen atoms are green for clarity).

The structure consists of a network of cations surrounded by the counterions. The cations are arranged in alternating layers. The view from above those layers looks like bows. They originate from crossing acid substituents of two imidazolium compounds from different layers (see Figure 95). All bromide anions are surrounded by six close hydrogen atoms of different imidazolium molecules. The H...Br distances are 3.033 Å, 3.020 Å, 2.965 Å, 2.861 Å, 2.797 Å and 2.591 Å. All hydrogen atoms involved are either from the aromatic moiety or the acid substituent. The methyl side chains only participate in another, more common, hydrogen bond type with the oxygen of the acid moiety (O...H). The given structure is mainly stabilized over these two H...Br and O...H bonding types and packing effects. $\pi\cdots\pi$ interactions could not be found.

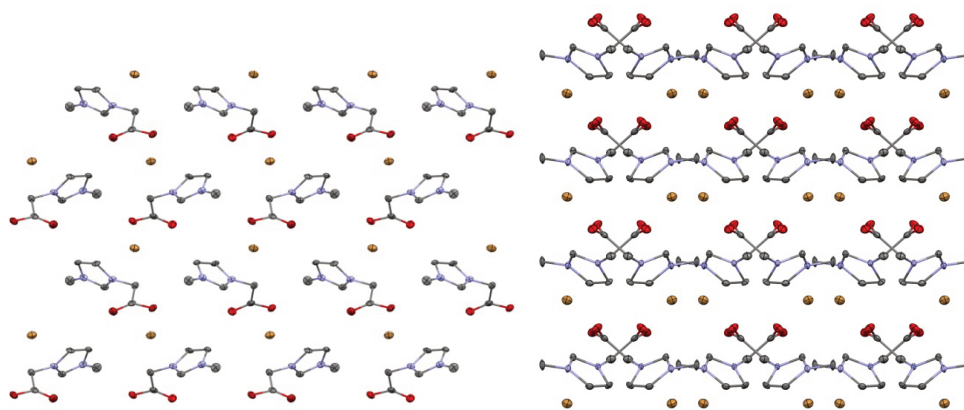
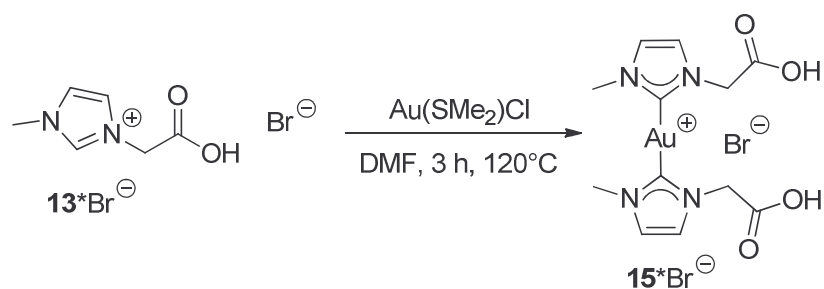


Figure 95: Crystal packing of the imidazolium salt **13*Br⁻** (50% probability level for the thermal ellipsoids). Hydrogen atoms have been omitted for clarity.

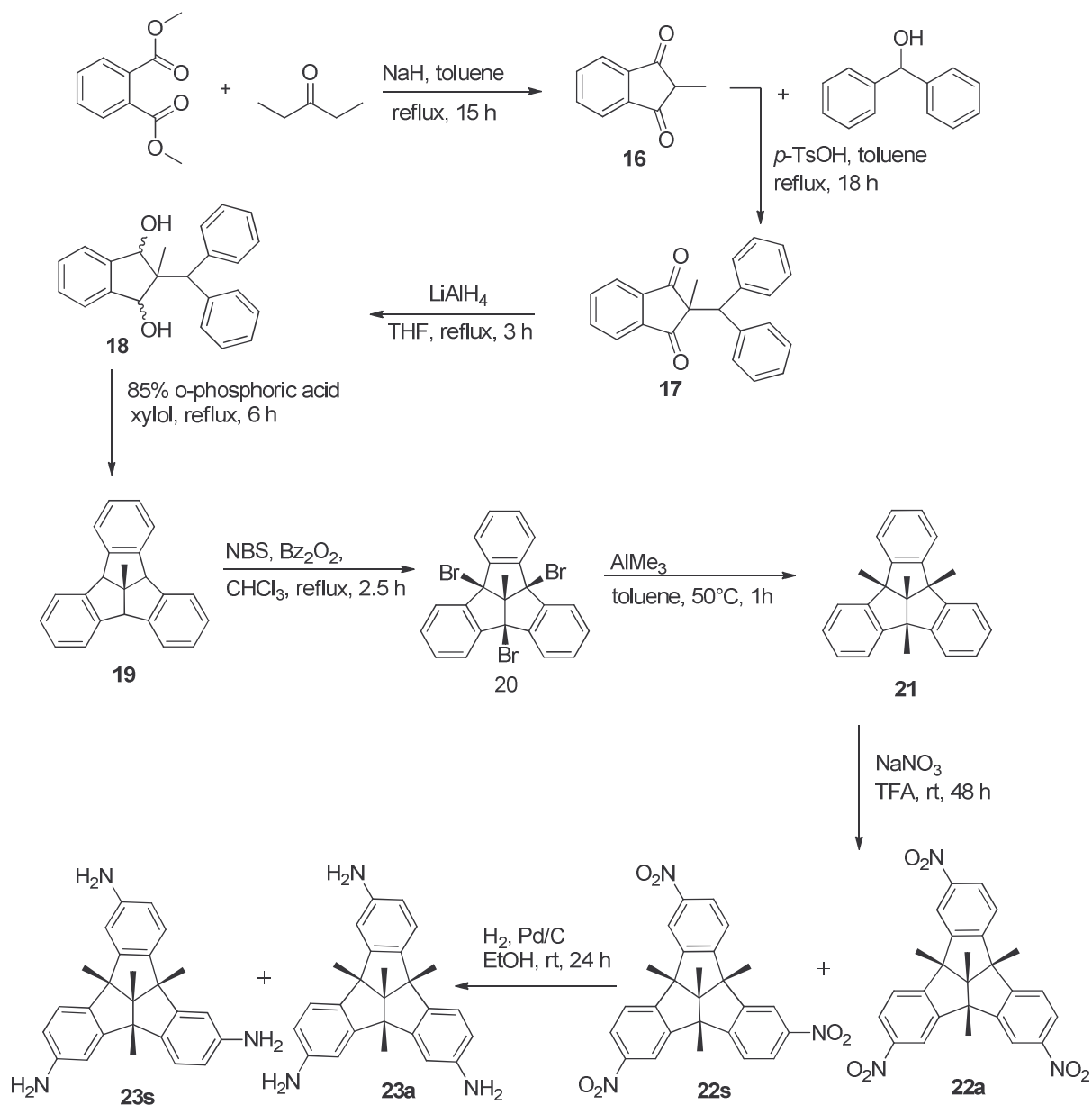
As a first attempt for the complexation, the imidazolium salt **13*Br⁻** was mixed with NaOAc and Au(SMe₂)Cl in DMF and stirred for three hours at 120°C. This method was adapted by a procedure from *Hemmert et al.*^[62f], which has already been used effectively in our work group.^[4f,63b] The reaction was immediately successful. For the best of our knowledge this complex is as yet unknown in the literature.



Scheme 11: Synthesis of the gold(I)NHC complex **15*Br⁻**.

Next to the imidazolium compound the amine containing backbone needed to be synthesized. As the centre piece of the planned C₃ symmetrical ligand precursor the corresponding amine TBTQ isomer **23s** was chosen. This already known molecule was first published by *Kuck et al.* in 1984.^[10a] The here presented synthesis is based on their procedures and some subsequently changes and improvements. The first step of the synthesis of the TBTQ derivative is the reaction of dimethylphthalat with 3-pentanone. The method was adapted from *Mosher et al.*^[10b] The highly cancer causing solvent benzene was replaced with toluene.^[10f,10h] Stirring under reflux, for 15 hours, led to a deep red solid. The

next three steps were performed according to the procedures described by *Kuck et al.*^[10c] Once again toluene was used instead of benzene for the synthesis of compound **17**.^[10f,10h] Even though *Kuck et al.*^[10d] had already published an effective bromination procedure, another instruction was followed for the synthesis of **20**. *Beaudoin et al.* have found the different route.^[10g] The new method does not require the use of elemental bromine and was therefore preferred. The synthesis of the compounds **21**, **22a** and **22s** as well as **23a** and **23s** were performed according to the literature.^[10d,10e] The trinitro derivatives were obtained as a mixture of the two isomers **22s** and **22a**. While those compounds are almost inseparable, the associated reduced amines **23a** and **23s** have a different elution behaviour.^[10e] Thus the next reaction step was performed without further purification or separation of the product mixture.



Scheme 12: Syntheses of the TBTQ backbone adapted from the literature.^{[10a] [10b] [10c-h]}

In contrast to the nitro TBTQ, the new amines **23a** and **23s** can easily be separated by liquid column chromatography.^[10e] The isomers show two different characteristic $^1\text{H-NMR}$ spectra. While the asymmetric species **23a** results in three multiplets, the spectrum of the symmetric compound **23s** shows two doublets (a+c) and one dd (b) (see Figure 96).

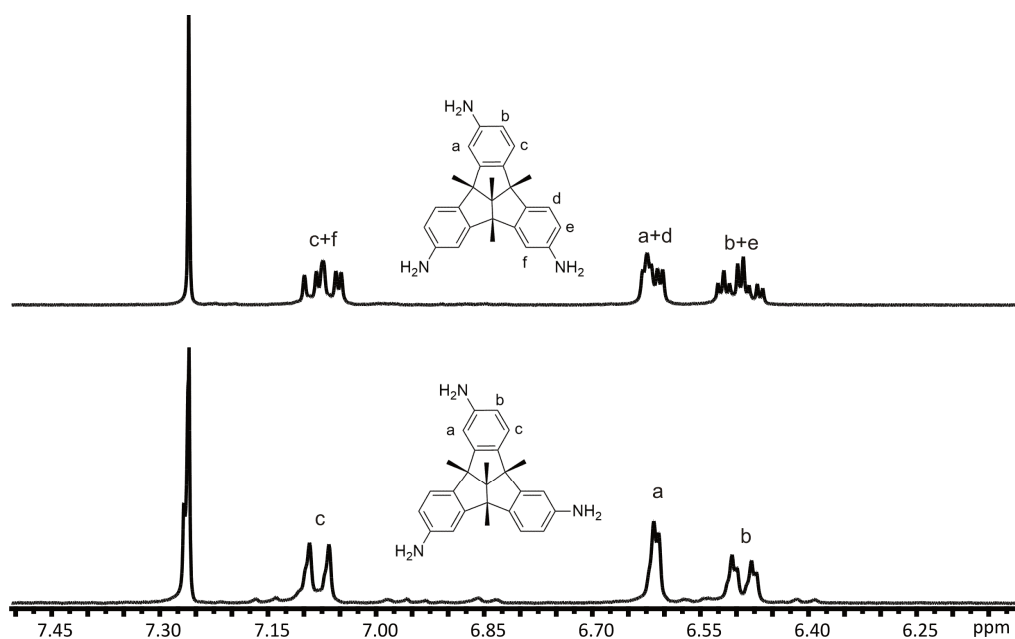
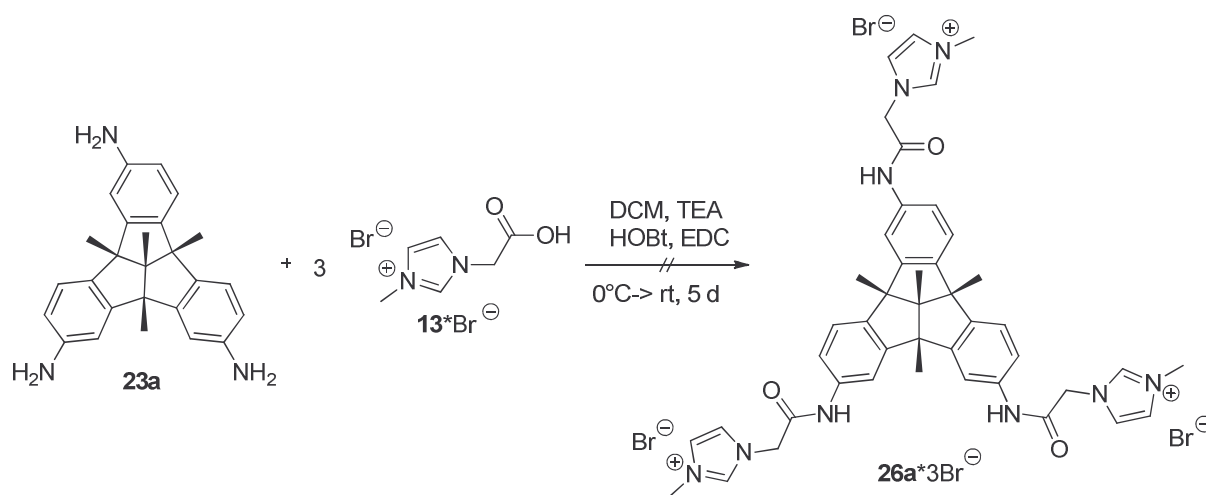


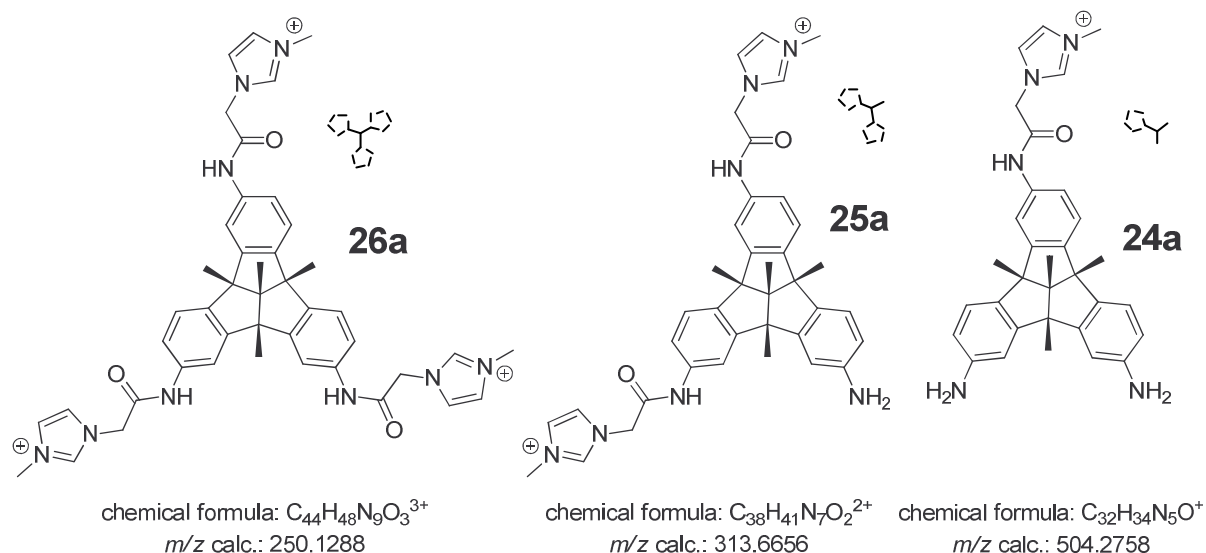
Figure 96: Enlargement of the aromatic area from the $^1\text{H-NMR}$ spectra of the two isomers **23a** and **23s**.

The last step of the synthesis of the ligand precursor is the amide coupling reaction. There are a variety of different organic coupling reagents and metallic catalysts known for this type of condensation reaction and a lot of them work quite well for aromatic amines.^[117] They usually play an important role in peptide synthesis, but can also be used for other compounds. For the following reactions, metal free routes were mainly chosen. Most of the here used coupling reagents are hygroscopic and dissociate during the reaction with water. Therefore all experiments were operated with dry solvents and under argon atmosphere. The first attempts were performed with the asymmetrical isomer of the triamino compound **23a**. The amine and the imidazolium salt **13**⁺Br⁻ were dissolved in dichloromethane and the solution cooled down to 0°C. Then HOBt, triethylamine (TEA) and EDC were added and the reacting solution allowed to warm up slowly to room temperature. Stirring was continued for five days at ambient temperature. A lot of colourless precipitate has formed. For purification ethyl acetate was added and the solution washed with NaHCO_{3(aq)} and NaCl_(aq) solutions and with pure H₂O. The organic layer was dried over Na₂SO₄ and the solvent removed under pressure.



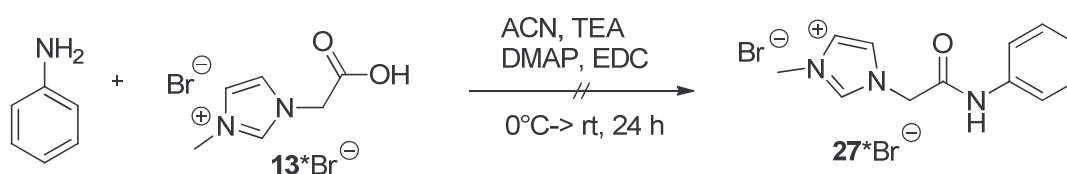
Scheme 13: Tested synthesis of **26a*3Br⁻** with **13*Br⁻**, **23a**, EDC, HOBT and TEA in dichloromethane at 0°C, with a reaction time of 5 days.

The evolution of the reacting species and the products was followed with ESI MS. Successful coupling reactions should lead to the new tripodal ligand precursor **26a*3Br⁻** with three imidazolium units. Additional products after only one or two successful amidation reactions are also plausible and would lead to the intermediates **25a** and **24a**. Due to a higher charge **26a** has the smallest m/z value and should be detectable at 250.1288. Because of their size and complexity the products will be shown as sketches in the spectra. The asymmetric conformation of the TBTQ scaffold provides three different isomers at a time for the compounds **24a** and **25a**, which cannot be transferred into each other by rotation. Since the isomers are isobaric they cannot be distinguished by mass spectrometric means. Here they are shown as one sketch respectively, which is representative for all possible isomers.



Scheme 14: Cationic species of the wanted asymmetric tripodal ligand precursor and the two intermediates with only one or two respectively successfully coupled NHC units; including their chemical formulas and calculated m/z values (a = asymmetric). The sketches for the asymmetric compounds are illustrated with dashed bonds.

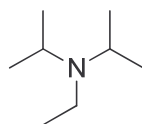
The only detectable TBTQ species in the first sample of the purified product was the triamino compound **23a** as cationized molecule $[M+H]^+$. Therefore the reaction parameters were changed. The next experiment was adapted from a procedure of *Barnard et al.*^[118] The synthesis is pretty similar to the first attempt, but involves ethanol as solvent. The ESI MS spectra of the reacting solution after 24 hours did not show any intended products. Further tests were transferred to the simpler aromatic amine aniline. This compound contains only one primary amine function. The reaction conditions were further varied for every step.



Scheme 15: Tested synthesis of 27^*Br^- with 13^*Br^- , anilin, EDC, DMAP and TEA in acetonitrile at 0°C , with a reaction time of 24 hours.

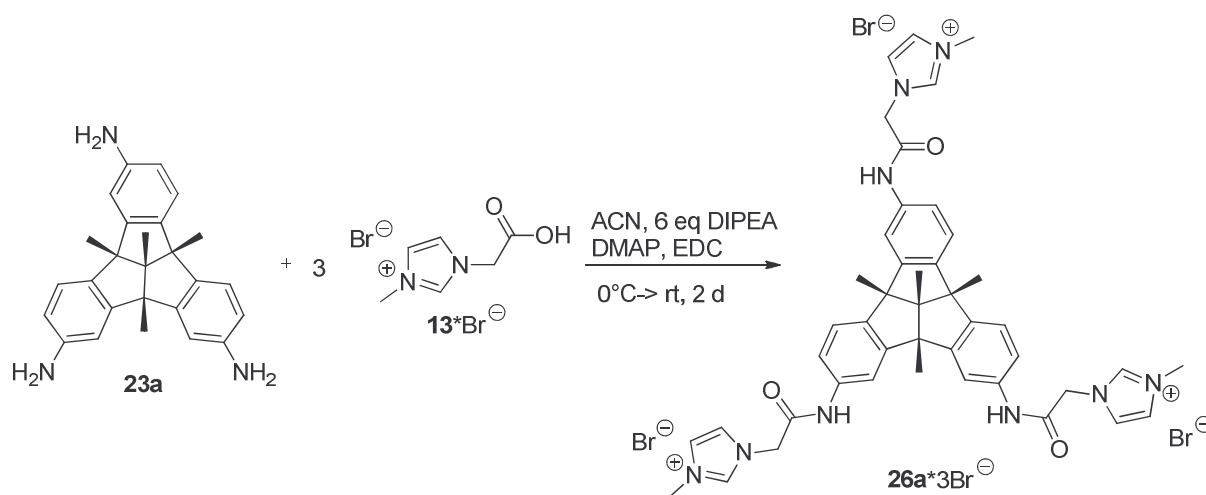
The next experiment was performed in acetonitrile at 0°C . The coupling reagents DMAP (instead of HOBt) and EDC were used. Measured by means of ESI MS, no product could be detected after 24 hours. Acetonitrile was chosen as solvent in this reaction, because all reactants have shown a good solubility even at low temperatures. So for the next

experiment acetonitrile was kept as solvent but the carbodiimid was changed from EDC to DCC. The changed coupling reagents did also not support the reaction. Another variable parameter is the temperature. The properties of the solvents like the boiling – or melting points do have a huge impact on the reaction. With different solvents the reaction temperature can be varied. For some reactions the transient intermediates are pretty reactive and dissolve in solution before they are able to react with another molecule. Lowering the temperature could support the coupling reaction by slowing down the dissociation step. Numerous instructions of amide coupling reactions suggest low temperatures under 0°C, so the transient intermediates exist long enough to react with the amine, without an early dissociation. Therefore the reaction was performed at -60°C in THF. The reaction mixture was kept at this temperature for 24 hours and then slowly warmed to room temperature and stirred for another 24 hours. Alongside with the temperature the base was changed to lithium diisopropylamide (LDA). The stronger base should support the deprotonation step of the amine. Unfortunately the change of the temperature and the base were not beneficial. However for the next reaction TEA and LDA were replaced with Huenig base. Intriguingly this was the first successful performed amide coupling reaction of **13***Br⁻ with aniline yielding the product **27***Br⁻.



Scheme 16: Huenig base (*N,N*-Diisopropylethylamine, DIPEA)

Huenig base (*N,N*-Diisopropylethylamine, DIPEA) turned out as the key to an effective coupling reaction. The non nucleophilic and steric hindered, but strong base supports the given synthesis. There are also several examples of successful amide coupling reactions with DIPEA in the literature.^[119] After that the promising reaction, the reactants were tested with the TBTQ compound **23a**.



Scheme 17: Performed synthesis of **26a*3Br⁻** with **13*Br⁻**, **23a**, EDC, DMAP and 6 eq. DIPEA in acetonitrile at 0°C, with a reaction time of 2 days.

The general amidation synthesis was performed by mixing two solutions **A** + **B** at 0°C in an ice bath (containing water, ice and NaCl; to keep the temperature, more ice was added when needed).

Solution A: The amine **23a** (1 eq) was dissolved in acetonitrile and cooled to 0°C. Then DIPEA (6 eq) was added to the solution.

Solution B: The imidazolium salt **13*Br⁻** (4 eq) was dissolved in acetonitrile and cooled to 0°C. After that EDC (4.5 eq) and DMAP (0.05 eq) were added to the solution.

The amount of acetonitrile was changed a little bit for each reacting solution to get clear, colourless solutions. Anyhow the compounds in solution **A** did dissolve much better than in solution **B**, therefore solution **B** always contains more solvent. E. g. while 50 mg of **23a** were dissolved in 10 mL acetonitrile, 40 mL had been needed for the belonging imidazolium solution **B**.

Both solutions were stirred for a few minutes and then **A** was slowly added to **B**. The reaction mixture was continuously stirred and slowly warmed up to room temperature (the ice bath was kept under the flask but no more ice was added). Most experiments have gone by with distinct colour changes. This reacting solution turned brown while adding **A** to **B**. After 24 hours a small sample was taken, diluted in acetonitrile and measured by ESI MS. The reaction mixture contained some positively charged reactants.

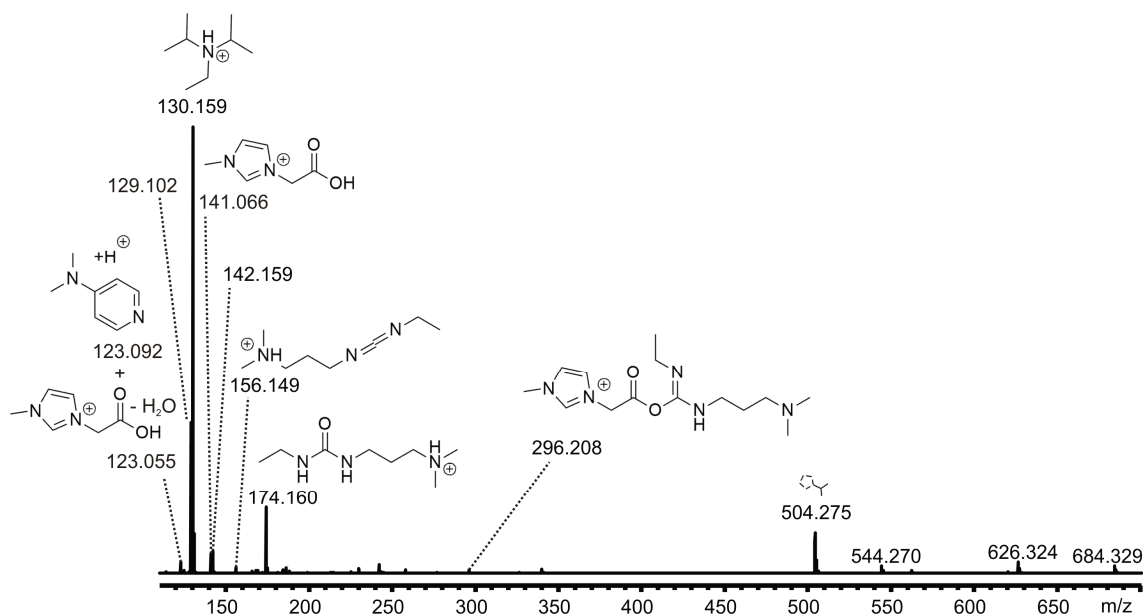


Figure 97: ESI(+) mass spectrum of a reacting solution containing 13^*Br^- , 23a, EDC and DMAP in acetonitrile at 0°C. The sample was taken after 24 hours and diluted with acetonitrile.

Huenigs base and DMAP are detectable after the addition of a proton, at $m/z = 123.092$ and 130.159 respectively. Both species show a high ESI response^[33,120] and therefore intensive signals. The NHC acid 13^*Br^- was detected at $m/z = 141.066$ and a fragment at $m/z = 123.055$ after the loss of H_2O , which is a common fragmentation of carbon acids during the ionization process. The two signals at $m/z = 123.092$ and 123.055 can easily be distinguished in an enlarged spectrum. The intensities in the given spectrum (see Figure 98) are almost equal, but alternate in the following investigations.

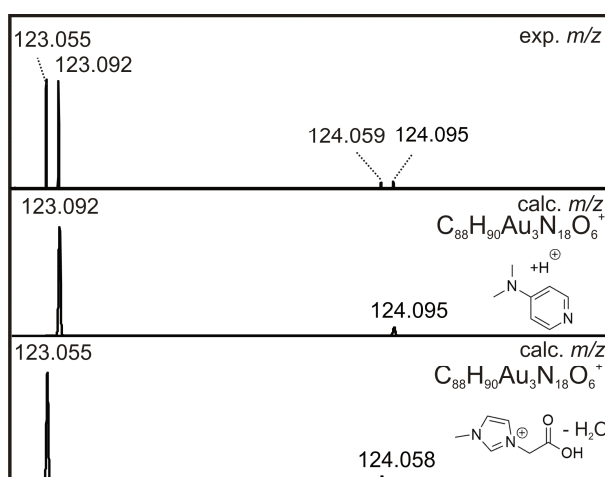
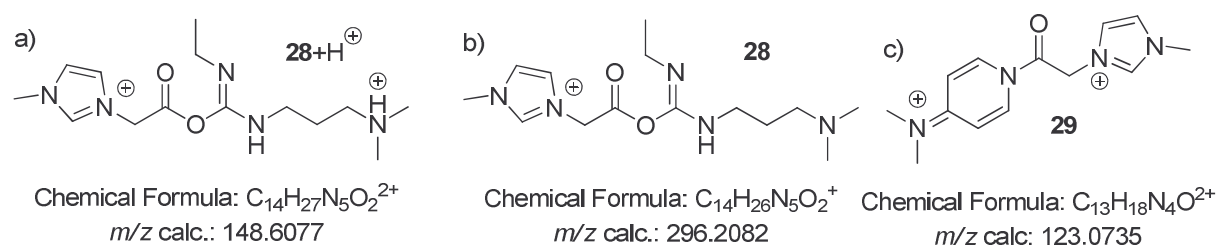


Figure 98: Partial ESI(+) mass spectrum of the reacting solution, showing the differences of the signals from $[DMAP+H]^+$ and $[13-H_2O]^+$.

The carbodiimid EDC and the corresponding carbamide are also visible after the addition of a proton at $m/z = 156.149$ and 174.160 respectively. Intriguingly at $m/z = 296.208$ is the first reactive intermediate (**28**) visible, occurring from the reaction of EDC with the acid.^[121] The intensity of this species is not very high but still a few times higher than the baseline noise. The detection of this active species indicates an adequate stability of the intermediate. Apart from this compound the protonated form could also exist in the reacting solution. This species has a higher charge (+2) and therefore a smaller m/z value of 148.608 . Due to the composition of the mixture both species are plausible and probably coexisting. However the given MS spectrum only shows the deprotonated form. The next reaction step is proposed as the substitution of the EDC moiety with the catalyst DMAP,^[117c,121c,122] leading to a new doubly charged reactive species **29** at $m/z = 123.0735$. DMAP as coupling reagent is often used for esterification but the mechanism is similar for the amide bonding reaction. The proposed transient species or the associated aggregates with anions could not be detected. The absence of this species does not necessary indicate the absence of this intermediate. Rather the transient species could be short lived or dissociate during the ionization process.



Scheme 18: Two possible species of the first intermediate a) 28 after the addition of a proton, b) 28 without the extra proton, c) the proposed second transient species 29, with two positive charges.

The species at $m/z = 504.275$ is identified as **24a** the product of the first successful coupling reaction of the TBTQ amine **23a** with acid 13^*Br^- . Due to the fact that **23a** is not charged, it can only be detected after the addition of a proton or sodium. In contrast to that, the ligand precursors contain permanent charges and therefore are simply detectable by ESI MS. The ESI spectrum in negative modulus shows the expected counterion bromide.

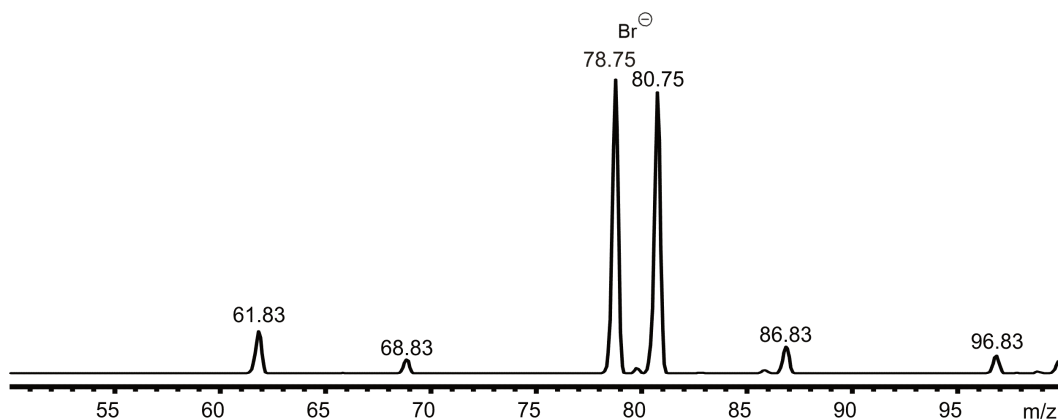


Figure 99: ESI(-) mass spectrum of a reacting solution containing 13^*Br^- , **23a**, EDC and DMAP in acetonitrile at $0^\circ C$. The sample was taken after 24 hours and diluted with acetonitrile.

After two days the reaction was ended. The solution turned brown and a dark precipitate has build. The suspension was filtered and the solvent removed under vacuum. The crude product was obtained as dark brown oil. ESI MS measurements of the product in methanol presented the species at $m/z = 504.276$ with a much higher intensity and new additional species. A new fragment is detectable at $m/z = 107.061$. This fragment does originate from the $[DMAP+H]^+$ species after the loss of the neutral methane molecule. A new doubly charged signal could also be detected at $m/z = 313.666$. The species was assigned to **25a**, which originates from the TBTQ amine **23a** after two successful coupling reactions. Even the final product **26a** of the reaction could be detected at $m/z = 250.129$ but with minor intensity. The charge of the acid 13^*Br^- used for the reaction contains the additional oligomeric species with repeating CH_2CO_2 units (each CH_2CO_2 unit is sketched in the spectra with a *). These reactants could also undergo the coupling reaction. Therefore some side products with small intensities were detected as well ($m/z = 342.668$ [**25a**+ CH_2CO_2], 562.281 [**24a**+ CH_2CO_2], 620.287 [**24a**+ CH_2CO_2]).

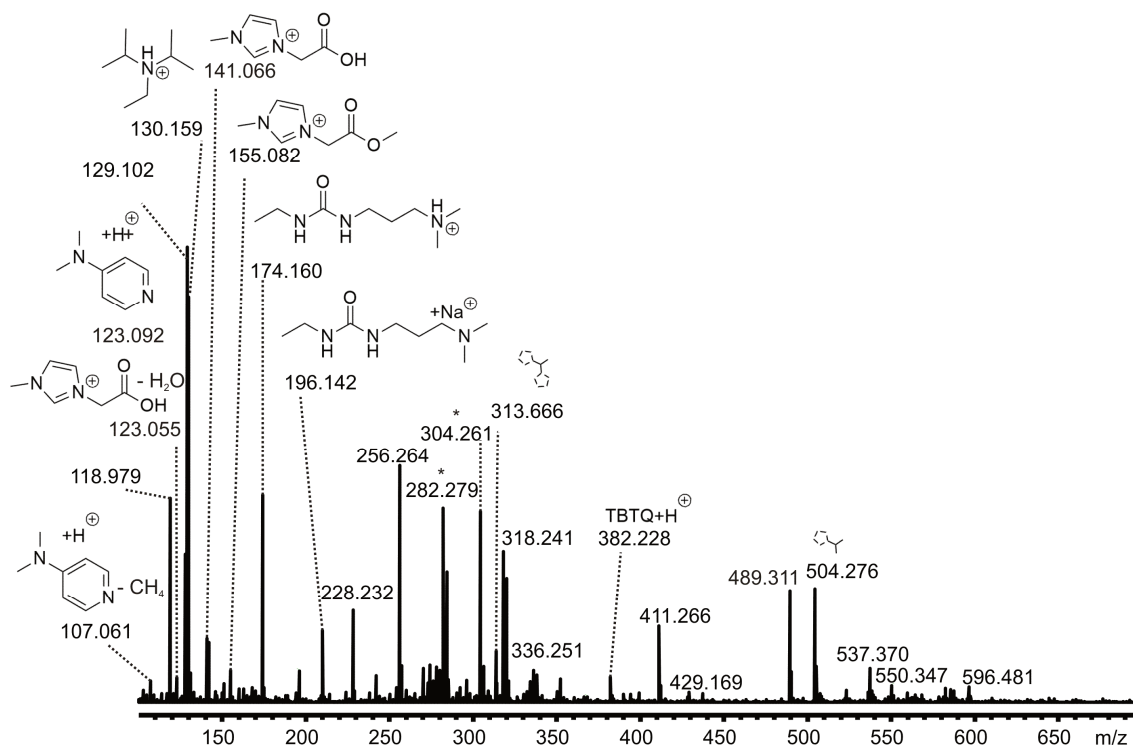
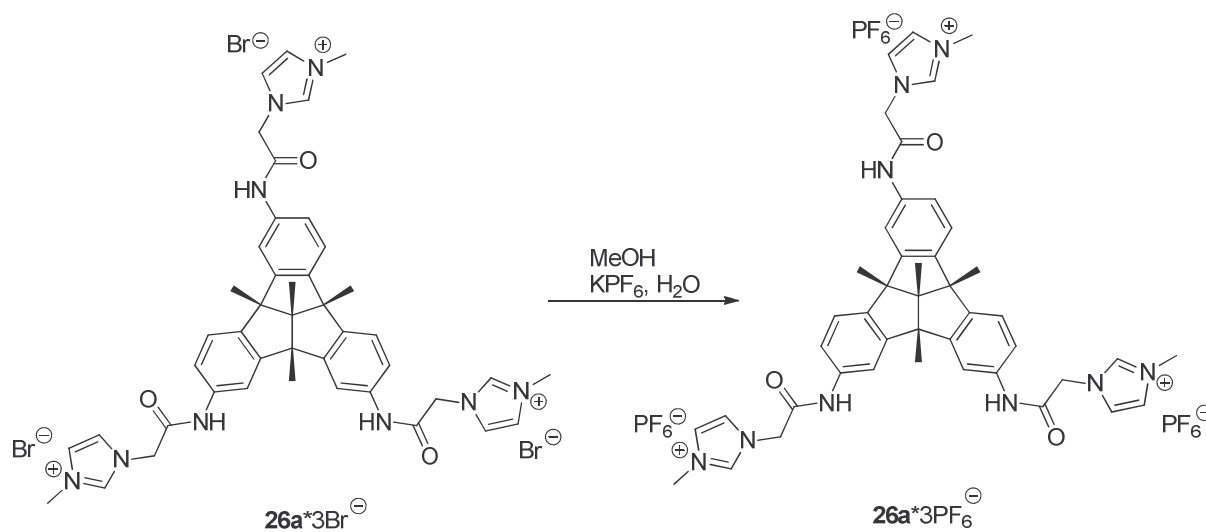


Figure 100: ESI(+) mass spectrum of a crude product containing 13^*Br^- , $23a$, EDC and DMAP in acetonitrile at $0^\circ C$. The sample was diluted with methanol. (* = common background contaminant ions).

The crude product was full of side products and remaining reactants. Purification and a subsequent change of the solubility should be accomplished by an anion exchange with an excess of PF_6^- (see Scheme 19). Therefore the dark brown oil (66.83 mg) was dissolved in methanol and a saturated solution of KPF_6 (66.45 mg) in water was added. The organic solvent was removed under vacuo and a light brown precipitate has formed. The product was filtered and investigated by MS.



Scheme 19: Counterion exchange of $26a^*3Br^-$ with KPF_6 in methanol/water.^[62f]

The ESI(-) MS spectrum of the product shows mainly the new counterion PF_6^- and small amounts of bromide which could not totally be replaced (see Figure 101). Due to the fact, that a hydrochloride was used as carbodiimid, chloride is also a plausible counterion. Hence the product probably consists of a mixture of bromide, chloride and hexafluorophosphate compounds. The confirmation of chloride by mass spectrometric means is difficult and requires special calibration steps. This additional effort was not taken for the crude product.

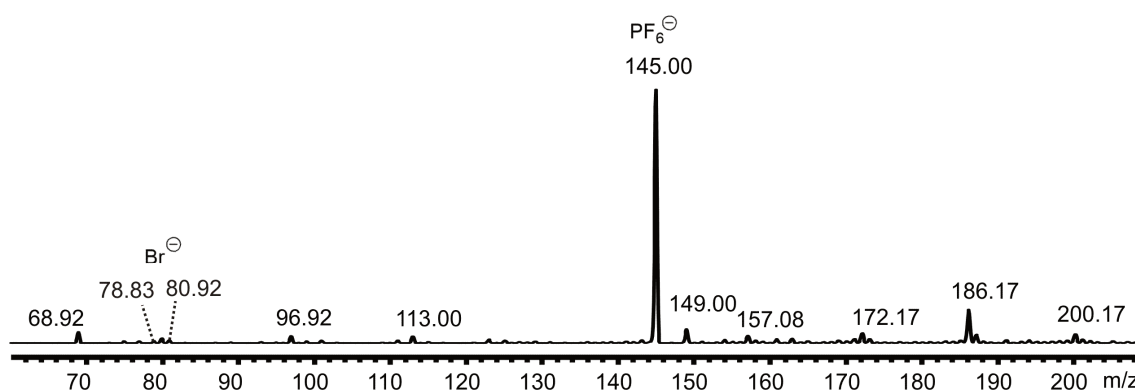


Figure 101: ESI(-) mass spectrum of the product after the counterion exchange from $26\text{a} \cdot 3\text{Br}^-$ with KPF_6 . The sample was diluted with methanol.

However the counterion exchange separated the positive species of the product by their solubility in water or methanol (see Figure 102). The intensities of the reactants and the side products decreased and the intensities of the three main products (**24a**, **25a** and **26a**) and the additional oligomeric species ($m/z = 342.668$ [**25a**+ CH_2CO_2], 371.670 [**25a**+ $(\text{CH}_2\text{CO}_2)_2$], 562.281 [**24a**+ CH_2CO_2], 620.287 [**24a**+ $(\text{CH}_2\text{CO}_2)_2$]) increased in the spectra of the residue from the organic phase. Next to those species some adducts of the ligand precursors and PF_6^- could be detected with small intensities (Figure 103). Aggregation of cations and anions during the ionization process is a common phenomenon. This behaviour is often tuneable by the ionization parameters and the concentration of the sample.

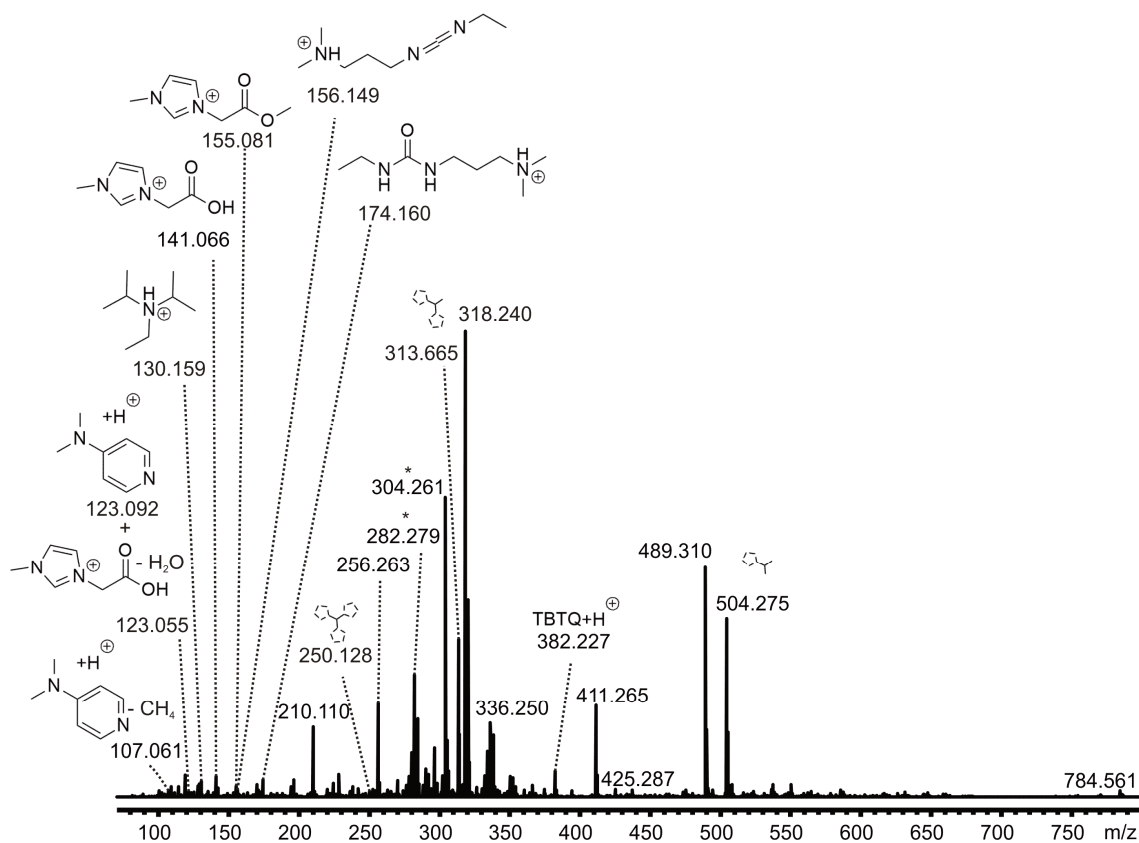


Figure 102: ESI(+) mass spectrum of the product after the counterion exchange from 26a*3Br⁻ with KPF₆. The sample was diluted with methanol. (* = common background contaminant ions).

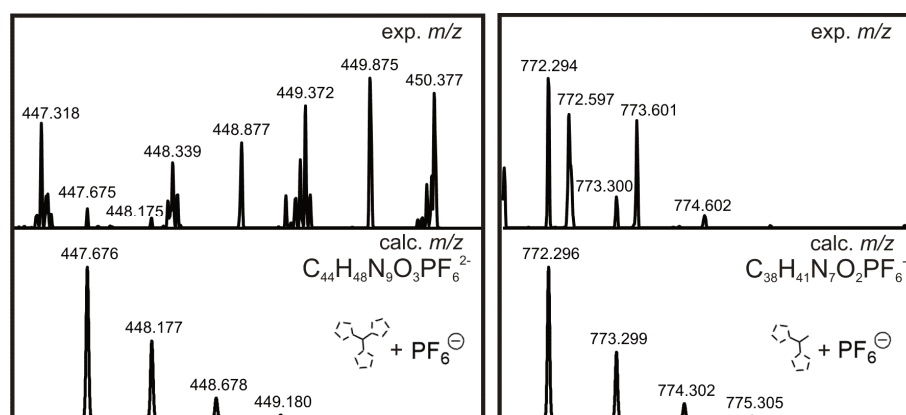


Figure 103: Partial ESI(+) mass spectrum of the product after the counterion exchange from 26a*3Br⁻ with KPF₆ (see Figure 102) showing the adducts of the NHC precursor molecules and PF₆⁻.

Most of the reactants remained in the water phase, due to their hydrophilic properties. Evaporation of the water leads to a residue, which was also investigated in the gas phase. The separation of the products and the reactants was incomplete but promising. Repeating the procedure could improve the result. Changing the solvent or the added counter ion (PF₆⁻

to other species like BF_4^- [123], OAc^- [4h] or other anions [124]) could also support the anion exchange and affect the solubility of different species.

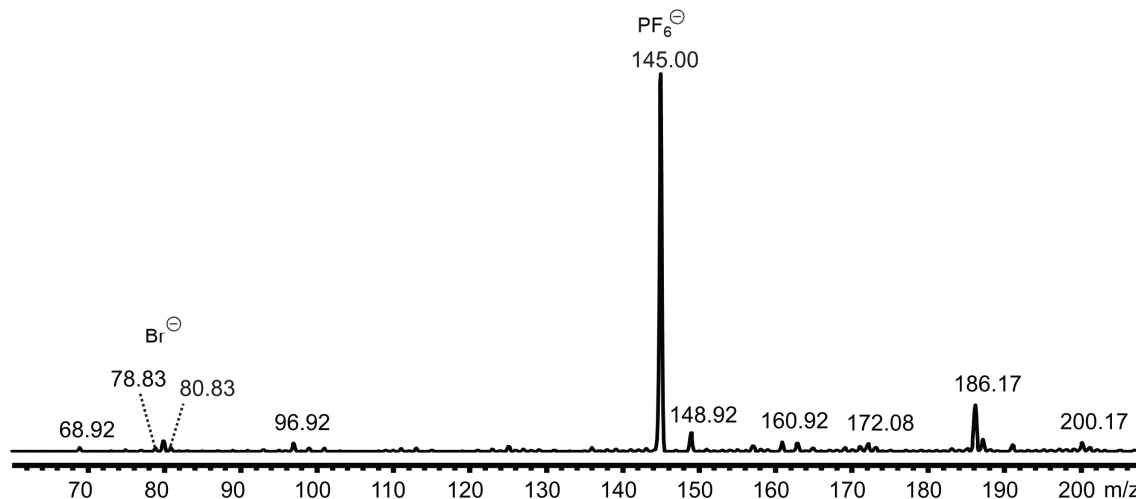


Figure 104: ESI(-) mass spectrum of the residue from the water phase after the counterion exchange from $26a \cdot 3\text{Br}^-$ with KPF_6 . The sample was diluted with methanol.

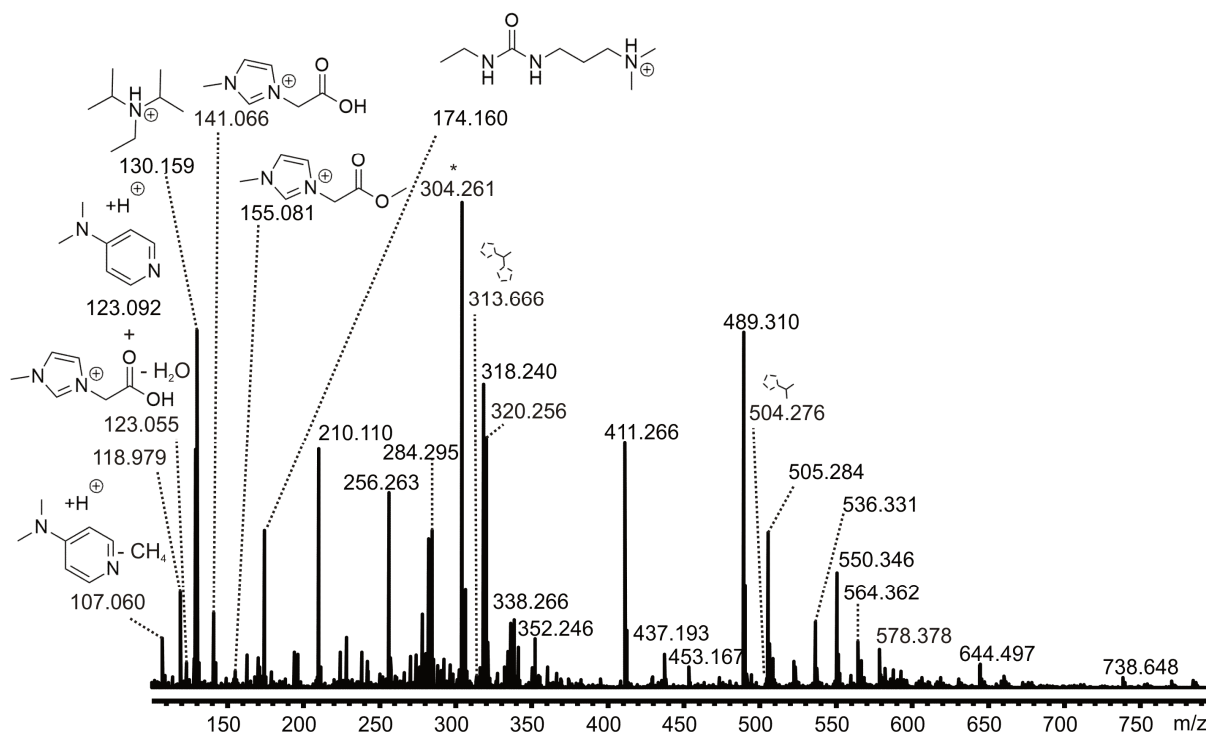


Figure 105: ESI(+) mass spectrum of the residue from the water phase after the counterion exchange from $26a \cdot 3\text{Br}^-$ with KPF_6 . The sample was diluted with methanol. (* = common background contaminant ions).

For a higher conversion the reaction time in the next experiment was doubled to eight days. The combination of the two mixtures **A** and **B** lead to an instant colour change of the solution to bright yellow. A colourless precipitate was quickly built. After four hours a small sample of the reacting solution was diluted in MeOH and measured by ESI MS. The first positive conversions to **24a** and **25a** could already be detected after this short period. Another sample was taken and measured after five days. The intensities of the interesting species were more intense and a small signal of **26a** could also be detected.

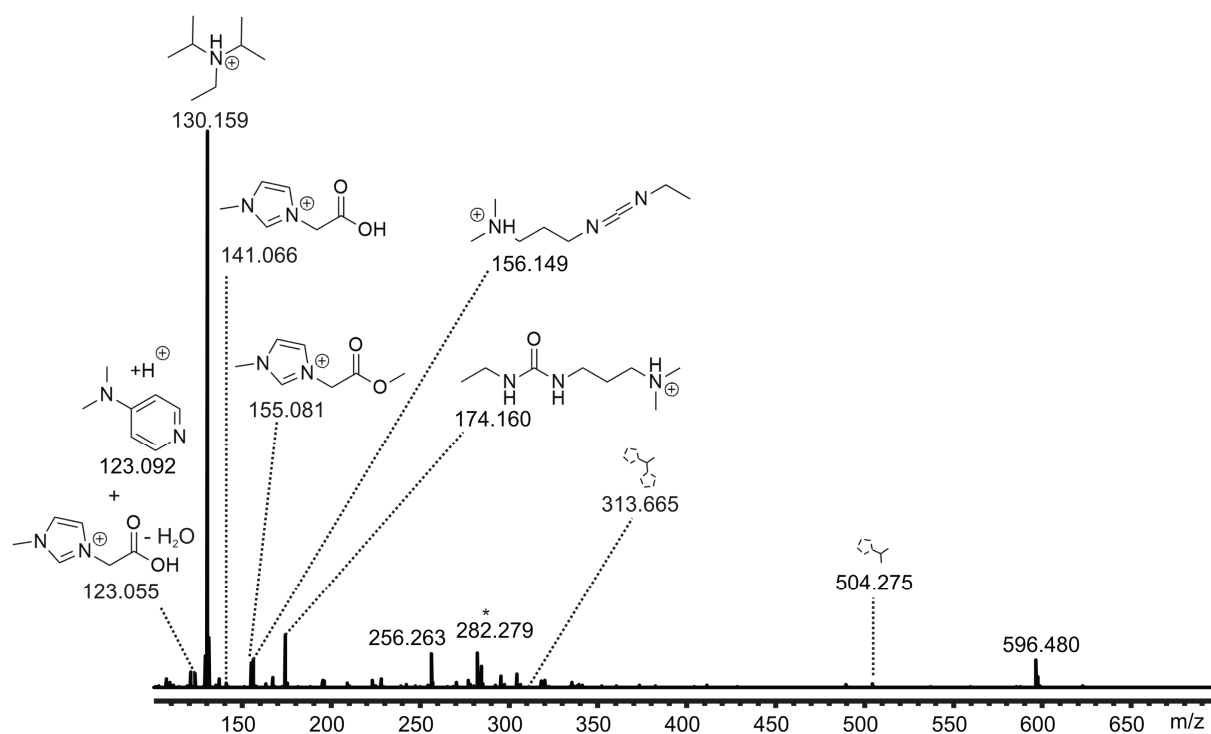


Figure 106: ESI(+)-mass spectrum of a reacting solution containing 13^*Br^- , **23a**, EDC, DMAP and DIPEA in acetonitrile at 0°C . The sample was taken after 4 hours and diluted with methanol. (* = common background contaminant ions).

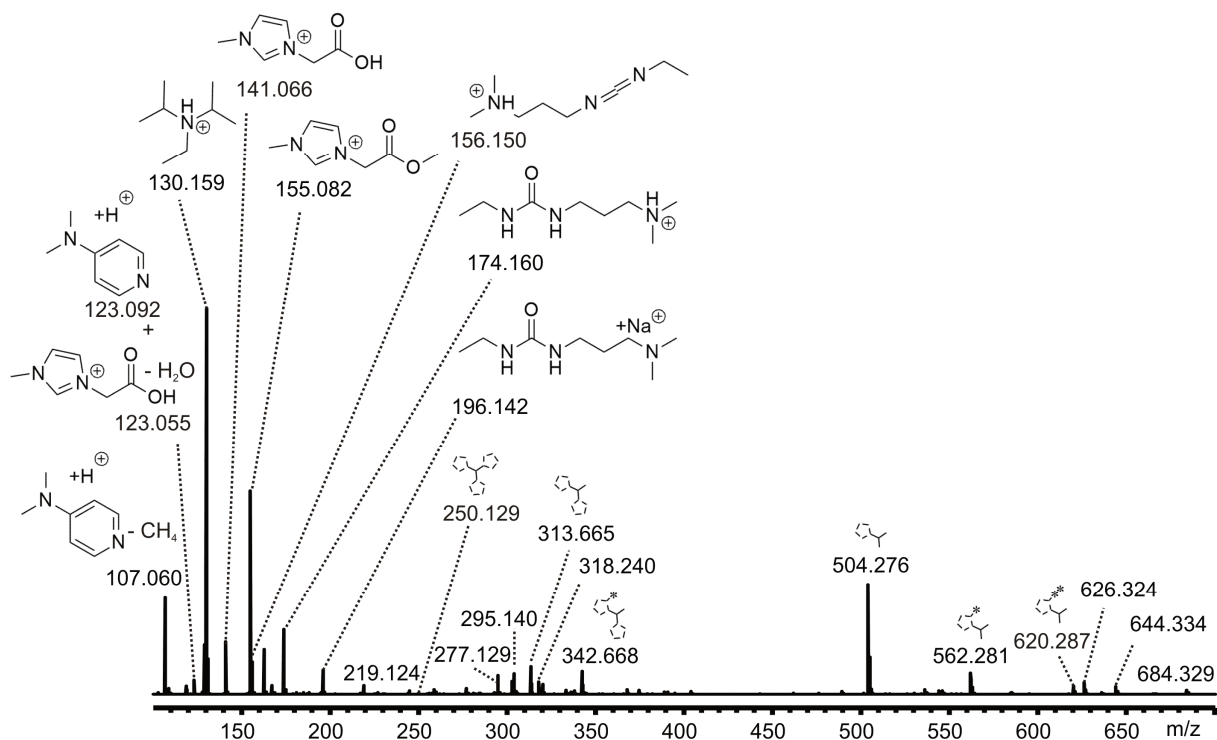


Figure 107: ESI(+) mass spectrum of a reacting solution containing 13^*Br^- , **23a**, EDC, DMAP and DIPEA in acetonitrile at $0^\circ C$. The sample was taken after five days and diluted with methanol.

The reaction was stopped after eight days. Removing the solvent in vacuo has led to the crude product as brown oil. The product was washed with water and a light brown precipitant was obtained. The solid was filtered and investigated by ESI MS (see Figure 108). The simple washing step, with water, lead to similar successful cleaning results in comparison with the counterion exchange. The dominating species in the ESI spectrum are the amides **24a** and **25a** followed by the oligomeric compounds. The preferred product **26a** was only found in small quantities (experimental and calculated isotopic pattern of the three interesting compounds are given in Figure 109, Figure 110 and Figure 111).

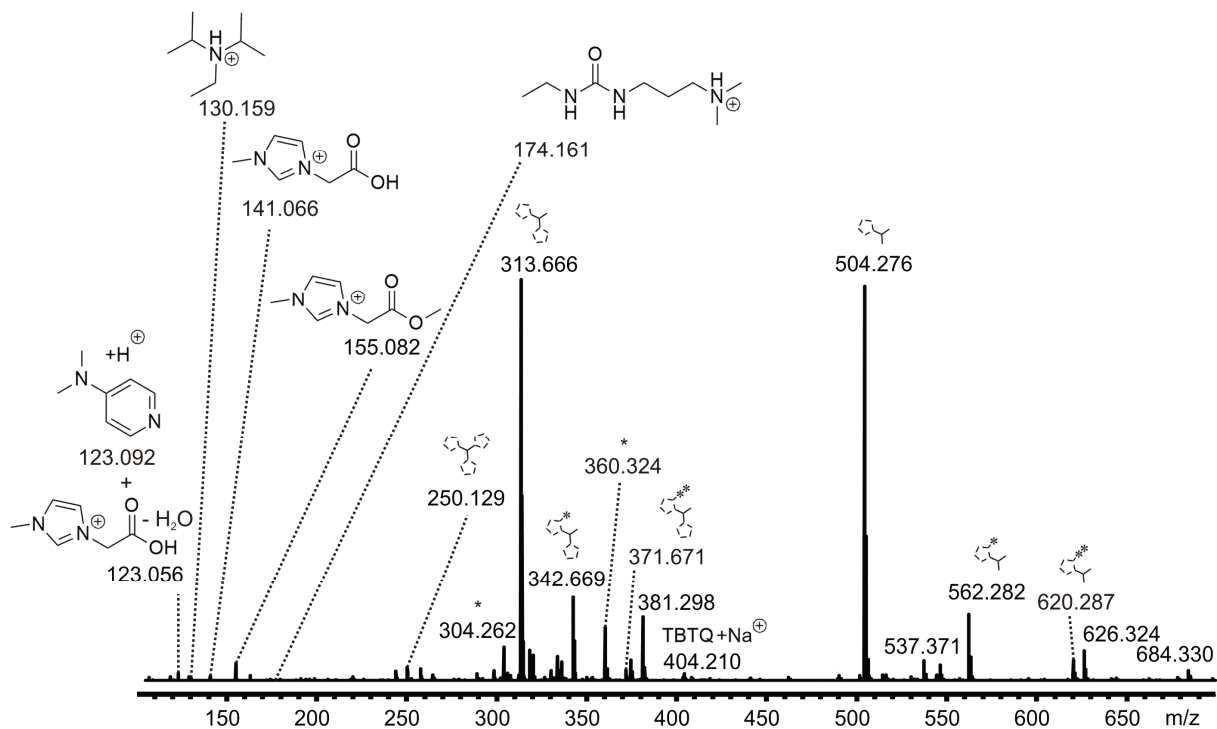


Figure 108: ESI(+) mass spectrum of the crude product from the reaction of 13*Br⁻, 23a, EDC, DMAP and DIPEA in acetonitrile at 0°C. The sample was diluted with methanol. (* = common background contaminant ions).

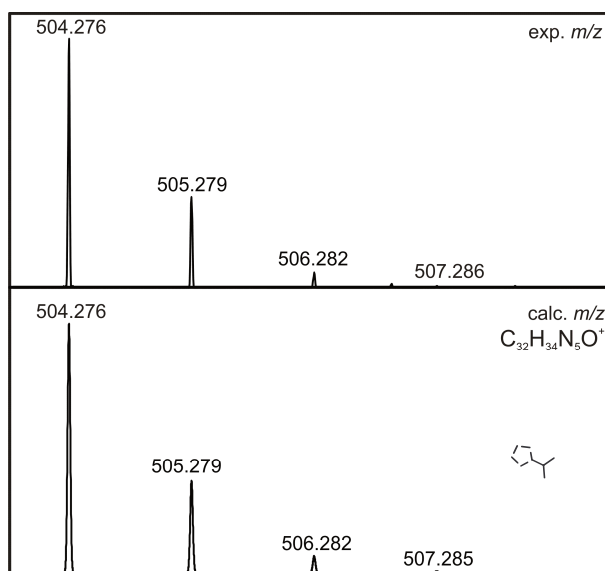


Figure 109: Partial ESI(+) mass spectrum of the crude product, showing the experimental and calculated isotopic pattern of 24a.

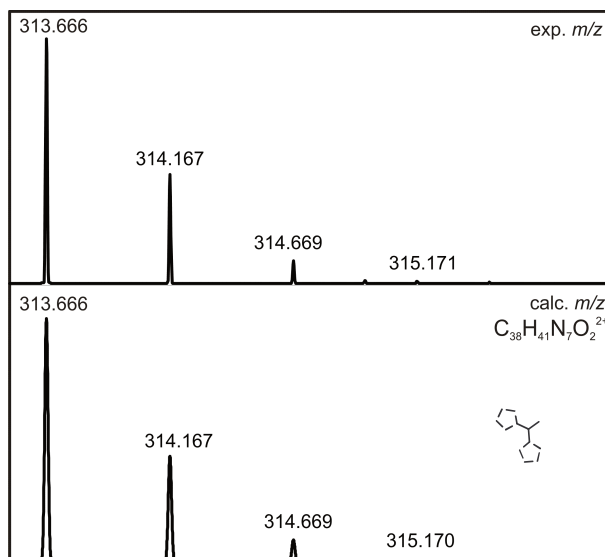


Figure 110: Partial ESI(+) mass spectrum of the crude product, showing the experimental and calculated isotopic pattern of 25a.

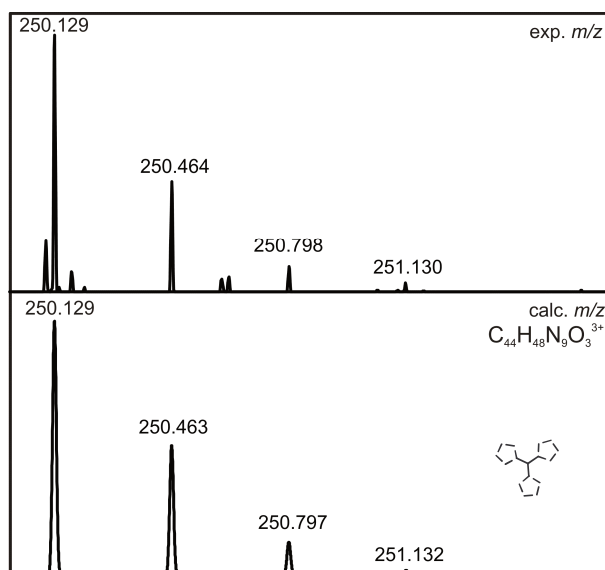


Figure 111: Partial ESI(+) mass spectrum of the crude product, showing the experimental and calculated isotopic pattern of 26a.

A plausible reason for the poor conversion is an incomplete deprotonation step. Therefore the next reaction should be improved by adding the doubled amount of the Huenig base. The colour changing of the reacting solution from yellow to brown and the building of a colourless precipitate was similar as in the reaction before. After five days a sample of the reacting solution was taken and diluted in methanol. The solution was transferred to the MS.

The resulting spectrum looks similar to the spectrum of the former experiment with half of the amount of Huenig base after five days (see Figure 107).

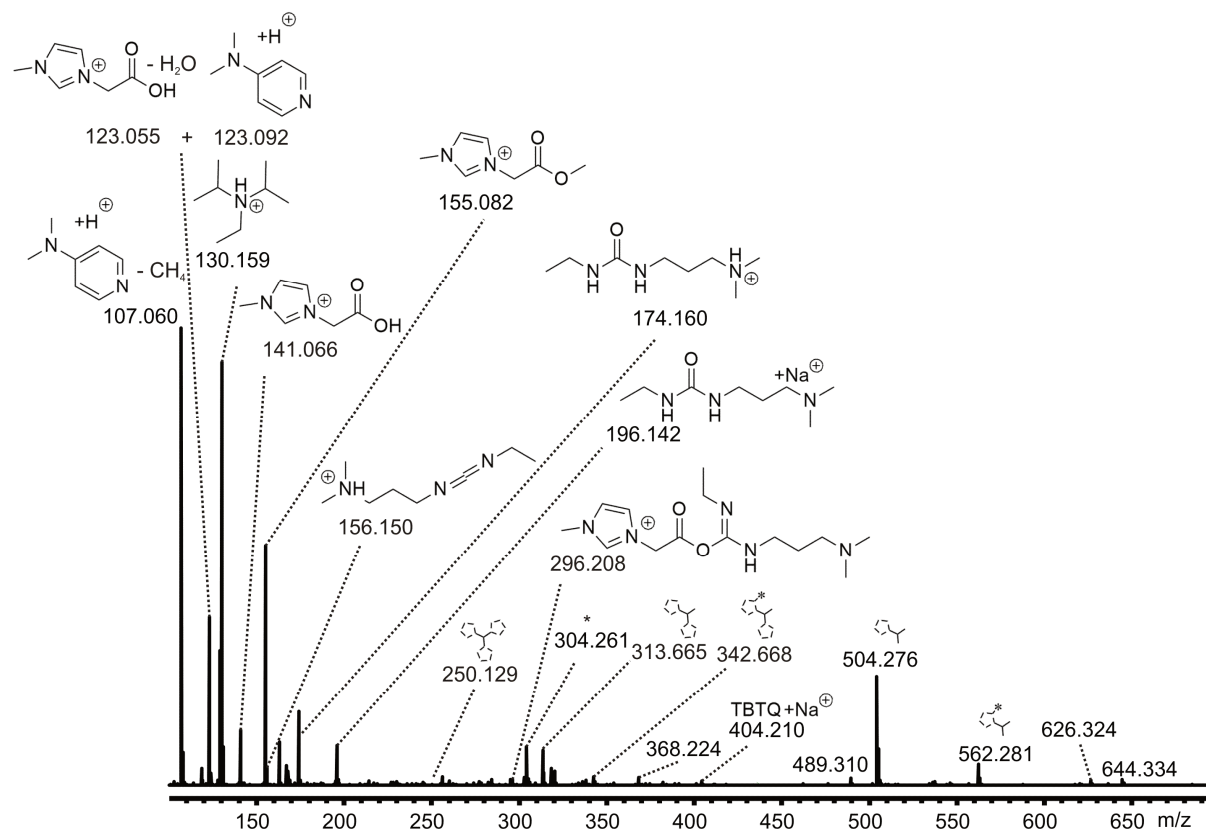


Figure 112: ESI(+)-mass spectrum of a reacting solution containing 13^*Br^- , **23a**, EDC, DMAP and DIPEA in acetonitrile at $0^\circ C$. The sample was taken after 5 days and diluted with methanol. (* = common background contaminant ions).

The reaction was again finished after eight days. The mixture was reduced to a minimum volume in vacuo and the generating dark brown precipitate was filtered and washed with acetonitrile. The MS spectrum of the crude product did not show higher intensities of the interesting species. The amount of **24a** and **25a** are almost unchanged in comparison with the spectrum after five days (see Figure 112). The tripodal ligand precursor **26a** could only be detected in small quantities. The previous reaction with half the amount of DIPEA has shown a much better turn over.

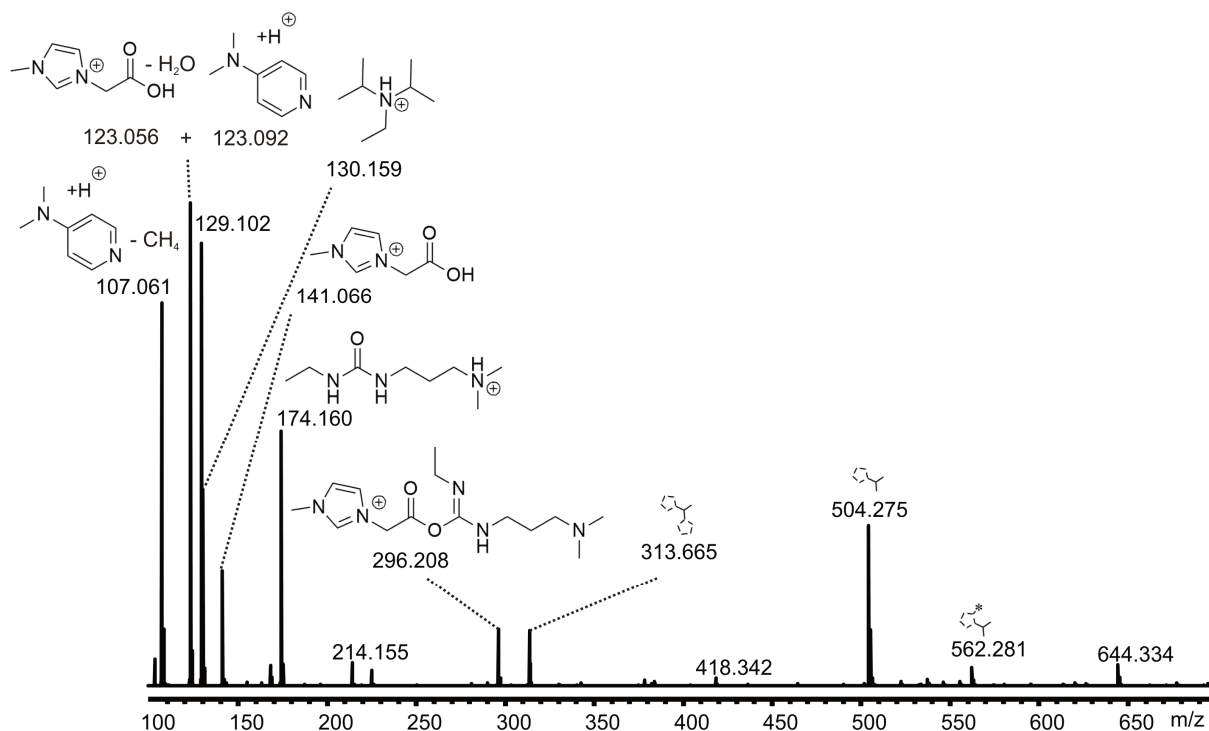


Figure 113: ESI(+) mass spectrum of the crude product from the reaction of 13^*Br^- , **23a**, EDC, DMAP and DIPEA in acetonitrile at 0°C . The sample was diluted with methanol and H_2O .

The combination of the two solutions has always been performed at low temperatures, in order to reduce the decomposition of the transient species. Due to the fact, that the previous reactions have shown good performance even after warming to room temperature, cooling seem unnecessary. So the reaction was now completely operated without ice bath. The procedure was performed as described above, by adding the two premixed solutions **A** and **B**, but the combination took place at room temperature. The impact of the changed reaction parameters was already visible after a short period of time. The colour change, from yellow to brown, was already apparent after a few hours and a lot of colourless precipitate has build at this stage. Differently than the previous results, all of the three possible ligand precursors (**24a**, **25a** and **26a**) and some of the oligomeric species were already detected after three hours (see Figure 114).

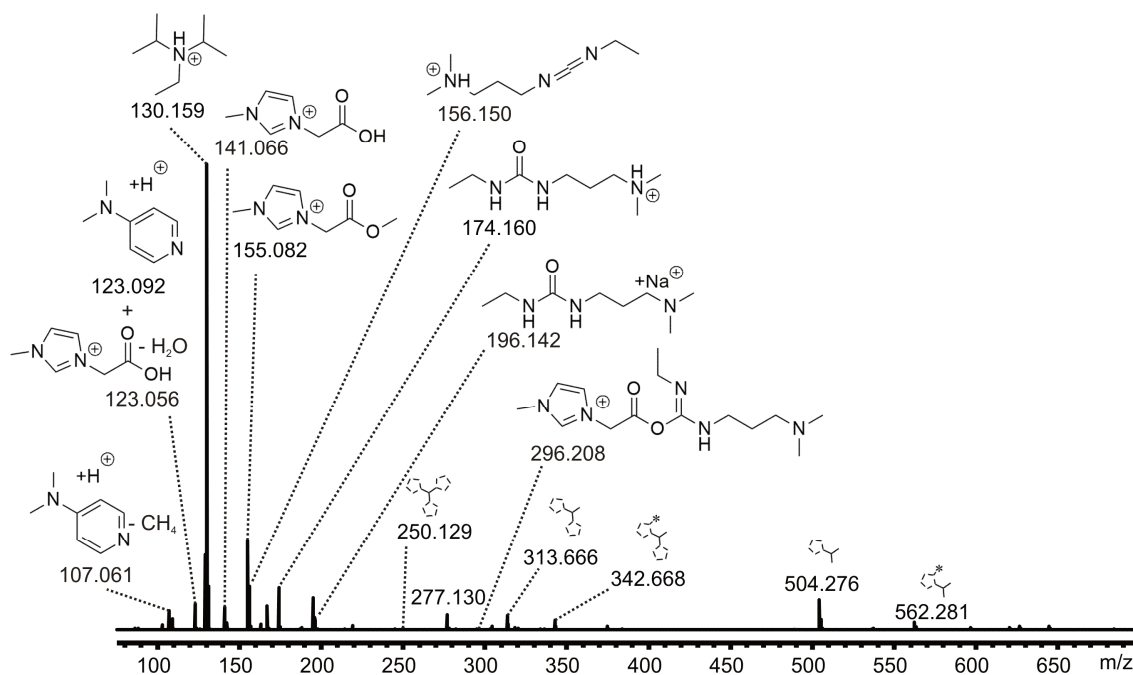


Figure 114: ESI(+) mass spectrum of a reacting solution containing 13^*Br^- , 23a, EDC, DMAP and DIPEA in acetonitrile at rt. The sample was taken after 3 hours and diluted with methanol.

After 24 hours the colour of the mixture and the ESI spectra of a sample did not changed significantly farther.

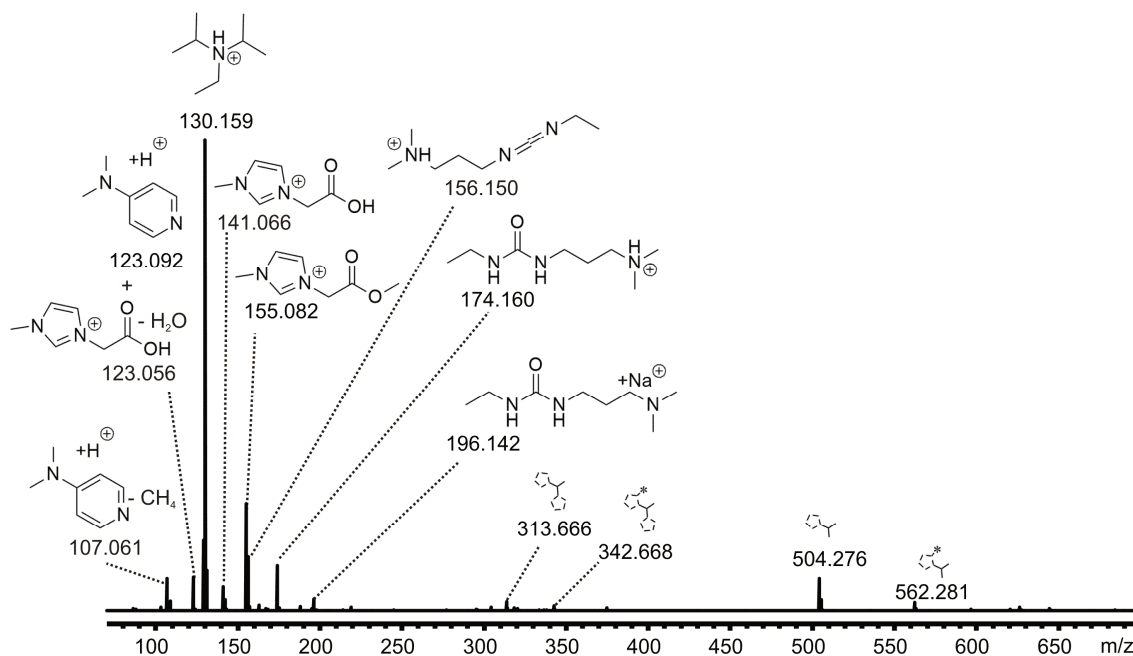


Figure 115: ESI(+) mass spectrum of a reacting solution containing 13^*Br^- , 23a, EDC, DMAP and DIPEA in acetonitrile at rt. The sample was taken after 24 hours and diluted with methanol.

Thus the reaction was ended after two days and the solvent was reduced to a minimum volume in vacuo. The dark solid was filtered and washed with acetonitrile. The ESI spectrum of the crude product, recorded from a methanol solution, reveals significant amounts of the three amide ligand precursors (**24a**, **25a** and **26a**). Washing the product with acetonitrile removed most of the reactants from the crude product. The amides are poorly soluble in acetonitrile and completely soluble in methanol. However washing with water has given better results, as seen before.

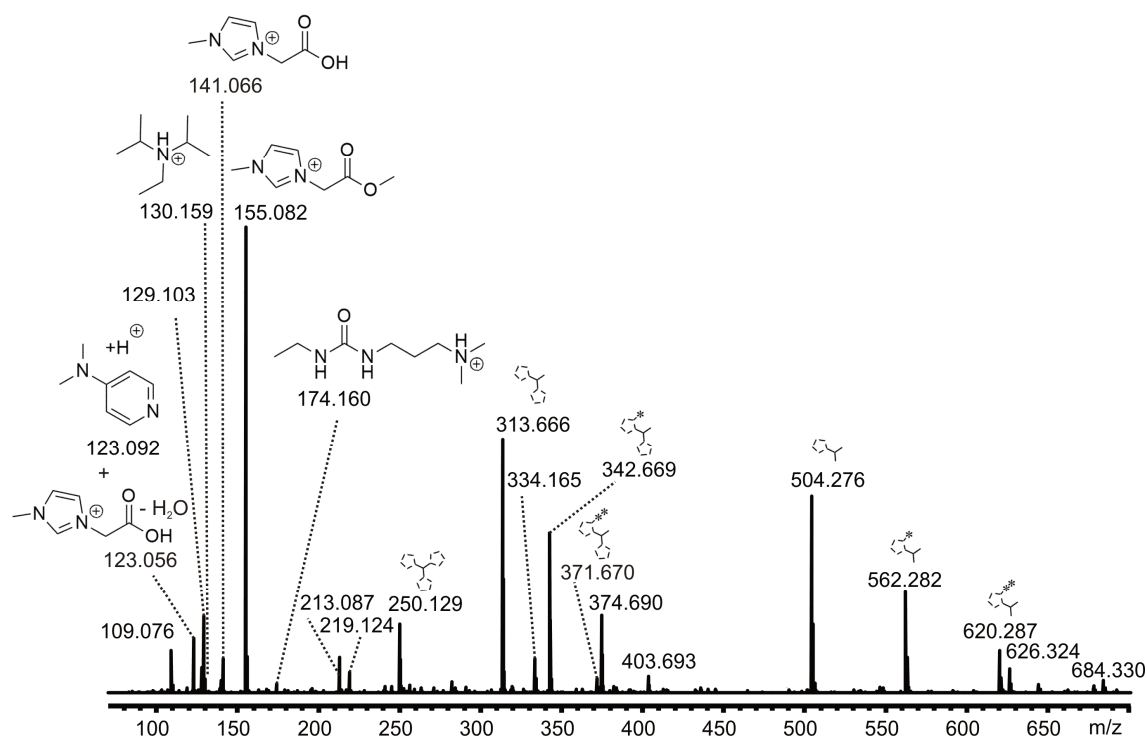


Figure 116: ESI(+)-mass spectrum of the crude product from the reaction of 13^*Br^- , **23a**, EDC, DMAP and DIPEA in acetonitrile at rt. The sample was diluted with methanol.

After the enhancement of the reaction at higher temperatures, the next experiment was driven at 50°C . Therefore the two mixtures **A** and **B** were mixed at room temperature and then heated. Similar to the experiment at ambient temperature, the colour of the solution turned bright yellow and changed to brown soon after the mixing step, accompanied by the building of a colourless precipitate. The first MS spectrum was taken after three hours. In contrast to the former experiments all three TBTQ NHC species (**24a**, **25a** and **26a**) could be detected with good intensities by that time.

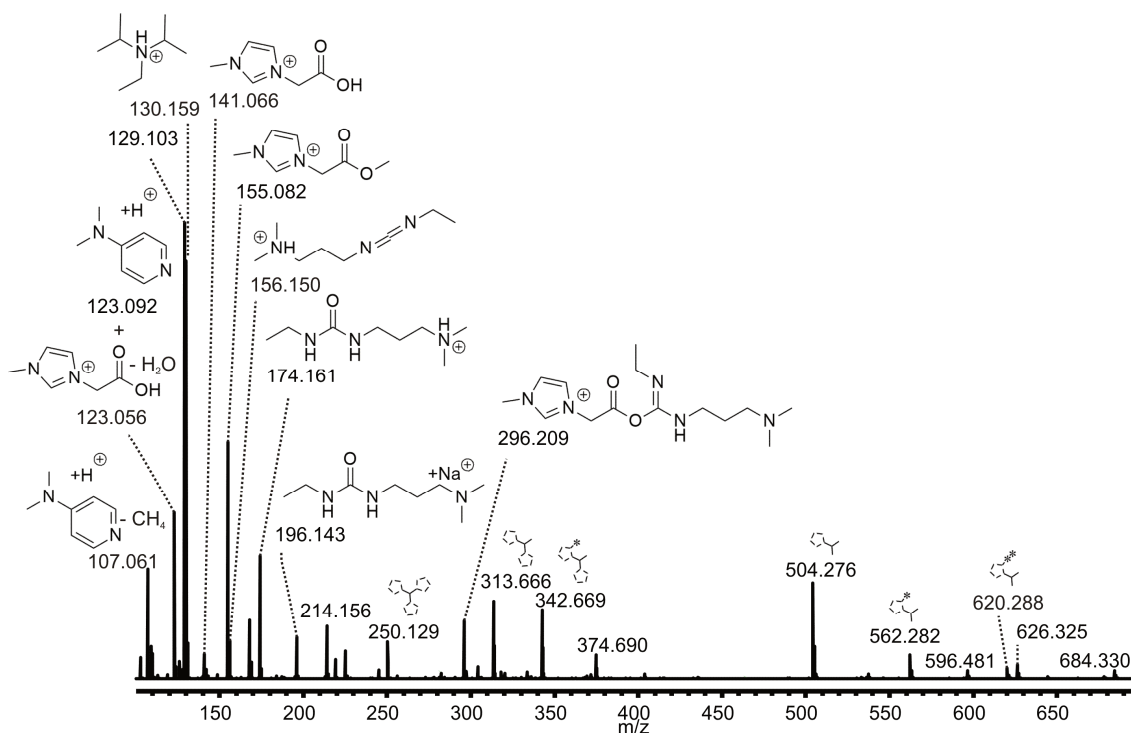


Figure 117: ESI(+)-mass spectrum of a reacting solution containing 13^*Br^- , 23a, EDC, DMAP and DIPEA in acetonitrile at 50°C. The sample was taken after 3 hours and diluted with methanol.

Stirring the mixture for 24 hours did not show significant changes in the composition of the detectable species in the gas phase (see Figure 118).

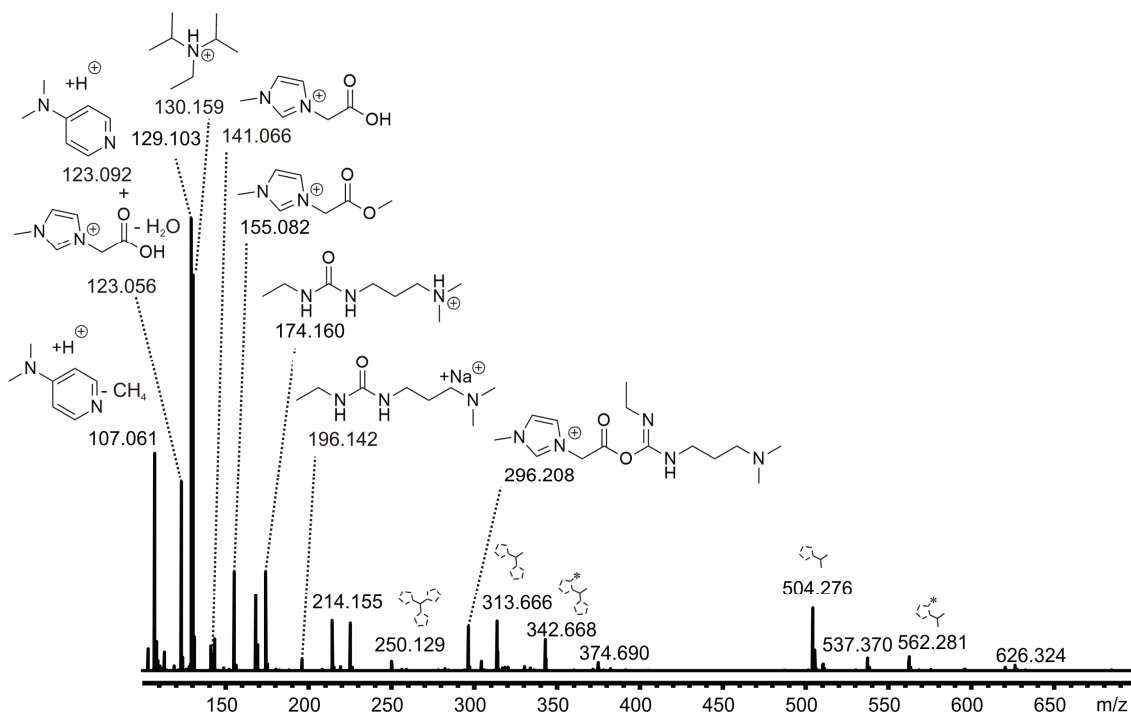


Figure 118: ESI(+)-mass spectrum of a reacting solution containing 13^*Br^- , 23a, EDC, DMAP and DIPEA in acetonitrile at 50°C. The sample was taken after 24 hours and diluted with methanol.

Stirring at 50°C was continued for another 24 hours. The mixture was then cooled to room temperature and filtered. The dark brown solid was washed with acetonitrile. Apart from the imidazolium ester **14** at $m/z = 155.08$ most of the reactants and side products could be separated from the mixture. The ESI MS spectrum of the product in methanol shows the tripod ligand precursor **26a** as the main product of the reaction (Figure 119). In the sample two additional aggregates of the tripod species **26a** have been detected. The doubly charged species **26a***Cl⁻ and **26a***Br⁻ are visible at $m/z = 392.678$ and $m/z = 414.653$ respectively (see Figure 119). Similar aggregates with PF₆⁻ have already been detected after the exchange of the counterion. Interestingly the oligomeric species of **24a** ([**24a**+CH₂CO₂]⁺ and [**24a**+(CH₂CO₂)₂]⁺) are detectable in an almost equal amount, while the ratio for **25a** is 3 : 11 : 1 (**25a** : [**25a**+CH₂CO₂]⁺ : [**25a**+(CH₂CO₂)₂]⁺) and for **26a** the oligomers are only detectable with negligible intensities. Apart from statistic arrangements, the bigger oligomers seem to hinder the building of the tripod ligand precursor **26a**. This is attributed to repulsive steric effects.

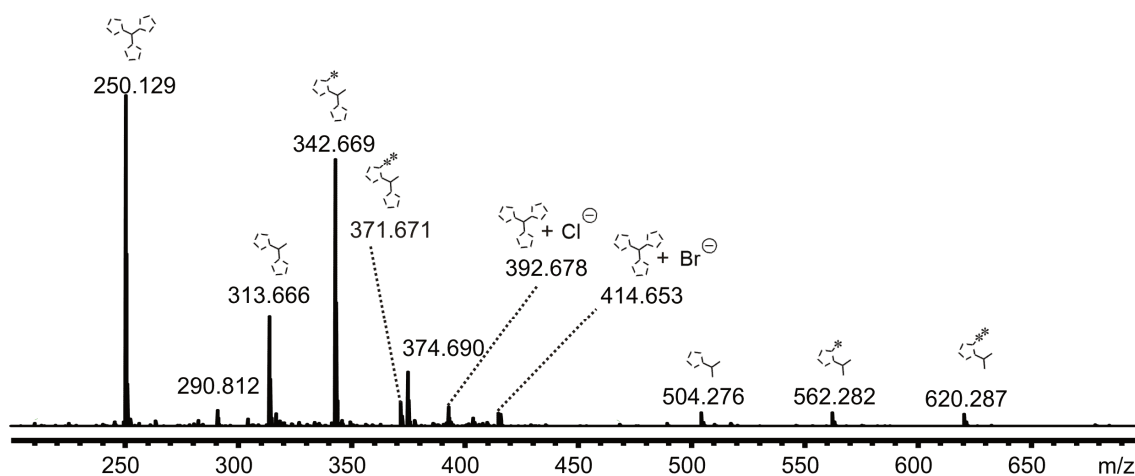


Figure 119: ESI(+) mass spectrum of the crude product (precipitate) from the reaction of **13***Br⁻, **23a**, EDC, DMAP and DIPEA in acetonitrile at 50°C. The sample was diluted with methanol (For full spectrum see Figure 173).

Investigations of the filtrate also show small signals of the crucial species **24a**, **25a** and **26a** as well as some oligomeric species, but the spectrum is dominated by side products and reactants (see Figure 120).

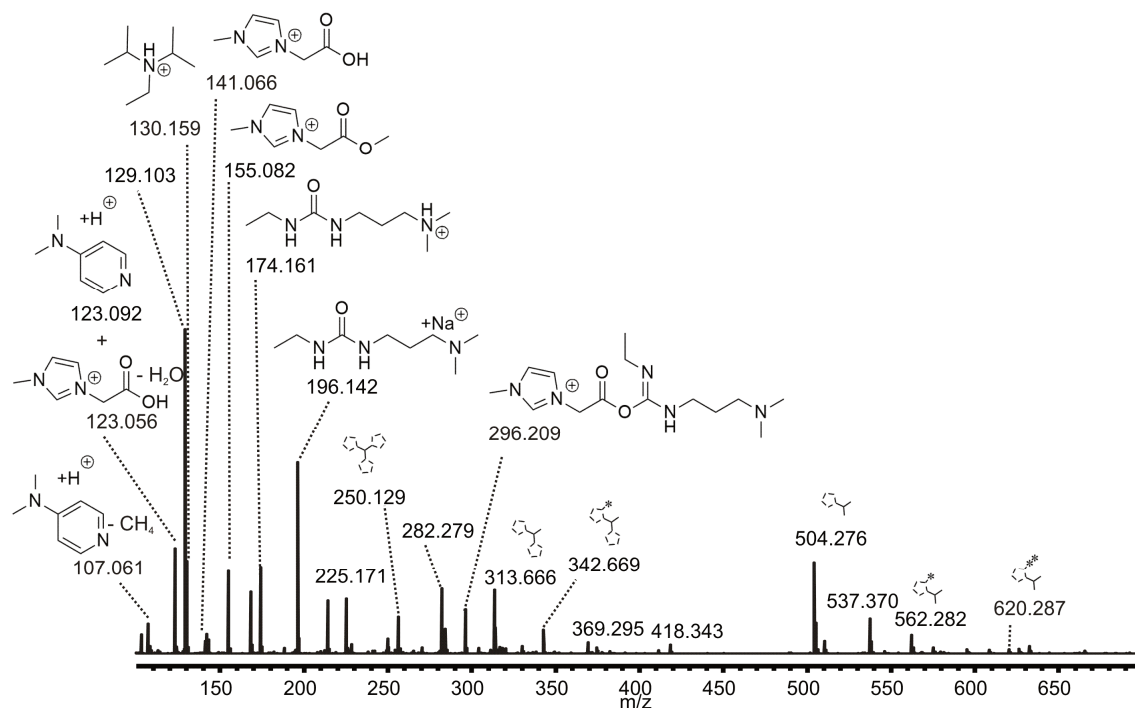


Figure 120: ESI(+) mass spectrum of the crude product (solid from the dried filtrate) from the reaction of 13^*Br^- , $23a$, EDC, DMAP and DIPEA in acetonitrile at $50^\circ C$. The sample was diluted with methanol.

The next experiment was performed with another increase of the temperature to $80^\circ C$. As described before, the two mixtures **A** and **B** were mixed at room temperature and then heated. The solution turned directly bright yellow and a colourless precipitate was formed. During the preheating the solution soon turned brown. The reaction mixture was stirred at $80^\circ C$ for three days. The red brown solid was filtered and washed with acetonitrile. The resulting MS spectrum is comparable with the spectra of the previous reaction at $50^\circ C$.

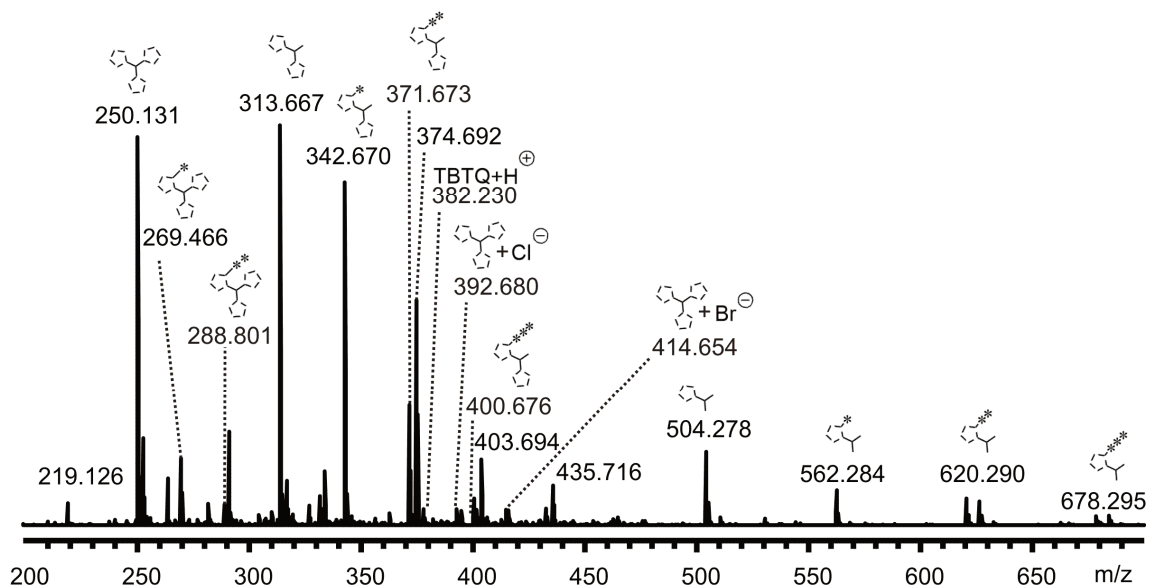
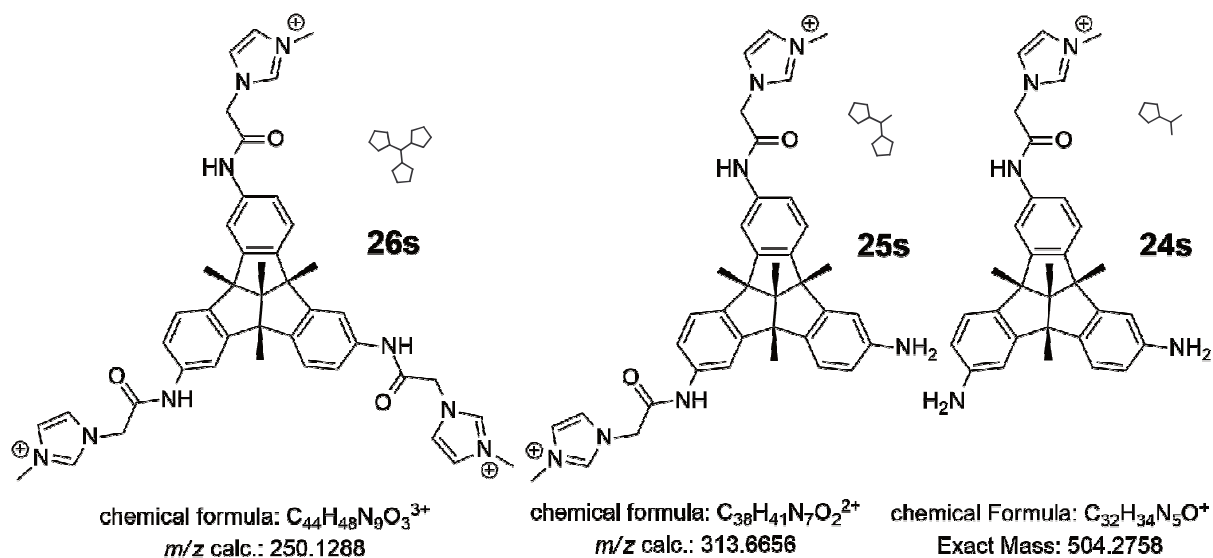


Figure 121: ESI(+) mass spectrum of the crude product from the reaction of 13^*Br^- , **23a**, EDC, DMAP and DIPEA in acetonitrile at $80^\circ C$. The sample was diluted with methanol (For full spectrum see Figure 174).

After the promising reaction with the asymmetric TBTQ backbone **23a**, the symmetrical isomer **23s** was tested. Based on the hitherto existing results, the reaction parameters were retained with 13^*Br^- , **23a**, EDC, DMAP and DIPEA in acetonitrile at $80^\circ C$.



Scheme 20: Cationic species of the wanted symmetric tripod ligand precursor and the two intermediates with only one or two respectively successfully coupled NHC units; including their chemical formulas and calculated m/z values (s=symmetric). The sketches for the symmetric compounds are illustrated with solid bonds.

Due to the symmetric conformation of the TBTQ backbone all possible combinations of the compounds **24s**, **25s** and **26s** respectively, can be transferred to each other by rotation. Therefore they consist of only one isomer in contrast to the asymmetric species. The synthesis with the symmetric compound was performed with the same reaction parameters as before (with **13***Br⁻, **23a**, EDC, DMAP and DIPEA in acetonitrile at 80°C). For this experiment a fresh charge of the acid **13***Br⁻ was used. This product did only contain pretty small amounts of the oligomeric species. The amount of the Huenig base was raised to 10 eq. to examine the impact at higher temperatures. Again the two mixtures **A** and **B** were mixed at room temperature and then heated to 80°C. The solution turned directly bright yellow and a colourless solid has formed. In contrast to the previously performed experiments, the colour of the solution turned orange and not brown. The reaction mixture was stirred at 80°C for two days. The then red brown solid was filtered and washed with acetonitrile. The MS spectrum of the crude product shows the two species **25s** and **26s** as main products of the reaction. Due to the fact, that the reaction solution only contained a small concentration of the oligomeric species of **13***Br⁻, the new product is almost free of oligomers. Only one species could be detected with minor intensity at $m/z = 342.667$ [**25s**+CH₂CO₂] (see Figure 122).

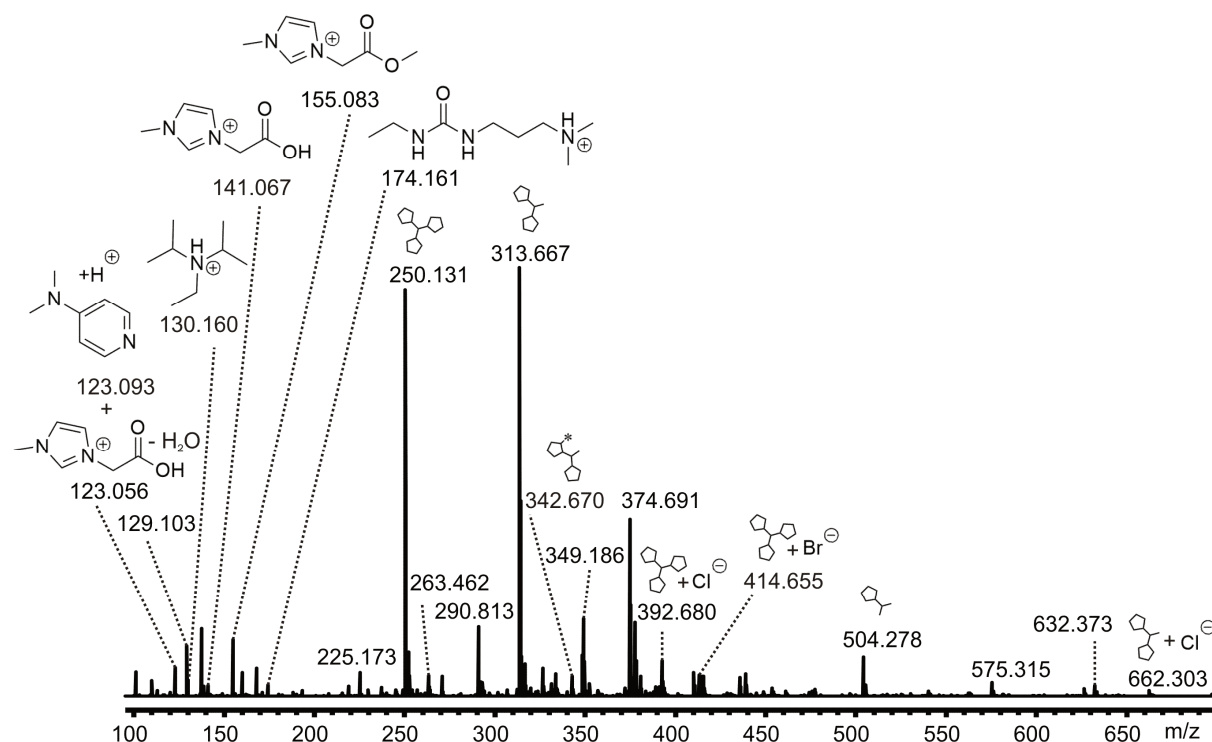


Figure 122: ESI(+) mass spectrum of the crude product from the reaction of **13***Br⁻, **23a**, EDC, DMAP and DIPEA in acetonitrile at 80°C. The sample was diluted with methanol.

Another attempt with the symmetric compound was performed with 6 eq. of the base. The two mixtures **A** and **B** were mixed at room temperature and then heated to 80°C. As seen before the solution turned directly bright yellow and a colourless precipitate was formed, which turned dark after a short period of time. The reaction mixture was stirred at 80°C for three days. The then red brown solid was filtered and washed with acetonitrile. Even though the cleaning step was incomplete, this reaction shows the best turn over. The tripod ligand precursor **26s** is the main product (see Figure 123). Interestingly the sample still contains the transient species **28** and also the protonated form $[\mathbf{28}+\text{H}]^{2+}$, so the reaction wasn't finished yet. Longer reaction times could lead to higher amounts of the tripod compound **26s**. Again the only detectable oligomer is $[\mathbf{25s}+\text{CH}_2\text{CO}_2]$. The absence of the species with the additional CH_2CO_2 groups is a benefiting reason for the better yields of the wanted compounds. Comparison of both isomers (symmetrical and asymmetrical) shows the best turn over for the symmetrical compound **26s**. This is probably attributed to steric repulsion. The crude products do also differ in their colour. While both appear brown, the symmetric compounds have an intense red undertone.

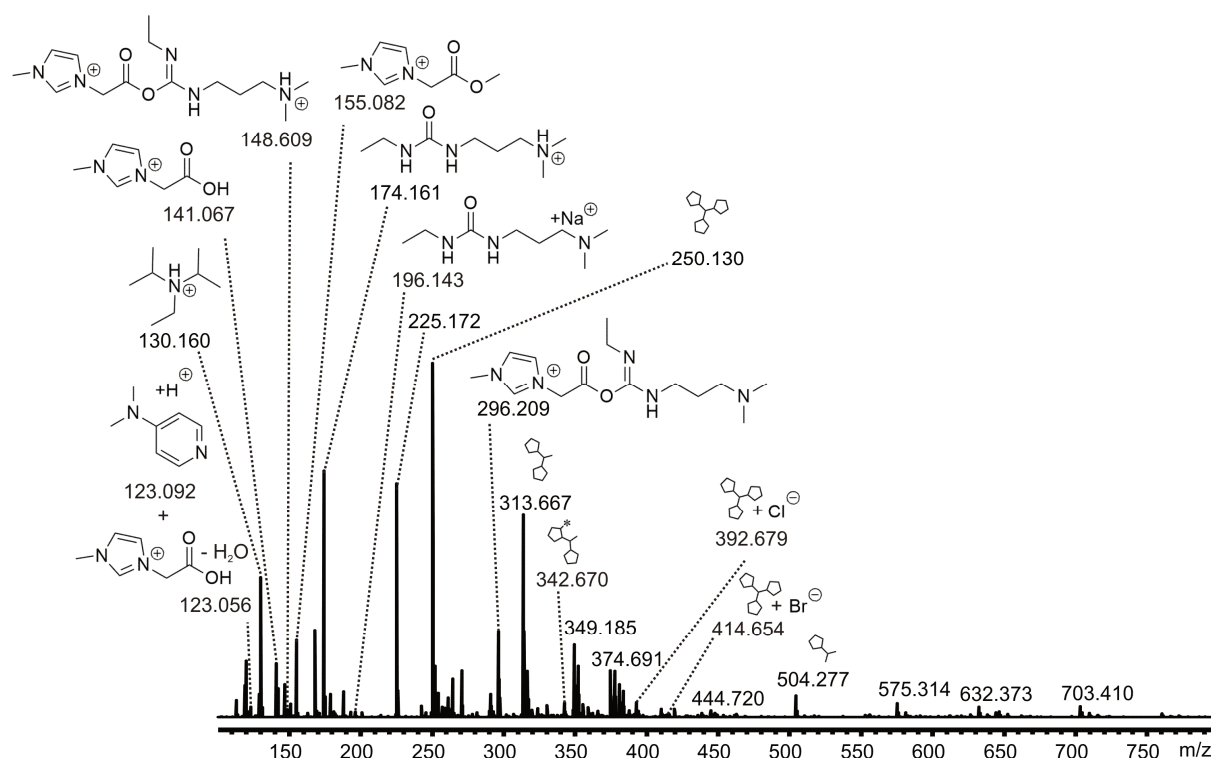
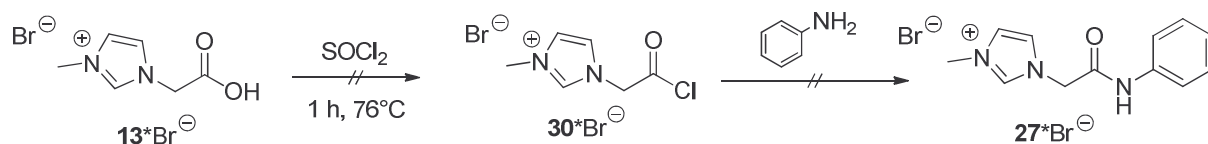


Figure 123: ESI(+) mass spectrum of the crude product from the reaction of $\mathbf{13}^*\text{Br}^-$, **23a**, EDC, DMAP and DIPEA in acetonitrile at 80°C. The sample was diluted with methanol.

Due to the fact, that the unfinished precursors **24a,s** and **25a,s** partially precipitate in acetonitrile, other solvents should be tested in the future. While most of the reactants could be separated from the product by a simple washing step, the mixtures of the three imidazolium compounds (**24a**, **25a** and **26a**) as well as (**24s**, **25s** and **26s**) respectively could not be separated. Several unsuccessful crystallization experiments were performed. Even though all tested column chromatography and TLC attempts have failed, to separate the ligand precursors to yield the pure tripod compound **26a** or **26s**.

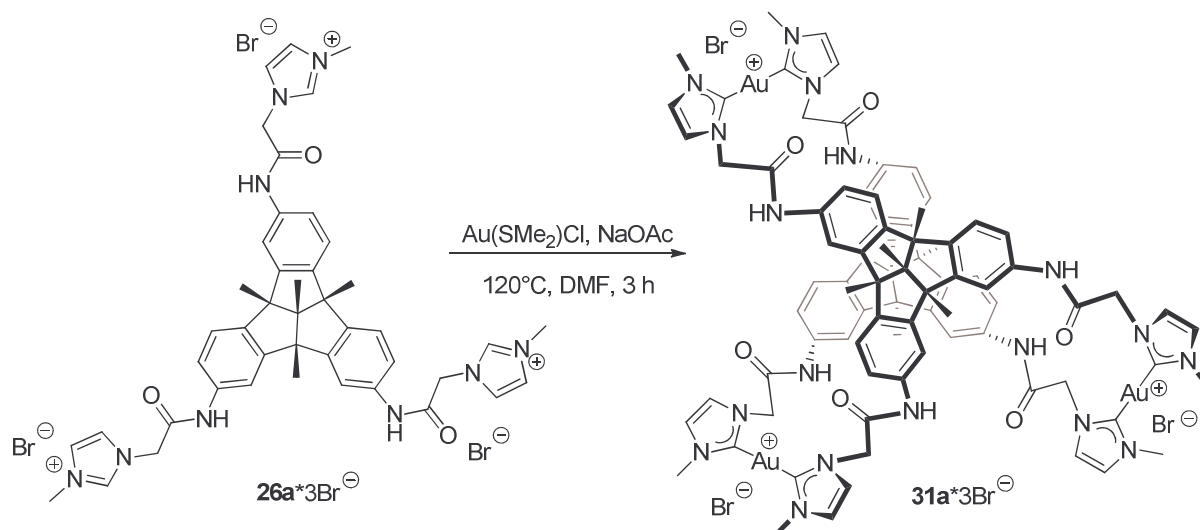
As an alternative route the coupling to the TBTQ framework could be realised with a more reactive acid chloride **30**. Similar reactions are known in the literature.^[125] These compounds are often reactive and dissociate fast. Therefore the acid chloride should be generated in situ and mixed with the amine without previous isolation and purification. The imidazolium salt **13*Br⁻** was heated in SOCl₂. The excess SOCl₂ was removed by distillation. The crude product was dissolved in THF and then aniline and Na₂CO₃ were tentatively added to the crude product. MS spectra of the product did not show the cation of the compound **27*Br⁻**. Since the reaction of the amine with the acid **13*Br⁻** was successful, this alternative approach was not further investigated.



Scheme 21: Alternative tested synthesis of the compound **27*Br⁻ with the acid chloride **30*Br⁻**.**

4.4 Synthesis of the metal TBTQ NHC complexes

Due to the lack of an effective separation method, the crude products of the ligand precursors were used without separation of the three different isomers **24a**, **25a** and **26a** (as well as **24s**, **25s** and **26s** respectively).



Scheme 22: Tested synthesis of **31a*Br⁻** with **26a*3Br⁻**, NaOAc and $\text{Au}(\text{SMe}_2)\text{Cl}$ in DMF at 120°C , with a reaction time of 3 hours.

The first complex building experiment was again adapted by the approved method from *Hemmert et al.*^[62f] Therefore the ligand precursors were heated in DMF and stirred for three hours, after the addition of NaOAc and $\text{Au}(\text{SMe}_2)\text{Cl}$. A small sample was taken, diluted in methanol and transferred to the MS. All possible Au(I) NHC complexes containing the three TBTQ NHC compounds **24a**, **25a** and **26a** and their oligomers are summarized in Table 6. For a better overview the detected gold species are shown as sketches in the MS spectra, as already seen for the ligand precursors. The explanation of these sketches is given in Scheme 26, Scheme 27 and Scheme 28.

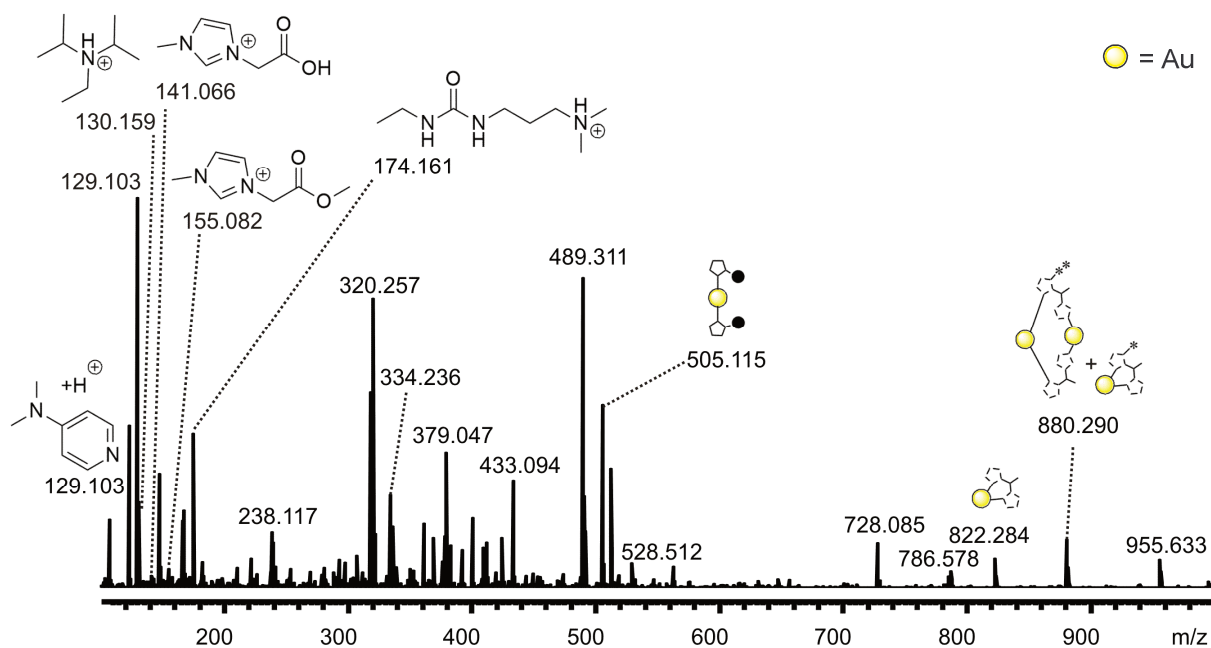


Figure 124: ESI(+)-mass spectrum of a reacting solution containing $24a^*Br^-$, $25a^*2Br^-$, $26a^*3Br^-$, $Au(SMe_2)Cl$ and $NaOAc$ in DMF $120^\circ C$. The sample was taken after 3 hours and diluted with methanol. (Includes small signals of $26a$, $25a$, $[25a+CH_2CO_2]$, $24a$, $[35a+CH_2CO_2]$; the crude product contains side products and starting materials from the synthesis of $26a^*3Br^-$).

The ESI spectrum shows some successful complexation products at $m/z = 505.115$ (**34**), 822.284 (**33a**) and 880.290 ($[35a+(CH_2CO_2)_2] + [33a+CH_2CO_2]$) two isobaric species with different charges). Also a signal at $m/z = 695.21$ could be detected. The accurate mass fits to the trinuclear gold cage, but the isotopic pattern does not fit the calculation. Thus the detected species is not the gold cage or the signal is perhaps superimposed by another signal (see Figure 125). The intensity of the signal was too small to perform fragmentation experiments and confirm the species. Even though the other four gold containing species are detectable with moderate intensities, the signals of the imidazolium species (**24a**, **25a** and **26a**) were only very small. Without available ligand precursors the building of more gold complexes is not possible. Hence the reaction was stopped and the reaction procedure was modified.

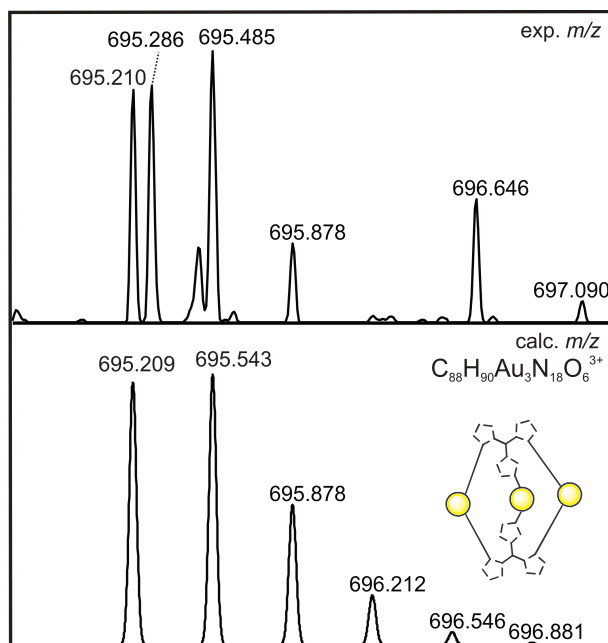


Figure 125: Partial ESI(+) mass spectrum of the reacting solution, showing the actual spectrum and calculated isotopic pattern of 31a.

There are some plausible explanations for the unsuccessful reaction. Depending on the fact, that the mixture of the imidazolium salts could not be purified, the concentration of the different species in the reacting solution is unknown. The reaction of imidazolium salts with a nonstoichiometric amount of the $\text{Au}(\text{SMe}_2)\text{Cl}$ usually leads to different complexes with only one NHC ligand and an additional chloride as ligand $[\text{NHC-Au-Cl}]$.^[2c,46a,89,113,126] These products are not charged and therefore not detectable by ESI MS, without further fragmentation or additional charged substituents. After the loss of the chloride ligand they can be found as $[\text{NHC-Au}]^+$ species. Another possible explanation is a mismatch of different ligands and the oligomerisation or polymerisation of the compounds. The imidazolium compounds **25a** and **26a** have more than one binding site available for complexation. The reaction between more than only two ligand precursors would lead to bigger and more complex structures. Next to the unwanted side reactions, the decomposition of the amide bonds through moisture is also possible and would therefore hamper the reaction. Since no effective purification method for the ligand precursors could be found so far and oligomerisation could not be excluded, the complexation routine was changed.

An alternative pathway for the synthesis of the trinuclear gold cage is the transmetalation of a silver complex.^[127] This type of complex contains partially reversible Ag-carbene bonds accompanied with an interesting dynamic behaviour in solution.^[62n,128] Ligand exchanges are

possible, to obtain the strongest versions of the complexes. Gold(I) NHC complexes however are mostly stable in solution and do not show the same behaviour. A mismatch of different ligand precursors or the combination of more than two of them could not be corrected. Therefore the prior synthesis of the silver complex templates seems helpful. Indeed this approach does not prevent oligomerisation, but the system stays dynamic and can still be corrected. The use of silver(I) NHC complexes are not limited to this practice, they do have several interesting properties and possible applications themselves.^[2c,51,114,129] A successful synthesis of an Ag containing cage could also provide a vulnerable sensor molecule. However the target compound for this work is the gold derivative. The higher stability of the end product provides a better handling for recognition processes. The first Ag(I) NHC complex in this work was synthesized via the silver base route.^[2c,57a,130] This routine is the most common preparation method and includes the treatment of the ligand precursor with Ag₂O. Some examples are known which do not need further additives as the silver source does act as a base itself, but most reactions are performed with an additional mild base and a phase transfer catalyst. However the synthesis does not need an inert gas atmosphere and can be performed at ambient temperature under mild conditions. The only challenge is to totally exclude the reacting mixture from light. The silver compounds are extremely light sensitive and dissociate fast in solution. Therefore all silver containing reactions and purification steps have to be performed without light exposure. The solid complexes after the removal of the solvent are indeed mostly stable under exposure to light.

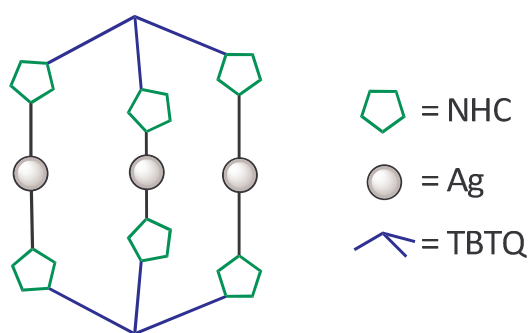
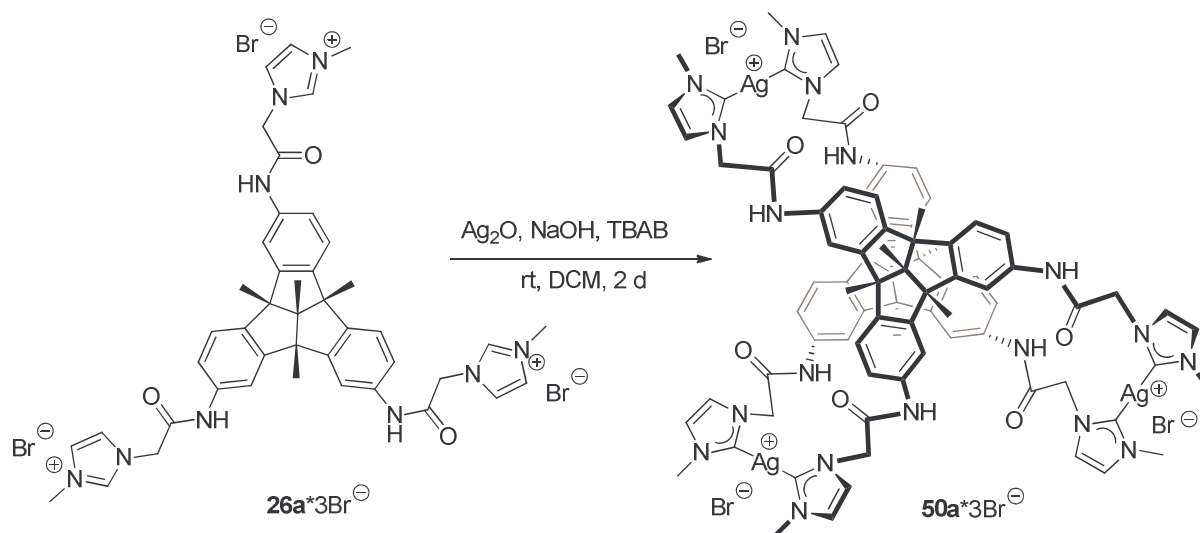


Figure 126: Sketch of the trinuclear silver(I) NHC tribenzotriquinacene cage molecule.

For the first reaction the crude product of the asymmetrical tripodal ligand precursors was dissolved in dichloromethane. A 2 N solution of NaOH_(aq), a catalytical amount of tetrabutylammonium bromide (TBAB) and AgO₂ were successively added, leading to a black suspension. After two hours a small sample of the now brown suspension was diluted in

methanol and transferred to the MS. All possible Ag(I) NHC complexes with their accurate masses are summarized in Table 7. As already seen for the gold species and the ligand precursors, the silver compounds are shown as sketches in the MS spectra. The explanation of these sketches is given in Scheme 26, Scheme 27 and Scheme 29.



Scheme 23: Tested synthesis of **50a***Br⁻ with **26a***3Br⁻, TBAB, NaOH_{aq} and Ag₂O in DCM at rt, with a reaction time of 2 days.

The cation of the phase transfer catalyst TBA⁺ has a pretty high ESI response, leading to an intense signal. Therefore most of the other detectable species are mainly suppressed. However the first successful complexation of silver was detected at $m/z = 427.636$, and confirmed by the accurate mass and the characteristic isotopic pattern of silver. The given complex **51a** consists of the ligand precursor **26a** and a silver atom. Complexation of one metal atom always involves two prior deprotonation steps leading to the carbene species. Unfortunately the reaction has linked two NHC units which originate from the same molecule. The intended cage complex should combine two different molecules. But nevertheless a first effective complexation step was achieved.

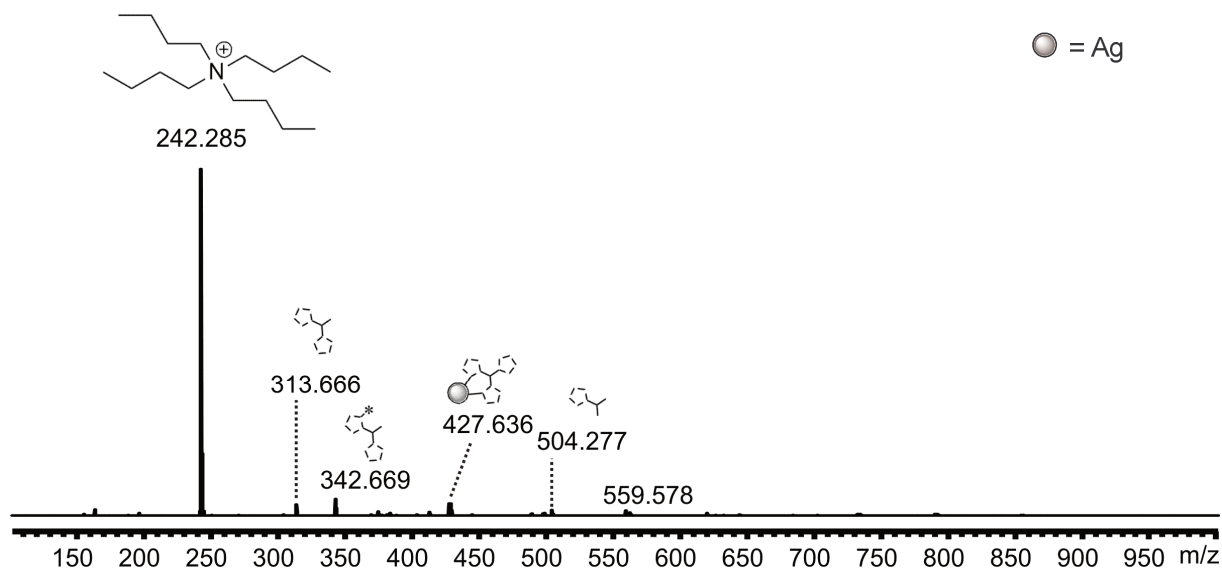


Figure 127: ESI(+)-mass spectrum of a reacting solution containing $24a^*Br^-$, $25a^*2Br^-$, $26a^*3Br^-$, TBAB, $NaOH_{aq}$ and AgO_2 in DCM at rt. The sample was taken after 2 hours and diluted with methanol.

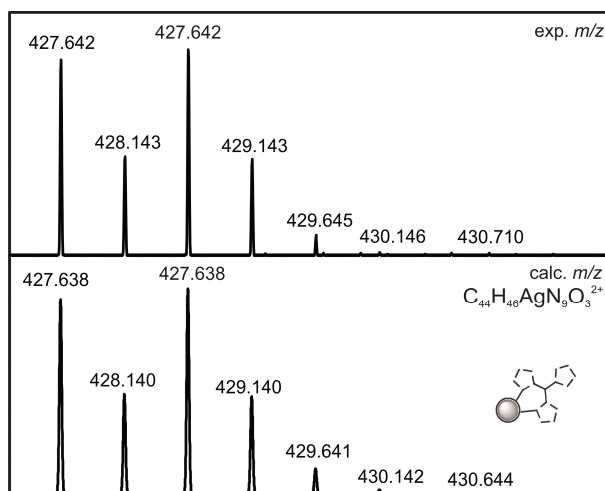


Figure 128: Partial ESI(+)-mass spectrum of a reacting solution, showing the experimental and calculated isotopic pattern of **51a**.

Changing the investigated m/z range above 250 supports the detection of other interesting species with moderate intensities, due to suppression of the intense TBA^+ signal. Next to the already known species from the crude product of the ligand precursor and the previously described silver complex, two new silver complexes are visible. They are produced by a complexation of **25a** with one silver ion (**52a**, $m/z = 732.227$) and the associated species with two additional $-CH_2CO_2$ groups ($[52a+(CH_2CO_2)_2]$, $m/z = 790.233$). Two other silver species with pretty small intensities could also be detected at $m/z = 618.254$ (**63a**), 647.260

[**63a**+CH₂CO₂]). Both complexes occur from the reaction of the two ligand precursors **24a** and **25a** as well as the oligomeric species. This is the first detected silver species with two different NHC ligands. Another detected species with a small intensity is **56a**, this complex also consists of two different NHCs (**25a** and **26a**). The spectrum also includes high intensities of the not yet reacted ligand precursors. Therefore stirring of the reacting solution was continued.

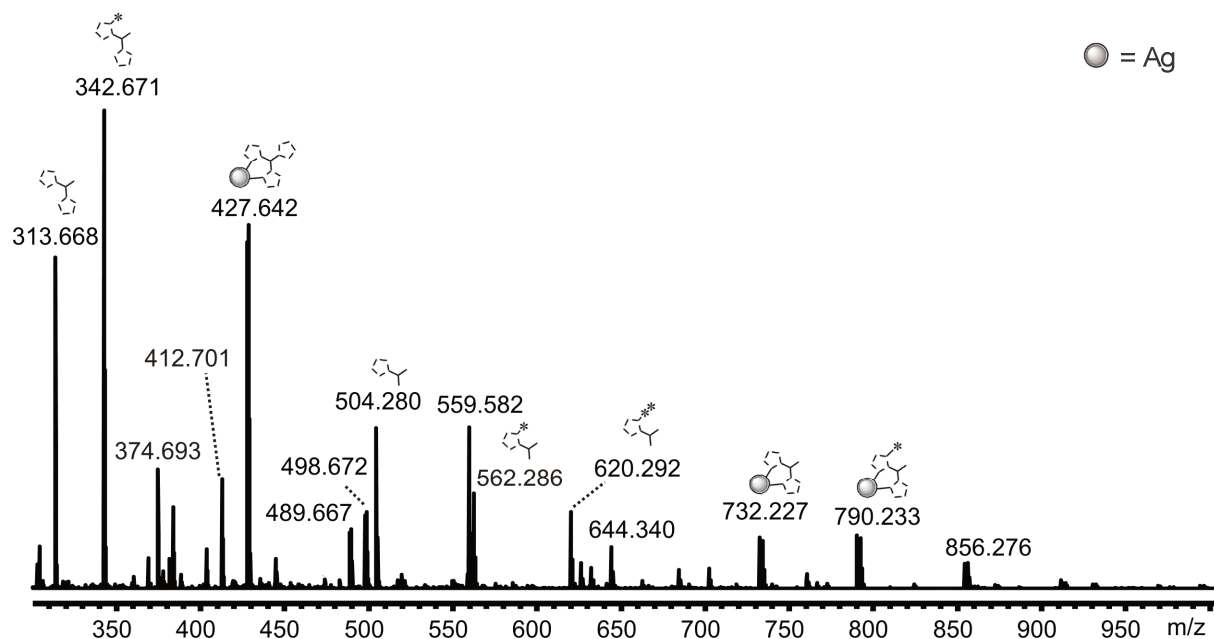


Figure 129: ESI(+)-mass spectrum of a reacting solution containing **24a***Br⁻, **25a***2Br⁻, **26a***3Br⁻, TBAB, NaOH_{aq} and AgO₂ in DCM at rt. The sample was taken after 2 hours and diluted with methanol. (Includes small signals of **56a**, **63a** and [**63a**+CH₂CO₂]).

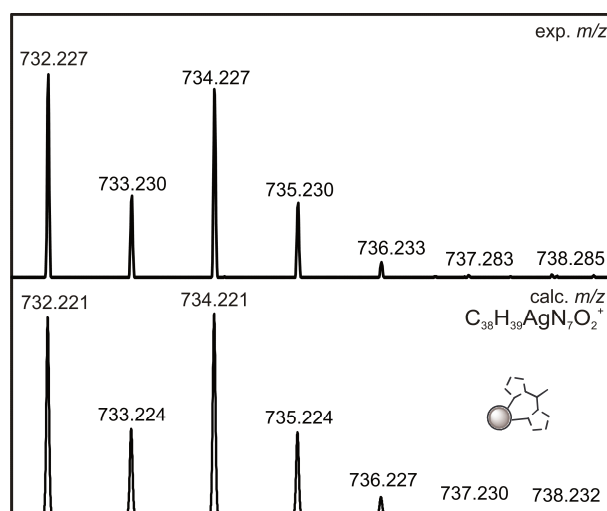


Figure 130: Partial ESI(+)-mass spectrum of a reacting solution, showing the experimental and calculated isotopic pattern of **52a**.

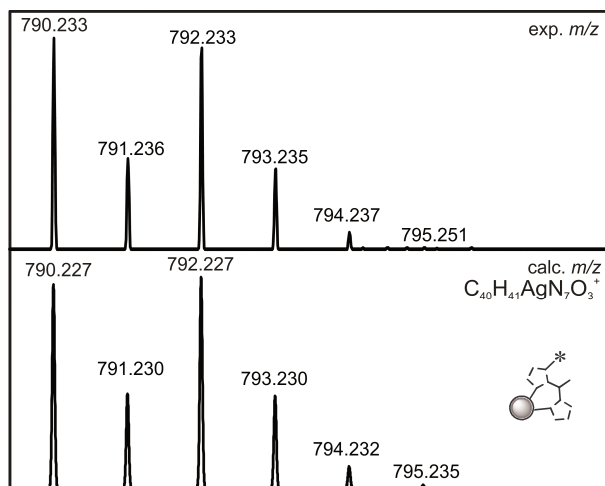


Figure 131: Partial ESI(+) mass spectrum of a reacting solution, showing the experimental and calculated isotopic pattern of [52a+CH₂CO₂].

After 24 hours the suspension was brown and contained a mixture of plenty bright and dark solids. Another sample of the mixture was taken and diluted in methanol. The ESI MS spectrum differs from the first one. The signal at $m/z = 732.221$ had changed because a second species with the same accurate mass but another charge occurred. The intensity of the new species **55a** is pretty small, but still recognizable. This species is the result of the complexation of two molecules of the ligand precursor **25a** and two silver atoms. The corresponding complex with one additional CH₂CO₂ unit could also be detected with a small intensity. The signal at $m/z = 610.173$ (C₃₂H₃₃N₅OAg) is probably a fragment of a former complex. Fragmentation of labile silver complexes [L₁-Ag-L₂]⁺ in the gas phase usually leads to two detectable fragments [L₁-Ag]⁺ and [Ag-L₂]⁺ after the loss of the other ligand. The distribution of the intensities depends on the dissociation energies of the ligands.^[131] The molecular formula of the detected species and the isotopic pattern fits to [24a-H+Ag]⁺. The constitution is characteristic for fragments of NHC-silver complexes. Species like that are marked with a # in the spectra. An overview of all detected fragment species and their probable assignments are given in Table 8 (this table is not limited to the current experiment).

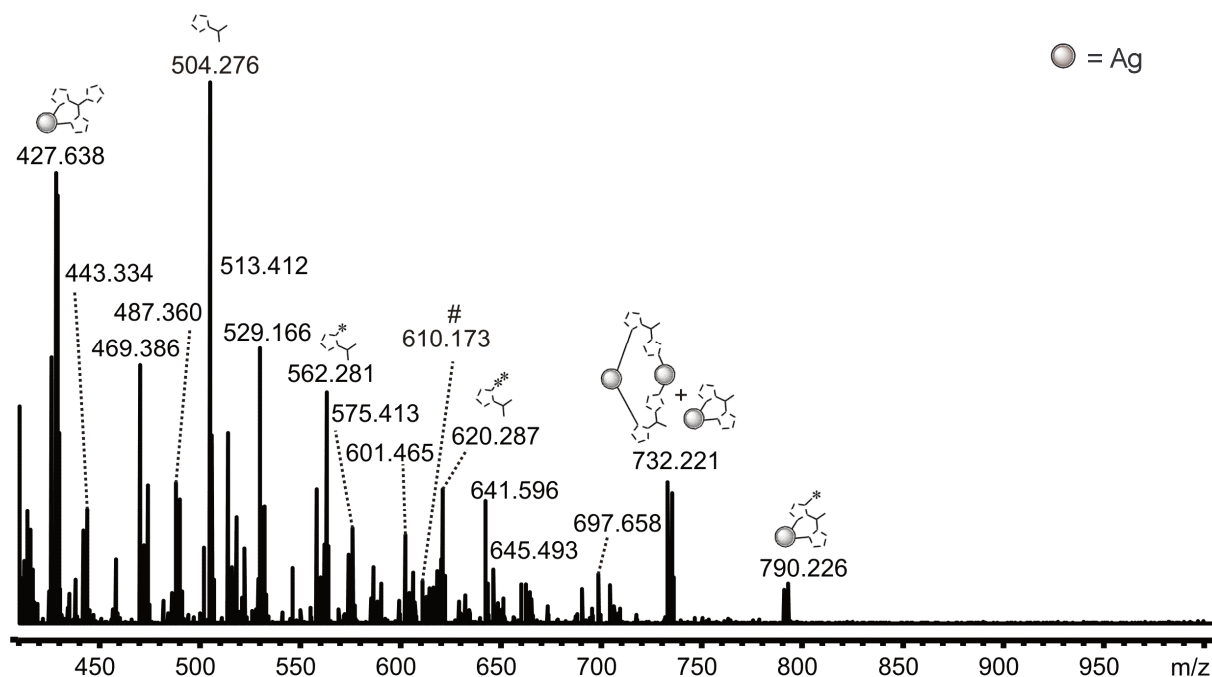


Figure 132: ESI(+) mass spectrum of a reacting solution containing $24a^*Br^-$, $25a^*2Br^-$, $26a^*3Br^-$, TBAB, $NaOH_{aq}$ and AgO_2 in DCM at rt. The sample was taken after 24 hours and diluted with methanol. (Includes small signals of $[TBTQ+H]^+$, $[63a+CH_2CO_2]$, $[55a+CH_2CO_2]$; for full spectrum see Figure 175, for explanation of the # see Table 8).

After two days a few more silver complexes could be detected in the solution. Next to the known isobaric species **52a** and **55a** are two complexes at $m/z = 427.66$ and 790.25 respectively. The new species are again Ag-NHC complexes with two different ligands. Due to the fact, that they have the same accurate mass as the previously found species with only one NHC ligand, the signals overlies. Since they have different charges the signals can be distinguished. The intensities of the species with only one NHC ligand are much higher but the small additional signals lead to deformed isotopic pattern (an example of the overlaying signals is given further down). The spectrum also contains several Ag-NHC species with minor intensities (see Figure 133). Suppression of the species with a smaller m/z value than 240 works pretty well with the used parameters at the QToF MS. Therefore the spectrum looks clean in that area, which is not representative for the sample but helpful for the detection of the interesting species. The intensities of the remaining ligand precursors in the solution are really small. Therefore the reaction was stopped and the reaction parameters were changed.

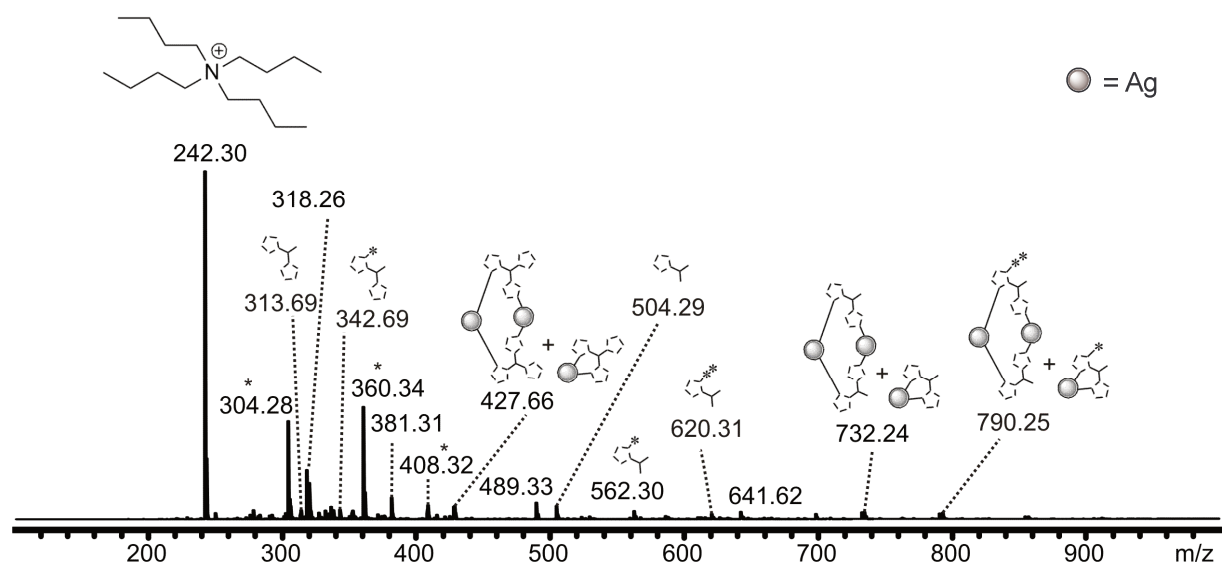


Figure 133: ESI(+)-mass spectrum of a reacting solution containing $24a^*Br^-$, $25a^*2Br^-$, $26a^*3Br^-$, TBAB, $NaOH_{aq}$ and AgO_2 in DCM at rt. The sample was taken after 2 days and diluted with methanol. (Includes small signals of $56a$, $[58a+(CH_2CO_2)_2]$, $[55a+CH_2CO_2]$, $[51a+(CH_2CO_2)_2]$, $59a/61a$, $63a$, * = common background contaminant ions).

For the next attempt another solvent was chosen. Replacing dichloromethane with methanol had a huge impact on the reaction. All reactants were mixed and stirred at room temperature as done before. The suspension turned directly black from the silver oxide. After one hour a sample was diluted in methanol and investigated. In contrast to the results of the reaction in dichloromethane, the given spectrum already shows two sets of isobaric species **52a** and **55a** as well as $[52a+CH_2CO_2]$ and $[55a+CH_2CO_2]$ and the signal for **51a**. The formation of the two dinuclear complexes only took one hour under the given conditions.

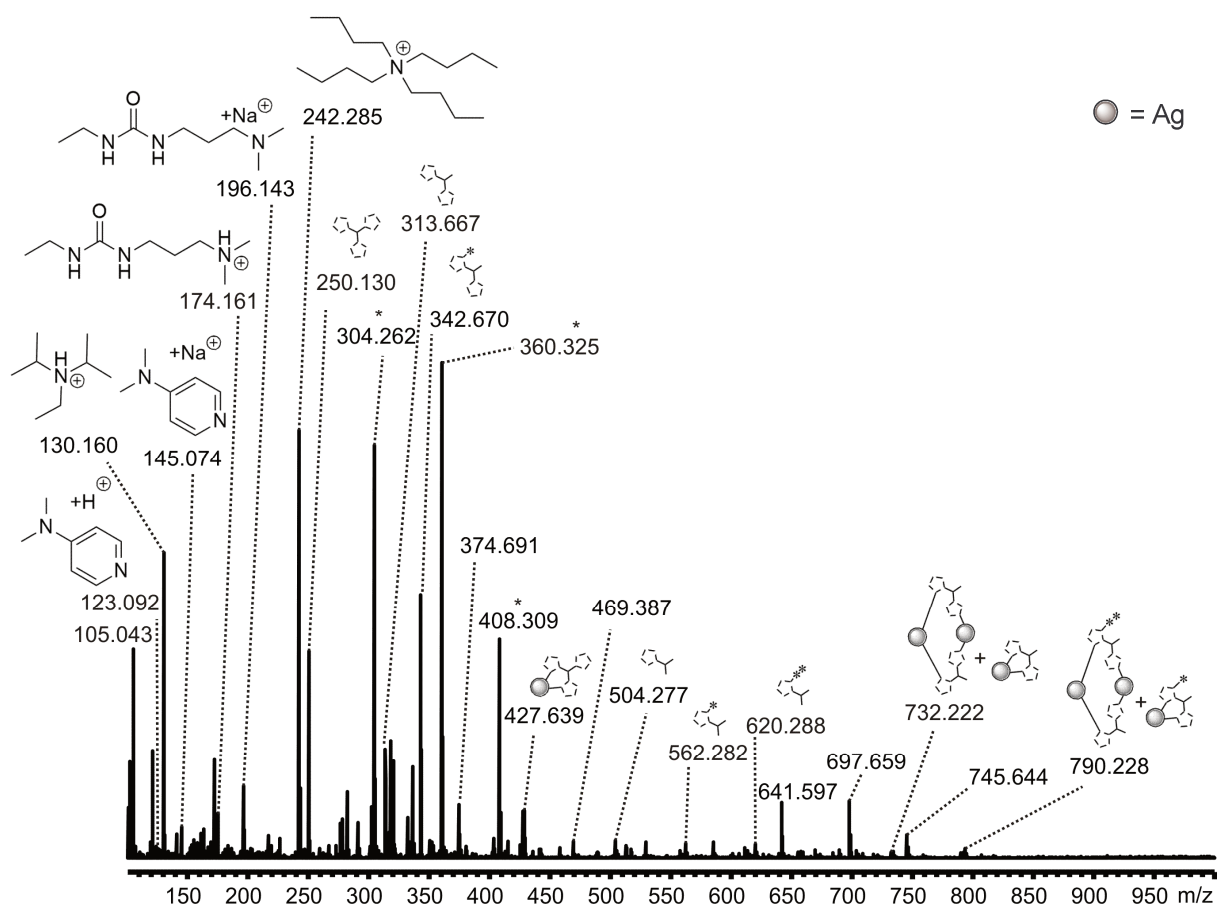


Figure 134: ESI(+) mass spectrum of a reacting solution containing **24a***Br⁻, **25a***2Br⁻, **26a***3Br⁻, TBAB, NaOH_{aq} and AgO₂ in MeOH at rt. The sample was taken after 1 hour and diluted with methanol. (Includes small signals of **59a**/**61a**, [**59a**+(CH₂CO₂)₂]/[**61a**+(CH₂CO₂)₂], **63a**, [**63a**+CH₂CO₂], [**63a**+(CH₂CO₂)₂], * = common background contaminant ions); the crude product contains side products and starting materials from the synthesis of **26a***3Br⁻).

Stirring for 24 hours resulted in the formation of another dinuclear complex **57a** next to the already detected silver complexes. The signal ($m/z = 668.18$, [C₃₂H₃₃N₅OAg+CH₂CO₂]⁺) was linked to another fragment [**24a**+CH₂CO₂-H+Ag]⁺ which probably originates from the fragmentation of a silver complex, similar to the previously explained species at $m/z = 610.18$. Measurements in the range above $m/z = 1000$ did not show any silver complexes with **24a**. Even though the intensities of the silver compounds did not increase significantly, the intensities of the ligand precursor species decreased. There are some plausible explanations for this observation as already mentioned for the gold compounds. One possibility is the dissociation of the amides in solution as well as the formation of neutral complexes [L-Ag-Cl] could be another reason.^[132] As already outlined above, the detection of these complexes by mass spectrometric means is difficult. A third possibility is the oligomerisation of the imidazolium compounds through the complexation of more than only two ligand precursors.

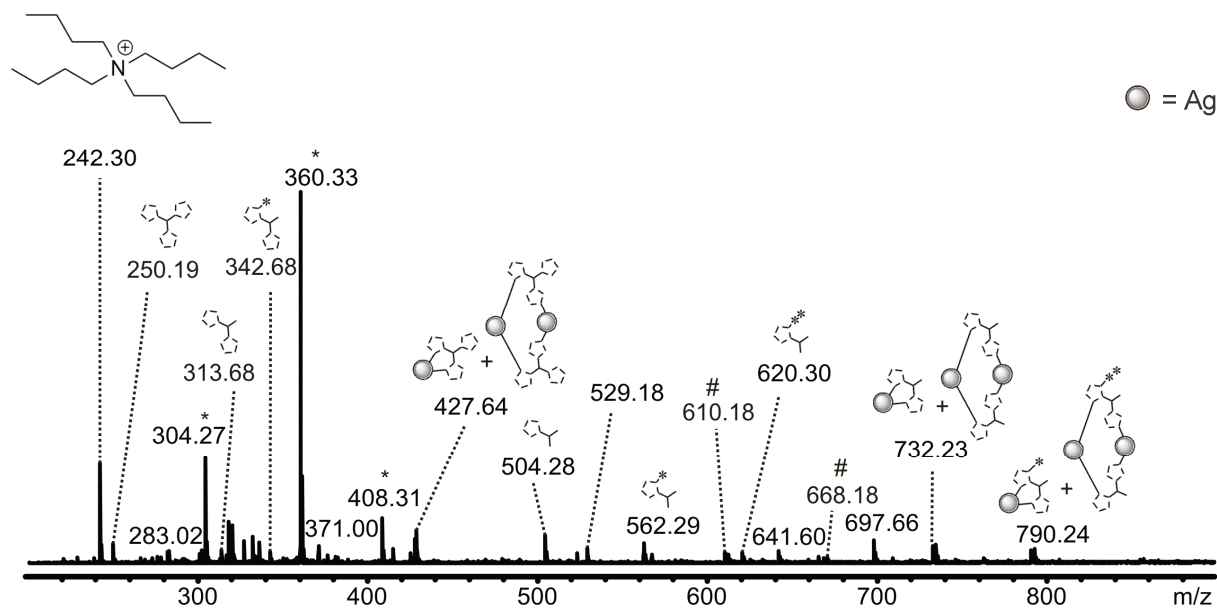


Figure 135: ESI(+)-mass spectrum of a reacting solution containing $24a^*Br^-$, $25a^*2Br^-$, $26a^*3Br^-$, TBAB, $NaOH_{aq}$ and AgO_2 in MeOH at rt. The sample was taken after 24 hours and diluted with methanol. (Includes small signals of $[55a+CH_2CO_2]$, $[63a+(CH_2CO_2)_2]$, * = common background contaminant ions, for explanation of the # see Table 8).

Even though the reaction seemed promising after only one hour and 24 hours, the composition of the reaction mixture did not change significantly after 5 days (see Figure 136), therefore the reaction was ended and other reaction parameters have been tested.

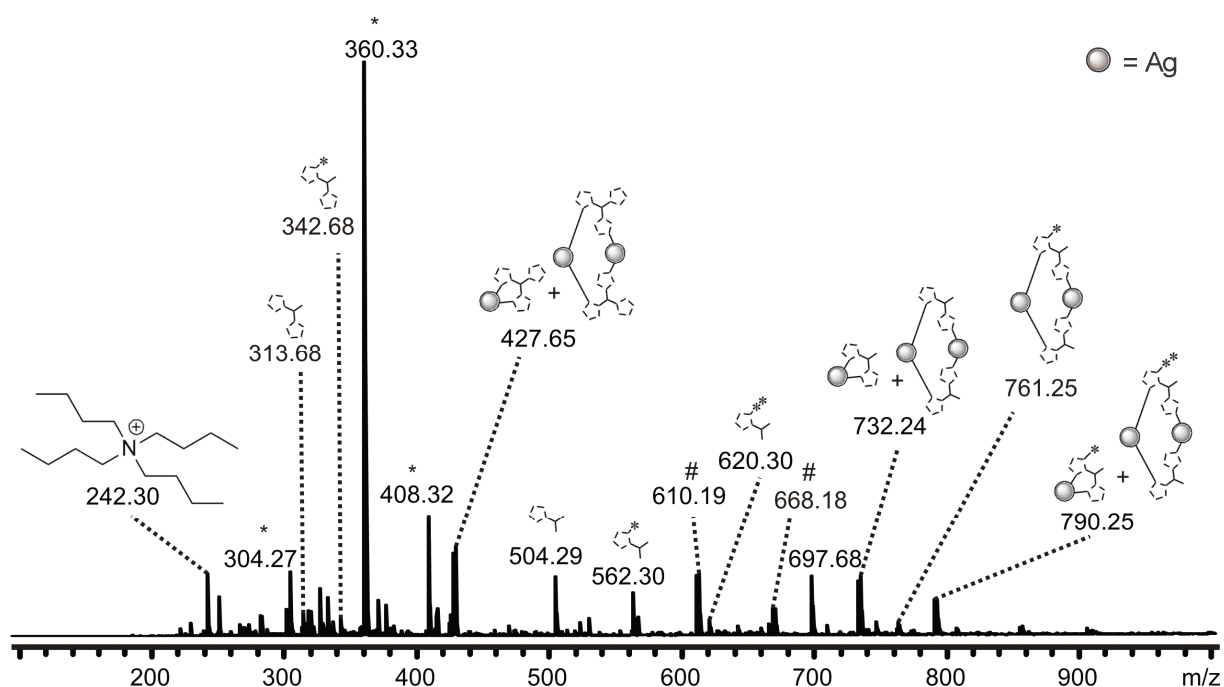
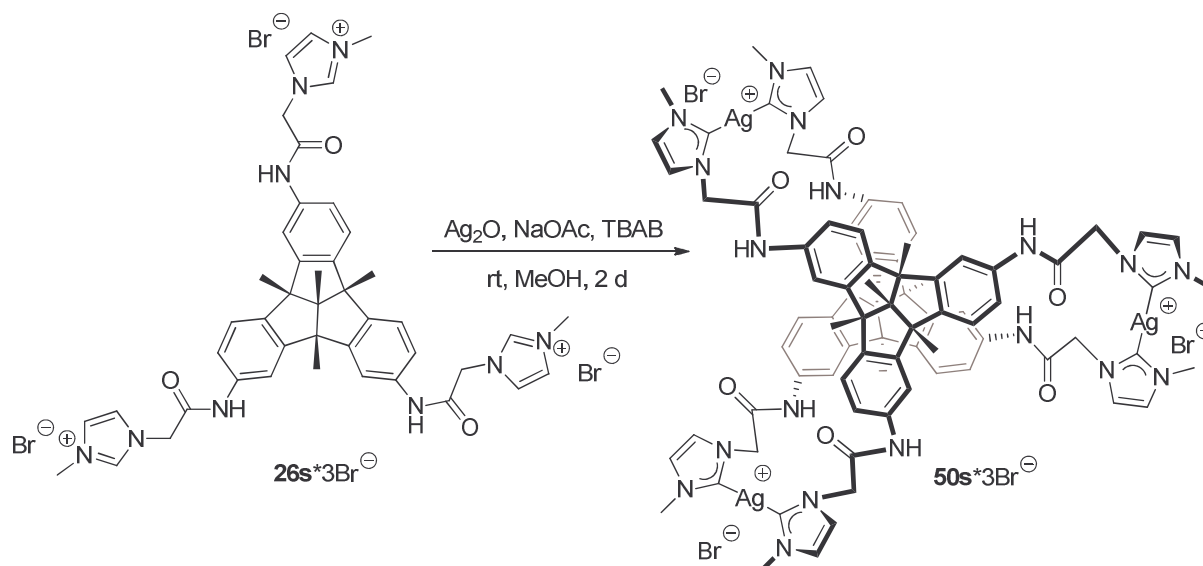


Figure 136: ESI(+)-mass spectrum of a reacting solution containing $24a^*Br^-$, $12a^*3Br^-$, $26a^*3Br^-$, TBAB, $NaOH_{aq}$ and AgO_2 in MeOH at rt. The sample was taken after 5 days and diluted with methanol. (* = common background contaminant ions, for explanation of the # see Table 8).



Scheme 24: Tested synthesis of $50s^*Br^-$ with $26s^*Br^-$, $TBAB$, $NaOAc$ and AgO_2 in $MeOH$ at rt , with a reaction time of 2 days.

Strong bases can cause the dissociation of amides, thus $NaOH_{(aq)}$ was replaced with $NaOAc$, to prevent the decomposition. The other reaction parameters were retained. This reaction was performed with the symmetric imidazolium TBTQ salts containing **24s**, **25s** and **26s**. The mixture was stirred for two days and a light brown precipitate has formed in the solution. Even though the intensities are small, the already known signals **51s** and **57s** as well as **52s** and **55s** could be detected. Both signals involve the isobaric mono- and dinuclear species respectively. Both overlying experimental spectra and the correlated calculated isotopic pattern are shown in Figure 138 and Figure 139. The additional higher charged species **55s** and **57s** have been detected before, but with much smaller intensities. The now moderate intensities allow the visualisation in the two schemes. The species can be identified by the small additional peaks inside the isotopic pattern of the species **52s** and **51s** at $\Delta m = \frac{1}{2}$ and $\frac{1}{4}$ respectively, due to the higher charges of the species.

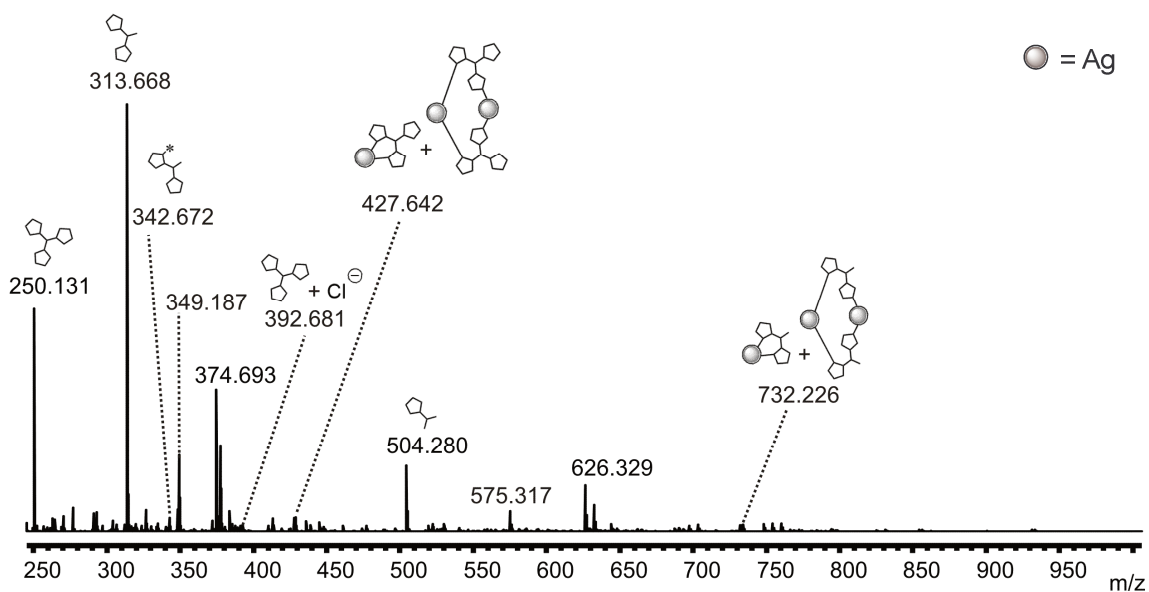


Figure 137: ESI(+) mass spectrum of the crude product from the reaction of 24s*3Br⁻, 25s*3Br⁻, 26s*Br⁻, TBAB, NaOAc and AgO₂ in MeOH at rt. The sample was diluted with methanol. (For full spectrum see Figure 176; Includes small signals of [24s+CH₂CO₂], [25s+Cl], 60s, 59s/61s, 56s, 50s, 63s).

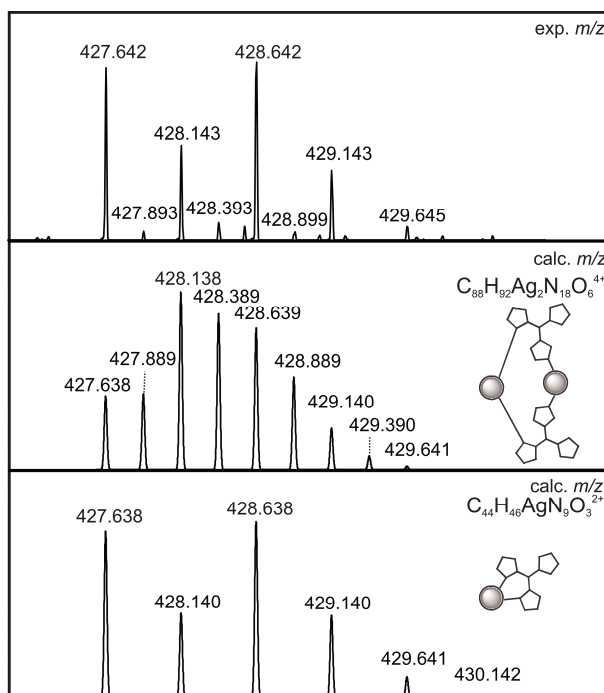


Figure 138: Partial ESI(+) mass spectrum of the crude product, showing the overlaying experimental and calculated isotopic pattern of 51s and 57s.

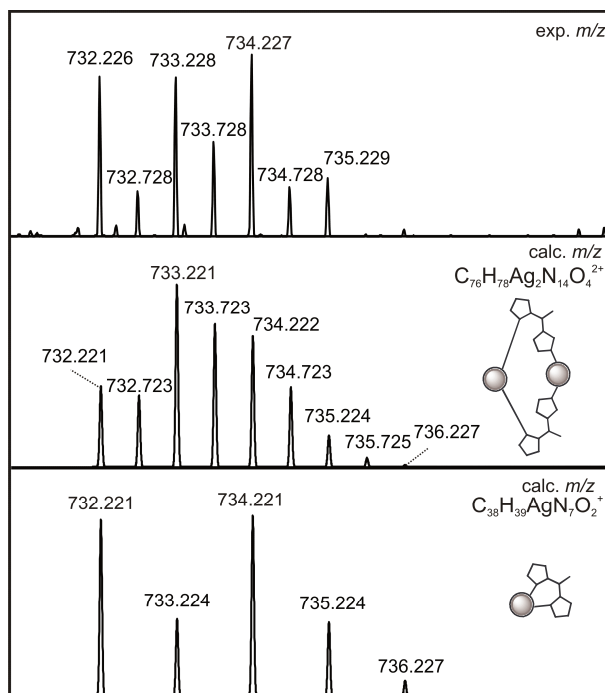


Figure 139: Partial ESI(+) mass spectrum of the crude product, showing the overlaying experimental and calculated isotopic pattern of 52s and 55s.

The signals of the remaining ligand precursors are still intense. Either they did not react or the formed complexes did already dissociate. With very small intensities (<1% of the intensity of the signal at 313.668) five more silver species could be detected. Some are superimposed with signals of other species (see Figure 140, Figure 141, Figure 142, Figure 143 and Figure 144). All five compounds consist of two ligands and at least one silver centre atom. Four of these complexes are especially interesting due to the combination of two different ligands ($m/z = 370.652$ (**60s**); $m/z = 453.184$ (**59s** or the isobaric species **61s**); $m/z = 529.166$ (**56s**); $m/z = 618.248$ (**63s**)). For the first time a signal with the confirming isotopic pattern of the wanted trinuclear silver complex **50s** could be detected (see Figure 144). Those new signals are small, but the currently used reaction conditions seem really promising. Some of these complexes have already been detected in previous experiments, but this spectrum includes all of them in combination with the cage molecule. The crude product still contains high signals of the ligand precursors. Therefore the reaction was incomplete and should be performed with longer reaction times or under other conditions.

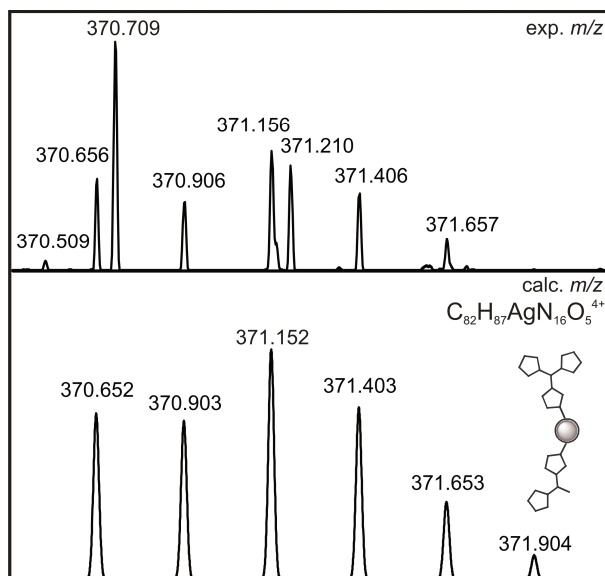


Figure 140: Partial ESI(+) mass spectrum of the crude product, showing the experimental and calculated isotopic pattern of 60s.

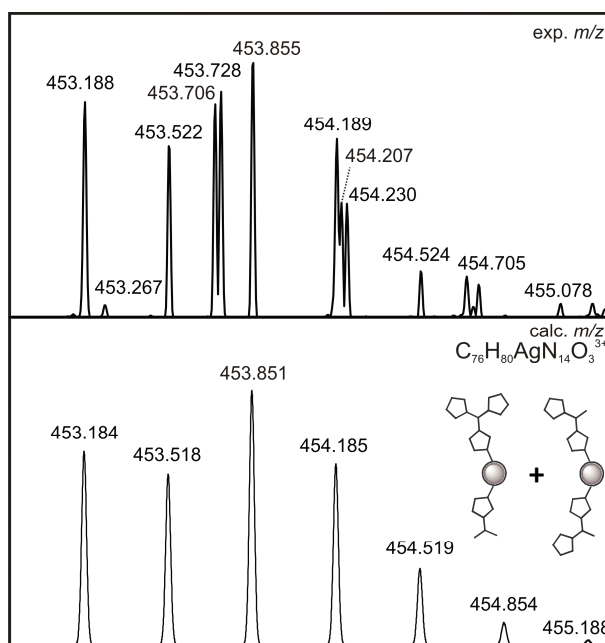


Figure 141: Partial ESI(+) mass spectrum of the crude product, showing the experimental and calculated isotopic pattern of 59s and 61s.

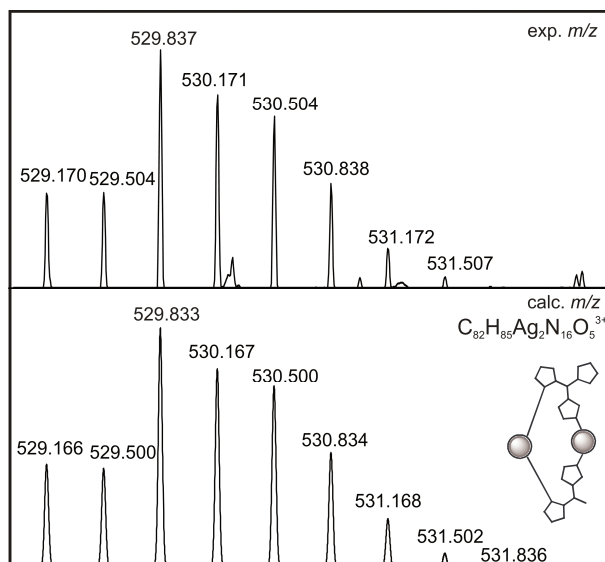


Figure 142: Partial ESI(+) mass spectrum of the crude product, showing the experimental and calculated isotopic pattern of 56s.

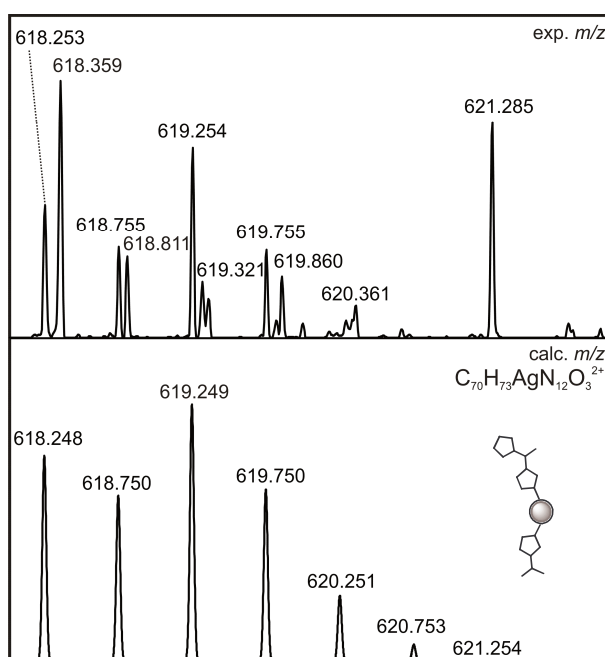


Figure 143: Partial ESI(+) mass spectrum of the crude product, showing the experimental and calculated isotopic pattern of 63s.

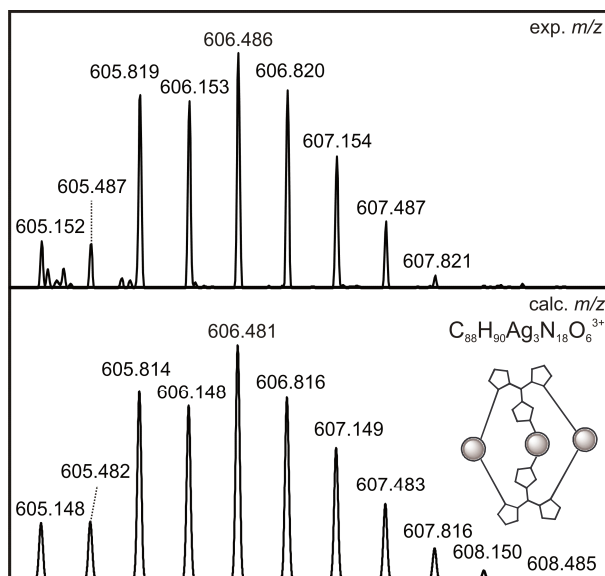


Figure 144: Partial ESI(+) mass spectrum of the crude product, showing the experimental and calculated isotopic pattern of 50s.

The influence of the phase transfer catalyst was investigated next and therefore the reaction was operated without TBAB. The solution of the ligand precursors was mixed with Ag_2O and NaOAc in methanol at room temperature. The first spectrum recorded after a reaction time of five hours contained some of the known mononuclear silver species (**51a**, **52a** and [**51a**+ CH_2CO_2]). Without the dominating signal of the ammonium compound, the other signals are detectable with good intensities.

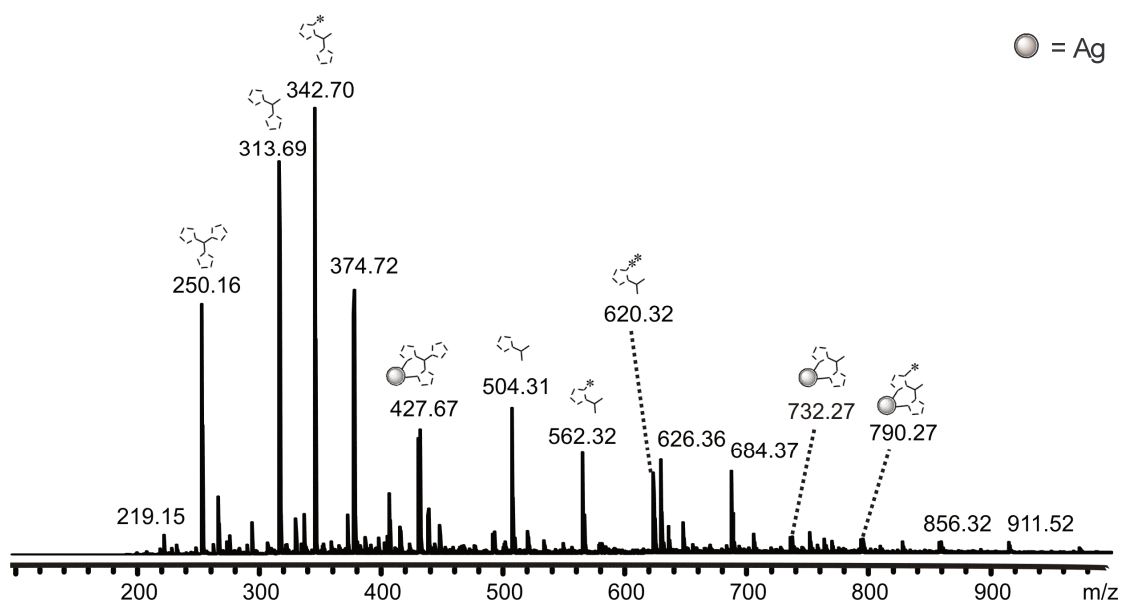


Figure 145: ESI(+) mass spectrum of a reacting solution containing $24\text{a}^*\text{Br}^-$, $25\text{a}^*\text{2Br}^-$, $26\text{a}^*\text{3Br}^-$, NaOAc and AgO_2 in MeOH at rt. The sample was taken after 5 hours and diluted with methanol.

The reaction was continued for four days and another sample was investigated by MS. The intensities of the three detected silver species increased in comparison with the ligand precursor. Even though, no new species could be detected.

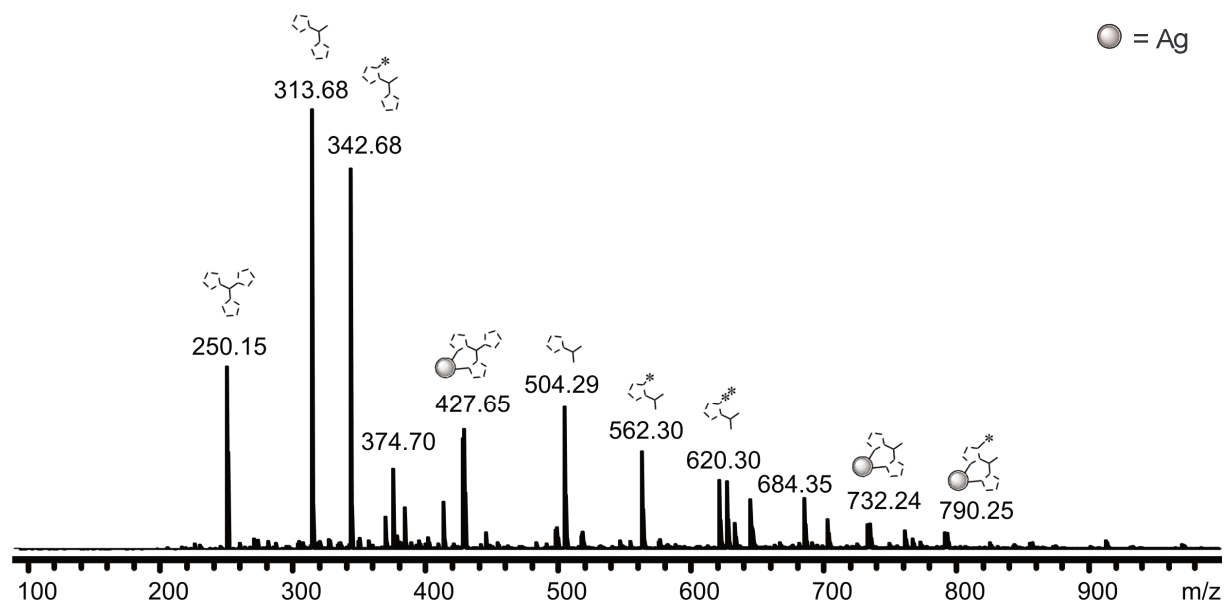


Figure 146: ESI(+) mass spectrum of a reacting solution containing $24a^*Br^-$, $25a^*2Br^-$, $26a^*3Br^-$, NaOAc and AgO_2 in MeOH at rt. The sample was taken after 4 days and diluted with methanol.

Stirring the mixture for 10 days, lead to higher intensities of the signals assigned to the silver species. The signals of the ligand precursors decreased in comparison with the complex signals, but they did not disappear, as seen before. This result supports the theory of the dissociation driven by the strong base NaOH. A new signal could be detected at $m/z = 415.053$. The signal was assigned to the Ag complex **53** with two NHC ligands which originated from the imidazolium compound **14** with the ester moiety.

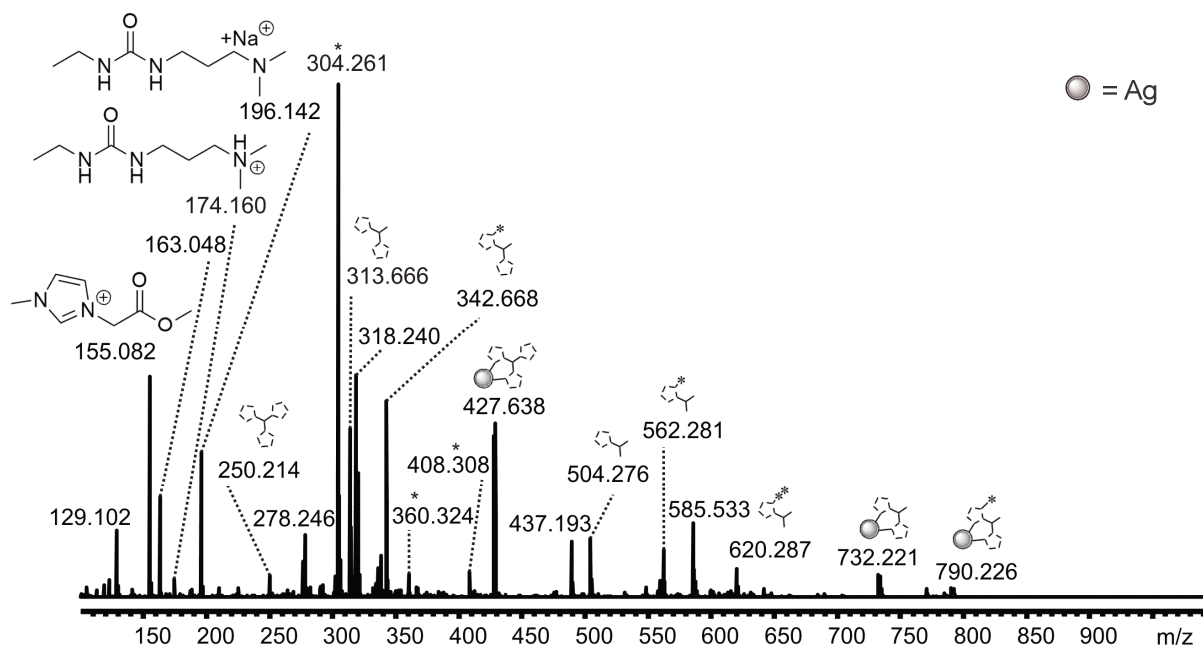


Figure 147: ESI(+) mass spectrum of a reacting solution containing $24a^*Br^-$, $25a^*2Br^-$, $26a^*3Br^-$, NaOAc and AgO_2 in MeOH at rt. The sample was taken after 10 days and diluted with methanol. (Includes small signals of **53**, * = common background contaminant ions; the crude product contains side products and starting materials from the synthesis of $26a^*3Br^-$).

After a reaction time of 13 days some additional species could be detected. The dinuclear complexes **55a** and $[55a+(CH_2CO_2)_2]$ now exist next to the mononuclear compounds. The intensity of the previously described signal of complex **53** increased strongly. The new detected species at $m/z = 260.979$ could be attributed to a fragment of this complex after the loss of one ligand. Due to the fact, that the intensities of the ligand precursor signals dropped dramatically, the reaction was stopped. The phase transfer catalyst seems to be a crucial factor for the intended complexation reaction. Therefore all following reactions were performed with catalytic amounts of TBAB.

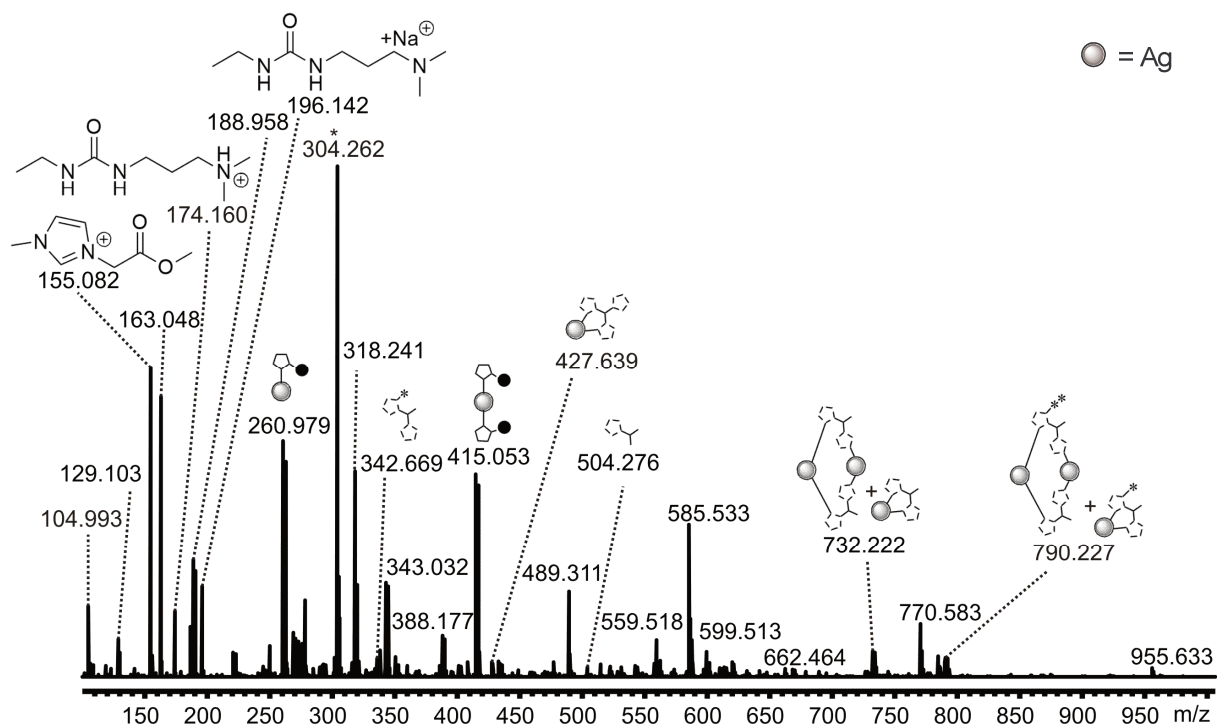


Figure 148: ESI(+) mass spectrum of a reacting solution containing $24a^*Br^-$, $25a^*2Br^-$, $26a^*3Br^-$, NaOAc and AgO_2 in MeOH at rt. The sample was taken after 13 days and diluted with methanol. (Includes small signals of $25a$ and $[55a+CH_2CO_2]$, * = common background contaminant ions; the crude product contains side products and starting materials from the synthesis of $26a^*3Br^-$).

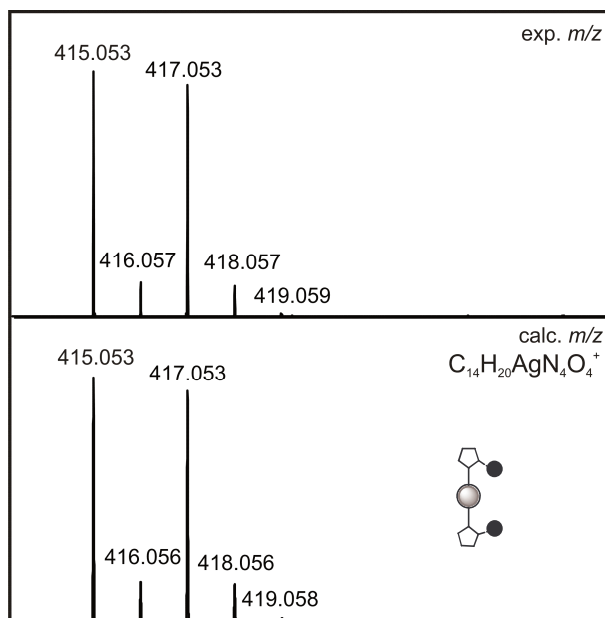


Figure 149: Partial ESI(+) mass spectrum of the crude product, showing the experimental and calculated isotopic pattern of 53.

The synthesis of Ag(I) NHC complexes by the silver base route is usually performed at ambient conditions. Some exceptional ligand precursors require additional activation energy through higher reaction temperatures.^[2c,57a,108b,133] Hence the reaction parameters were changed again to promote the complexation. The reactants were mixed at room temperature and then stirred under reflux for 24 hours. A brown solid remained in the solution and was filtered. The MS spectrum of the crude product does only include small signals of two mononuclear silver complexes **51a** and **52a** but no new species. Therefore this approach was dropped.

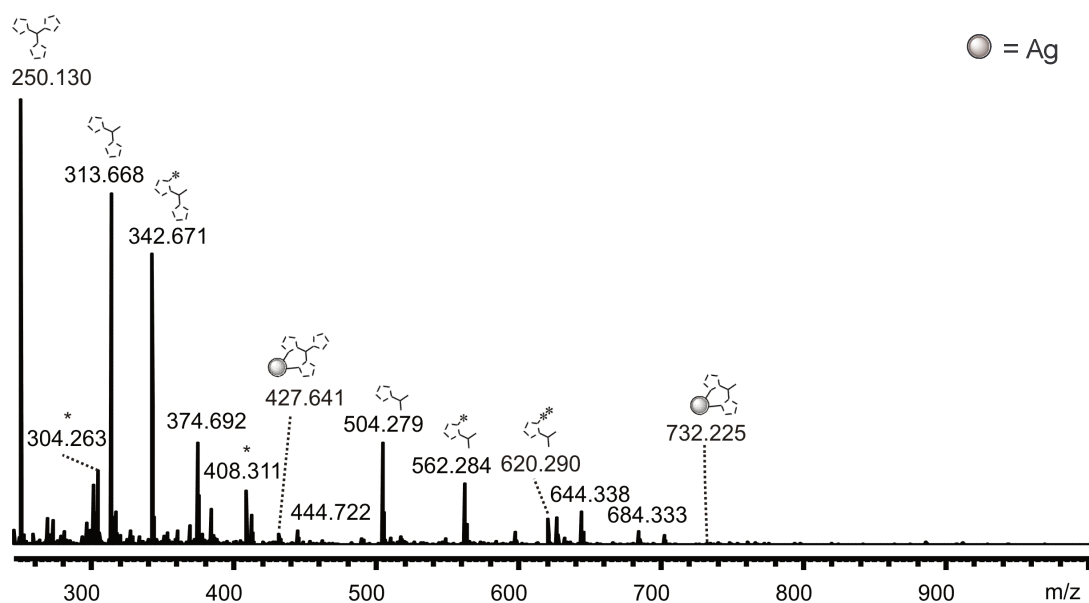


Figure 150: ESI(+) mass spectrum of the crude product from the reaction of **24a*Br⁻**, **25a*2Br⁻**, **26a*3Br⁻**, TBAB, NaOAc and AgO₂ in MeOH under reflux. The sample was diluted with methanol. (For full spectrum see Figure 177; Includes small signals of [23+H]⁺, [25a+Cl]⁻, [26a+Cl]⁻, * = common background contaminant ions).

The higher temperature did not yield new compounds or increasing intensities of the known signals. On that account the temperature was switched back to ambient conditions. Based on the results of the former experiments the following reaction was again performed with the combination of the phase transfer catalyst TBAB, NaOAc and Ag₂O in methanol at room temperature. For a better turn over the reaction mixture was now stirred for seven days. The suspension turned red brown similar to the ligand precursor. The first sample was taken after three days. The results are alike the previous recorded spectrum of the experiment with the same reaction conditions (see Figure 137).

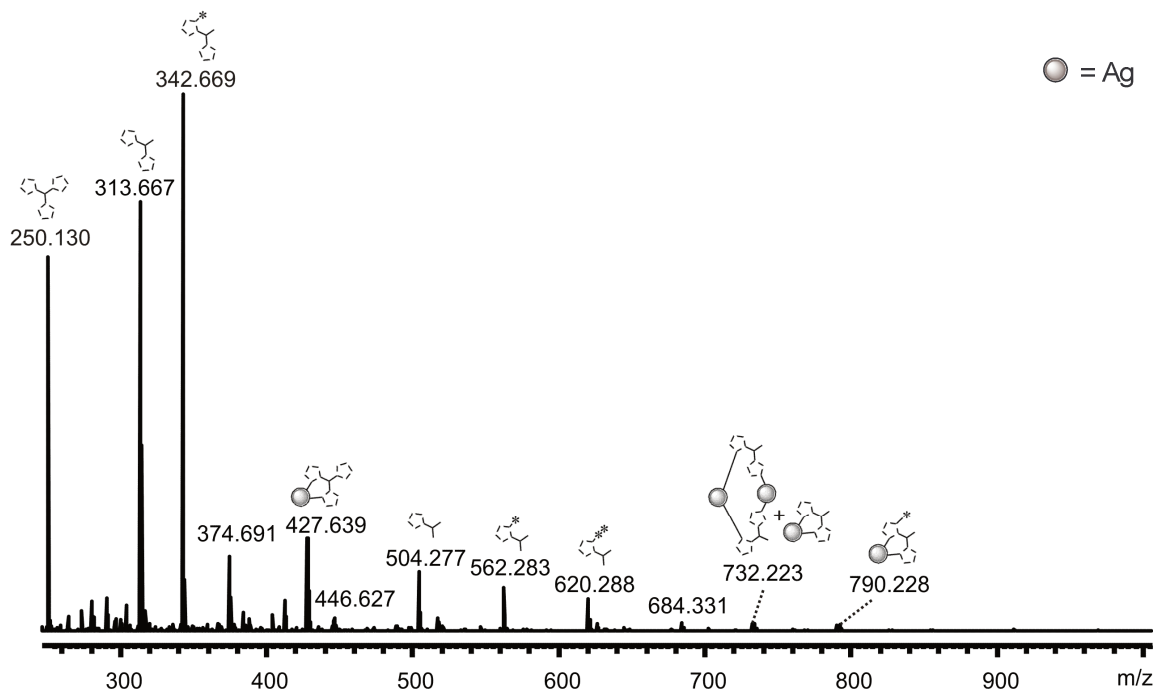


Figure 151: ESI(+) mass spectrum of a reacting solution containing $24a^*Br^-$, $25a^*2Br^-$, $26a^*3Br^-$, TBAB, NaOAc and AgO_2 in MeOH at rt. The sample was taken after 3 days and diluted with methanol. (For full spectrum see Figure 178; Includes small signals of $[23+H]^+$, 60a, $[60a+CH_2CO_2]$, 59a/61a, $[59a+CH_2CO_2]/[61a+CH_2CO_2]$, $[59a+(CH_2CO_2)_2]/[61a+(CH_2CO_2)_2]$, 56a, $[56a+CH_2CO_2]$, 63a, $[63a+CH_2CO_2]$, $[63a+(CH_2CO_2)_2]$, $[55a+CH_2CO_2]$, $[26a+Cl]$).

24 hours later several more silver species could be detected, including the trinuclear silver complex **50a**. A new compound in the reacting solution is **45**. This complex contains the plain acid NHC originating from compound **1** as ligands. Since the purification was incomplete, the imidazolium compound **1** is still available in the reacting solution. This also led to some new complexes, containing this ligand and another NHC compound (**67a** at $m/z = 436.647$, $[67a+(CH_2CO_2)]$ at $m/z = 456.650$ and **65a** at $m/z = 750.238$). These side products prevent the complexation of the TBTQ containing species. Nevertheless these are some more successful synthesized complexes in the mixture. Next to these new species are several more signals detectable, which were attributed to fragments of prior complexes and marked with a # in the spectra. The mixture also contained small amounts of the cage molecule **50a**, but the isotopic pattern is superimposed from another unknown species.

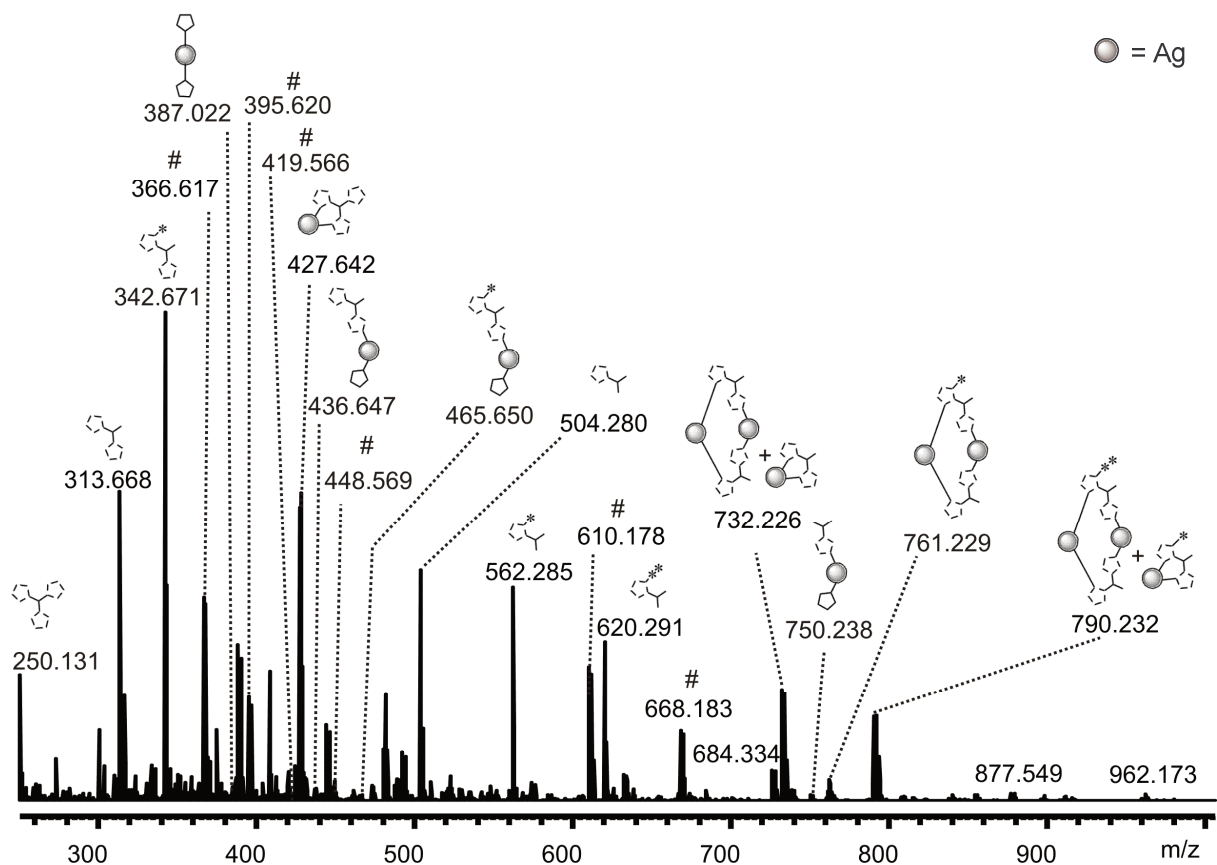


Figure 152: ESI(+) mass spectrum of a reacting solution containing 24a*Br⁻, 25a*2Br⁻, 26a*3Br⁻, TBAB, NaOAc and AgO₂ in MeOH at rt. The sample was taken after 4 days and diluted with methanol. (For full spectrum see Figure 179; Includes small signals of [51a+CH₂CO₂], 56a, [56a+CH₂CO₂], 50a, [63a+CH₂CO₂], [63a+(CH₂CO₂)₂], for explanation of the # see Table 8).

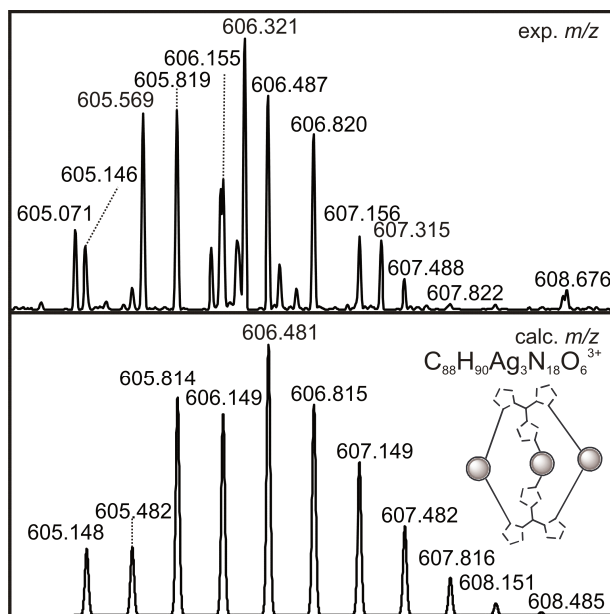


Figure 153: Partial ESI(+) mass spectrum of the crude product, showing the experimental and calculated isotopic pattern of 50a.

After seven days the solvent was removed in vacuo. The resulting crude product was used as a template for the transmetallation with gold. Accordingly the solid was dissolved in dry DMF leading to a brown solution. After the addition of the gold source ($\text{Au}(\text{SMe}_2)\text{Cl}$) the solution turned purple. The colour change usually indicates the decomposition of the gold compound and the building of nano particles.^[134] The mixture was stirred for 2 hours at room temperature. After the addition of diethyl ether, stirring was continued for 30 min. The resulting dark precipitate was filtered and washed with diethyl ether. The solvent of the filtrate was removed and both products were dried under vacuo.

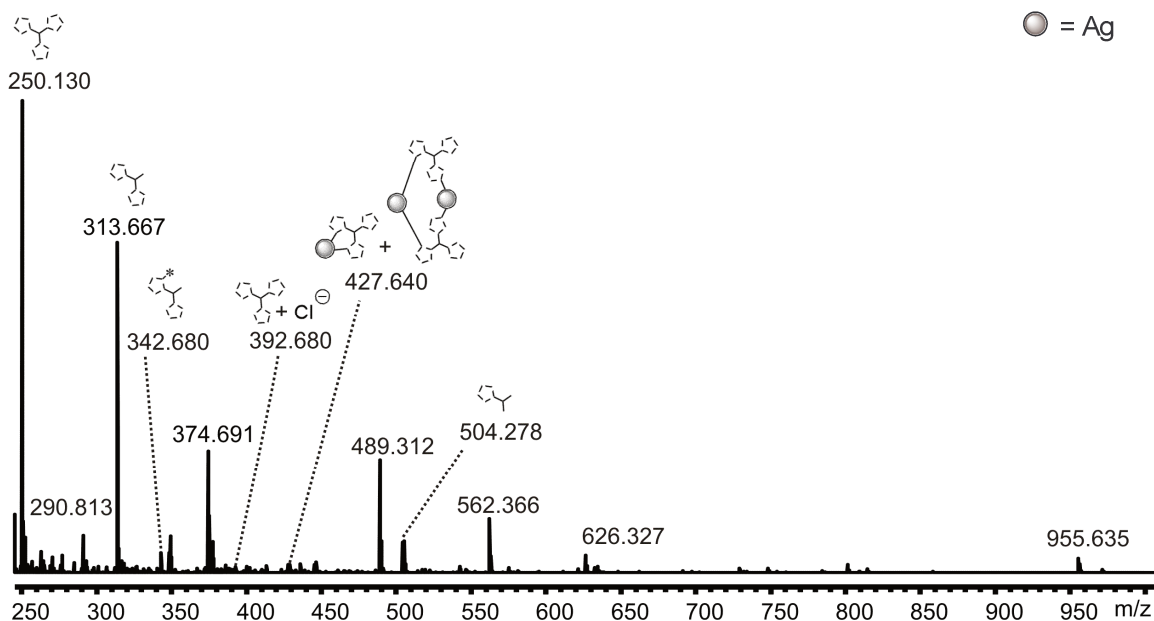


Figure 154: ESI(+) mass spectrum of the residue of the filtrate from the reaction of $14a^*Br^-$ and $Au(SMe_6)Cl$ in DMF at rt. The sample was diluted with methanol. (For full spectrum see Figure 180, Includes small signals of $[25a+Cl]$, $[24a+CH_2CO_2]$, 38a, 32a, 37a, 39a/41a, 33a, 35a, 52s, 55a, 56a, 50a).

The spectrum of the solid originating from the filtrate provides a mixture of silver and gold containing complexes with small intensities and the remaining unbound ligand precursors (**24a**, **25a** and **26a**) with higher intensities. The MS spectrum from the collected precipitate provides similar species but with much smaller intensities.

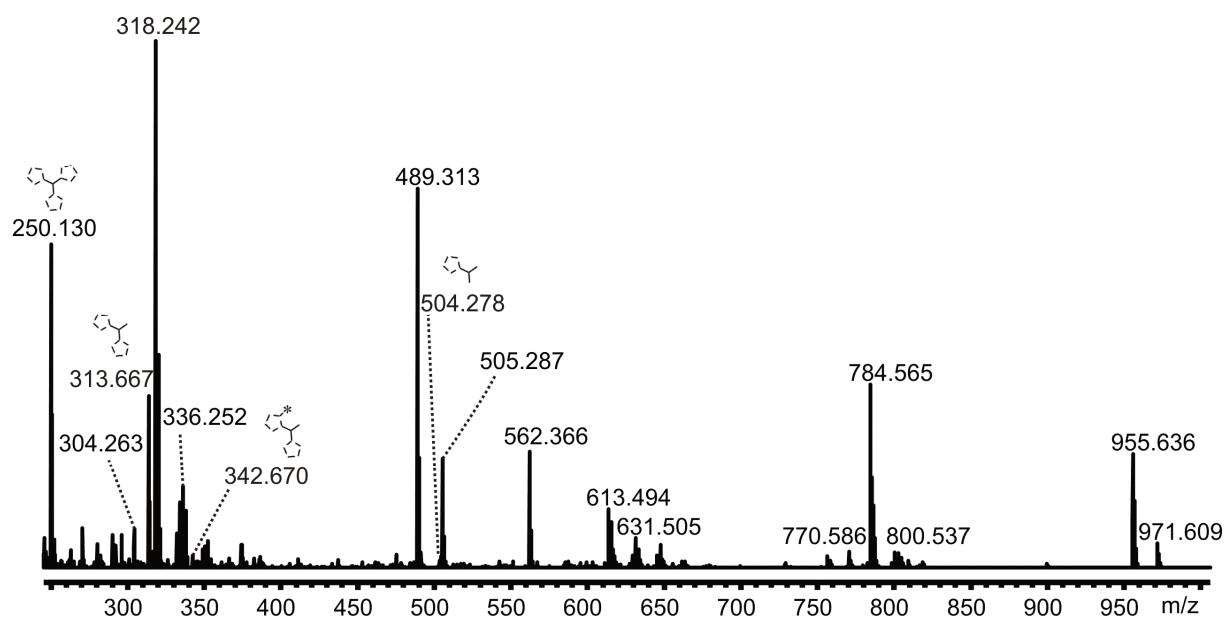
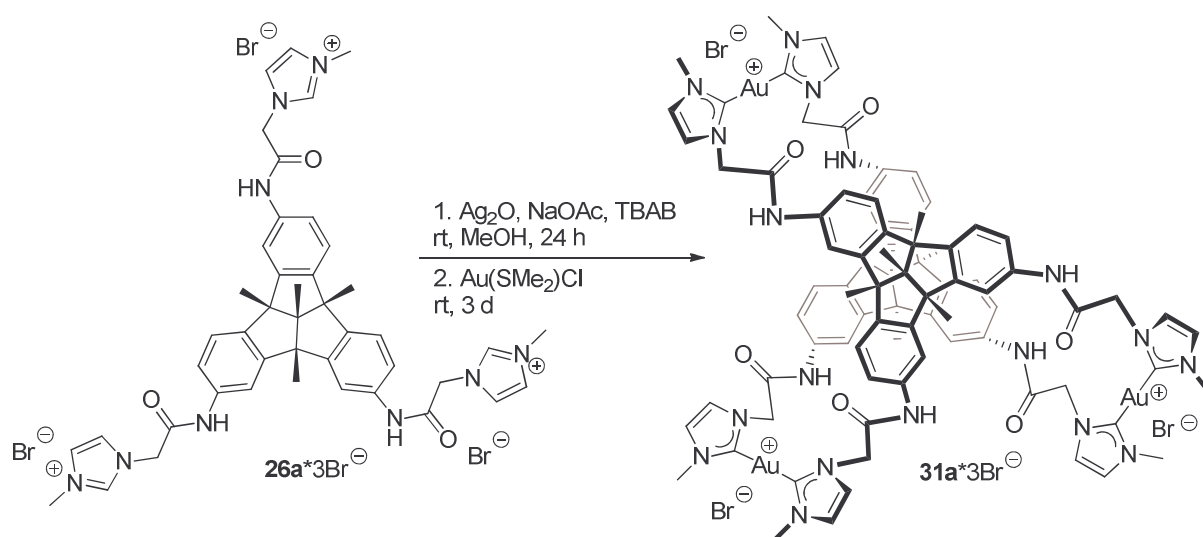


Figure 155: ESI(+) mass spectrum of the crude product from the reaction of $14a^*Br^-$ and $Au(SMe_6)Cl$ in DMF at rt. The sample was diluted with methanol. (For full spectrum see Figure 181, Includes small signals of 34, 51a).

The crude product still contained silver compounds, so the transmetallation step was incomplete and should be improved. In addition the intensities of the gold complexes are much smaller than for the previously found silver species. This indicates the decomposition of the complexes. Perchance the solution was unintentional exposed to light during the purification step, or they are not stable over a longer period of time. To exclude these reasons for the dissociation, the drying step was neglected during the next experiment and the reaction time was shortened.



Scheme 25: 1. Tested synthesis of $50\text{a}^*\text{Br}^-$ with $26\text{a}^*\text{3Br}^-$, TBAB, NaOAc and AgO_2 in MeOH at rt, with a reaction time of 24 hours. 2. Transmetallation step with $\text{Au}(\text{SMe}_2)\text{Cl}$ with a reaction time of 4 days.

Accordingly as alternative version the transmetallation was now realized without further isolation of the silver compounds. The first step of the synthesis was performed as before with NaOAc and TBAB in methanol at room temperature. Besides the reaction conditions, the tuning parameters during the MS experiments and the solvents used for them are crucial for meaningful reaction monitoring. For example the detection of the interesting species could be hindered by the aggregation behaviour of cations and anions in the gas phase, which could lead to uncharged compounds. Some aggregates with an unstoichiometric composition of cations and anions have been described before. This phenomenon is often tuneable by the concentration of the sample or different interactions with the solvent. For an investigation of this behaviour, the first sample of the reacting solution was taken after

two hours and diluted in three different ways. The first measurements have been performed in pure methanol. The second sample was recorded after ingesting a concentrated methanol solution into the tube of the mass spectrometer and then flushing with pure methanol. This method leads to a higher dilution of the sample. The last experiment was performed by adding H₂O to the methanol solution (1:1) to separate the anions by solvation (some other ratios were tested, but the spectra are not given in this work). The concentrated sample in methanol yielded a spectrum with high intensities for the usual species **51a**, **52a**, **55a**, [**52a**+CH₂CO₂] and [**55a**+(CH₂CO₂)₂]. The signal of the cage complex **50a** is small but the typical isotopic pattern is noticeable (see Figure 157). Next to the known complex **53a** some other complexes containing the ligand precursor **14** could be detected this time. Interestingly three species in the range over $m/z = 1000$ could be detected for the first time (**62a**, [**62a**+CH₂CO₂] and [**62a**+(CH₂CO₂)₂]).

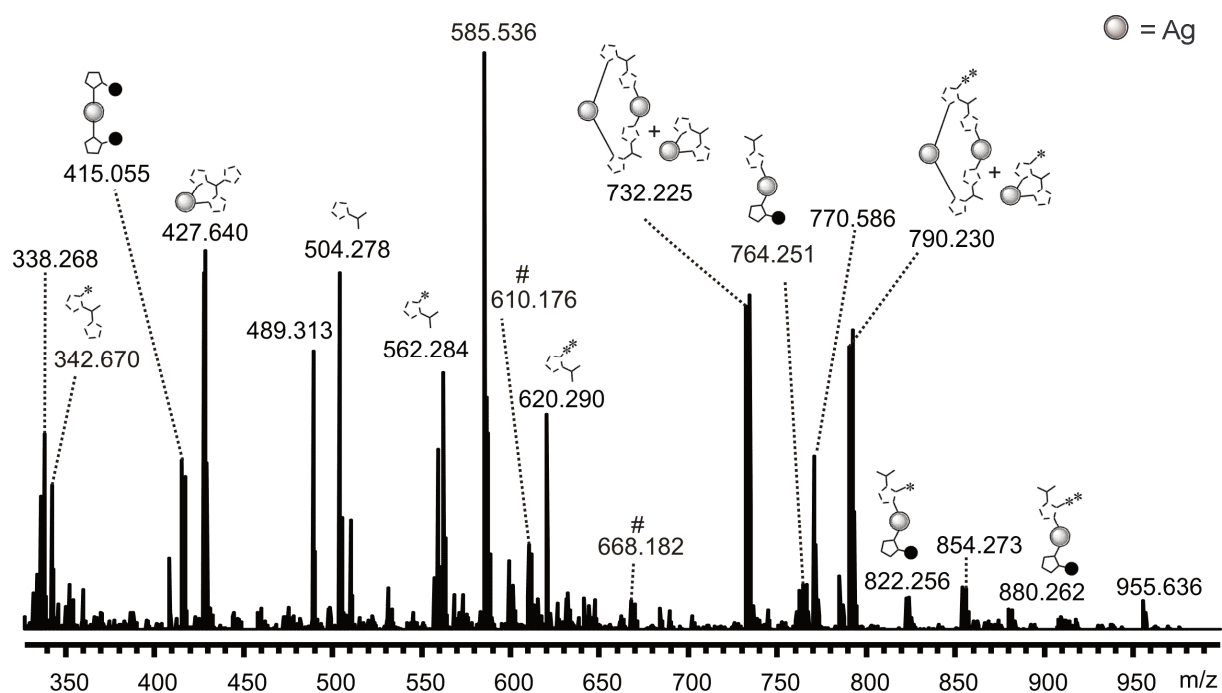


Figure 156: ESI(+) mass spectrum of a reacting solution containing **24a***Br⁻, **25a***2Br⁻, **26a***3Br⁻, TBAB, NaOAc and AgO₂ in MeOH at rt. The sample was taken after 2 hours and diluted with methanol. (For full spectrum see Figure 182, Includes small signals of [23+H]⁺, **50a**, [**63a**+CH₂CO₂], [**63a**+(CH₂CO₂)₂], [**55a**+CH₂CO₂], for explanation of the # see Table 8).

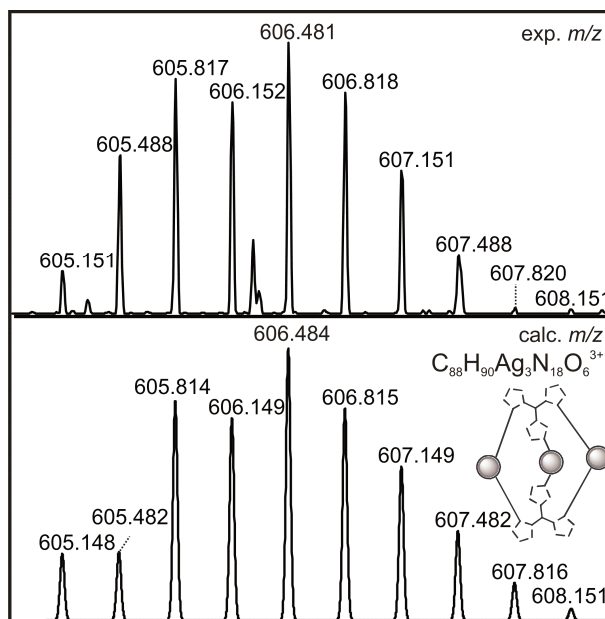


Figure 157: Partial ESI(+) mass spectrum of the crude product, showing the experimental and calculated isotopic pattern of 50a.

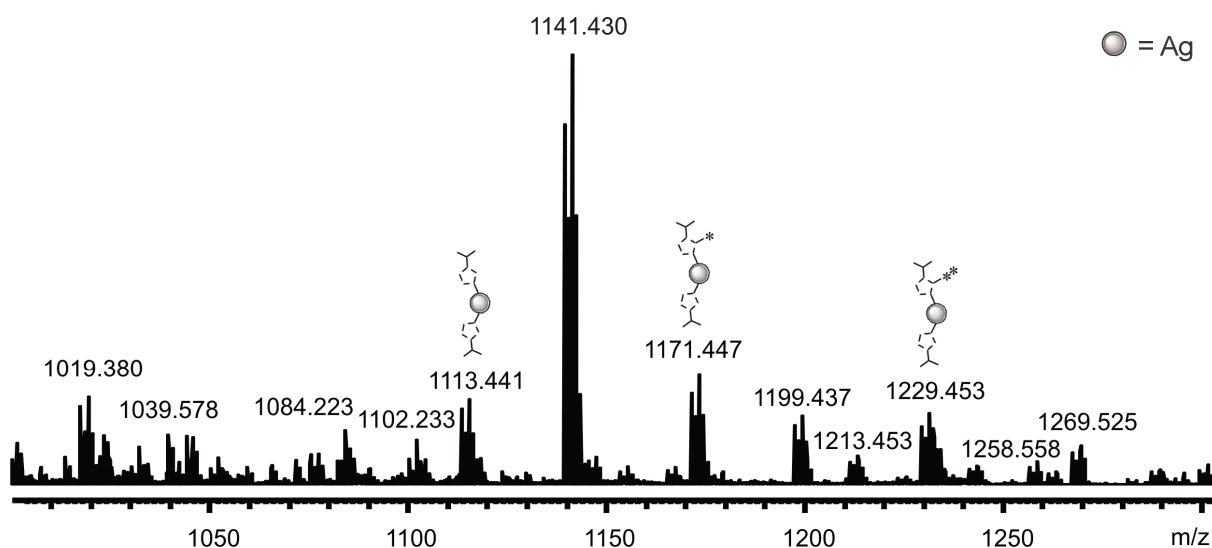


Figure 158: ESI(+) mass spectrum of a reacting solution containing $24a^*Br^-$, $25a^*2Br^-$, $26a^*3Br^-$, TBAB, NaOAc and AgO_2 in MeOH at rt. The sample was taken after 2 hours and diluted with methanol.

The next spectrum was recorded after ingesting a high concentrated methanol solution of the sample and then pure methanol. Sometimes this technique helps preventing the aggregation of the ion pairs. Using smaller concentrations of the sample led to an increase of the background contaminant ions. The intensities of the five usual species (**51a**, **52a**, **55a**, [**52a**+ CH_2CO_2] and [**55a**+ $(CH_2CO_2)_2$]) stay almost the same. The signal of the cage molecule **50a** is still present, even though the isotopic pattern is slightly blended by the electronic

noise (see Figure 160). Interestingly the intensities of the species linked to fragments of former complexes (marked with a #) are increasing. So the strong dilution promotes the fragmentation of the compounds. The intensity of the signal of complex **53** is also much higher as in the former spectrum. The associated fragment of the complex after the loss of one ligand is also visible in the full spectrum (Figure 183). Based on that observation the aggregation of the big TBTQ containing complexes with the counterions seems already hindered. The small complex with the ester unit appears more likely to build undetectable ion pairs or aggregates. This behaviour could be suppressed by the strong dilution. Another possible explanation for a missing ion separation of the cations and anions is a strong binding inside the cavity. These capsule like molecules are specifically designed to bind small molecules or ions inside of them. Separation of the aggregates does may need more activation and is not promoted by simple solvation processes. Also recognizable is the increase of the signals from the carbamate (see Figure 183). Dilution supports the detection of this species. However this behaviour is not important for the complexation reaction.

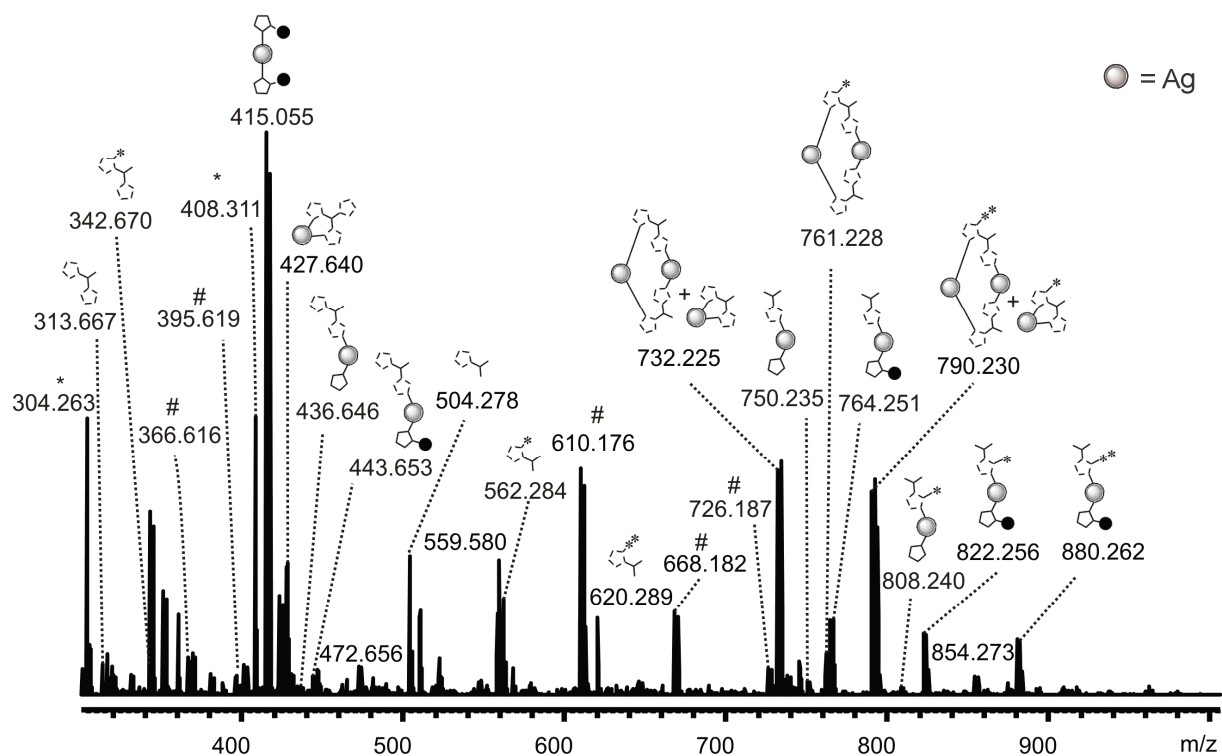


Figure 159: ESI(+) mass spectrum of a reacting solution containing $24a^*Br^-$, $25a^*2Br^-$, $26a^*3Br^-$, TBAB, NaOAc and AgO_2 in MeOH at rt. The sample was taken after 2 hours and diluted with methanol. (For full spectrum see Figure 183, Includes small signals of $[23a+H]^+$, $[23a+Na]^+$, 56a, 63a, $[63a+(CH_2CO_2)_2]$, 50a, $[56a+CH_2CO_2]$, * = common background contaminant ions, for explanation of the # see Table 8).

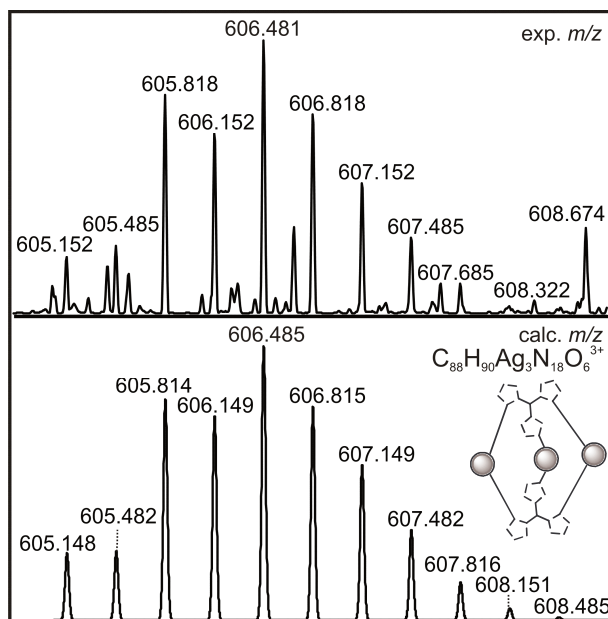


Figure 160: Partial ESI(+) mass spectrum of the crude product, showing the experimental and calculated isotopic pattern of **50a**.

For the next measurement the sample was diluted in a mixture of methanol and H₂O (1:1). The additional water could lead to a better solvation of the anions and therefore prevent the aggregation with the complexes. Unfortunately the experiment did not realize the intended effect. Instead of an increase the intensities of the signals decreased. Also the signal of complex **50a** could no longer be detected. The water changed the ESI response of the complexes for the worse. Even the addition of smaller amounts of H₂O did not promote the detection of the separated cations. After this experiment the reaction monitoring was furthermore performed by simply diluting the sample in methanol. After each sample pure methanol was ingested in the mass spectrometer and another spectrum recorded to compare differences.

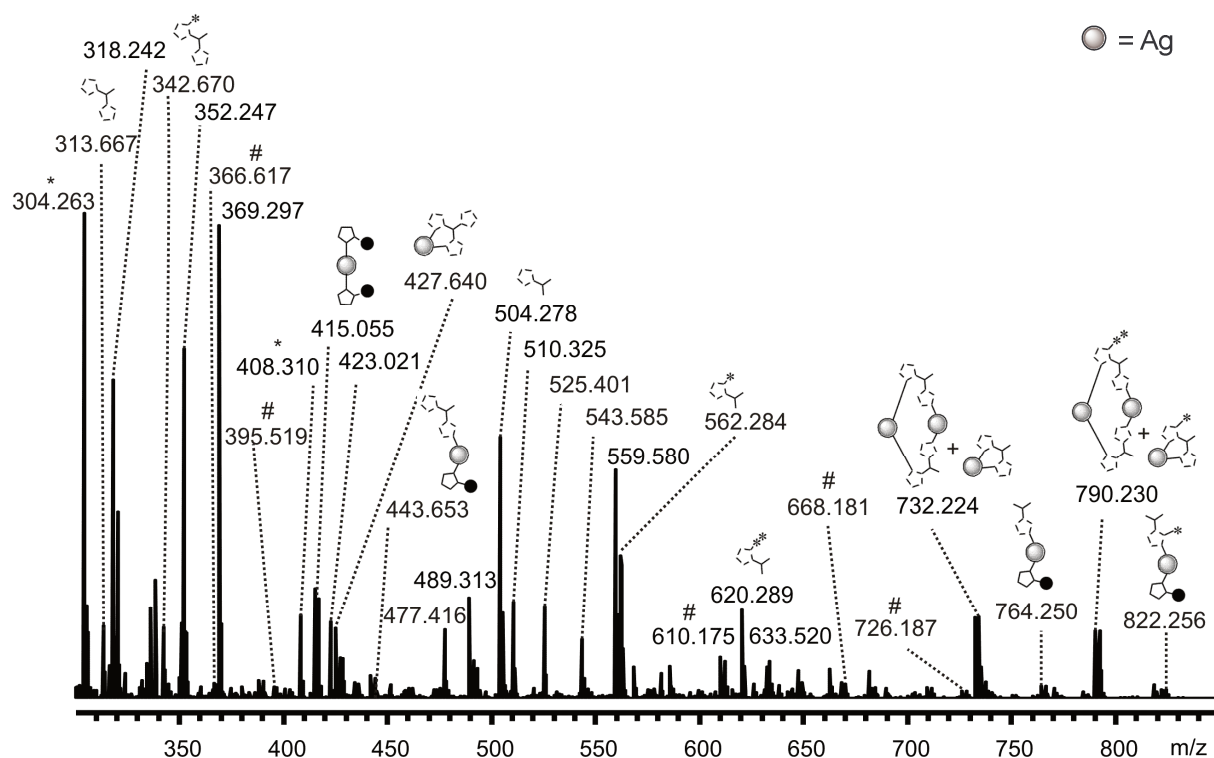


Figure 161: ESI(+) mass spectrum of a reacting solution containing $24a^*Br^-$, $25a^*2Br^-$, $26a^*3Br^-$, TBAB, NaOAc and AgO_2 in MeOH at rt. The sample was taken after 2 hours and diluted with methanol and H_2O . (For full spectrum see Figure 184, Includes small signals of $63a$, $[63a+CH_2CO_2]$, $[63a+(CH_2CO_2)_2]$, $[55a+CH_2CO_2]$, $[51a+CH_2CO_2]$, * = common background contaminant ions, for explanation of the # see Table 8).

The composition of the reacting mixture did not change much over night. The recorded spectrum is similar to the spectrum of the day before (see Figure 162 and Figure 163).

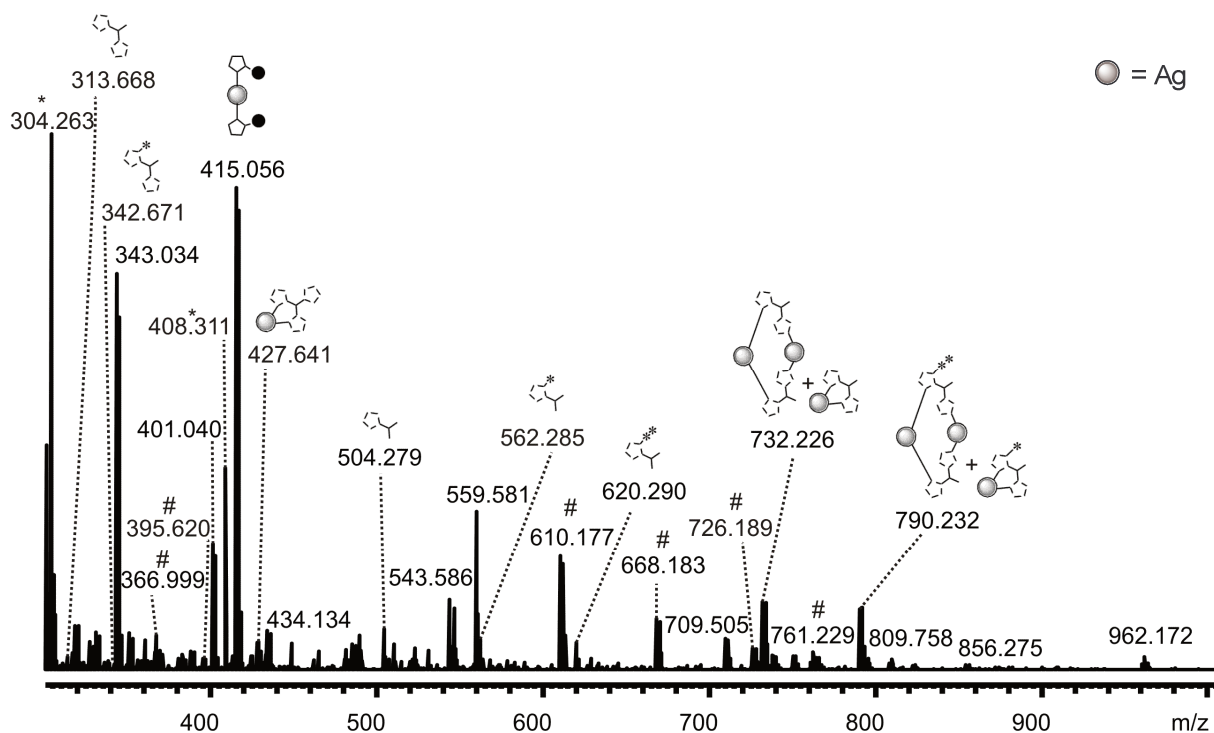


Figure 162: ESI(+) mass spectrum of a reacting solution containing $24a^*Br^-$, $25a^*2Br^-$, $26a^*3Br^-$, TBAB, NaOAc and AgO_2 in MeOH at rt. The sample was taken after 24 hours and diluted with methanol. (For full spectrum see Figure 185, Includes small signals of $[23a+H]^+$, $[23a+Na]^+$, 41a, 50a). * = common background contaminant ions).

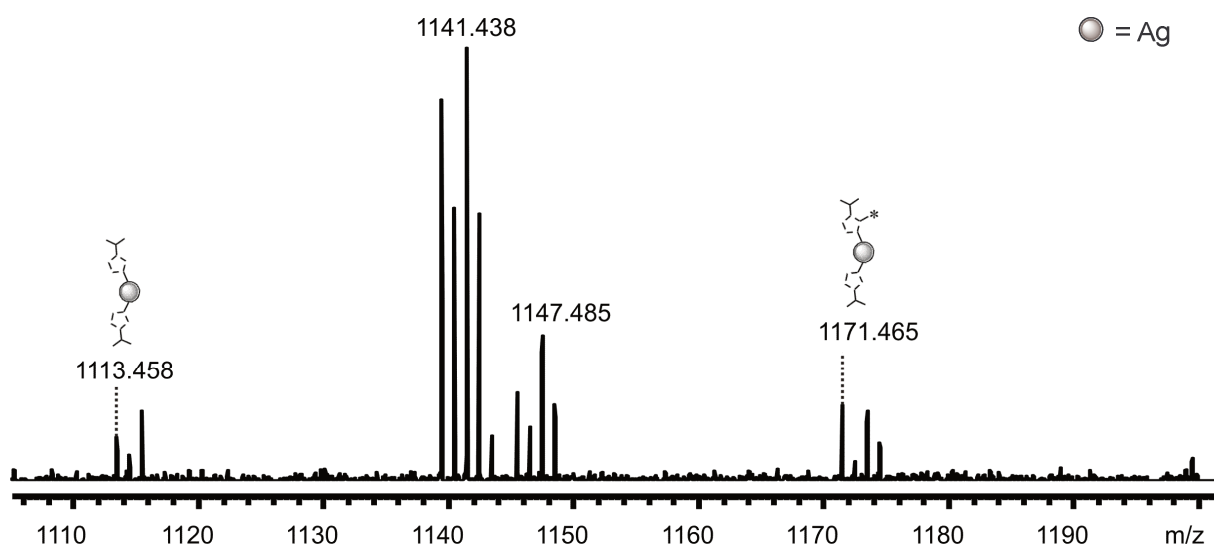


Figure 163: ESI(+) mass spectrum of a reacting solution containing $24a^*Br^-$, $25a^*2Br^-$, $26a^*3Br^-$, TBAB, NaOAc and AgO_2 in MeOH at rt. The sample was taken after 24 hours and diluted with methanol.

As the next step of the reaction, Au(SMe₂)Cl was added to the solution and the mixture was stirred for three days (still under the absence of light). A sample of the reacting solution showed several gold containing species with moderate intensities (**34**, **33a**, **35a**, [**33a**+CH₂CO₂] and [**35a**+(CH₂CO₂)₂]). Therefore the transmetalation reaction in methanol, without the purification step was way more successful. The total absence of fragments of the type [Au-L]⁺ indicates the higher dissociation energy of the gold complexes in comparison with the silver complexes. The fragmentation of the Au species does usually need further activation.

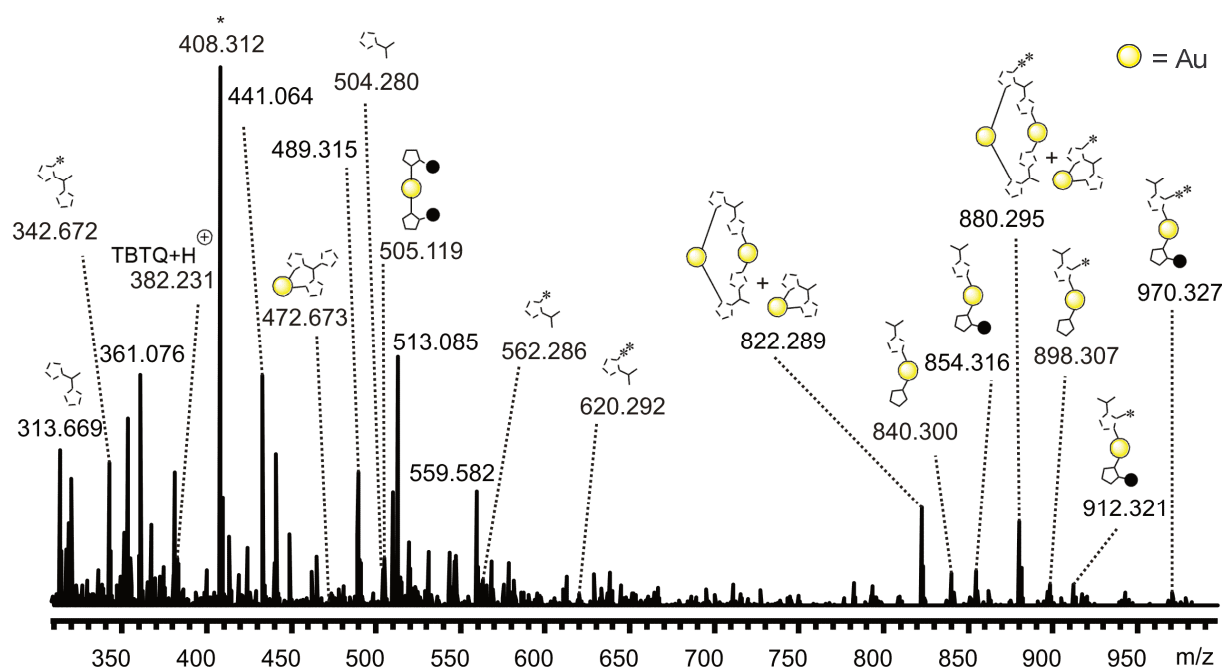


Figure 164: ESI(+) mass spectrum of a reacting solution containing **24a***Br⁻, **25a***2Br⁻, **26a***3Br⁻, TBAB, NaOAc, AgO₂ and Au(SMe₂)Cl in MeOH at rt. The sample was taken 3 days after the addition of the gold compound and diluted with methanol. (For full spectrum see Figure 186, Includes small signals of **51a**, [**52a**+CH₂CO₂], [**41a**+CH₂CO₂], * = common background contaminant ions, for explanation of the # see Table 8).

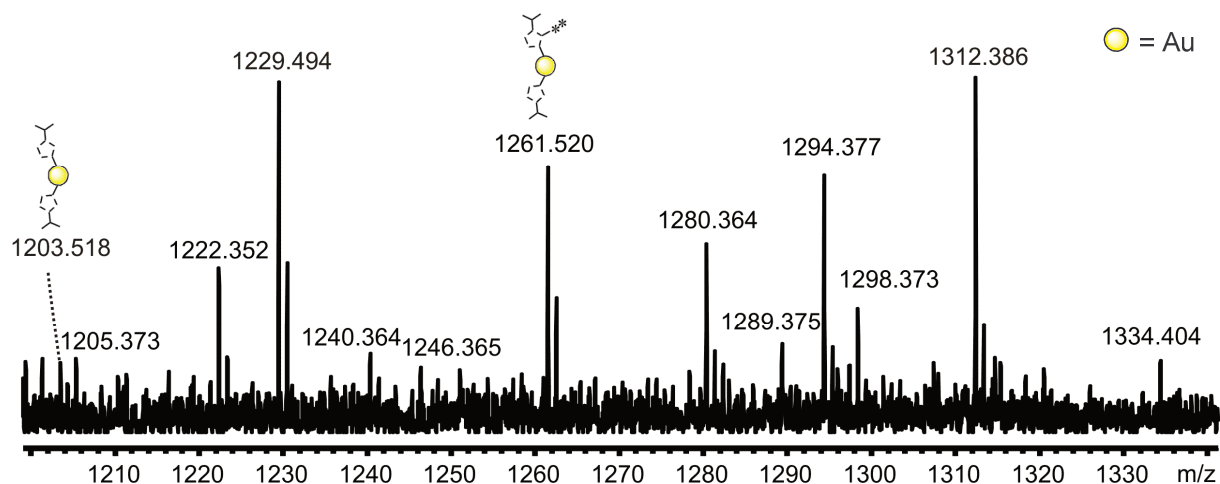


Figure 165: ESI(+) mass spectrum of a reacting solution containing $24a^*Br^-$, $25a^*2Br^-$, $26a^*3Br^-$, TBAB, NaOAc, AgO_2 and $Au(SMe_2)Cl$ in MeOH at rt. The sample was taken 3 days after the addition of the gold compound and diluted with methanol.

There are almost no remaining silver species detectable in the tested sample. Therefore the reaction was stopped. Further transmetallation would require more Ag-NHC compounds. Decomposition of the complexes in solution is possible. The silver complexes are sensitive to light and the gold compounds are sensitive to air and moisture during the reaction. To avoid the dissociation of the Ag complexes, $Au(SMe_2)Cl$ should be added after a shorter period of time.

A comparison of the silver containing crude products of the different isomers, shows a better rate of yield for the symmetrical compound **50s**. The experimental isotopic pattern does match the calculated one, while it is more intense in contrast to the baseline noise. Similar as the ligand precursors the solids of the symmetrical compounds are more red-brown and the asymmetrical products have a darker brown-black colour. Using the symmetrical compounds would probably yield more of the intended main product. This is attributed to the steric hindered conformation of the asymmetrical compounds. Therefore the symmetric complexes were used for the following synthesis.

The mixture for the next reaction was treated with Ag_2O and stirred for only 45 min, before the gold source was added. The reaction was then ended after a total of 42 hours. The solvent was removed in vacuo leading to a light brown solid. The intriguing ESI MS spectrum of the crude product shows several Au(I) NHC species. Noticeable is the absence of most of the oligomeric species, due to the improved reaction conditions for the symmetric

compounds. For a better view of the small signals the range under $m/z = 320$ with intense signals was excluded. In combination with another spectrum above $m/z = 1000$ (Figure 168), all possible combinations of two of the ligand precursors **24s**, **25s** and **26s** with one, two or three gold atoms could be detected. As seen before, the spectrum contains several signals of gold complexes, with ligands occurring from the ligand precursor **14**. An improvement of the purification conditions is mandatory for a better rate of yield. Hence these side products prevent the combination with the TBTQ species. For the first time a species linked to the trinuclear cage **31s** could be detected (see Figure 167). The signal is small and superimposed with the electronic noise.

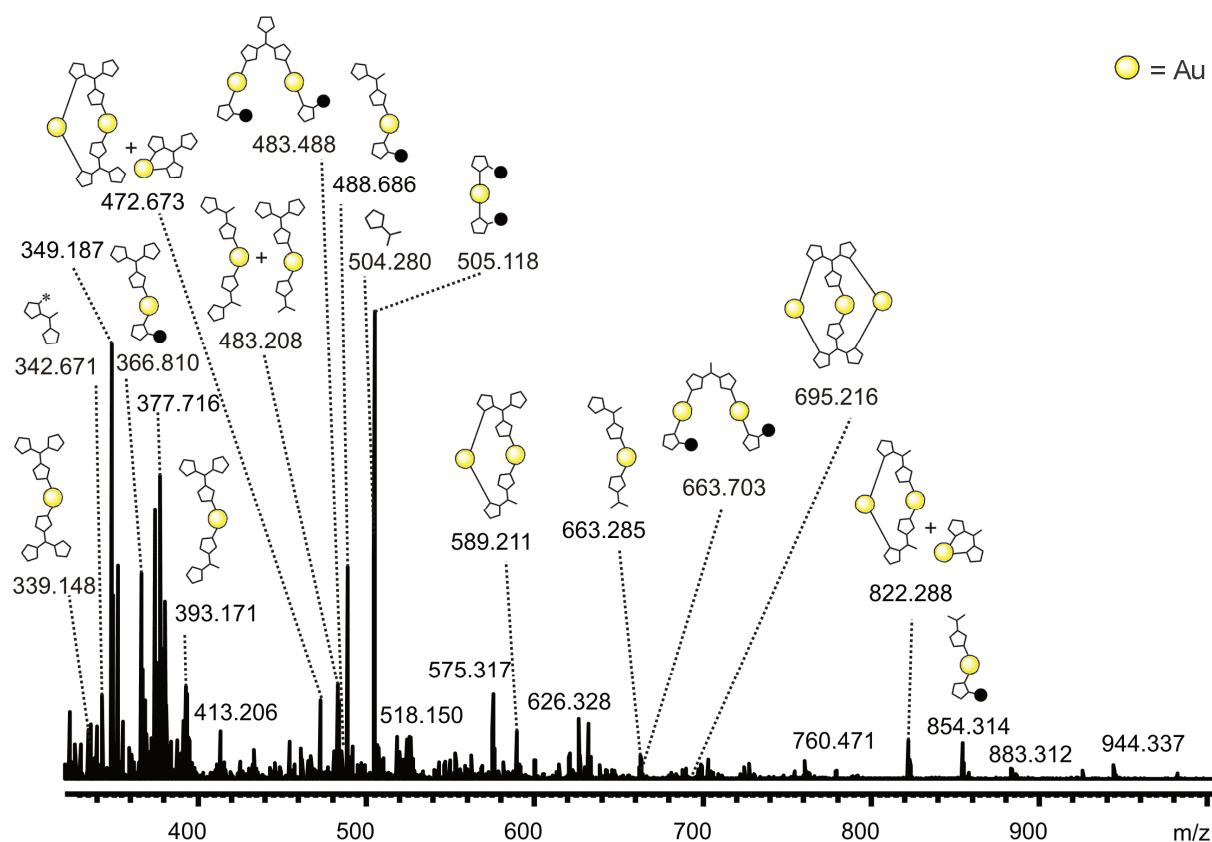


Figure 166: ESI(+)-mass spectrum of the crude product from the reaction of **24s***3Br⁻, **25s***3Br⁻, **26s***Br⁻, TBAB, NaOAc, AgO₂ and Au(SMe₂)Cl in MeOH at rt. The sample was diluted with methanol. (For full spectrum see Figure 187, Includes small signals of [39s+CH₂CO₂]/ [41 s+CH₂CO₂], [40s+CH₂CO₂], [36s+CH₂CO₂]).

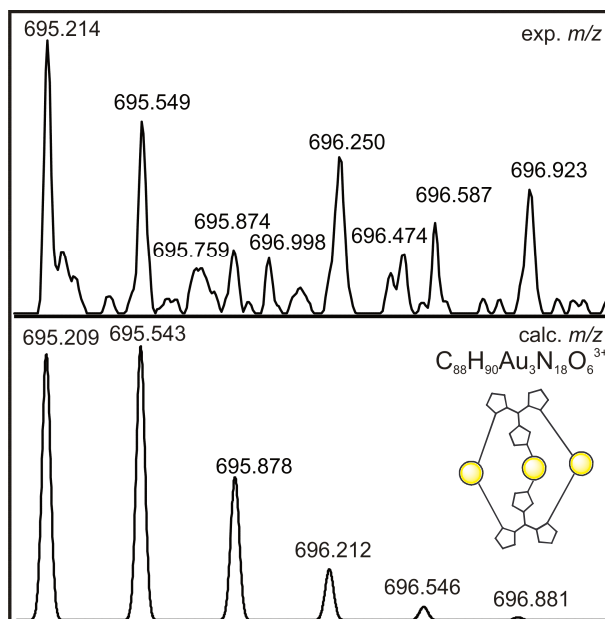


Figure 167: Partial ESI(+) mass spectrum of the crude product, showing the experimental and calculated isotopic pattern of 31s.

All of the 12 interesting gold-TBTQ species and the free ligand precursors (**24s**, **25s** and **26s**), but none of the silver containing species could be detected in the product sample. This result confirms the success of the intended transmetallation step. The two step synthesis including the prior formation of the silver complexes yields in more different gold TBTQ species than the previous used methods. It yielded the expected 11 different species in the range between $m/z = 245 - 1000$, and an additional species at $m/z = 1203$ (see Figure 168). Measurements in the range above $m/z = 1000$ need further calibration. Due to the fact that the most interesting species are detectable in another range, this tuning step was not implemented. Therefore the accurate masses are even more imprecise and the random noise is higher than in the area below.

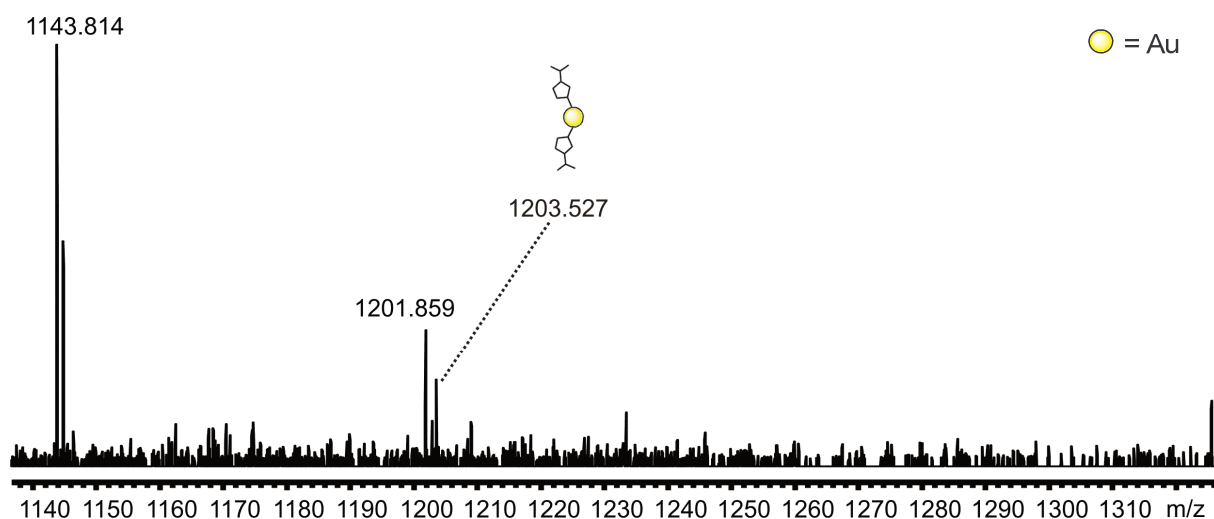


Figure 168: ESI(+) mass spectrum of the crude product from the reaction of $24s^*3Br^-$, $25s^*3Br^-$, $26s^*Br^-$, TBAB, NaOAc, AgO_2 and $Au(SMe_2)Cl$ in MeOH at rt. The sample was diluted with methanol.

Variation of the gold source could improve the reaction. Therefore another compound was tested. The last reaction was performed almost as the reaction before, but $Au(tht)Cl$ was used as gold source. This compound is a common and reactive alternative to $Au(SMe_2)Cl$.^[2c,135] The crude product of the reaction was received as light brown solid. The ESI MS spectra of the two gold containing crude products are almost identical. Therefore a preference of one of the gold sources is not recommended yet. Both reactions yielded nearly the same interesting detectable species, with similar intensities of the signals.

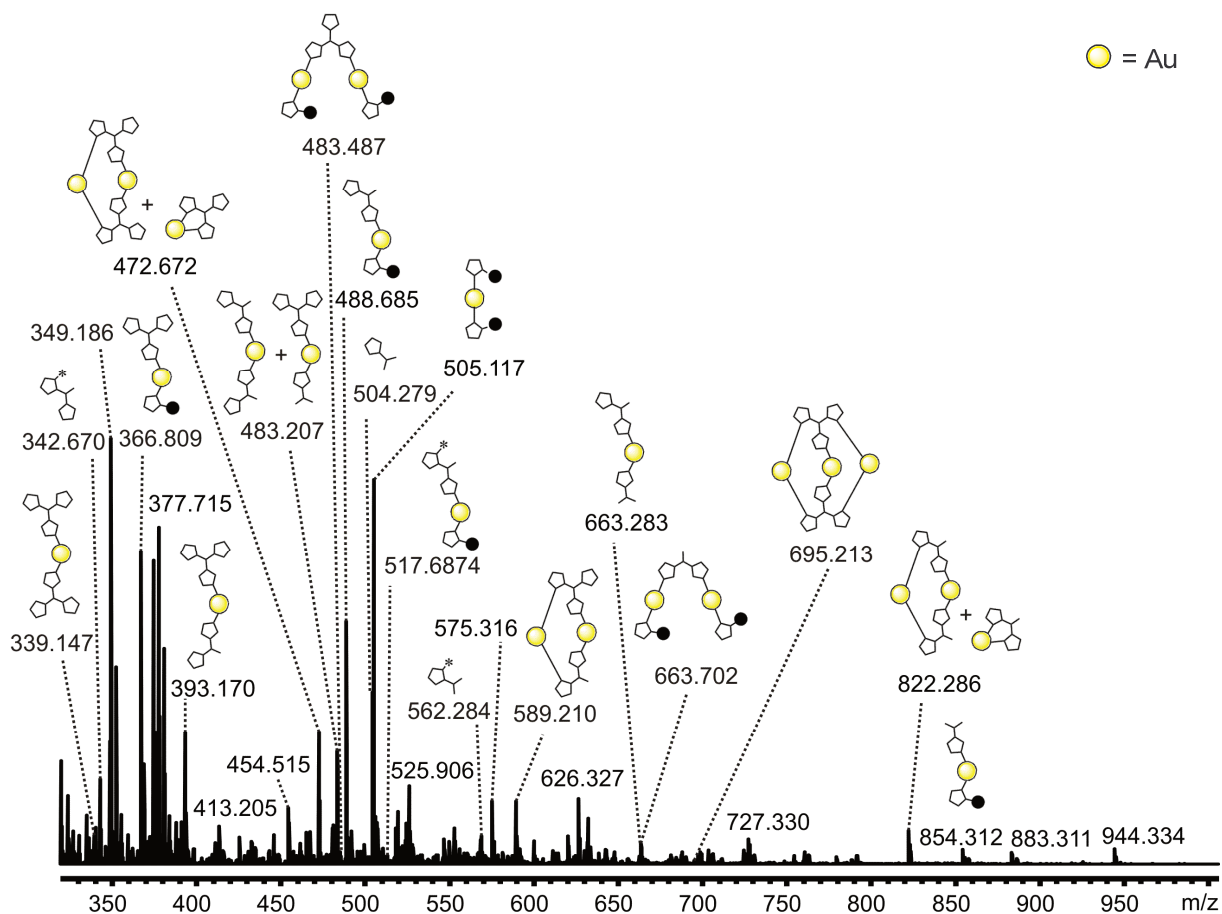


Figure 169: ESI(+) mass spectrum of the crude product from the reaction of 24s*3Br⁻, 25s*3Br⁻, 26s*Br⁻, TBAB, NaOAc, AgO₂ and Au(tht)Cl in MeOH at rt. The sample was diluted with methanol. (For full spectrum see Figure 188, Includes small signals of [39s+CH₂CO₂]/[41s+CH₂CO₂], [40s+CH₂CO₂], [36s+CH₂CO₂]).

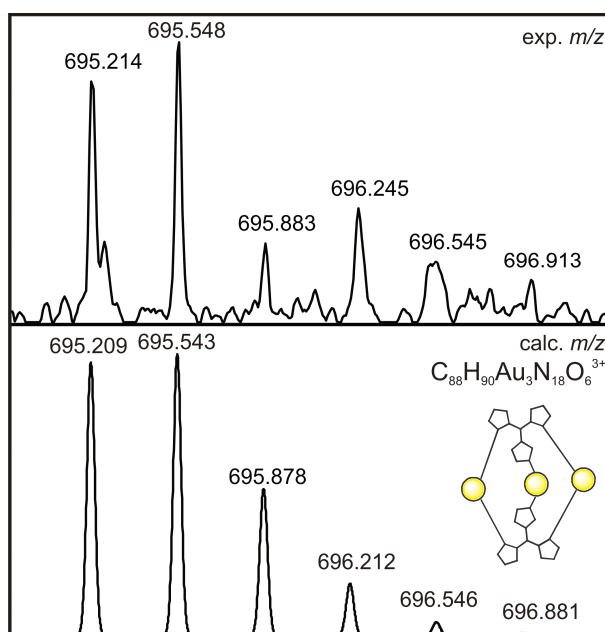


Figure 170: Partial ESI(+) mass spectrum of the crude product, showing the experimental and calculated isotopic pattern of 31s.

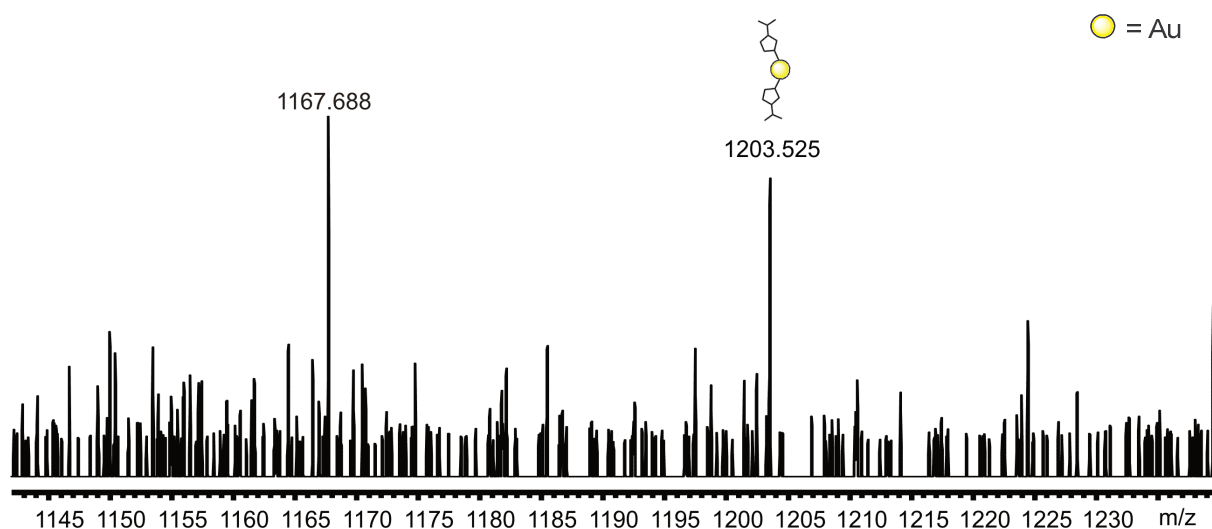


Figure 171: ESI(+) mass spectrum of the crude product from the reaction of $24s^*3Br^-$, $25s^*3Br^-$, $26s^*Br^-$, TBAB, NaOAc, AgO_2 and $Au(tht)Cl$ in MeOH at rt. The sample was diluted with methanol.

Purification of all the new complexes by crystallization in different solvents was unsuccessful. Dissolving the product in DMF however leads to a bright yellow solution. Further investigations of this behaviour could be interesting. The colour change from brown in methanol to yellow in DMF could indicate different interactions of the complexes with the counterions or the solvent. Another source for the bright colour could be silver nanoparticles. They are generated after the transmetalation reaction and therefore could also exist in the crude product.

4.5 Conclusion

In conclusion the design and a promising synthesis route for a new C_3 symmetrical tribenzotriquinacene NHC ligand precursor and the respective conversion to the unique trinuclear silver and gold complexes were presented. Next to them the C_1 symmetrical isomers of the imidazolium compounds were synthesized with similar results. The imidazolium moieties are linked to the aromatic backbone over an amide bonding. The coupling reaction led to a mixture of three different compounds with one, two or three imidazolium units respectively. The key for this reaction is the combination of the coupling compounds EDC and DMAP with the strong but non nucleophilic base DIPEA. In addition the reaction needs a higher activation through a temperature of at least 50°C, to achieve the three coupling steps in an adequate rate of yield. All purification attempts to yield the pure tripodal compounds were ineffective, so the conversion to the corresponding cage molecules was drastically limited. Therefore the reaction parameters need further improvement. Different solvents or anion exchanges could support the reaction. However this is the first example of a tripodal ligand precursor consisting of the TBTQ framework and NHC moieties linked over amide bonds. The crude product was successfully used to construct several heteroleptic and homoleptic Ag(I) NHC complexes via the silver base route. Nevertheless the right combination of base (NaOAc), solvent (MeOH) and phase transfer catalyst (TBAB) is important for the reaction. Intriguingly 11 possible combinations of the ligand precursors **24a,s**, **25a,s** and **26a,s** and silver could be detected by mass spectrometric means. Additionally some complexes containing the plain imidazolium acid precursor **1** without the TBTQ unit or the corresponding ester derivative **17** could be detected. Transmetallation of the silver complexes with two different gold sources (Au(SMe₂)Cl and Au(tht)Cl) lead to all 12 possible gold complexes of the symmetrical isomers and some of the additional compounds with acid and ester moieties. So the silver compounds proved to be suitable transmetallation agents. The reaction conditions for this step are really soft, at room temperature without prior purification and do not need further activation. All complexes have been confirmed several times by mass spectrometric means. Comparing both sets of ligand precursors (symmetric and asymmetric) does not show striking differences during the synthesis. The symmetrical compounds appear to have slightly better yield rate for the silver complexes which is attributed to the steric configuration. But nevertheless both tripodal Ag cage molecules could be synthesized. The successful synthesis of so many different

complexes provides a large array for possible sensor molecules. Screening experiments can be performed with small molecules or ions and all of these compounds to find the best host-guest pair in the herein provided library of complexes. Due to the fact that NHC compounds are easy tuneable by different substituents, the ligand precursors can be improved and modulated to fit for a specific substrate. The different isomers lead to different colours of the complexes. This could also be interesting for the recognition application. Further luminescence spectroscopic experiments with the 3D-metallocavitands are planned. The interesting results open up the opportunity as potential highly selective chiral phosphorescent receptor molecules. The cavity inside the given silver and gold cage molecules could probably bind different specific hosts. However the described capturing of small molecules or ions over Au...Au bonding and other supramolecular interactions still has to be observed.

4.6 Experimental section

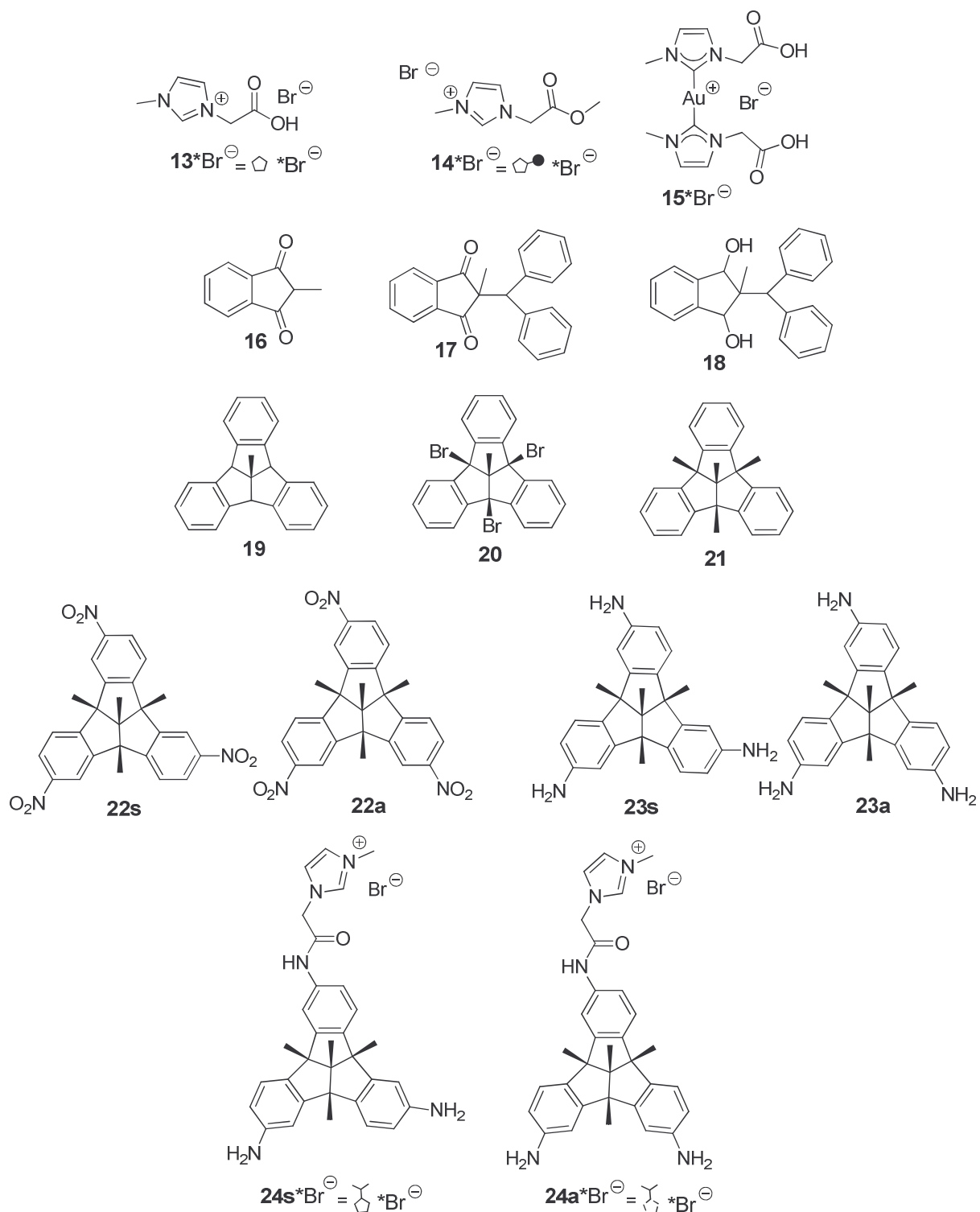
If not mentioned otherwise, all operations were performed under argon atmosphere using standard schlenk techniques with conventional glassware. Most solvents were dried, distilled, and stored under argon according to standard procedures. All starting materials were used as received from commercial sources. NMR data were recorded on a Bruker Avance 300 or 400 spectrometer at 25°C. The references for NMR spectra are as follows: ^1H MeOD (3.31 ppm), $^{13}\text{C}\{^1\text{H}\}$ MeOD (49.0 ppm).^[93] The known compounds of **16** – **23a**, **23s** were mainly synthesized as described in the literature. For some steps the solvent benzene was replaced with toluene (see Scheme 12). The spectroscopic characterization matches the reported data.^{[10e], [10b-d,10f-h]} X-ray crystallographic data were collected on a STOE IPDS2T diffractometer at 123 K. Intensities were measured by fine-slicing ϕ - and ω -scans and corrected for background, polarization and Lorentz effects. A semi-empirical absorption correction was applied for the data sets following Blessing's method.^[94] The structures were solved by direct methods and refined anisotropically by the least squares procedure implemented in the ShelX program system.^[95] The hydrogen atoms were included isotropically using the riding model on the bound atoms.^[96]

13*Br⁻: Yield 1.40 g (25%); 2.20 mL 1-methyl imidazole (27.9 mmol) and 3.60 g bromo acetic acid (25.9 mmol) were stirred in acetonitrile at 75°C for 20 h. The solvent was removed under vacuo, yielding a colourless oil. White crystals were obtained after the addition of concentrated hydrochloric acid. The product was washed with acetonitrile and dried in vacuo. ¹H-NMR (400.0 MHz, MeOD, δ in ppm, RT): 3.91 (s, 3H, H-1), 5.17 (s, 2H, H-4), 7.73-7.76 (m, 2H, H-2,3), 9.14 (s, 1H, H-7); ¹³C-NMR (125.0 MHz, MeOD, δ in ppm, RT): 36.0 (C-1), 49.7 (C-5), 123.2 (C-2), 123.7 (C-3), 137.6 (C-7), 168.2 (C-4); HR-ESI-MS(+) *m/z*: 141.0652 [M-Br]⁺, calc. for C₆H₉N₂O₂⁺: 141.0659, 281.1231 [2M-Br-HBr]⁺, calc. C₁₂H₁₇N₄O₄⁺: 281.1244.

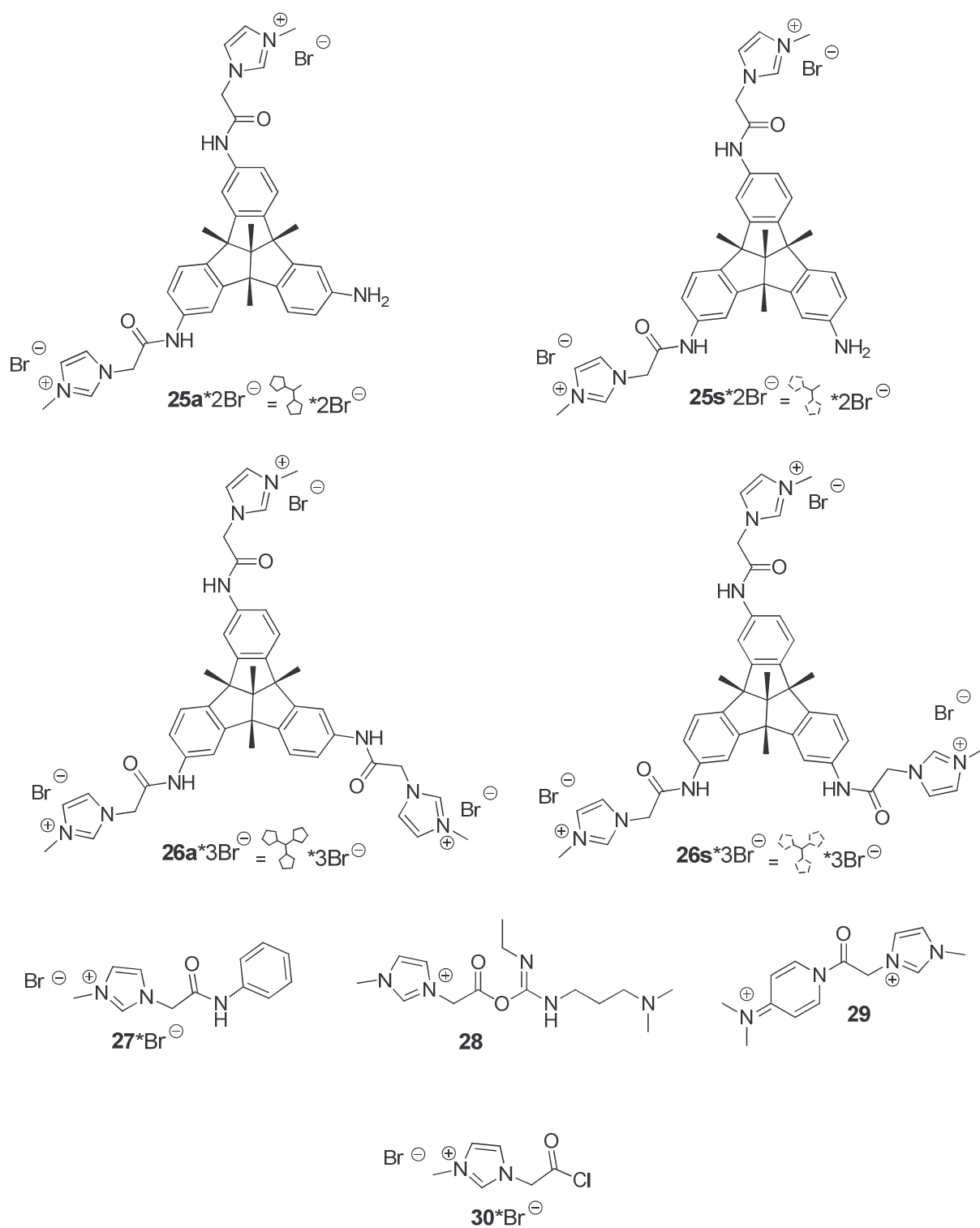
15*Br⁻: Yield 181 mg (82%); 176 mg (796 μmol, 2.0 eq) 3-(carboxymethyl)-1-methyl-1*H*-imidazol-3-ium-bromide, 142 mg (1.73 mmol, 4.3) sodium acetate and 119 mg (404 μmol, 1.0 eq) Chloro(dimethylsulfid)gold(I) were stirred under reflux in 15 mL DMF for 3 h. The solution was reduced in volume and precipitated with diethyl ether. The crude product was filtered, washed with diethyl ether and dried under vacuo. The product was obtained as light pink crystals. ¹H-NMR (300.0 MHz, MeOD, δ in ppm, RT): 3.89 (s, 6H, H-1), 4.76 (s, 4H, H-5), 7.23 (d, 2H, H-2, ³*J*_{H-2,H-3} = 1.9 Hz), 7.24 (d, 2H, H-3, ³*J*_{H-3,H-2} = 1.9 Hz); ¹³C-NMR (75.0 MHz, MeOD, δ in ppm, RT): 38.0 (C-1), 55.2 (C-5), 123.3 (C-2), 124.2 (C-3), 174.1 (C-6), 186.8 (C-4); HR-ESI-MS(+) *m/z*: 477.0840 [M-Br]⁺, calc. for C₁₂H₁₆AuN₄O₄⁺: 477.0832.

4.7 Appendix

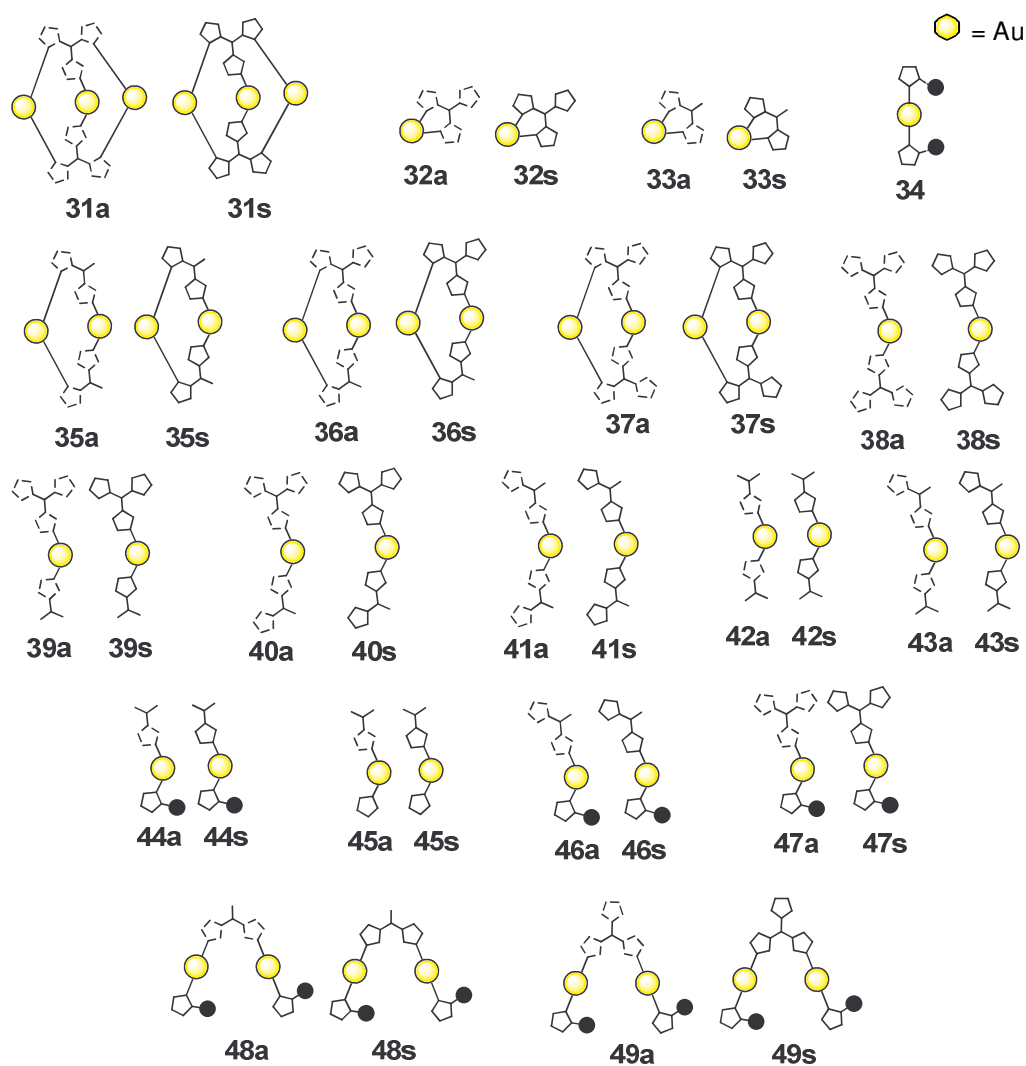
Overview of the synthesized compounds and proposed transient species



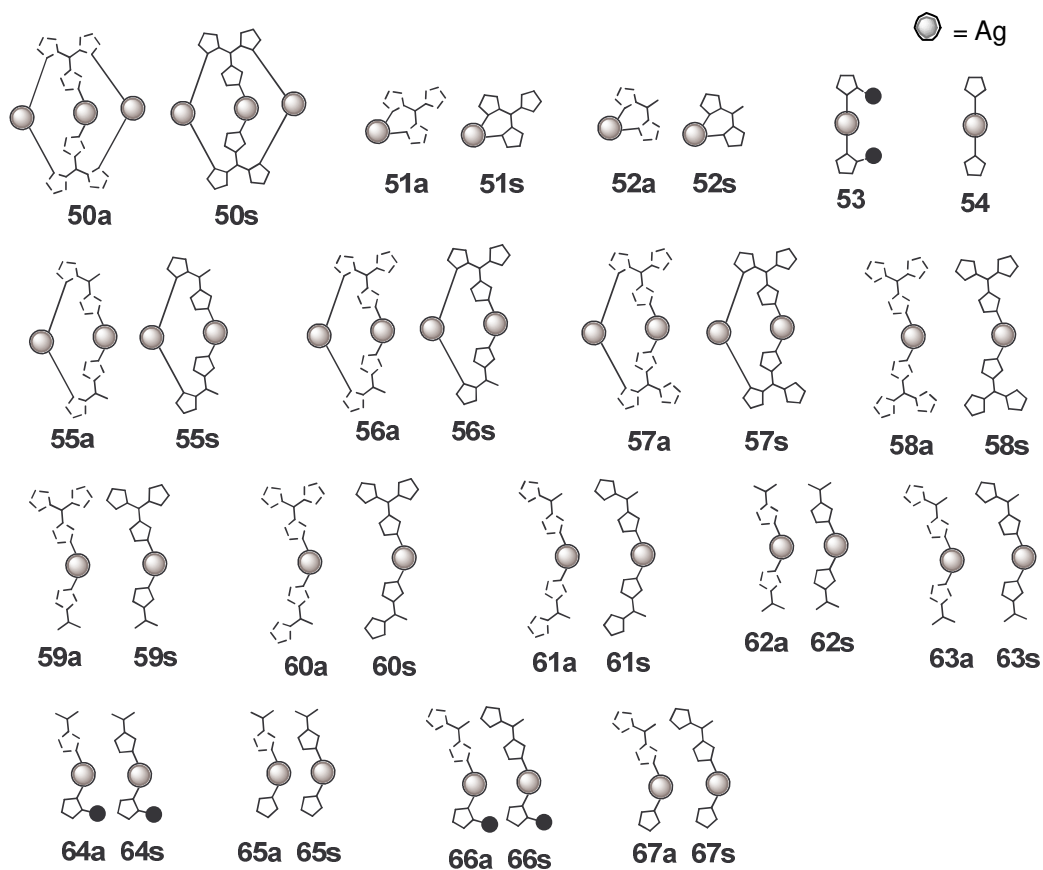
Scheme 26: Overview of the synthesized compounds. The additional sketches of the cations are used for the visualization in the mass spectra.



Scheme 27: Overview of the synthesized compounds and proposed transient species. The additional sketches of the cations are used for the visualization in the mass spectra.



Scheme 28: For a better Overview the following complexes are shown as simple sketches. They are mainly used for the visualization in the mass spectra. The complexation of a metal atom always includes deprotonation of the ligand precursors. Therefore each drawn bond between a ligand and a metal atom is also indicating the loss of one proton. The sketches for the asymmetric compounds are illustrated with dashed bonds and the symmetrical compounds are illustrated with solid bonds. Explanations of the ligands are given in Scheme 26 and Scheme 27



Scheme 29: For a better Overview the following complexes are shown as simple sketches. They are mainly used for the visualization in the mass spectra. The complexation of a metal atom always includes deprotonation of the ligand precursors. Therefore each drawn bond between a ligand and a metal atom is also indicating the loss of one proton. The sketches for the asymmetric compounds are illustrated with dashed bonds and the symmetrical compounds are illustrated with solid bonds. Explanations of the ligands are given in Scheme 26 and Scheme 27.

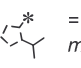
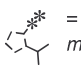
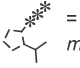
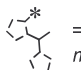
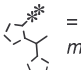
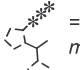
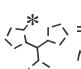
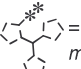
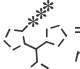
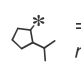
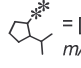
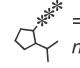
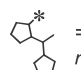
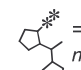
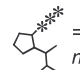
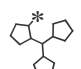
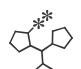
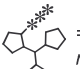
 = [11a+(CH ₂ CO ₂)] m/z = 562.2813	 = [11a+(CH ₂ CO ₂) ₂] m/z = 620.2867	 = [11a+(CH ₂ CO ₂) ₃] m/z = 678.2922
 = [12a+(CH ₂ CO ₂)] m/z = 342.6683	 = [12a+(CH ₂ CO ₂) ₂] m/z = 371.6710	 = [12a+(CH ₂ CO ₂) ₃] m/z = 400.6738
 = [13a+(CH ₂ CO ₂)] m/z = 269.4639	 = [13a+(CH ₂ CO ₂) ₂] m/z = 288.7991	 = [13a+(CH ₂ CO ₂) ₃] m/z = 308.1343
 = [11s+(CH ₂ CO ₂)] m/z = 562.2813	 = [11s+(CH ₂ CO ₂) ₂] m/z = 620.2867	 = [11s+(CH ₂ CO ₂) ₃] m/z = 678.2922
 = [12s+(CH ₂ CO ₂)] m/z = 342.6683	 = [12s+(CH ₂ CO ₂) ₂] m/z = 371.6710	 = [12s+(CH ₂ CO ₂) ₃] m/z = 400.6738
 = [13s+(CH ₂ CO ₂)] m/z = 269.4639	 = [13s+(CH ₂ CO ₂) ₂] m/z = 288.7991	 = [13s+(CH ₂ CO ₂) ₃] m/z = 308.1343

Figure 172: Overview of the possible asymmetrical and symmetrical ligand precursors with 1-3 additional -CH₂CO₂ groups and their calculated m/z values.

Table 6: Overview of all possible gold complexes consisting of 1, 2 or 3 Au ions, 1 or 2 of the ligand precursors 24a,s; 25a,s; 26a,s and one or two additional CH₂CO₂ groups. Two touching blue areas mark two different molecules with the same charge and molecular formula, but different conformations. Red, green, brown and purple areas mark two different molecules with different charges and different molecular formulas but the same m/z values. The sketches show the symmetrical compounds but the asymmetrical compounds are isobaric.





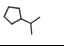
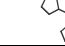
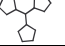
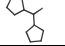
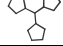
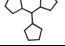
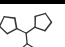
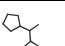
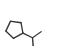
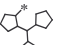
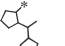
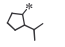
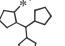
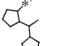
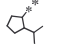
bounded metal ions second ligand first ligand	+ 	+ 			+ 		+ 
	no second ligand						
	C ₄₄ H ₄₆ AuN ₉ O ₅ ²⁺ m/z = 472.6689	C ₇₆ H ₈₀ AuN ₁₄ O ₈ ³⁺ m/z = 483.2045	C ₈₂ H ₈₇ AuN ₁₆ O ₈ ⁴⁺ m/z = 393.1672	C ₈₈ H ₉₄ AuN ₁₈ O ₈ ⁵⁺ m/z = 339.1449	C ₈₂ H ₈₅ Au ₂ N ₁₆ O ₈ ³⁺ m/z = 589.2968	C ₈₂ H ₉₂ Au ₂ N ₁₈ O ₈ ⁴⁺ m/z = 472.6689	C ₈₈ H ₉₀ Au ₃ N ₁₈ O ₈ ³⁺ m/z = 695.5090
	C ₃₈ H ₃₈ AuN ₇ O ₂ ⁺ m/z = 822.2826	C ₇₀ H ₇₂ AuN ₁₂ O ₃ ²⁺ m/z = 663.2792	C ₇₆ H ₈₀ AuN ₁₄ O ₄ ³⁺ m/z = 483.2045		C ₇₈ H ₇₈ Au ₂ N ₁₄ O ₄ ²⁺ m/z = 822.2826		
		C ₆₄ H ₆₆ AuN ₁₀ O ₂ ⁺ m/z = 1203.5030					
	C ₄₆ H ₄₈ AuN ₉ O ₅ ²⁺ m/z = 501.6716	C ₇₈ H ₈₂ AuN ₁₄ O ₆ ³⁺ m/z = 502.5397	C ₈₄ H ₈₉ AuN ₁₆ O ₇ ⁴⁺ m/z = 407.6686	C ₉₀ H ₉₆ AuN ₁₈ O ₈ ⁵⁺ m/z = 350.7459	C ₈₄ H ₈₇ Au ₂ N ₁₆ O ₇ ³⁺ m/z = 608.5419	C ₉₀ H ₉₄ Au ₂ N ₁₈ O ₈ ⁴⁺ m/z = 487.1703	C ₉₀ H ₉₂ Au ₃ N ₁₈ O ₈ ³⁺ m/z = 714.5442
	C ₄₀ H ₄₁ AuN ₇ O ₄ ⁺ m/z = 880.2880	C ₇₂ H ₇₅ AuN ₁₂ O ₅ ²⁺ m/z = 692.2819	C ₇₈ H ₈₂ AuN ₁₄ O ₆ ³⁺ m/z = 502.5397		C ₇₈ H ₈₀ Au ₂ N ₁₄ O ₆ ²⁺ m/z = 851.2853		
		C ₆₈ H ₆₈ AuN ₁₀ O ₄ ⁺ m/z = 1261.5085					
	C ₄₈ H ₅₀ AuN ₉ O ₇ ²⁺ m/z = 530.6744	C ₈₀ H ₈₄ AuN ₁₄ O ₈ ³⁺ m/z = 521.8749	C ₈₆ H ₉₁ AuN ₁₆ O ₉ ⁴⁺ m/z = 422.1700	C ₉₂ H ₉₈ AuN ₁₈ O ₁₀ ⁵⁺ m/z = 362.3470	C ₈₆ H ₈₉ Au ₂ N ₁₆ O ₉ ³⁺ m/z = 627.7889	C ₉₂ H ₉₆ Au ₂ N ₁₈ O ₁₀ ⁴⁺ m/z = 501.6716	C ₉₂ H ₉₄ Au ₃ N ₁₈ O ₁₀ ³⁺ m/z = 733.8793
	C ₄₂ H ₄₃ AuN ₇ O ₆ ⁺ m/z = 938.2935	C ₇₄ H ₇₇ AuN ₁₂ O ₇ ²⁺ m/z = 721.2846	C ₈₀ H ₈₄ AuN ₁₄ O ₈ ³⁺ m/z = 521.8749		C ₈₀ H ₈₂ Au ₂ N ₁₄ O ₈ ²⁺ m/z = 880.2880		
		C ₆₈ H ₇₀ AuN ₁₀ O ₆ ⁺ m/z = 1319.5140					

Table 7: Overview of all possible silver complexes consisting of 1, 2 or 3 Ag ions, 1 or 2 of the ligand precursors 24a,s; 25a,s; 26a,s and one or two additional CH₂CO₂ groups. Two touching blue areas mark two different molecules with the same charge and molecular formula, but different conformations. Red, green, brown and purple areas mark two different molecules with different charges and different molecular formulas but the same *m/z* values. The sketches show the symmetrical compounds but the asymmetrical compounds are isobaric.





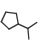
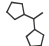
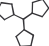
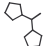
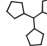
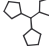
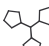
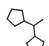
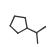
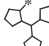
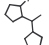
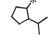
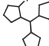
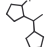
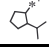
bounded metal ions second ligand first ligand	+ 	+ 			+ 		+ 
	no second ligand						
	C ₄₄ H ₄₆ AgN ₆ O ₃ ²⁺ <i>m/z</i> = 427.6382	C ₇₆ H ₈₀ AgN ₁₄ O ₄ ³⁺ <i>m/z</i> = 453.1840	C ₈₂ H ₈₇ AgN ₁₆ O ₅ ⁴⁺ <i>m/z</i> = 370.6519	C ₈₈ H ₉₄ AgN ₁₈ O ₆ ⁵⁺ <i>m/z</i> = 321.1325	C ₈₂ H ₈₅ Ag ₂ N ₁₆ O ₅ ³⁺ <i>m/z</i> = 529.1658	C ₈₈ H ₉₂ Ag ₂ N ₁₈ O ₆ ⁴⁺ <i>m/z</i> = 427.6382	C ₈₈ H ₉₀ Ag ₃ N ₁₈ O ₆ ³⁺ <i>m/z</i> = 605.1476
	C ₃₈ H ₃₉ AgN ₇ O ₂ ⁺ <i>m/z</i> = 732.2211	C ₇₀ H ₇₃ AgN ₁₂ O ₃ ²⁺ <i>m/z</i> = 618.2484	C ₇₆ H ₈₀ AgN ₁₄ O ₄ ³⁺ <i>m/z</i> = 453.1840		C ₇₆ H ₇₈ Ag ₂ N ₁₄ O ₄ ²⁺ <i>m/z</i> = 732.2211		
		C ₆₄ H ₆₈ AgN ₁₀ O ₂ ⁺ <i>m/z</i> = 1113.4416					
	C ₄₆ H ₄₈ AgN ₆ O ₅ ²⁺ <i>m/z</i> = 456.6409	C ₇₈ H ₈₂ AgN ₁₄ O ₆ ³⁺ <i>m/z</i> = 472.5192	C ₈₄ H ₈₉ AgN ₁₆ O ₇ ⁴⁺ <i>m/z</i> = 385.1532	C ₉₀ H ₉₆ AgN ₁₈ O ₈ ⁵⁺ <i>m/z</i> = 332.7336	C ₈₄ H ₈₇ Ag ₂ N ₁₆ O ₇ ³⁺ <i>m/z</i> = 548.5010	C ₉₀ H ₈₄ Ag ₂ N ₁₈ O ₈ ⁴⁺ <i>m/z</i> = 442.1395	C ₉₀ H ₈₂ Ag ₃ N ₁₈ O ₈ ³⁺ <i>m/z</i> = 624.4827
	C ₄₀ H ₄₁ AgN ₇ O ₄ ⁺ <i>m/z</i> = 790.2265	C ₇₂ H ₇₅ AgN ₁₂ O ₅ ²⁺ <i>m/z</i> = 647.2512	C ₇₈ H ₈₂ AgN ₁₄ O ₆ ³⁺ <i>m/z</i> = 472.5192		C ₇₈ H ₈₀ Ag ₂ N ₁₄ O ₆ ²⁺ <i>m/z</i> = 761.2238		
		C ₆₆ H ₆₈ AgN ₁₀ O ₄ ⁺ <i>m/z</i> = 1171.4470					
	C ₄₈ H ₅₀ AgN ₆ O ₇ ²⁺ <i>m/z</i> = 485.6437	C ₈₀ H ₈₄ AgN ₁₄ O ₈ ³⁺ <i>m/z</i> = 491.8544	C ₈₈ H ₉₁ AgN ₁₆ O ₉ ⁴⁺ <i>m/z</i> = 399.6546	C ₉₂ H ₉₈ AgN ₁₈ O ₁₀ ⁵⁺ <i>m/z</i> = 344.3347	C ₈₆ H ₈₈ Ag ₂ N ₁₆ O ₉ ³⁺ <i>m/z</i> = 567.9361	C ₉₂ H ₈₉ Ag ₂ N ₁₈ O ₁₀ ⁴⁺ <i>m/z</i> = 456.6409	C ₉₂ H ₈₄ Ag ₃ N ₁₈ O ₁₀ ³⁺ <i>m/z</i> = 643.8179
	C ₄₂ H ₄₃ AgN ₇ O ₆ ⁺ <i>m/z</i> = 848.2320	C ₇₄ H ₇₇ AgN ₁₂ O ₇ ²⁺ <i>m/z</i> = 676.2539	C ₈₀ H ₈₄ AgN ₁₄ O ₈ ³⁺ <i>m/z</i> = 491.8544		C ₈₀ H ₈₂ Ag ₂ N ₁₄ O ₈ ²⁺ <i>m/z</i> = 790.2265		
		C ₆₈ H ₇₀ AgN ₁₀ O ₆ ⁺ <i>m/z</i> = 1229.4525					

Table 8: Explanation of the detected fragments [L-Ag]⁺ with their accurate mass, molecular formula and the proposed composition.

accurate mass of the fragment	molecular formula	proposed fragment composition
366.6142	[C ₃₈ H ₄₀ AgN ₇ O ₂] ²⁺	[25a/s-H+Ag] ²⁺
395.6169	[C ₃₈ H ₄₀ AgN ₇ O ₂ +(CH ₂ CO ₂)] ²⁺	[25a/s-H+Ag+(CH ₂ CO ₂)] ²⁺
419.5628	[C ₃₈ H ₃₉ Ag ₂ N ₇ O ₂] ²⁺	[25a/s-2H+2Ag] ²⁺
448.5655	[C ₃₈ H ₃₉ Ag ₂ N ₇ O ₂ +(CH ₂ CO ₂)] ²⁺	[25a/s-2H+2Ag+(CH ₂ CO ₂)] ²⁺
610.1731	[C ₃₂ H ₃₃ AgN ₅ O] ⁺	[24a/s-H+Ag] ⁺
668.1785	[C ₃₂ H ₃₃ AgN ₅ O+(CH ₂ CO ₂)] ⁺	[24a/s-H+Ag+(CH ₂ CO ₂)] ⁺
726.1840	[C ₃₂ H ₃₃ AgN ₅ O+(CH ₂ CO ₂) ₂] ⁺	[24a/s-H+Ag+2(CH ₂ CO ₂)] ⁺

Table 9: Crystallographic Data.

	1*Br⁻
formula	C₆H₉BrN₂O₂
cryst size [mm³]	0.31 x 0.06 x 0.03
cryst syst	orthorhombic
space group	Pca2₁
a [Å]	13.3978(3)
b [Å]	6.43648(24)
c [Å]	9.77754(24)
α [°]	90
β [°]	90
γ [°]	90
V [Å³]	843.16(4)
Z	4
ρ_{calc} [mg m³]	1.741
F₀₀₀	440.0
μ [mm⁻¹]	4.829
θ range [°]	6.082 – 55.982
reflns collected	27209
reflns unique	2028
R_{int}	0.0925
GOF	1.214
refined params	103
R1 [I>2σ(I)]	0.0528
wR2 (all data)	0.1446
largest diff peak [e Å⁻³]	1.24/-0.91

Spectra

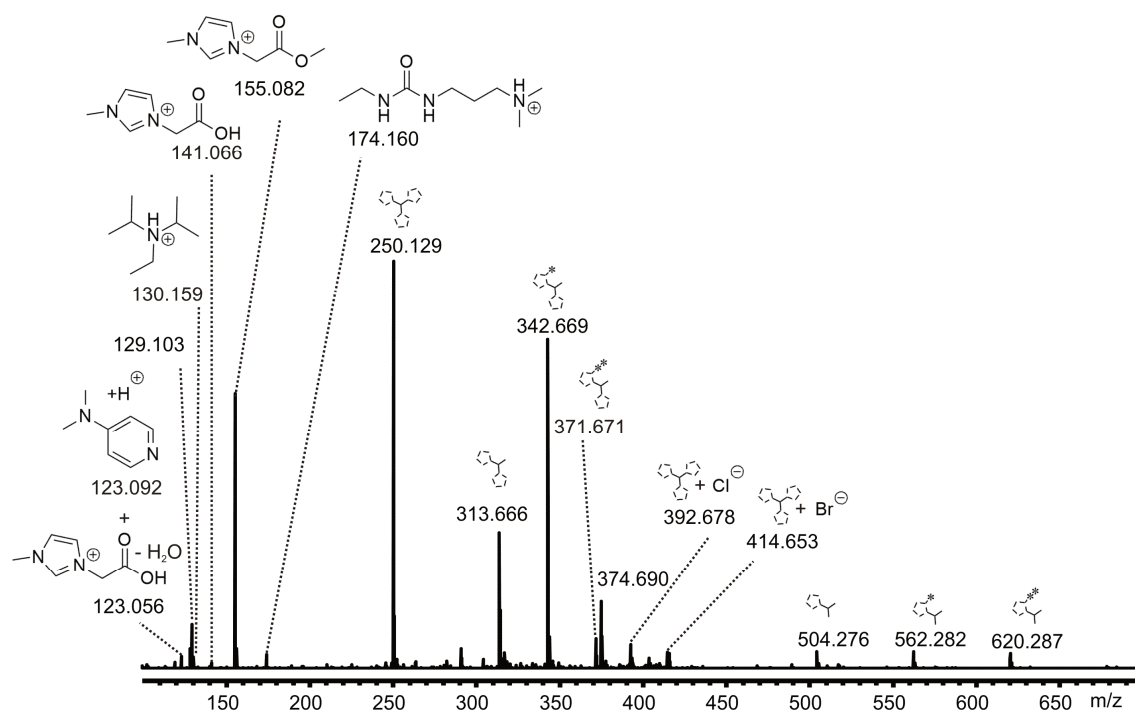


Figure 173: ESI(+) mass spectrum of the crude product from the reaction of 13^*Br^- , 23a, EDC, DMAP and DIPEA in acetonitrile at 50°C. The sample was diluted with methanol.

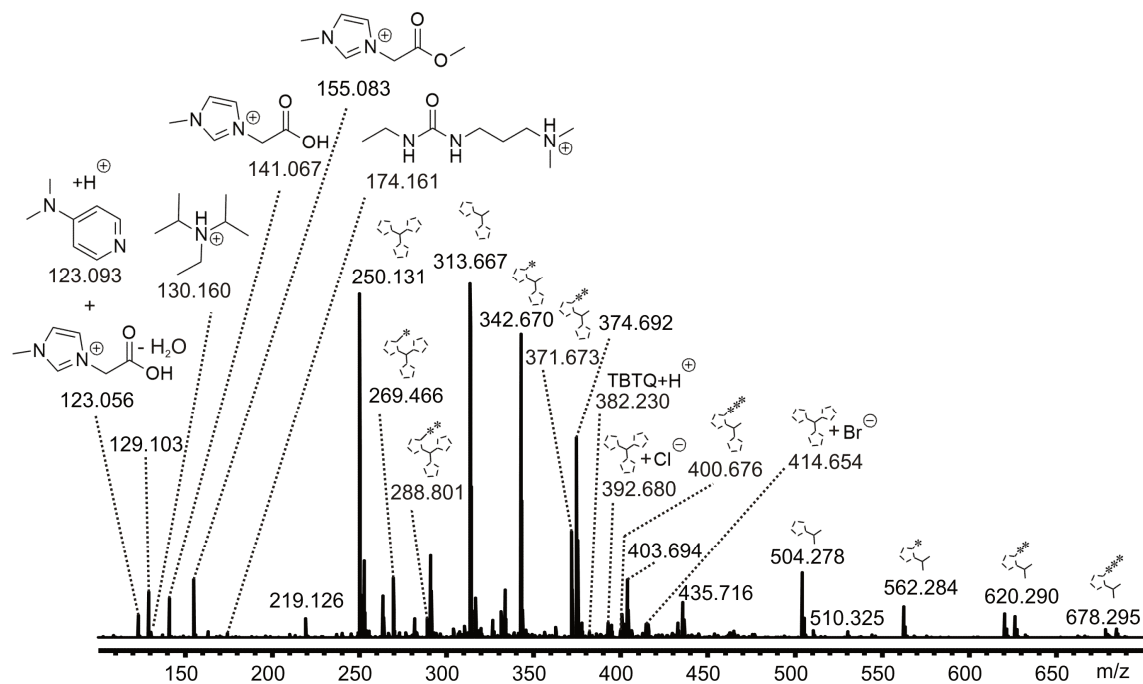


Figure 174: ESI(+) mass spectrum of the crude product from the reaction of 13^*Br^- , 23a, EDC, DMAP and DIPEA in acetonitrile at 80°C. The sample was diluted with methanol.

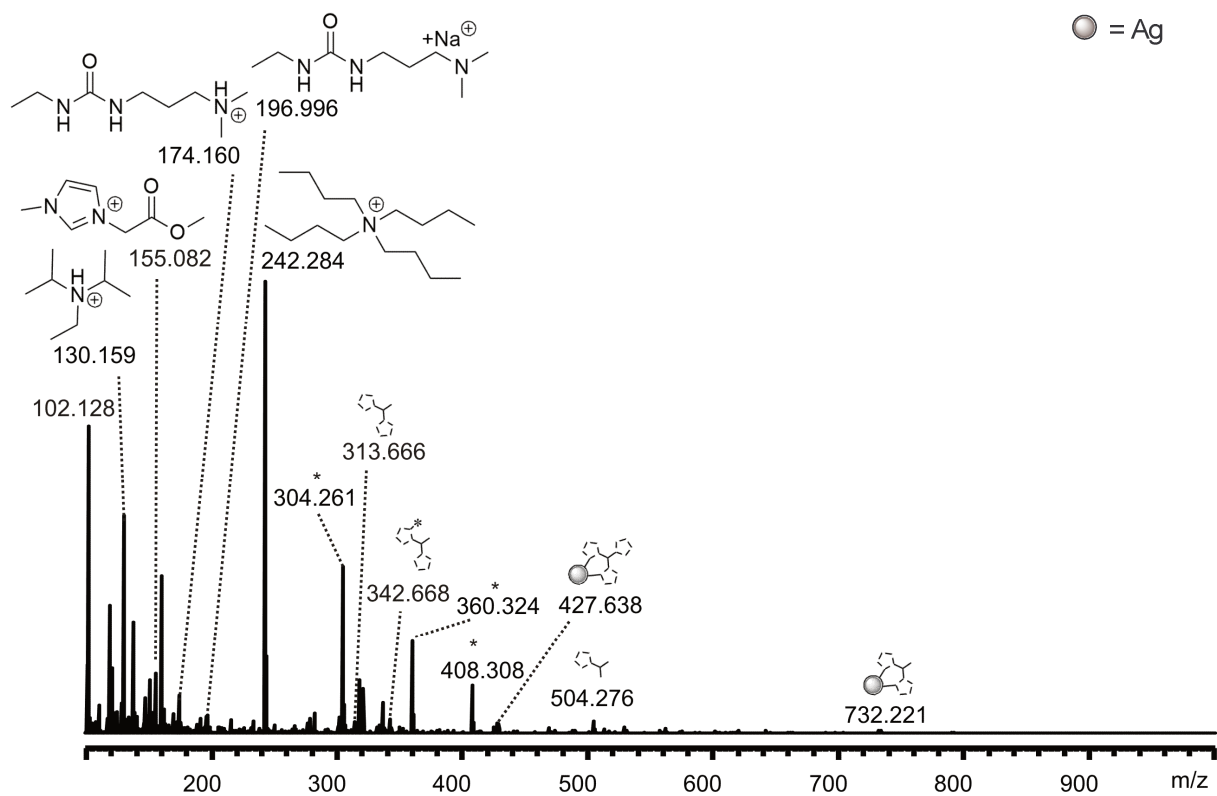


Figure 175: ESI(+)-mass spectrum of a reacting solution containing $24a^*Br^-$, $25a^*2Br^-$, $26a^*3Br^-$, TBAB, $NaOH_{aq}$ and AgO_2 in DCM at rt. The sample was taken after 24 hours and diluted with methanol. * = common background contaminant ions; the crude product contains side products and starting materials from the synthesis of $26a^*3Br^-$.

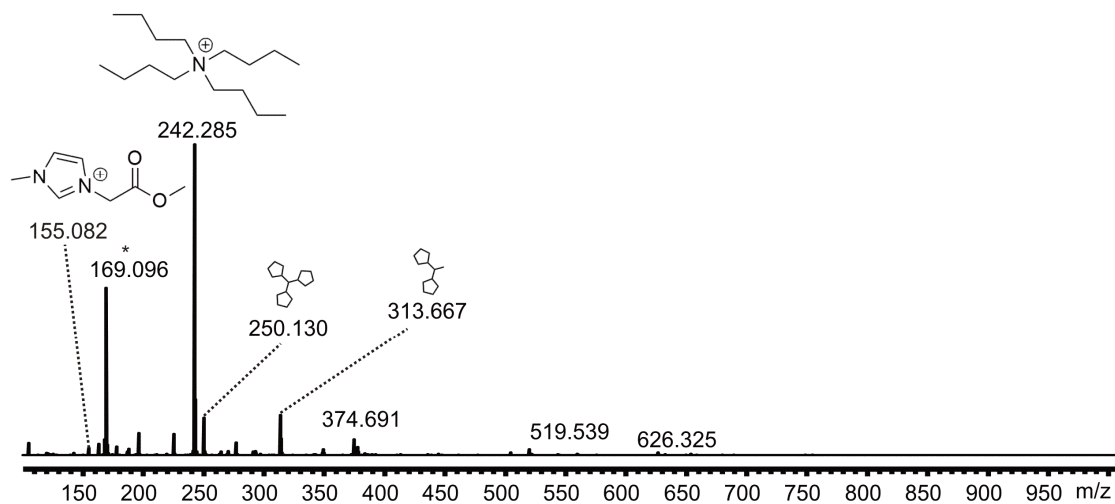


Figure 176: ESI(+)-mass spectrum of the crude product from the reaction of $24s^*3Br^-$, $25s^*3Br^-$, $26s^*Br^-$, TBAB, $NaOAc$ and AgO_2 in MeOH at rt. The sample was diluted with methanol.

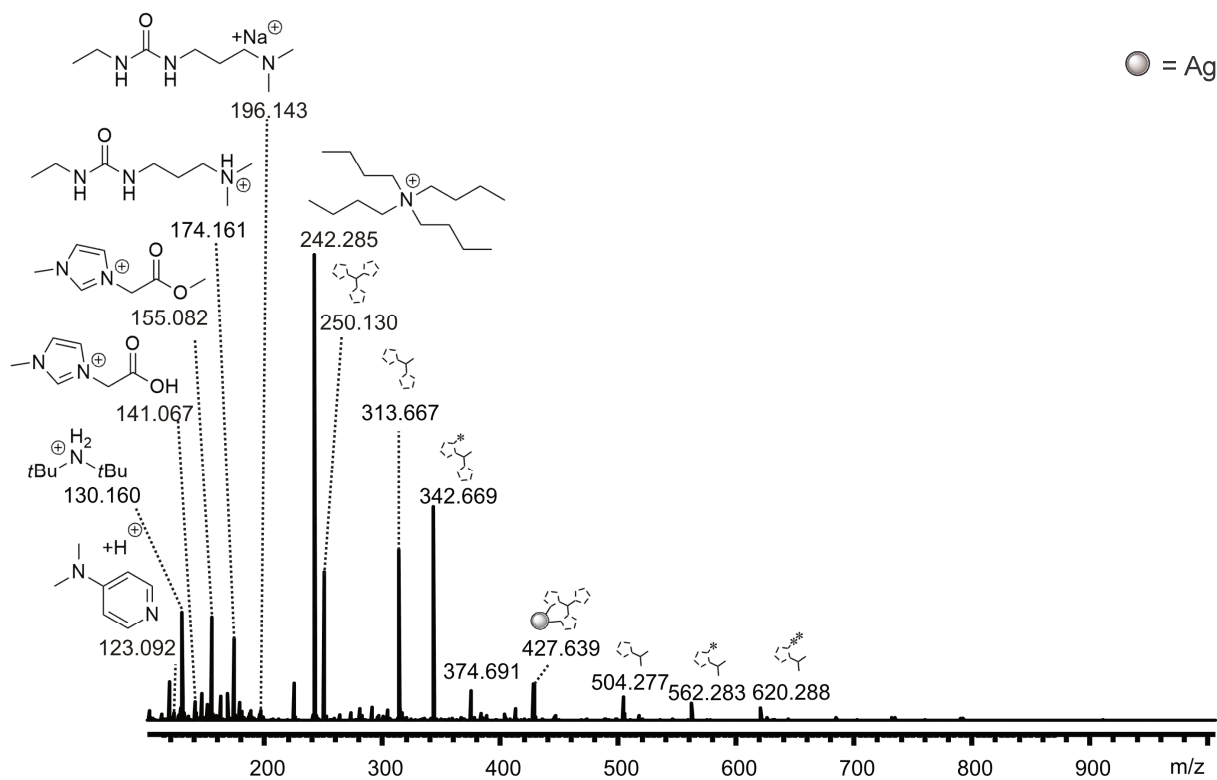


Figure 178: ESI(+) mass spectrum of a reacting solution containing $24a^*Br^-$, $25a^*2Br^-$, $26a^*3Br^-$, TBAB, NaOAc and AgO_2 in MeOH at rt. The sample was taken after 3 days and diluted with methanol; the crude product contains side products and starting materials from the synthesis of $26a^*3Br^-$.

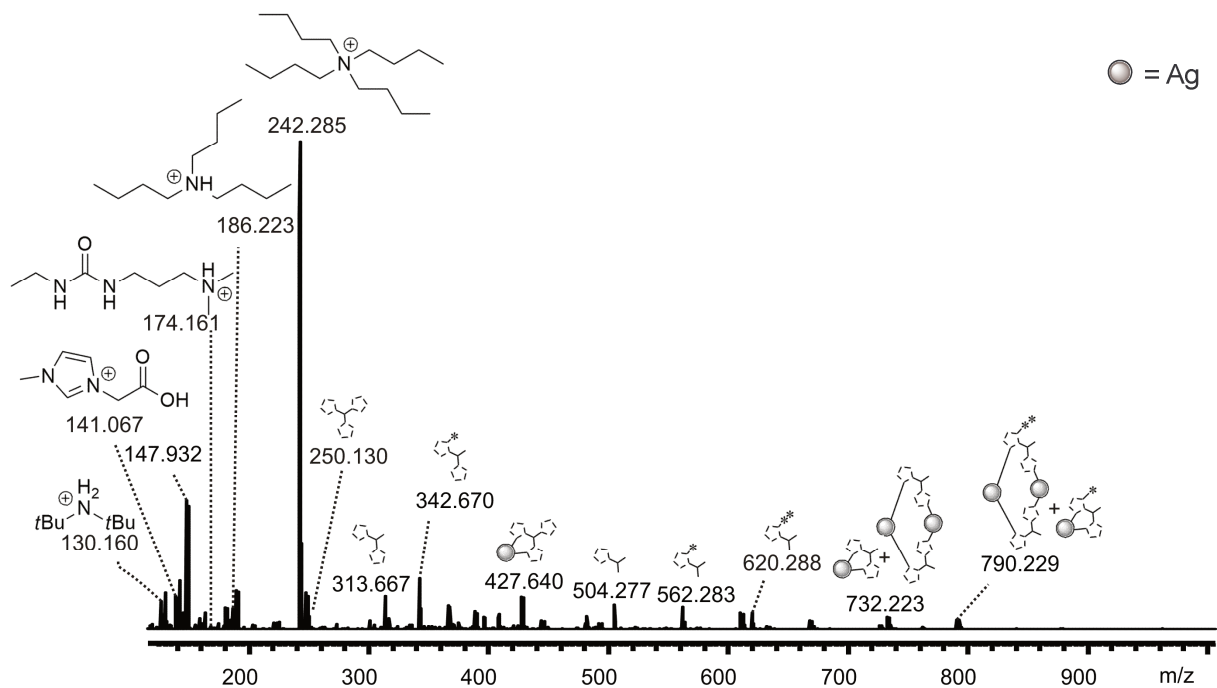


Figure 179: ESI(+) mass spectrum of a reacting solution containing $24a^*Br^-$, $25a^*2Br^-$, $26a^*3Br^-$, TBAB, NaOAc and AgO_2 in MeOH at rt. The sample was taken after 4 days and diluted with methanol; the crude product contains side products and starting materials from the synthesis of $26a^*3Br^-$.

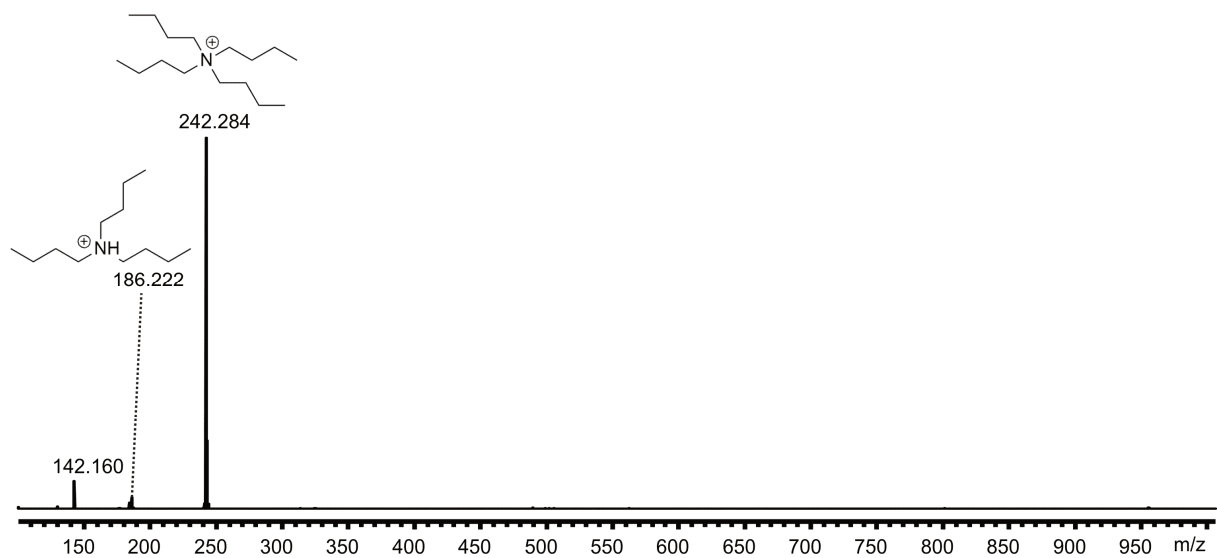


Figure 180: ESI(+) mass spectrum of the residue of the filtrate from the reaction of $17a^*Br^-$ and $Au(SMe_2)Cl$ in DMF at rt. The sample was diluted with methanol.

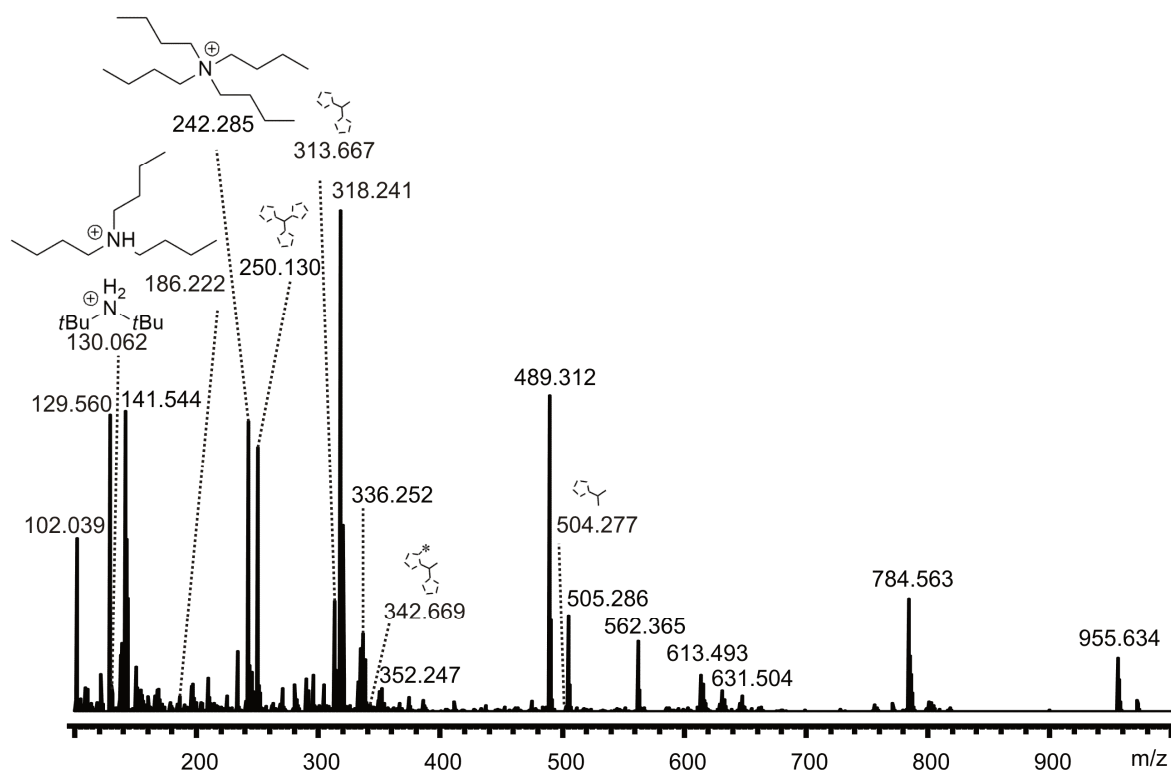


Figure 181: ESI(+) mass spectrum of the crude product from the reaction of 50a*Br⁻ and Au(SMe₆)Cl in DMF at rt. The sample was diluted with methanol. * = common background contaminant ions.

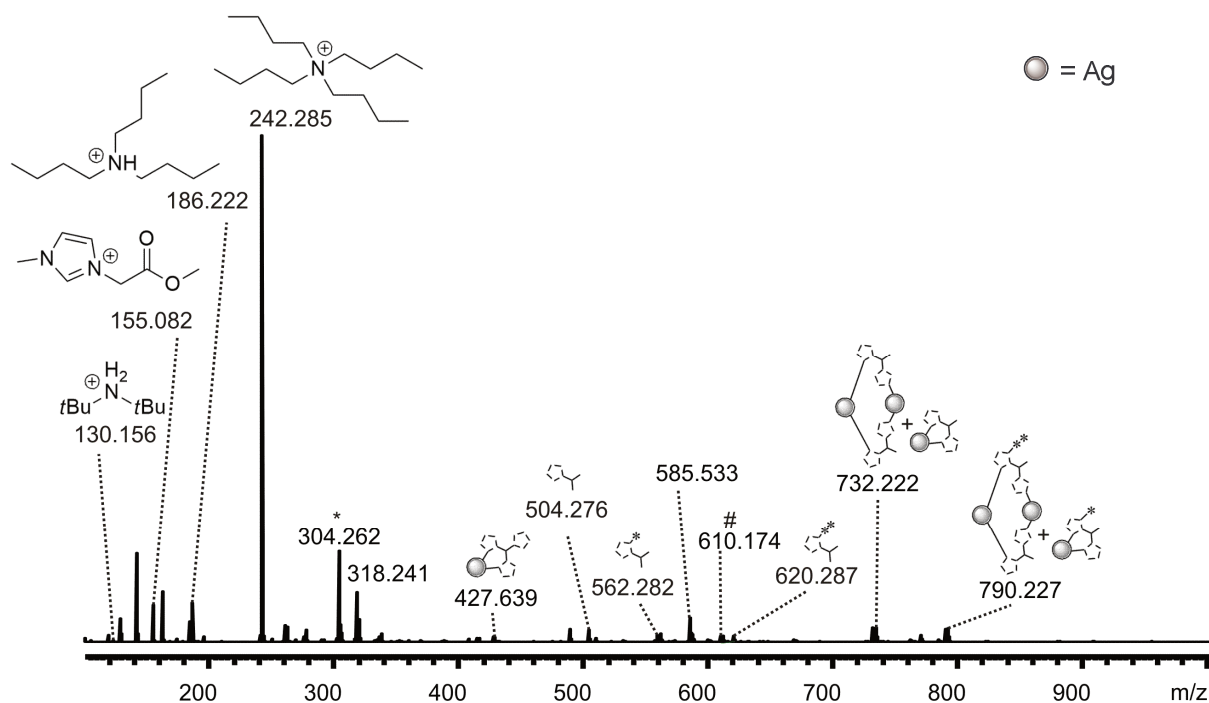


Figure 182: ESI(+) mass spectrum of a reacting solution containing 24a*Br⁻, 25a*2Br⁻, 26a*3Br⁻, TBAB, NaOAc and AgO₂ in MeOH at rt. The sample was taken after 2 hours and diluted with methanol. * = common background contaminant ions; the crude product contains side products and starting materials from the synthesis of 26a*3Br⁻.

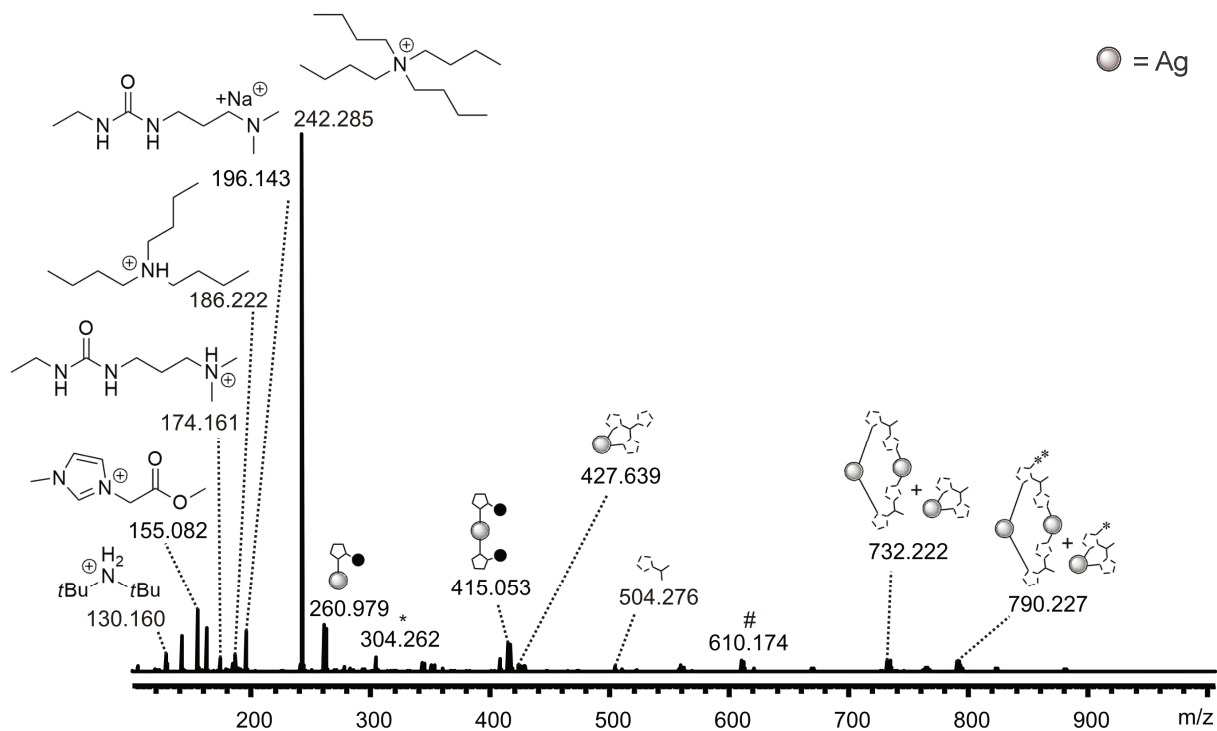


Figure 183: ESI(+) mass spectrum of a reacting solution containing $24a^*Br^-$, $25a^*2Br^-$, $26a^*3Br^-$, TBAB, NaOAc and AgO_2 in MeOH at rt. The sample was taken after 2 hours and diluted with methanol. * = common background contaminant ions; the crude product contains side products and starting materials from the synthesis of $26a^*3Br^-$.

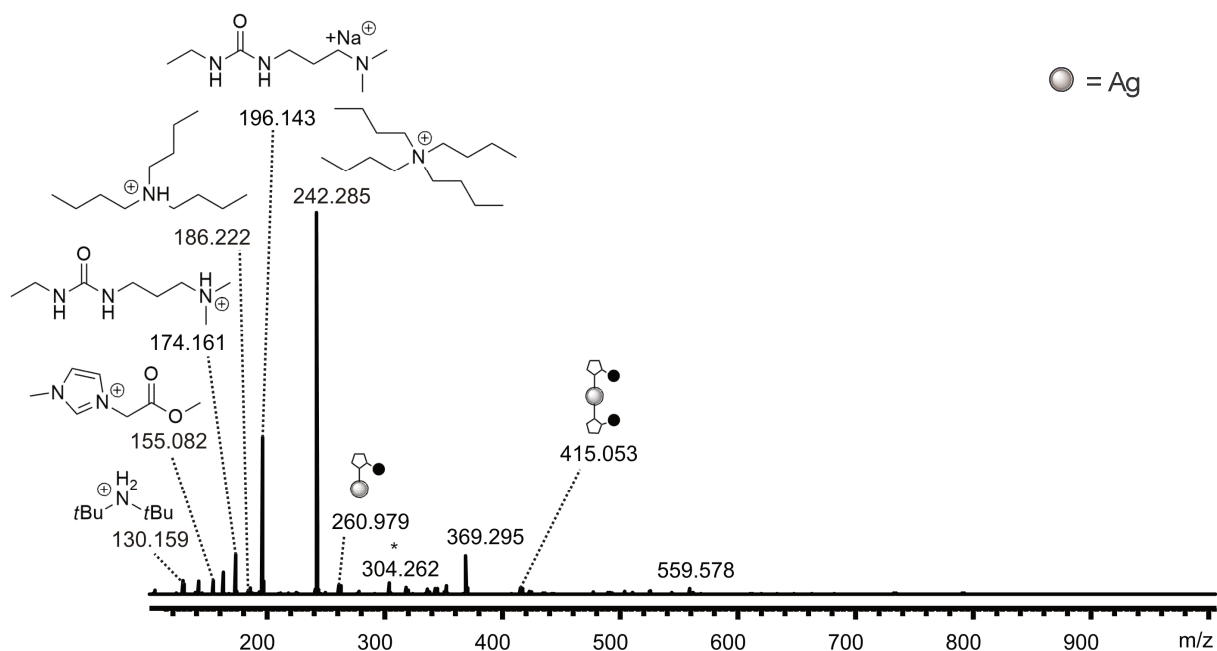


Figure 184: ESI(+) mass spectrum of a reacting solution containing $24a^*Br^-$, $25a^*2Br^-$, $26a^*3Br^-$, TBAB, NaOAc and AgO_2 in MeOH at rt. The sample was taken after 2 hours and diluted with methanol and H_2O . * = common background contaminant ions; the crude product contains side products and starting materials from the synthesis of $26a^*3Br^-$.

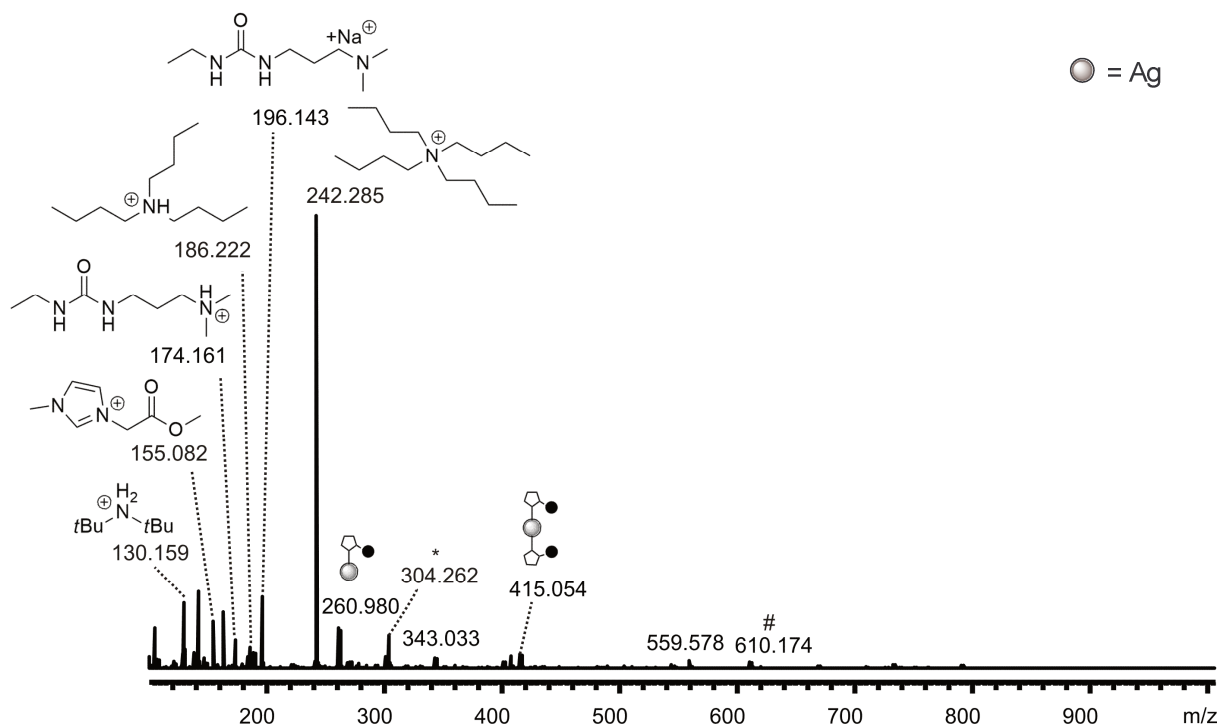


Figure 185: ESI(+)-mass spectrum of a reacting solution containing $24a^*Br^-$, $25a^*2Br^-$, $26a^*3Br^-$, TBAB, NaOAc and AgO_2 in MeOH at rt. The sample was taken after 24 hours and diluted with methanol. * = common background contaminant ion; the crude product contains side products and starting materials from the synthesis of $26a^*3Br^-$.

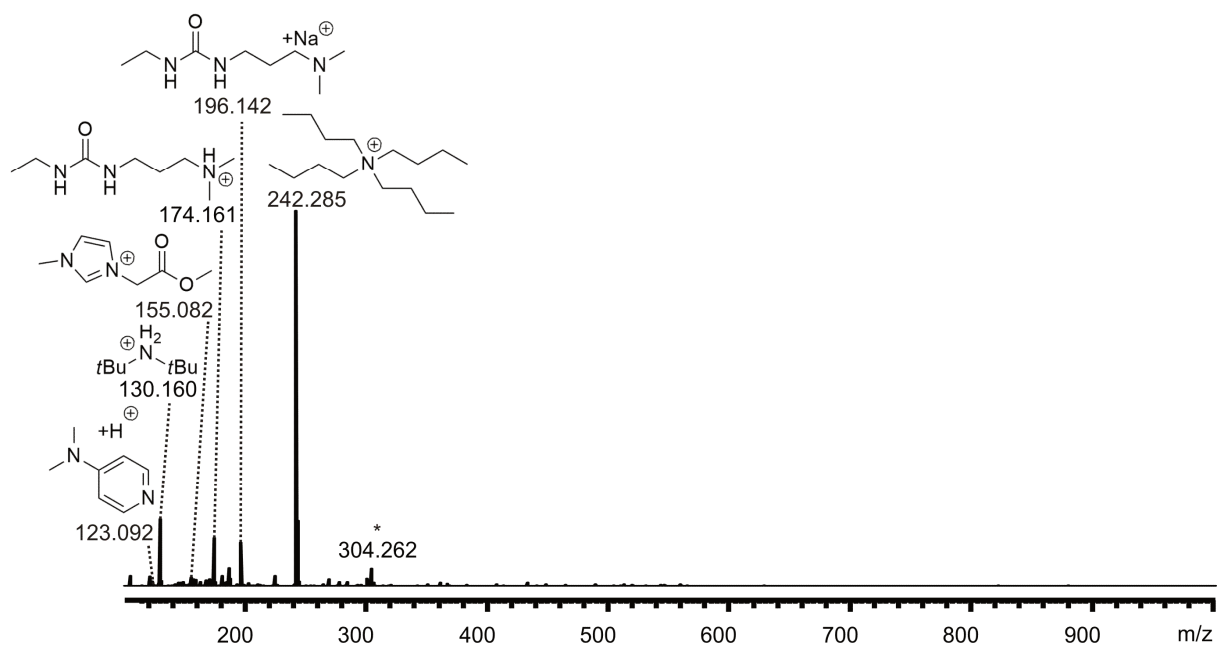


Figure 186: ESI(+)-mass spectrum of a reacting solution containing $24a^*Br^-$, $25a^*2Br^-$, $26a^*3Br^-$, TBAB, NaOAc, AgO_2 and $Au(SMe_2)Cl$ in MeOH at rt. The sample was taken 3 days after the addition of the gold compound and diluted with methanol. * = common background contaminant ions; the crude product contains side products and starting materials from the synthesis of $26a^*3Br^-$.

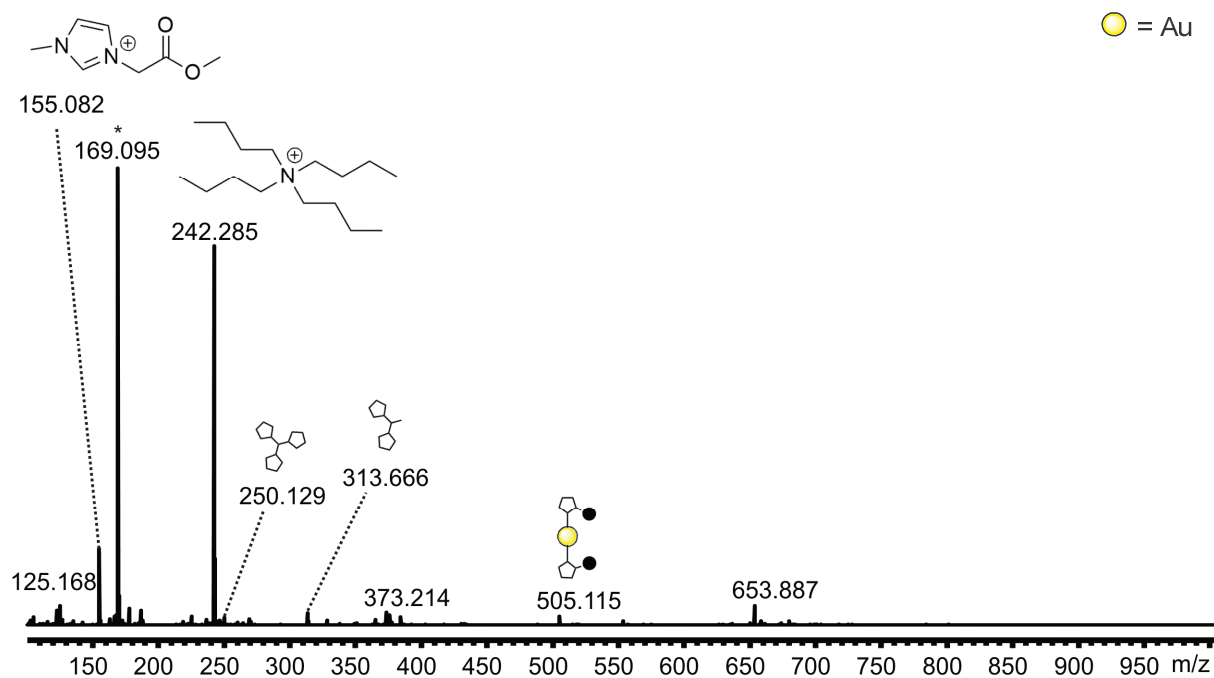


Figure 187: ESI(+)-mass spectrum of the crude product from the reaction of $24s^*3Br^-$, $25s^*3Br^-$, $26s^*Br^-$, TBAB, NaOAc, Ag_2O_2 and $Au(SMe_2)Cl$ in MeOH at rt. The sample was diluted with methanol. * = common background contaminant ions; the crude product contains side products and starting materials from the synthesis of $26a^*3Br^-$.

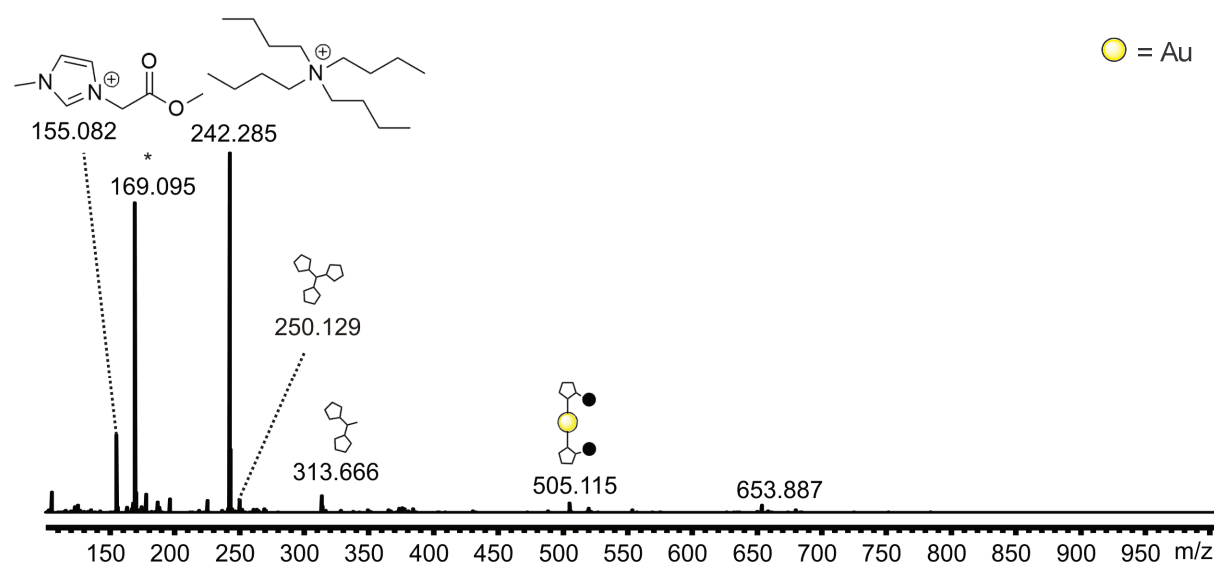


Figure 188: ESI(+)-mass spectrum of the crude product from the reaction of $24s^*3Br^-$, $25s^*3Br^-$, $26s^*Br^-$, TBAB, NaOAc, Ag_2O_2 and $Au(tht)Cl$ in MeOH at rt. The sample was diluted with methanol. * = common background contaminant ions; the crude product contains side products and starting materials from the synthesis of $26a^*3Br^-$.

5 Summarizing conclusion and brief outlook

The first part of the given work presented the investigation of the gold(III)-catalyzed domino cyclization and oxidative coupling reaction, for the synthesis of dicoumarin derivatives, by mass spectrometric means. Electrospray mass spectrometry should give an insight of the reaction mechanism and the transient species, by transferring the molecules to the gas phase. The easy deprotonation of the catalyst and the traceability as $[\text{AuCl}_4]^-$ species seemed promising for the use of this powerful analysis technique. The required substrates were synthesized via Steglich esterification.^[22] Two different derivatives of the substrate (with *tert*-butyl substituent and without additional substituent) were tested in this work. Unfortunately different challenges hindered the measurements and necessitated changes in the technical working routine. First of all the strong corrosivity of the catalyst HAuCl_4 strictly excluded the use of any stainless steel equipment, which normally includes spatula, syringes, the ESI needle and all connectors. All of the metal compounds were replaced by different materials (with PTFE compounds when possible). The ion source was assembled with an inert *fused-silica* capillary. Usually these sprayers are used for capillary electrophoresis mass spectrometry experiments. With these simple exchanging steps the complications provoked by corrosion could be reduced to a minimum. A crucial element for the successful reaction is the solvent DCE. Due to its bad ability to form a stable spray, the investigation required another solvent. However the problem could be sorted out by diluting the reacting mixture with acetonitrile, right before the measurement. This step also prevented the blockage of the capillaries by high concentrated solutions. Even though the catalyst could easily be detected after deprotonation as the negative $[\text{AuCl}_4]^-$ species, the organic compounds needed the addition of sodium or a proton $[\text{M}+\text{H}]^+$ and $[\text{M}+\text{Na}]^+$. Therefore these species could only be followed in the positive ESI modus. This behaviour was a huge drawback for the simultaneous monitoring of all participating species. Hence the ESI modus had to be changed constantly during the measurements. An internal standard was used for the correct normalization of the intensities throughout the monitoring experiments. The identification of all postulated transient intermediates of the reaction could be achieved by mass spectrometric means. Therefore the main goal of the given work was accomplished. All species were detected with negative charge, which was expected due to the nature of the catalyst. The ligand sphere of the gold centre involves only chloride ligands and one respectively two molecules of the substrates (**A**). In summary the species $[\text{AuCl}_2]^-$; $[\text{AuCl}_4]^-$;

$[A+AuCl_4]^- = B/ C+Cl^-$; $[A-H+AuCl_3]^- = D$; $[2A-H+AuCl_3]^- = D+A$; $[2A-2H+AuCl_2]^- = E$, $F =$ coumarin, $G =$ dicoumarin, could be detected (The nomenclature of the species **A**, **B**, **C**, **D**, **E**, **F** and **G** originated from the postulated mechanism and is listed consecutively with the reaction steps). The characterization of the compounds was achieved by their accurate masses and the characteristic isotopic pattern of the chloride ligands. Supporting fragmentations were also performed with CID experiments, to assist the results. The monitoring of the progress from the interesting species represented the next problem of the project. The reaction conditions require high temperatures of 60°C. The turn over is so fast, that it could not be monitored under the ideal reaction conditions. Therefore some parameters had to be adjusted to slow down the reaction. The temperature was set down to room temperature, the oxidant was omitted and on that account stoichiometric or smaller amounts of the catalyst used. With these adjustments the reaction was followed over one hour. The success of the reaction and the rate of monomer and dimer are highly dependent on the concentration of the substrate. Changing the concentration from 50 mmolL⁻¹ to 20 mmolL⁻¹ lengthened the reaction time a few minutes. Varying the amount of the catalyst from 5 mol% - 20 mol% indeed had a bigger impact. The intensities of the product species were higher than the substrate signals after ~5 min (for 20 mol%), while it took almost 30 min for the less concentrated solution (5 mol%). Due to differing ESI response factors the intensities of the signals are not consistent with the real concentrations in solution, but they provide a good reference point.

Dinuclear gold(I) NHC complexes are a fascinating and highly investigated type of compounds for supramolecular aggregation processes. Intra- and intermolecular interactions of the compounds are highly tuneable by even small changes in the NHC complexes. Due to the multitude of possible aggregation it is sometimes like playing around with all the different binding sites to find the right receptor substrate pair. The goal is to get a deeper inside of all these interactions to be able to design an intrinsic host compound for a given guest, without the trial and error method. Therefore we investigated the potential interactions by hydrogen-, ion...ion-, cation...π-, anion...π- and π...π bonding. The intriguing gold complexes used in this work are also able to provide metallophilic interactions. All complexes of the four comparative series were synthesized as bromide and hexafluorophosphate complexes (the primary differences are: imidazolium -/ benzimidazolium moiety; C1-C3 alkylene bridge; methyl- / ethyl wingtip). Some of the

complexes were already synthesized and partly characterized before but all benzimidazolium PF_6^- compounds were herein produced for the first time in our group. Several analytical measurements were performed, starting with NMR spectroscopy. These experiments clearly showed the influence of the counterions to the chemical shifts of the signals. Whereas the differences in the linker length and the aromatic systems are crucial for the interplay of the cations and anions, depending on the NHC moiety, the signals of the wingtip groups do not change with the counterions. Visible downfield shifting of different proton resonances clearly hints the aggregation or rather interaction with the counterions. This phenomenon is strongly affected by the configuration of the complexes. While the aromatic resonances of the imidazolium compounds show a significant shift, the signals of the alkylene bridges go through a bigger change for the benzimidazolium complexes. However, the intensities of the changes are reverse correlating with the alkylene chain length. The compounds with the shortest bridges show the strongest impact. This is attributed to an unhampered and faster dynamic of the longer alkylene chains in solution. Due to the existing cavity in the complexes, the aggregation of small molecules was supposed to take place between the metal centres. This could be achieved by interactions with the gold atoms. However the different aromatic moieties enable various binding sites and therefore lead to different bonding motifs. The counterions and complexes could form aggregates by $\pi \cdots X$, $\text{Au} \cdots X$ and/or $\text{H} \cdots X$ interactions. Hence the differences in the NMR spectra are seen as shifting of some resonances (not only the resonances of the bridge around the cavity).

Even though hydrogen bonds with halides or hexafluorophosphate are unusual, they are possible and could already be demonstrated herein by NMR spectroscopic means. Due to the non coordinating properties of PF_6^- , the aggregation of the better coordinating bromide could be detected by the shifting of the involved proton resonances, as described above. Fortunately those interactions are not limited to the two counterions (PF_6^- and Br^-). The addition of BF_4^- , NO_3^- and OTf^- to solutions of the hexafluorophosphate complex resulted in similar shifting processes, while adding more PF_6^- did not result in any observable alteration. The comparison experiments were mainly performed with the $[\text{Au}_2(\text{bisEt}_2\text{Melm})_2]^{2+}$ complex in acetonitrile. Based on the intensity of the downfield shift, the affinity of the complex to the counterions could be ranked $\text{PF}_6^- < \text{BF}_4^- < \text{OTf}^- \ll \text{NO}_3^- \sim \text{Br}^-$. The rather non coordinating anions PF_6^- and BF_4^- show a similar behaviour. The aggregation of tetrafluoroborate is probably preferred because it is less sterically hindered. The triflate

counterion shows a slightly stronger interaction but is also quite bulky. The interaction with bromide and nitrate are comparable. Triflate and nitrate can be stabilized by several H...O/H...Br bonds. All salts were added as silver- and tetrabutylammonium compounds respectively. The shifting for both additives is comparable. Thus the peculiar interaction of the cations with the complexes was excluded. The coulomb repulsion of three positive charges seems stronger than potential metallophilic Au...Ag interactions. Aggregation processes though are not limited to the cations and anions. Several examples in the literature have documented interactions between the gold complexes and solvent molecules, but not all complexes are soluble in the same solvent. Hence the comparability is not preserved and the experiments presented here are only limited to a few examples, which are able to illustrate the effects. Even though the NMR spectroscopic experiments have demonstrated differing aggregations via hydrogen bonding, they are no proof for aurophilic interactions.

X-ray diffraction experiments should give a better insight to the interactions in solid state. Single crystals suitable for the measurements were obtained for all complexes **1a,b** - **12a,b** and some additional compounds with different counterions ($[\text{Au}_2(\text{bisEt}_2\text{Melm})_2](\text{NO}_3)_2$, $[\text{Au}_2(\text{bisMe}_2\text{PrIm})_2](\text{BF}_4)_2$, $[\text{Au}_2(\text{bisEt}_2\text{MeBlm})_2](\text{PO}_2\text{F}_2)_2$ and $[\text{Au}_2(\text{bisEt}_2\text{EtBlm})_2](\text{PO}_2\text{F}_2)_2$). The geometry of the resulting crystal structures is not only influenced by attractive interactions (hydrogen bonding, Au...Au-, ion...ion-, cation... π - and anion... π interaction as well as π stacking) but also by packing effects. Some compounds, mostly bromide complexes, need additional solvent molecules to form single crystals. This hampers the identification of trends inside the complex series. However, a few intriguing geometries with short aurophilic interactions could be shown. The overall structures include cations which are mostly interacting with other cations via π stacking and the surrounding layers of counterions. They are mainly stabilized by hydrogen bonding to the complexes or solvent molecules. Those H...X interactions could be found with distances of 2.255 – 3.034 Å (H...F distances are shorter than H...Br distances, due to different atomic radii). Some of the counterions are also aggregated via anion... π interactions. Keep in mind, that all small distances could also be forced by packing effects. The configuration of the methylene complexes is mainly U shaped. The flexibility of the cations is limited due to the fixed N-(CH₂)-N angle and the resulting distances of the alkylene bridges. While the imidazolium compounds provide coplanar NHC moieties the benzimidazolium rings are twisted due to steric repulsion. Some

of the C-Au-C axes are slightly bended to each other and therefore allow the formation of short Au...Au bonds, but there is no clear correlation depending on the counterions or side chains. None of the crystal structures investigated in this work contain C-Au-C axis with an unusual small angle. The angle ranges from 169.3 - 179.71° and could therefore be considered as almost linear. The longer ethylene and propylene linkers provide more flexibility of the cations. Hence the geometry could be either folded (flat or twisted) or stretched out. This provides a wider array of possible geometry motifs and resulted in some pretty interesting structures. An outstanding crystal structure was found for the $[\text{Au}_2(\text{bisMe}_2\text{PrIm})_2](\text{BF}_4)_2$ complex. The intramolecular Au...Au distances are only 2.999 Å, which are the shortest aurophilic interactions of all complexes investigated in our group so far. This unique geometry could be achieved due to the flexible propylene bridges. Thereby the C-Au-C axes could be vertical arranged and the NHC moieties are not located one upon the other. This leads to minimal steric repulsion and provides short metal – metal distances. Some exceptional structures contain Au...X distances, which are shorter than the sum of their corresponding van der Waals radii (no real Au-X bonds were found, those would require an oxidation of the metal centres to gold(III) or the substitution of the ligands by the counterions). This hints to rather weak interactions of the counterions with the metal centres in solid state. The interactions in the crystal structures are influenced by several parameters like the configuration and conformation of the compounds, attractive interactions as well as packing effects. The application of solids for the recognition of other compounds is limited (e.g. vapours are possible) but they are still interesting, for instance to create OLEDs or heat sensitive material (provoked by colour changes due to thermochromism^[49a,91]).

The last mentioned property leads to the also executed fascinating UV/Vis and fluorescence measurements of the complexes in solution. For a further insight of the cation...counterion interactions in-depth UV/Vis- and fluorescence spectroscopic experiments in acetonitrile and methanol were performed. All compounds show intense high energy absorption bands which are attributed to metal perturbed π - π^* ligand centred transition processes. While the absorption maxima of the imidazolium complexes **1a,b** - **3a,b** and **7a,b** – **9a,b** are between 255 and 265 nm, the λ_{max} of the corresponding benzimidazole complexes **4a,b** - **6a,b** and **10a,b** – **12a,b** undergo a red shift to 282 - 289 nm. The counterion exchange does not strongly change those absorption spectra. The intensities are differing with the anions but

do not show clear correlations throughout the four series. The excitation at those wavelengths leads to the interesting emission spectra. All propylene and the imidazolium ethylene complexes induce a strong maximum between 350 and 400 nm (λ_{exc} (imidazolium)= 255 nm, λ_{exc} (benzimidazolium)= 289 nm). The emission is caused by the formation of a stable exciplex ($^3[\text{d}\sigma^*\text{p}\sigma]$ excited state). Au...Au interactions in the complexes with long alkylene chains are probably enabled by folded structures. Compounds with the shorter bridges are more rigid and in the case of the benzimidazolium compounds probably also steric hindered. The bended structures could be supported by hydrogen bonding with the counterions. The emission spectra of the methylene compounds are similar to spectra of the ligand precursors. The absence of similar aurophilic interactions is stated to their hindered flexibility. Even though the emission maxima could be observed for both Br^- and PF_6^- complexes, the intensities are increasing after the counterion exchange. This quenching behaviour is attributed to the aggregation of the anion to the cation and the formation of association compounds with other emission properties. This effect with a simultaneous appearance of an aggregated complex could be demonstrated by adding a huge excess of bromide to the solutions. For the given experiments, 300 eq TBAB were added. This led to the quenching of the high energy emission with a concurrent increase of a new maxima at ~ 460 nm for the imidazolium complexes and ~ 540 nm for the benzimidazole complexes. It is worth mentioning that all compounds are showing the emission attributed to the association complex, even when they are not emissive at the higher energy attributed to the uncoordinated compound. Interestingly the increases of the intensities from the emission bands are the strongest for the benzimidazolium methylene complexes.

For a broader insight to the solvent - complex interaction, the same experiments were performed with the benzimidazolium complexes in methanol ($[\text{Au}_2(\text{bisMe}_2\text{PrIm})_2]^{2+}$, $[\text{Au}_2(\text{bisMe}_2\text{PrIm})_2]^{2+}$ and $[\text{Au}_2(\text{bisMe}_2\text{PrIm})_2]^{2+}$). All three complexes were investigated as hexafluorophosphate and bromide compound respectively. The propylene complexes are again the strongest emitters but with less intense maxima and almost not distinguishable curves for the different counterions. This behaviour is attributed to the aggregation of methanol to the complexes in a comparable association complex as seen for bromide. Adding a huge excess of TBAB does again quench the emission and lead to the increase of the low energy maxima. All experiments with the addition of bromide (in acetonitrile and methanol) lead to another emission band at ~ 350 nm. Those are attributed to aurophilic

interactions with varying Au...Au distances. While most compounds have shown these maxima only after the addition of an excess of bromide, the rigid methylene compounds always feature those emission. The propylene and ethylene compounds are more flexible in solution and therefore able to change the bond lengths via folded or stretched conformations. The herein demonstrated photophysical performance could be explained by the formation of aurophilic interactions. The high energy emission is attributed to the the $^3[d\sigma^*p\sigma]$ excited state of a non coordinated free complex and the low energy emission to the association complex with aggregated counterions and/ or coordinated solvent molecules.

A clear correlation of the different counterions and the complex behaviour in solution could be shown. The potential application as optical sensors for small molecules, especially coordinating anions, seems promising. The interactions of the complexes with an other complex molecule, the counterions or the solvent is highly tuneable and in some cases explicit unique for just one compound. We hope, that we provided a better insight of the intriguing aggregation of the counterions to the cations, but there is still a lot room for following investigations with varying complex substitution or other counterions as potential guest molecules.

The dinuclear gold(I) NHC complexes used up till now in this work are providing a rather small cavity. An enlargement of alkylene bridges would provide bigger but pretty dynamic compounds. Tribenzotriquinacene was chosen as a rigid but blarger backbone for a good preorganisation of the host molecule. This bowl shaped compound could provide a capsule like template for cage molecules. Due to the possibility of several substitution motifs of TBTQ, the imidazolium precursors could be planned as tripodal ligands. The addition of NHC moieties allows the synthesis of trinuclear gold complex structures. The third metal centre was inserted for extended aurophilic interactions. The coupling of the imidazolium compounds to the aromatic backbone should be realized over an amide coupling. Therefore the imidazolium compound should bear an acid group and the TBTQ scaffold three amine groups. The corresponding TBTQ derivative was synthesized via a known reaction pathway.^[10] The reaction always yields a *C3* symmetrical product and a *C1* symmetrical compound as side product. Due to the chirality of the compounds they could probably be used for racemic recognition experiments and maybe separate isomers. The imidazolium

moiety was synthesized with 1-methyl imidazole and bromo acetic acid. The following coupling of the amide bonds needed several adjustments of the reaction parameters. The effective combination of EDC, DMAP, DIPEA at 80°C in acetonitrile, yielded a mixture containing the intended tripodal ligand precursor. The influence of the non nucleophilic but strong Huenigs base (DIPEA) and the high temperature were absolute crucial. Usually amide coupling is performed at ambient conditions, due to the temperature sensitivity of amino acids and peptides. However all compounds used here are heat stable. All reaction products contained a combination of compounds with either one or two or even three successful linked imidazolium units (from the *C1* or *C3* symmetric precursors, both were used separately). Despite several purification attempts, the mixture of the three respective TBTQ compounds could not be separated. Hence the reactions to the complexes had to be executed with the impure ligand precursor mixtures. However these crude products were used to construct almost all possible heteroleptic and homoleptic combinations of symmetrical and asymmetrical silver(I) NHC complexes via the silver base route (AgO_2 , tetrabutylammonium bromide as phase transfer catalyst and methanol as solvent), under the exclusion of light. Most importantly the intended trinuclear cage molecule could be detected in the crude product by mass spectrometric means. The reaction parameters were a combination of NaOAc as base, tetrabutylammonium bromide as phase transfer catalyst and methanol as solvent, at room temperature. Transmetalation of these products was achieved with two different gold sources ($\text{Au}(\text{SMe}_2)\text{Cl}$ and $\text{Au}(\text{tth})\text{Cl}$). Both tested compounds were suitable for the intended application with similar turn over. The intriguing trinuclear gold(I) NHC compounds could be detected in the product mixture. Several crystallization attempts were performed, but did not yielded suitable single crystals or at least a clean product. Even though all purification steps were unsuccessful, the present reaction pathway seems really promising. Due to the multiplicity of the products, a library of different metal NHC compounds was achieved. Hence they could also be used for screening experiments in the future, to find the right receptor for a given substrate. Further experiments for recognition applications as luminescence active 3D-metallocavitands are outstanding but planned.

6 Abbreviations

ACN	acetonitrile
calc.	calculated
CID	collision induced dissociation
DCC	<i>N,N'</i> -dicyclohexylcarbodiimide
DCE	1,2-dichloroethane
DCM	dichloromethane
DIPEA	<i>N,N</i> -Diisopropylethylamine
DMAP	4-dimethylaminopyridine
DMF	<i>N,N</i> -dimethylformamide
DMSO	dimethylsulfoxide
EDC	1-ethyl-3-(3-dimethylaminopropyl)carbodiimide
ESI	electrospray ionization
<i>et al.</i>	<i>et alia</i> , and others
exp.	experimental
HOBt	benzotriazol-1-ol
<i>J</i>	coupling constant
LDA	lithium diisopropylamide
MeOH	methanol
MS	mass spectrometry
<i>m/z</i>	mass to charge ratio

NHC	<i>N</i> -heterocyclic carbene
NMR	nuclear magnetic resonance
ORTEP	Oak Ridge Thermal-Ellipsoid Plot
rt	room temperature
TBAB	tetrabutylamino bromide
TBTQ	tribenzotriquinacene
TEA	triethylamine
<i>tert</i> -Bu	<i>tert</i> -butyl
<i>tert</i> -BuOOH	<i>tert</i> -butylhydroperoxide
TFA	trifluoro acetic acid
THF	tetrahydrofuran
UV/Vis	ultraviolet-visible light

7 References

- [1] H.A. Wegner, S. Ahles, M. Neuburger; *Chem. Eur. J.* **2008**, *14*, 11310-11313.
- [2] (a) K. Öfele; *J. Organomet. Chem.* **1968**, *12*, P42-P43; (b) H.W. Wanzlick, Schonher.Hj; *Angew. Chem., Int. Edit.* **1968**, *7*, 141-&; (c) J.C.Y. Lin, R.T.W. Huang, C.S. Lee, A. Bhattacharyya, W.S. Hwang, I.J.B. Lin; *Chem. Rev.* **2009**, *109*, 3561-3598; (d) B. Ranieri, I. Escofet, A.M. Echavarren; *Org. Biomol. Chem.* **2015**, *13*, 7103-7118.
- [3] (a) A.S.K. Hashmi; *Chem. Rev.* **2007**, *107*, 3180-3211; (b) M. Alcarazo, T. Stork, A. Anoop, W. Thiel, A. Fürstner; *Angew. Chem., Int. Edit.* **2010**, *49*, 2542-2546; (c) N. Krause, C. Winter; *Chem. Rev.* **2011**, *111*, 1994-2009; (d) A. Corma, A. Leyva-Perez, M.J. Sabater; *Chem. Rev.* **2011**, *111*, 1657-1712; (e) X.Y. Xu, S.H. Kim, X. Zhang, A.K. Das, H. Hirao, S.H. Hong; *Organometallics* **2013**, *32*, 164-171; (f) D. Gatineau, J.P. Goddard, V. Mouries-Mansuy, L. Fensterbank; *Isr. J. Chem.* **2013**, *53*, 892-900; (g) M. Guitet, P.L. Zhang, F. Marcelo, C. Tugny, J. Jimenez-Barbero, O. Buriez, C. Amatore, V. Mouries-Mansuy, J.P. Goddard, L. Fensterbank, Y.M. Zhang, S. Roland, M. Menand, M. Sollogoub; *Angew. Chem., Int. Edit.* **2013**, *52*, 7213-7218; (h) R. Manzano, F. Rominger, A.S.K. Hashmi; *Organometallics* **2013**, *32*, 2199-2203; (i) R.H. Crabtree; *Coord. Chem. Rev.* **2013**, *257*, 755-766; (j) L.A. Schaper, S.J. Hock, W.A. Herrmann, F.E. Kuhn; *Angew. Chem., Int. Edit.* **2013**, *52*, 270-289; (k) D.A. Rosca, J.A. Wright, M. Bochmann; *Dalton Trans.* **2015**, *44*, 20785-20807; (l) R. Dorel, A.M. Echavarren; *Chem. Rev.* **2015**, *115*, 9028-9072; (m) A.C.H. Jans, A. Gomez-Suarez, S.P. Nolan, J.N.H. Reek; *Chem. Eur. J.* **2016**, *22*, 14836-14839; (n) P. Zargarán, T. Wurm, D. Zahner, J. Schiessl, M. Rudolph, F. Rominger, A.S.K. Hashmi; *Adv. Synth. Catal.* **2018**, *360*, 106-111.
- [4] (a) M. Baron, C. Tubaro, A. Biffis, M. Basato, C. Graiff, A. Poater, L. Cavallo, N. Armadori, G. Accorsi; *Inorg. Chem.* **2012**, *51*, 1778-1784; (b) R. Visbal, M.C. Gimeno; *Chem. Soc. Rev.* **2014**, *43*, 3551-3574; (c) F.-F. Hung, W.-P. To, J.-J. Zhang, C. Ma, W.-Y. Wong, C.-M. Che; *Chem. Eur. J.* **2014**, *20*, 8604-8614; (d) Y. Chen, G. Cheng, K. Li, D.P. Shelar, W. Lu, C.M. Che; *Chem. Sci.* **2014**, *5*, 1348-1353; (e) R. Zhong, A. Pothig, D.C. Mayer, C. Jandl, P.J. Altmann, W.A. Herrmann, F.E. Kuhn; *Organometallics* **2015**, *34*, 2573-2579; (f) S. Kobialka, C. Muller-Tautges, M.T.S. Schmidt, G. Schnakenburg, O. Holloczki, B. Kirchner, M. Engeser; *Inorg. Chem.* **2015**, *54*, 6100-6111; (g) P.F. Ai, A.A. Danopoulos, P. Braunstein; *Inorg. Chem.* **2015**, *54*, 3722-3724; (h) P.J. Altmann, A. Pothig; *J. Am. Chem. Soc.* **2016**, *138*, 13171-13174; (i) M. Monticelli, C. Tubaro, M. Baron, M. Basato, P. Sgarbossa, C. Graiff, G. Accorsi, T.P. Pell, D.J.D. Wilson, P.J. Barnard; *Dalton Trans.* **2016**, *45*, 9540-9552.
- [5] (a) F. Scherbaum, A. Grohmann, B. Huber, C. Kruger, H. Schmidbaur; *Angew. Chem., Int. Ed.* **1988**, *27*, 1544-1546; (b) H. Schmidbaur; *Gold Bull* **2000**, *33*, 3-10; (c) H. Schmidbaur, A. Schier; *Chem. Soc. Rev.* **2008**, *37*, 1931-1951; (d) H. Schmidbaur, A. Schier; *Chem. Soc. Rev.* **2012**, *41*, 370-412.
- [6] S. Kobialka; *doctor thesis*, Rheinische Friedrich-Wilhelms-Universität Bonn, **2014**.

- [7] (a) C. Hemmert, R. Poteau, F.J.B.D. Dominique, P. Ceroni, G. Bergamini, H. Gornitzka; *Eur. J. Inorg. Chem.* **2012**, 3892-3898; (b) S.P. Wei, X.Y. Li, Z. Yang, J.B. Lan, G. Gao, Y. Xue, J.S. You; *Chem. Sci.* **2012**, 3, 359-363; (c) M. Viji, A.K. Nair, P.C. Nandajan, D. Ramaiah; **2014**, 4, 47982-47986; (d) Q. Liu, M. Xie, X.Y. Chang, S. Cao, C. Zou, W.F. Fu, C.M. Che, Y. Chen, W. Lu; *Angew. Chem., Int. Edit.* **2018**, 57, 6279-6283.
- [8] (a) E.P. Kyba, R.C. Helgeson, K. Madan, G.W. Gokel, T.L. Tarnowski, S.S. Moore, D.J. Cram; *J. Am. Chem. Soc.* **1977**, 99, 2564-2571; (b) R.D. Hancock; *J Chem Educ* **1992**, 69, 615-621; (c) G. Ercolani; *J. Am. Chem. Soc.* **2003**, 125, 16097-16103.
- [9] (a) D.J. Cram; *Angew. Chem., Int. Ed.* **1986**, 25, 1039-1057; (b) D.J. Cram, K.M. Doxsee; *J. Org. Chem.* **1986**, 51, 5068-5071; (c) J.W. Steed, J.L. Atwood *Supramolecular chemistry*; 2nd ed.; Wiley: Chichester, UK, p.17 ff., **2009**; (d) J.W. Steed, J.L. Atwood *Supramolecular chemistry*; 2nd ed.; Wiley: Chichester, UK, p.22 ff., **2009**.
- [10] (a) D. Kuck; *Angew. Chem., Int. Ed.* **1984**, 23, 508-509; (b) R.W.S. W. A. Mosher; *J. Org. Chem.* **1971**, 36, 1561-1563; (c) T.L. D. Kuck, A. Schuster; *Chem. Ber.* **1992**, 125, 1449-1460; (d) A.S. D. Kuck, R. A. Krause, J. Tellenbröcker, C. P. Exner, M. Penk, H. Böggw, A. Müller; *Tetrahedron* **2001**, 57, 3587-3613; (e) D.K. J. Tellenbröcker; *Beilstein J. Org. Chem.* **2011**, 7, 329-337; (f) S. Müller, *Master thesis*, Rheinische Friedrich-Wilhelms-Universität Bonn, **2013**; (g) F.R. D. Beaudoin, M. Mastalerz; *Synthesis* **2015**, 47, 3846-3848; (h) S. Götz, *personal correspondence*, Rheinische Friedrich-Wilhelms-Universität Bonn, **2016**.
- [11] (a) N. Marion, S.P. Nolan; *Chem. Soc. Rev.* **2008**, 37, 1776-1782; (b) D. Pflasterer, A.S.K. Hashmi; *Chem. Soc. Rev.* **2016**, 45, 1331-1367; (c) W.W. Zi, F.D. Toste; *Chem. Soc. Rev.* **2016**, 45, 4567-4589.
- [12] (a) A.S.K. Hashmi, M. Rudolph; *Chem. Soc. Rev.* **2008**, 37, 1766-1775; (b) M. Rudolph, A.S.K. Hashmi; *Chem. Soc. Rev.* **2012**, 41, 2448-2462.
- [13] (a) D. Pflasterer, E. Rettenmeier, S. Schneider, E.D. Ruiz, M. Rudolph, A.S.K. Hashmi; *Chem. Eur. J.* **2014**, 20, 6752-6755; (b) D. Pflasterer, S. Schumacher, M. Rudolph, A.S.K. Hashmi; *Chem. Eur. J.* **2015**, 21, 11585-11589.
- [14] X. Yin, M. Mato, A.M. Echavarren; *Angew. Chem., Int. Edit.* **2017**, 56, 14591-14595.
- [15] A. Ahlers, T. de Haro, B. Gabor, A. Fürstner; *Angew. Chem., Int. Edit.* **2016**, 55, 1406-1411.
- [16] (a) A.M. Echavarren, A.S.K. Hashmi, F.D. Toste; *Adv. Synth. Catal.* **2016**, 358, 1347-1347; (b) R.E. Ebule, D. Malhotra, G.B. Hammond, B. Xu; *Adv. Synth. Catal.* **2016**, 358, 1478-1481; (c) D.B. Huple, S. Ghorpade, R.-S. Liu; *Adv. Synth. Catal.* **2016**, 358, 1348-1367; (d) P. Kothandaraman, Y. Zhao, B.R. Lee, C.J. Le Ng, J.Y. Lee, B.J. Ayers, P.W.H. Chan; *Adv. Synth. Catal.* **2016**, 358, 1385-1391; (e) E. Manoni, M. Daka, M.M. Mastandrea, A.D. Nisi, M. Monari, M. Bandini; *Adv. Synth. Catal.* **2016**, 358, 1404-1409; (f) D. Gasperini, L. Maggi, S. Dupuy, R.M.P. Veenboer, D.B. Cordes, A.M.Z. Slawin, S.P. Nolan; *Adv. Synth. Catal.* **2016**, 358, 3857-3862; (g) M.N. Hopkinson, A. Tlahuext-Aca, F. Glorius; *Acc.*

- Chem. Res.* **2016**, *49*, 2261-2272; (h) Z. Zeng, H. Jin, J. Xie, B. Tian, M. Rudolph, F. Rominger, A.S.K. Hashmi; *Org. Lett.* **2017**, *19*, 1020-1023.
- [17] (a) H.A. Wegner, M. Auzias; *Angew. Chem., Int. Edit.* **2011**, *50*, 8236-8247; (b) Z.T. Zheng, Z.X. Wang, Y.L. Wang, L.M. Zhang; *Chem. Soc. Rev.* **2016**, *45*, 4448-4458.
- [18] J. Hiort, K. Maksimenka, M. Reichert, S. Perovic-Ottstadt, W.H. Lin, V. Wray, K. Steube, K. Schaumann, H. Weber, P. Proksch, R. Ebel, W.E.G. Müller, G. Bringmann; *J. Nat. Prod.* **2004**, *67*, 1532-1543.
- [19] M.G. Auzias, M. Neuburger, H.A. Wegner; *Synlett* **2010**, 2443-2448.
- [20] C. Efe, I.N. Lykakis, M. Stratakis; *Chem. Comm.* **2011**, *47*, 803-805.
- [21] D. Tang, Z. Chen, J. Zhang, Y. Tang, Z. Xu; *Organometallics* **2014**, *33*, 6633-6642.
- [22] H.A. Wegner, S. Ahles, M. Neuburger; *Chem. Eur. J.* **2008**, *14*, 11310-11313.
- [23] J.B. Fenn; *Angew. Chem., Int. Edit.* **2003**, *42*, 3871-3894.
- [24] (a) P. Chen; *Angew. Chem.* **2003**, *115*, 2938-2954; (b) L.S. Santos, L. Knaack, J.O. Metzger; *Int. J. Mass Spectrom.* **2005**, *246*, 84-104; (c) M. Eberlin; *Eur. J. Mass Spectrom.* **2007**, *13*, 19-28; (d) D. Schröder; *Acc. Chem. Res.* **2012**, *45*, 1521-1532; (e) L. Jasikova, M. Anania, S. Hybelbauerova, J. Roithova; *J. Am. Chem. Soc.* **2015**, *137*, 13647-13657; (f) K.L. Vikse, J.S. McIndoe; *Pure Appl. Chem.* **2015**, *87*, 361-377; (g) C. Iacobucci, A. Lebon, F. De Angelis, A. Memboeuf; *Chem. Eur. J.* **2016**, *22*, 18690-18694; (h) A. Tsybizova, J. Roithova; *Mass Spectrom. Rev.* **2016**, *35*, 85-110.
- [25] J.H. Gross *Mass Spectrometry. A Textbook*; Springer, **2017**; Vol. 3rd ed.
- [26] (a) L.S. Santos, C.H. Pavam, W.P. Almeida, F. Coelho, M.N. Eberlin; *Angew. Chem., Int. Edit.* **2004**, *43*, 4330-4333; (b) A.A. Sabino, A.H.L. Machado, C.R.D. Correia, M.N. Eberlin; *Angew. Chem., Int. Edit.* **2004**, *43*, 4389-4389; (c) C. Marquez, J.O. Metzger; *Chem. Comm.* **2006**, 1539-1541; (d) C.A. Marquez, F. Fabbretti, J.O. Metzger; *Angew. Chem., Int. Edit.* **2007**, *46*, 6915-6917; (e) H.Y. Wang, J.O. Metzger; *Organometallics* **2008**, *27*, 2761-2766; (f) W. Schrader, P.P. Handayani, J. Zhou, B. List; *Angew. Chem., Int. Edit.* **2009**, *48*, 1463-1466; (g) T.D. Fernandes, B.G. Vaz, M.N. Eberlin, A.J.M. da Silva, P.R.R. Costa; *J. Org. Chem.* **2010**, *75*, 7085-7091; (h) M.W. Alachraf, P.P. Handayani, M.R.M. Huttli, C. Grondal, D. Enders, W. Schrader; *Org. Biomol. Chem.* **2011**, *9*, 1047-1053; (i) L. Jasikova, J. Roithova; *Organometallics* **2013**, *32*, 7025-7033; (j) K.L. Vikse, Z. Ahmadi, J.S. McIndoe; *Coord. Chem. Rev.* **2014**, *279*, 96-114; (k) J. Schulz, E. Shcherbachenko, J. Roithova; *Organometallics* **2015**, *34*, 3979-3987; (l) M.W. Alachraf, R.C. Wende, S.M.M. Schuler, P.R. Schreiner, W. Schrader; *Chem. Eur. J.* **2015**, *21*, 16203-16208; (m) A. Noor, J.W. Li, G.N. Khairallah, Z. Li, H. Ghari, A.J. Canty, A. Ariaifard, P.S. Donnelly, R.A.J. O'Hair; *Chem. Comm.* **2017**, *53*, 3854-3857.
- [27] K.L. Vikse, M.P. Woods, J.S. McIndoe; *Organometallics* **2010**, *29*, 6615-6618.
- [28] (a) S. Meyer, R. Koch, J.O. Metzger; *Angew. Chem.* **2003**, *115*, 4848-4851; (b) S. Furmeier, J.O. Metzger; *J. Am. Chem. Soc.* **2004**, *126*, 14485-14492; (c) R. Beel, S. Kobialka, M.L. Schmidt, M.

- Engeser; *Chem. Comm.* **2011**, *47*, 3293-3295; (d) J.A. Willms, R. Beel, M.L. Schmidt, C. Mundt, M. Engeser; *Beilstein J. Org. Chem.* **2014**, *10*, 2027-2037.
- [29] (a) A.A. Sabino, A.H.L. Machado, C.R.D. Correia, M.N. Eberlin; *Angew. Chem., Int. Edit.* **2004**, *43*, 2514-2518; (b) C.A. Marquez, F. Fabbretti, J.O. Metzger; *Angew. Chem.* **2007**, *119*, 7040-7042.
- [30] R.J. Oeschger, D.H. Ringger, P. Chen; *Organometallics* **2015**, *34*, 3888-3892.
- [31] (a) K.L. Vikse, M.A. Henderson, A.G. Oliver, J.S. McIndoe; *Chem. Comm.* **2010**, *46*, 7412-7414; (b) A. Putau, K. Koszinowski; *Organometallics* **2010**, *29*, 3593-3601; (c) A. Putau, H. Brand, K. Koszinowski; *J. Am. Chem. Soc.* **2012**, *134*, 613-622; (d) T.D. Blumke, T. Klatt, K. Koszinowski, P. Knochel; *Angew. Chem., Int. Edit.* **2012**, *51*, 9926-9930; (e) A. Putau, M. Wilken, K. Koszinowski; *Chem. Eur. J.* **2013**, *19*, 10992-10999.
- [32] M. Kolter, K. Koszinowski; *Chem. Eur. J.* **2016**, *22*, 15744-15750.
- [33] N.B. Cech, C.G. Enke; *Mass Spectrom. Rev.* **2001**, *20*, 362-387.
- [34] (a) J. Roithova, D. Schroder; *Coord. Chem. Rev.* **2009**, *253*, 666-677; (b) J. Roithova, S. Jankova, L. Jasikova, J. Vana, S. Hybelbauerova; *Angew. Chem., Int. Edit.* **2012**, *51*, 8378-8382; (c) J. Roithová, Š. Janková, L. Jašíková, J. Váňa, S. Hybelbauerová; *Angew. Chem.* **2012**, *124*, 8503-8507; (d) L. Batiste, P. Chen; *J. Am. Chem. Soc.* **2014**, *136*, 9296-9307.
- [35] S. Ivanova, V. Pitchon, C. Petit, H. Herschbach, A. Van Dorselaer, E. Leize; *Appl. Catal. a-Gen* **2006**, *298*, 203-210.
- [36] (a) M. Abonnenc, L.A. Qiao, B.H. Liu, H.H. Girault; *Annu. Rev. Anal. Chem.* **2010**, *3*, 231-254; (b) J.Y. Pei, C.C. Hsu, Y.H. Wang, K.F. Yu; *Rsc Adv.* **2017**, *7*, 43540-43545.
- [37] (a) I. Braun, A.M. Asiri, A.S.K. Hashmi; *Acs Catal.* **2013**, *3*, 1902-1907; (b) M.M. Hansmann, M. Rudolph, F. Rominger, A.S.K. Hashmi; *Angew. Chem., Int. Edit.* **2013**, *52*, 2593-2598.
- [38] M.L. Schmidt, M. Engeser; *J. Mass Spectrom.* **2017**, *52*, 367-371.
- [39] A.J. Arduengo, R.L. Harlow, M. Kline; *J. Am. Chem. Soc.* **1991**, *113*, 361-363.
- [40] A. Biffis, M. Baron, C. Tubaro; *Adv. Organomet. Chem.* **2015**, *63*, 203-288.
- [41] (a) L. Mercs, M. Albrecht; *Chem. Soc. Rev.* **2010**, *39*, 1903-1912; (b) M. Bardají; *Inorganics* **2014**, *2*, 433; (c) M.R. Narouz, K.M. Osten, P.J. Unsworth, R.W.Y. Man, K. Salorinne, S. Takano, R. Tomihara, S. Kaappa, S. Malola, C.T. Dinh, J.D. Padmos, K. Ayoo, P.J. Garrett, M. Nambo, J.H. Horton, E.H. Sargent, H. Hakkinen, T. Tsukuda, C.M. Crudden; *Nat. Chem.* **2019**, *11*, 419-425.
- [42] (a) H.G. Raubenheimer, S. Cronje; *Chem. Soc. Rev.* **2008**, *37*, 1998-2011; (b) K.M. Hindi, M.J. Panzner, C.A. Tessier, C.L. Cannon, W.J. Youngs; *Chem. Rev.* **2009**, *109*, 3859-3884; (c) I. Ott; *Coord. Chem. Rev.* **2009**, *253*, 1670-1681; (d) T.T. Zou, C.T. Lum, C.N. Lok, J.J. Zhang, C.M. Che; *Chem. Soc. Rev.* **2015**, *44*, 8786-8801.

- [43] (a) C. Chao, Q. Hua-Yu, L. Ai-Ling, C. Dan, T. Gu-Ping, C. Wan-Zhi; *Chinese J. Inorg. Chem.*, **2011**, *27*, 1423-1430; (b) R. Visbal, V. Fernandez-Moreira, I. Marzo, A. Laguna, M.C. Gimeno; *Dalton Trans.* **2016**, *45*, 15026-15033.
- [44] (a) L.E. Wedlock, P.J. Barnard, A. Filipovska, B.W. Skelton, S.J. Berners-Price, M.V. Baker; *Dalton Trans.* **2016**, *45*, 12221-12236; (b) C. Hemmert, H. Gornitzka; *Dalton Trans.* **2016**, *45*, 440-447.
- [45] (a) P.J. Barnard, M.V. Baker, S.J. Berners-Price, D.A. Day; *J. Inorg. Biochem.* **2004**, *98*, 1642-1647; (b) M.V. Baker, P.J. Barnard, S.J. Berners-Price, S.K. Brayshaw, J.L. Hickey, B.W. Skelton, A.H. White; *Dalton Trans.* **2006**, 3708-3715; (c) J. Lemke, A. Pinto, P. Niehoff, V. Vasylyeva, N. Metzler-Nolte; *Dalton Trans.* **2009**, 7063-7070.
- [46] (a) H.M.J. Wang, C.Y.L. Chen, I.J.B. Lin; *Organometallics* **1999**, *18*, 1216-1223; (b) P.J. Barnard, M.V. Baker, S.J. Berners-Price, B.W. Skelton, A.H. White; *Dalton Trans.* **2004**, 1038-1047; (c) P.J. Barnard, L.E. Wedlock, M.V. Baker, S.J. Berners-Price, D.A. Joyce, B.W. Skelton, J.H. Steer; *Angew. Chem., Int. Edit.* **2006**, *45*, 5966-5970; (d) V.W.W. Yam, E.C.C. Cheng; *Top. Curr. Chem.* **2007**, *281*, 269-309; (e) A. Gomez-Suarez, D.J. Nelson, D.G. Thompson, D.B. Cordes, D. Graham, A.M.Z. Slawin, S.P. Nolan; *Beilstein J. Org. Chem.* **2013**, *9*, 2216-2223; (f) R. Visbal, I. Ospino, J.M. Lopez-de-Luzuriaga, A. Laguna, M.C. Gimeno; *J. Am. Chem. Soc.* **2013**, *135*, 4712-4715; (g) N. Sinha, L. Stegemann, T.T.Y. Tan, N.L. Doltsinis, C.A. Strassert, F.E. Hahn; *Angew. Chem., Int. Ed.* **2017**, *56*, 2785-2789.
- [47] (a) M.A. Mansour, W.B. Connick, R.J. Lachicotte, H.J. Gysling, R. Eisenberg; *J. Am. Chem. Soc.* **1998**, *120*, 1329-1330; (b) X.M. He, V.W.W. Yam; *Coord. Chem. Rev.* **2011**, *255*, 2111-2123; (c) X. Zhang, B. Li, Z.H. Chen, Z.N. Chen; *J. Mater. Chem.* **2012**, *22*, 11427-11441; (d) O.S. Wenger; *Chem. Rev.* **2013**, *113*, 3686-3733.
- [48] (a) S. Han, Y.Y. Yoon, O.S. Jung, Y.A. Lee; *Chem. Comm.* **2011**, *47*, 10689-10691; (b) C.X. Lin, X.F. Kong, Q.S. Li, Z.Z. Zhang, Y.F. Yuan, F.B. Xu; **2013**, *15*, 6948-6962; (c) Q.X. Liu, D.C. Wei, D.X. Zhao, X.F. Sun, Z.X. Zhao, J. Yan; *New J. Chem.* **2017**, *41*, 4843-4852; (d) Q.X. Liu, X.F. Sun, D.X. Zhao, Z.X. Zhao, R. Liu, S.Z. Lv; *Sens. Actuator B Chem.* **2017**, *249*, 203-209.
- [49] (a) M. Kriechbaum, J. Holbling, H.G. Stammer, M. List, R.J.F. Berger, U. Monkowius; *Organometallics* **2013**, *32*, 2876-2884; (b) Q.Q. Teng, H.V. Huynh; *Chem. Comm.* **2015**, *51*, 1248-1251; (c) Q.X. Liu, J.R. Chen, X.F. Sun, X.J. Zhao, Z.X. Zhao, K.Q. Cai; *Rsc Adv.* **2016**, *6*, 12256-12262.
- [50] (a) C.E. Strasser, V.J. Catalano; *J. Am. Chem. Soc.* **2010**, *132*, 10009-10011; (b) K. Chen, M.M. Nenzel, T.M. Brown, V.J. Catalano; *Inorg. Chem.* **2015**, *54*, 6900-6909.
- [51] N. Sinha, F.E. Hahn; *Acc. Chem. Res.* **2017**, *50*, 2167-2184.
- [52] (a) N. Sinha, F. Roelfes, A. Hepp, C. Mejuto, E. Peris, F.E. Hahn; *Organometallics* **2014**, *33*, 6898-6904; (b) C. Mejuto, G. Guisado-Barrios, D. Gusev, E. Peris; *Chem. Comm.* **2015**, *51*, 13914-13917.

- [53] (a) C.S.T. Brinke, T. Pape, F.E. Hahn; *Dalton Trans.* **2013**, *42*, 7330-7337; (b) P.J. Altmann, D.T. Weiss, C. Jandl, F.E. Kuhn; *Chem. Asian J.* **2016**, *11*, 1597-1605.
- [54] V. Camara, N. Masciocchi, J. Gil-Rubio, J. Vicente; *Chem. Eur. J.* **2014**, *20*, 1389-1402.
- [55] (a) J. Gil-Rubio, V. Camara, D. Bautista, J. Vicente; *Organometallics* **2012**, *31*, 5414-5426; (b) A. Poethig, T. Strassner; *Organometallics* **2012**, *31*, 3431-3434; (c) J. Vaughan, D.J. Carter, A.L. Rohl, M.I. Ogden, B.W. Skelton, P.V. Simpson, D.H. Brown; *Dalton Trans.* **2016**, *45*, 1484-1495.
- [56] (a) Y. Hou, L.N. Zakharov, M. Nyman; *J. Am. Chem. Soc.* **2013**, *135*, 16651-16657; (b) O. Sadeghi, L.N. Zakharov, M. Nyman; *Science* **2015**, *347*, 1359-1362.
- [57] (a) V.J. Catalano, M.A. Malwitz, A.O. Etogo; *Inorg. Chem.* **2004**, *43*, 5714-5724; (b) M. Tominaga, T. Kawaguchi, K. Ohara, K. Yamaguchi, H. Masu, I. Azumaya; *CrystEngComm* **2016**, *18*, 266-273; (c) C.C. Chou, C.C. Yang, H.C. Chang, W.Z. Lee, T.S. Kuo; *New J. Chem.* **2016**, *40*, 1944-1947; (d) J. Gil-Rubio, J. Vicente; *Chem. Eur. J.* **2018**, *24*, 32-46.
- [58] (a) C.E. Strasser, L. Dobrzanska, H. Schmidbaur, S. Cronje, H.G. Raubenheimer; *J. Mol. Struct.* **2010**, *977*, 214-219; (b) H. Schmidbaur, H.G. Raubenheimer, L. Dobrzanska; *Chem. Soc. Rev.* **2014**, *43*, 345-380; (c) H. Schmidbaur, H.G. Raubenheimer; *Angew. Chem., Int. Edit.* **2020**.
- [59] V.W.W. Yam, V.K.M. Au, S.Y.L. Leung; *Chem. Rev.* **2015**, *115*, 7589-7728.
- [60] B. Pinter, L. Broeckaert, J. Turek, A. Růžička, F. De Proft; *Chem. Eur. J.* **2014**, *20*, 734-744.
- [61] (a) C. Tubaro, M. Baron, M. Costante, M. Basato, A. Biffis, A. Gennaro, A.A. Isse, C. Graiff, G. Accorsi; *Dalton Trans.* **2013**, *42*, 10952-10963; (b) A. Sathyanarayana, S. Nakamura, K. Hisano, O. Tsutsumi, K. Srinivas, G. Prabusankar; *Sci. China Chem.* **2018**, *61*, 957-965.
- [62] (a) R. Frankel, J. Kniczek, W. Ponikwar, H. Noth, K. Polborn, W.P. Fehlhammer; *Inorg. Chim. Acta* **2001**, *312*, 23-39; (b) J.W. Wang, H.B. Song, Q.S. Li, F.B. Xu, Z.Z. Zhang; *Inorg. Chim. Acta* **2005**, *358*, 3653-3658; (c) F.E. Hahn, C. Radloff, T. Pape, A. Hepp; *Chem. Eur. J.* **2008**, *14*, 10900-10904; (d) G. Papini, G. Bandoli, A. Dolmella, G.G. Lobbia, M. Pellei, C. Santini; *Inorg. Chem. Comm.* **2008**, *11*, 1103-1106; (e) A. Liu, X. Zhang, W. Chen, H. Qiu; *Inorg. Chem. Comm.* **2008**, *11*, 1128-1131; (f) F.J.B.D. Dominique, H. Gornitzka, A. Sournia-Saquet, C. Hemmert; *Dalton Trans.* **2009**, 340-352; (g) C. Carcedo, J.C. Knight, S.J.A. Pope, I.A. Fallis, A. Dervisi; *Organometallics* **2011**, *30*, 2553-2562; (h) M. Baron, C. Tubaro, M. Basato, A. Biffis, M.M. Natile, C. Graiff; *Organometallics* **2011**, *30*, 4607-4615; (i) A. Rit, T. Pape, A. Hepp, F.E. Hahn; *Organometallics* **2011**, *30*, 334-347; (j) J. Cure, R. Poteau, I.C. Gerber, H. Gornitzka, C. Hemmert; *Organometallics* **2012**, *31*, 619-626; (k) M. Baron, C. Tubaro, M. Basato, A. Biffis, C. Graiff; *J. Organomet. Chem.* **2012**, *714*, 41-46; (l) V. Gierz, A. Seybold, C. Maichle-Mossmer, K.W. Tornroos, M.T. Speidel, B. Speiser, K. Eichele, D. Kunz; *Organometallics* **2012**, *31*, 7893-7901; (m) C. Hemmert, R. Poteau, M. Laurent, H. Gornitzka; *J. Organomet. Chem.* **2013**, *745*, 242-250; (n) J. Gil-Rubio, V. Camara, D. Bautista, J. Vicente; *Inorg. Chem.* **2013**, *52*, 4071-4083; (o) A. Biffis, M. Cipani, C. Tubaro, M. Basato, M. Costante, E. Bressan, A. Venzo, C. Graiff; *New J. Chem.*

- 2013**, 37, 4176-4184; (p) Y.F. Han, G.X. Jin, F.E. Hahn; *J. Am. Chem. Soc.* **2013**, 135, 9263-9266; (q) S. Canteri, M. Baron, C. Tubaro, A. Biffis, C. Graiff; *Z. Anorg. Allg. Chem.* **2015**, 641, 2272-2276; (r) T. Simler, P. Braunstein, A.A. Danopoulos; *Dalton Trans.* **2016**, 45, 5122-5139; (s) T.P. Pell, D.J.D. Wilson, B.W. Skelton, J.L. Dutton, P.J. Barnard; *Inorg. Chem.* **2016**, 55, 6882-6891.
- [63] (a) O. Kuhl; *Chem. Soc. Rev.* **2007**, 36, 592-607; (b) T. Diehl, M.T.S. Krause, S. Ueberlein, S. Becker, A. Trommer, G. Schnakenburg, M. Engeser; *Dalton Trans.* **2017**, 46, 2988-2997.
- [64] (a) L. Guo, X.Z. Song, C.X. Lin, Q.S. Li, C. Liu, W.H. Wang, F.B. Xu; *Polyhedron* **2015**, 85, 732-739; (b) T. Wagner, A. Pothig, H.M.S. Augenstein, T.D. Schmidt, M. Kaposi, E. Herdtweck, W. Brutting, W.A. Herrmann, F.E. Kuhn; *Organometallics* **2015**, 34, 1522-1529.
- [65] (a) C.K. Lee, C.S. Vasam, T.W. Huang, H.M.J. Wang, R.Y. Yang, C.S. Lee, I.J.B. Lin; *Organometallics* **2006**, 25, 3768-3775; (b) B. Ballarin, L. Busetto, M.C. Cassani, C. Femoni, A.M. Ferrari, I. Miletto, G. Caputo; *Dalton Trans.* **2012**, 41, 2445-2455; (c) A.M. Ortiz, P. Gomez-Sal, J.C. Flores, E. De Jesus; *Organometallics* **2014**, 33, 600-603; (d) S.R. Patrick, A. Collado, S. Meiries, A.M.Z. Slawin, S.P. Nolan; *J. Organomet. Chem.* **2015**, 775, 152-154; (e) P.F. Ai, C. Gourlaouen, A.A. Danopoulos, P. Braunstein; *Inorg. Chem.* **2016**, 55, 1219-1229.
- [66] B.N. Ahamed, R. Dutta, P. Ghosh; *Inorg. Chem.* **2013**, 52, 4269-4276.
- [67] R. Kishore, S.K. Das; *J. Mol. Struct.* **2013**, 1053, 38-47.
- [68] (a) D. Rios, D.M. Pham, J.C. Fettingner, M.M. Olmstead, A.L. Balch; *Inorg. Chem.* **2008**, 47, 3442-3451; (b) M. Saitoh, A.L. Balch, J. Yuasa, T. Kawai; *Inorg. Chem.* **2010**, 49, 7129-7134.
- [69] (a) L. Biasiolo, M. Trinchillo, P. Belanzoni, L. Belpassi, V. Busico, G. Ciancaleoni, A. D'Amora, A. Macchioni, F. Tarantelli, D. Zuccaccia; *Chem. Eur. J.* **2014**, 20, 14594-14598; (b) G. Ciancaleoni, L. Belpassi, D. Zuccaccia, F. Tarantelli, P. Belanzoni; *ACS Catal.* **2015**, 5, 803-814.
- [70] (a) F. Mendizabal, P. Pyykko; *Phys. Chem. Chem. Phys.* **2004**, 6, 900-905; (b) J. Muniz, C. Wang, P. Pyykko; *Chem. Eur. J.* **2011**, 17, 368-377; (c) J. Ruiz, L. Garcia, D. Sol, M. Vivanco; *Angew. Chem., Int. Edit.* **2016**, 55, 8386-8390.
- [71] A. Velle, A. Cebollada, M. Iglesias, P.J.S. Miguel; *Inorg. Chem.* **2014**, 53, 10654-10659.
- [72] A.A. Penney, V.V. Sizov, E.V. Grachova, D.V. Krupenya, V.V. Gurzhiy, G.L. Starova, S.P. Tunik; *Inorg. Chem.* **2016**, 55, 4720-4732.
- [73] L.E. Wedlock, J.B. Aitken, S.J. Berners-Price, P.J. Barnard; *Dalton Trans.* **2013**, 42, 1259-1266.
- [74] M. Baron, A. Dall'Anese, C. Tubaro, L. Orian, V. Di Marco, S. Bogialli, C. Graiff, M. Basato; *Dalton Trans.* **2018**, 47, 935-945.
- [75] H.G. Raubenheimer, P.J. Olivier, L. Lindeque, M. Desmet, J. Hrusak, G.J. Kruger; *J. Organomet. Chem.* **1997**, 544, 91-100.
- [76] T. Baron, A. Bencsik, S. Nicot, E. Morignat, J. Verchere, L. Lakhdar, S. Legastelois, A.L. Mougnot; *Prion* **2012**, 6, 21-21.

- [77] C. Biz, S. Ibáñez, M. Poyatos, D. Gusev, E. Peris; *Chem. Eur. J.* **2017**, *23*, 14439-14444.
- [78] M. Osawa, H. Yamayoshi, M. Hoshino, Y. Tanaka, M. Akita; *Dalton Trans.* **2019**, *48*, 9094-9103.
- [79] (a) R. Jothibas, H.V. Huynh, L.L. Koh; *J. Organomet. Chem.* **2008**, *693*, 374-380; (b) H.V. Huynh, S. Guo, W. Wu; *Organometallics* **2013**, *32*, 4591-4600.
- [80] I.J.B. Lin, C.S. Vasam; *Can. J. Chem.* **2005**, *83*, 812-825.
- [81] K. Nomiya, S. Morozumi, Y. Yanagawa, M. Hasegawa, K. Kurose, K. Taguchi, R. Sakamoto, K. Mihara, N.C. Kasuga; *Inorg. Chem.* **2018**, *57*, 11322-11332.
- [82] A. Bondi; *Am. J. Phys. Chem.* **1964**, *68*, 441.
- [83] S.S. Batsanov; *Inorg. Mater.* **2001**, *37*, 871-885.
- [84] (a) S.V. Lindeman, J.K. Kochi; *Cryst. Growth Des.* **2004**, *4*, 563-571; (b) K. Chellappan, N.J. Singh, I.C. Hwang, J.W. Lee, K.S. Kim; *Angew. Chem., Int. Edit.* **2005**, *44*, 2899-2903; (c) W.M. Reichert, J.D. Holbrey, R.P. Swatloski, K.E. Gutowski, A.E. Visser, M. Nieuwenhuyzen, K.R. Seddon, R.D. Rogers; *Cryst. Growth Des.* **2007**, *7*, 1106-1114; (d) C.A. Hollis, L.R. Hanton, J.C. Morris, C.J. Sumby; *Cryst. Growth Des.* **2009**, *9*, 2911-2916; (e) K.K. Pandey, R. Vishwakarma, P.K. Bariya; *J. Organomet. Chem.* **2015**, *795*, 34-39.
- [85] J.W. Steed, J.L. Atwood *Supramolecular chemistry*; 2nd ed.; Wiley: Chichester, UK, p.28 ff., **2009**.
- [86] M. Baron, C. Tubaro, M. Basato, A.A. Isse, A. Gennaro, L. Cavallo, C. Graiff, A. Dolmella, L. Falivene, L. Caporaso; *Chem. Eur. J.* **2016**, *22*, 10211-10224.
- [87] (a) R. Fernandezgalan, B.R. Manzano, A. Otero, M. Lanfranchi, M.A. Pellinghelli; *Inorg. Chem.* **1994**, *33*, 2309-2312; (b) S. Orbisaglia, B. Jacques, P. Braunstein, D. Hueber, P. Pale, A. Blanc, P. de Fremont; *Organometallics* **2013**, *32*, 4153-4164.
- [88] (a) K. Matsumoto, R. Hagiwara; *Inorg. Chem.* **2009**, *48*, 7350-7358; (b) M.G. Freire, C.M.S.S. Neves, I.M. Marrucho, J.A.P. Coutinho, A.M. Fernandes; *J. Phys. Chem. A* **2010**, *114*, 3744-3749.
- [89] H.V. Huynh, S. Guo, W.Q. Wu; *Organometallics* **2013**, *32*, 4591-4600.
- [90] (a) H.R.C. Jaw, M.M. Savas, R.D. Rogers, W.R. Mason; *Inorg. Chem.* **1989**, *28*, 1028-1037; (b) W.-F. Fu, K.-C. Chan, V.M. Miskowski, C.-M. Che; *Angew. Chem., Int. Ed.* **1999**, *38*, 2783-2785; (c) K.H. Leung, D.L. Phillips, M.-C. Tse, C.-M. Che, V.M. Miskowski; *J. Am. Chem. Soc.* **1999**, *121*, 4799-4803; (d) H.-X. Zhang, C.-M. Che; *Chem. Eur. J.* **2001**, *7*, 4887-4893; (e) W.F. Fu, K.C. Chan, K.K. Cheung, C.M. Che; *Chem. Eur. J.* **2001**, *7*, 4656-4664.
- [91] K. Chen, V.J. Catalano; *Eur. J. Inorg. Chem.* **2015**, 5254-5261.
- [92] (a) L. Suber, I. Sondi, E. Matijevic, D.V. Goia; *J. Colloid Interf. Sci.* **2005**, *288*, 489-495; (b) S. Papp, R. Patakfalvi, I. Dekany; *Croat. Chem. Acta* **2007**, *80*, 493-502; (c) R.M. El-Shishtawy, A.M. Asiri, M.M. Al-Otaibi; *Spectrochim Acta A* **2011**, *79*, 1505-1510; (d) L. Farzampour, M. Amjadi; *J. Lumin.* **2014**, *155*, 226-230.
- [93] H.E. Gottlieb, V. Kotlyar, A. Nudelman; *J. Org. Chem.* **1997**, *62*, 7512-7515.

- [94] R.H. Blessing; *Acta Cryst. A* **1995**, *51*, 33-38.
- [95] G.M. Sheldrick *SHELXS97 and SHELXL97*; University of Göttingen, Germany, 1997.
- [96] O.V. Dolomanov, L.J. Bourhis, R.J. Gildea, J.A.K. Howard, H. Puschmann; *J. Appl. Crystallogr.* **2009**, *42*, 339-341.
- [97] (a) Z. Shi, R.P. Thummel; *J. Org. Chem.* **1995**, *60*, 5935-5945; (b) K. Ito, N. Nishina, H. Ohno; *Electrochim. Acta* **2000**, *45*, 1295-1298; (c) K. Okuyama, J. Sugiyama, R. Nagahata, M. Asai, M. Ueda, K. Takeuchi; *J. Mol. Catal. Chem.* **2003**, *203*, 21-27; (d) X.M. Wu, Q.X. Liu, X.G. Wang, H.B. Song, Z.Y. Zheng; *Acta Cryst. E* **2007**, *63*, O4263-U2866; (e) Y. Watanabe, K. Yamashita, J. Kimura, H. Satoh, T. Urushida, H. Hayashi, T. Iwamoto; *J. Pharmacol. Sci.* **2008**, *106*, 265-265; (f) K. Iwamoto, H. Kimura, M. Oike, M. Sato; *Org. Biomol. Chem.* **2008**, *6*, 912-915; (g) J. Berding, M. Lutz, A.L. Spek, E. Bouwman; *Organometallics* **2009**, *28*, 1845-1854; (h) Q.X. Liu, M.C. Shi, Z.Q. Wang, S.W. Liu, S.S. Ge, Y. Zang, X.G. Wang, J.H. Guo; *Polyhedron* **2010**, *29*, 2121-2126; (i) S.K.U. Riederer, P. Gigler, M.P. Hogerl, E. Herdtweck, B. Bechlars, W.A. Herrmann, F.E. Kuhn; *Organometallics* **2010**, *29*, 5681-5692; (j) R. Kishore, S.K. Das; *Cryst. Growth Des.* **2012**, *12*, 3684-3699.
- [98] J.W. Steed, J.L. Atwood *Supramolecular chemistry*; 2nd ed.; Wiley: Chichester, UK, p. 27 ff., **2009**.
- [99] M. Krause, *Master Thesis*, Rheinische Friedrich-Wilhelms-Universität Bonn, **2014**.
- [100] (a) C.D. Abernethy, G.M. Codd, M.D. Spicer, M.K. Taylor; *J. Am. Chem. Soc.* **2003**, *125*, 1128-1129; (b) M. Engeser, D. Schroder, H. Schwarz; *Chem. Eur. J.* **2005**, *11*, 5975-5987; (c) H.C. Lin, P.W. de Oliveira, V. Huch, M. Veith; *Chem. Mater* **2010**, *22*, 6518-6523; (d) K. Fukudome, N. Ikenaga, T. Miyake, T. Suzuki; *Catal. Sci. Technol.* **2011**, *1*, 987-998; (e) A. El-Batta, A.W. Waltman, R.H. Grubbs; *J. Organomet. Chem.* **2011**, *696*, 2477-2481; (f) B.L. Tran, B. Pinter, A.J. Nichols, F.T. Konopka, R. Thompson, C.H. Chen, J. Krzystek, A. Ozarowski, J. Telser, M.H. Baik, K. Meyer, D.J. Mindiola; *J. Am. Chem. Soc.* **2012**, *134*, 13035-13045; (g) G.M. Miyake, M.N. Akhtar, A. Fazal, E.A. Jaseer, C.S. Daeffler, R.H. Grubbs; *J. Organomet. Chem.* **2013**, *728*, 1-5; (h) M. Erben, J. Merna, O. Hylsky, J. Kredatusova, A. Lycka, L. Dostal, Z. Padelkova, M. Novotny; *J. Organomet. Chem.* **2013**, *725*, 5-10; (i) J.F. Wang, W.H. Fang, D.S. Li, L. Zhang, J. Zhang; *Inorg. Chem.* **2017**, *56*, 2367-2370.
- [101] X.F. Jiang, F.K.W. Hau, Q.F. Sun, S.Y. Yu, V.W.W. Yam; *J. Am. Chem. Soc.* **2014**, *136*, 10921-10929.
- [102] (a) Q.-X. Liu, Z.-Q. Yao, X.-J. Zhao, Z.-X. Zhao, X.-G. Wang; *Organometallics* **2013**, *32*, 3493-3501; (b) F.K.W. Hau, K.L. Cheung, N. Zhu, V.W.W. Yam; *Org. Chem. Front.* **2019**, *6*, 1205-1213.
- [103] N.S. Venkataramanan, A. Suvitha; *J. Incl. Phenom. Macro.* **2017**, *88*, 53-67.
- [104] U. Kernbach, M. Ramm, P. Luger, W.P. Fehlhammer; *Angew. Chem., Int. Ed. in English* **1996**, *35*, 310-312.
- [105] A. Jacobi, G. Huttner, U. Winterhalter, S. Cunsakis; *Eur. J. Inorg. Chem.* **1998**, *1998*, 675-692.
- [106] X. Hu, K. Meyer; *J. Organomet. Chem.* **2005**, *690*, 5474-5484.

- [107] (a) H.V.R. Dias, W. Jin; *Tetrahedron Lett* **1994**, *35*, 1365-1366; (b) M. Tominaga, T. Kawaguchi, K. Ohara, K. Yamaguchi, H. Masu, I. Azumaya; *CrystEngComm* **2016**, *18*, 266-273.
- [108] (a) X.L. Hu, Y.J. Tang, P. Gantzel, K. Meyer; *Organometallics* **2003**, *22*, 612-614; (b) X.L. Hu, I. Castro-Rodriguez, K. Olsen, K. Meyer; *Organometallics* **2004**, *23*, 755-764.
- [109] E.K. Bullough, C.A. Kilner, M.A. Little, C.E. Willans; *Org. Biomol. Chem.* **2012**, *10*, 2824-2829.
- [110] (a) Y. Chun, N.J. Singh, I.C. Hwang, J.W. Lee, S.U. Yu, K.S. Kim; *Nat. Commun.* **2013**, *4*; (b) P.J. Altmann, A. Pothig; *Chem. Comm.* **2016**, *52*, 9089-9092.
- [111] D. Kuck, T. Lindenthal, A. Schuster; *Chemische Berichte* **1992**, *125*, 1449-1460.
- [112] (a) T. Diehl, *Diploma Thesis*, Rheinische Friedrich-Wilhelms-Universität Bonn, **2013**; (b) B. Staacke, *Diploma thesis*, Rheinische Friedrich-Wilhelms-Universität Bonn, **2013**; (c) M. Fetzer *Bachelor thesis*, Rheinische Friedrich-Wilhelms-Universität Bonn, **2013**; (d) S. Überlein, *Bachelor Thesis*, Rheinische Friedrich-Wilhelms-Universität Bonn, **2013**.
- [113] C. Segarra, J. Linke, E. Mas-Marza, D. Kuck, E. Peris; *Chem. Comm.* **2013**, *49*, 10572-10574.
- [114] M. Poyatos, J.A. Mata, E. Peris; *Chem. Rev.* **2009**, *109*, 3677-3707.
- [115] (a) R.A. Bartsch, S.V. Dzyuba; *Am. Chem. Soc.* **2003**, *856*, 289-299; (b) A. Singh, T. Raj, N. Singh; *Catal. Lett.* **2015**, *145*, 1606-1611.
- [116] (a) N. Kuhn, A. Abu-Rayyan, K. Eichele, S. Schwarz, M. Steimann; *Inorg. Chim. Acta* **2004**, *357*, 1799-1804; (b) B. Ballarin, L. Busetto, M.C. Cassani, C. Femoni; *Inorg. Chim. Acta* **2010**, *363*, 2055-2064.
- [117] (a) C.K. Narang, V. Kachhawaha, N.K. Mathur; *React. Polym.* **1988**, *8*, 189-192; (b) B. Zacharie, G. Sauve, C. Penney; *Tetrahedron* **1993**, *49*, 10489-10500; (c) C.A.G.N. Montalbetti, V. Falque; *Tetrahedron* **2005**, *61*, 10827-10852; (d) J. Charton, S. Girault-Mizzi, M.A. Debreu-Fontaine, F. Foufelle, I. Hainault, J.G. Bizot-Espiard, D.H. Caignard, C. Sergheraert; *Bioorg. Med. Chem.* **2006**, *14*, 4490-4518; (e) P. Conti, L. Tamborini, A. Pinto, L. Sola, R. Ettari, C. Mercurio, C. De Micheli; *Eur. J. Med. Chem.* **2010**, *45*, 4331-4338; (f) G. Brahmachari, S. Laskar, S. Sarkar; *J. Chem. Res.* **2010**, 288-295; (g) S.M. Smith, G.L. Hoang, R. Pal, M.O.B. Khaled, L.S.W. Pelter, X.C. Zeng, J.M. Takacs; *Chem. Comm.* **2012**, *48*, 12180-12182; (h) T. Suzuki, Y. Kasuya, Y. Itoh, Y. Ota, P. Zhan, K. Asamitsu, H. Nakagawa, T. Okamoto, N. Miyata; *Plos One* **2013**, *8*, e68669; (i) Y. Tang, M.C. Lv, X.F. Liu, H.J. Feng, L.W. Liu; *Org. Lett.* **2013**, *15*, 1382-1385; (j) M.D.M. Traore, V. Zwick, C.A. Simoes-Pires, A. Nurisso, M. Issa, M. Cuendet, M. Maynadier, S. Wein, H. Vial, H. Jamet, Y.S. Wong; *Acs Omega* **2017**, *2*, 1550-1562.
- [118] C.Y. Chan, P.A. Pellegrini, I. Greguric, P.J. Barnard; *Inorg. Chem.* **2014**, *53*, 10862-10873.
- [119] (a) J.L. Moore, S.M. Taylor, V.A. Soloshonok; *Arkivoc* **2005**, 287-292; (b) J. Charton, S. Girault-Mizzi, C. Sergheraert; *Chem. Pharm. Bull.* **2005**, *53*, 492-497; (c) S. Wacharasindhu, S. Montha, J. Boonyiseng, A. Potisatityuenyong, C. Phollookin, G. Tumcharern, M. Sukwattanasinitt;

Macromolecules **2010**, *43*, 716-724; (d) J.D. Goodreid, P.A. Duspara, C. Bosch, R.A. Batey; *J. Org. Chem.* **2014**, *79*, 943-954.

[120] B. Cole; *Electrospray Ionization Mass Spectrometry*; Wiley: New York, **1997**.

[121] (a) E.J. Breitmaier, G. In *Organische Chemie Grundlagen, Stoffklassen, Reaktionen, Konzepte, Molekülstruktur*; 4. ed.; Georg Thieme Verlag: Stuttgart, **2001**, p. 790 ff; (b) D. Lehnher, J. Gao, F.A. Hegmann, R.R. Tykwinski; *J. Org. Chem.* **2009**, *74*, 5017-5024; (c) Z. Wang *Comprehensive Organic Name Reactions and Reagents*, John Wiley & Sons, Hoboken, **2010**; (d) D. Gao, Y. Liu, W. Li, F. Zhong, X. Zhang, Y. Diao, N. Gao, X. Wang, W. Jiang, G. Jin; *Bioorg. Med. Chem. Lett.* **2014**, *24*, 5792-5795; (e) M.W. Amjad, M.C.I.M. Amin, H. Katas, A.M. Butt, P. Kesharwani, A.K. Iyer; *Mol. Pharm.* **2015**, *12*, 4247-4258; (f) J. Lei, Y. Liu, Y. Cao, D. Zheng, M. Luo, M. Xiao; Beijing Forestry University, Peop. Rep. China . 2018, p 15pp; (g) K. Liu, D. Zheng, H. Lei, J. Liu, J. Lei, L. Wang, X. Ma; *ACS Biomater. Sci. Eng.* **2018**, *4*, 1730-1737.

[122] (a) U. Ragnarsson, L. Grehn; *Acc. Chem. Res.* **1998**, *31*, 494-501; (b) A.C. Spivey, S. Arseniyadis; *Angew. Chem.* **2004**, *116*, 5552-5557.

[123] J. Dupont, C.S. Consorti, P.A.Z. Suarez, R.F. de Souza; *Org. Synth.* **2003**, *79*, 236-243.

[124] I. Krossing, I. Raabe; *Chem. Eur. J.* **2004**, *10*, 5017-5030.

[125] Y. Wei, W. Huang, Y. Zhou, S. Zhang, D. Hua, X. Zhu; *Int. J. Biol. Macromol.* **2013**, *62*, 365-369.

[126] (a) P. Kumar, I. Cisarova; *J. Organomet. Chem.* **2013**, *735*, 32-37; (b) K.R. Sampford, J.L. Carden, E.B. Kidner, A. Berry, K.J. Cavell, D.M. Murphy, B.M. Kariuki, P.D. Newman; *Dalton Trans.* **2019**, *48*, 1850-1858.

[127] H.M.J. Wang, I.J.B. Lin; *Organometallics* **1998**, *17*, 972-975.

[128] U. Hintermair, U. Englert, W. Leitner; *Organometallics* **2011**, *30*, 3726-3731.

[129] (a) H. Schmidbaur, A. Schier; *Angew. Chem., Int. Edit.* **2015**, *54*, 746-784; (b) Y.S. Wang, T. Feng, Y.Y. Wang, F.E. Hahn, Y.F. Han; *Angew. Chem., Int. Edit.* **2018**, *57*, 15767-15771.

[130] (a) B. Liu, W.Z. Chen, S.W. Jin; *Organometallics* **2007**, *26*, 3660-3667; (b) I.J.B. Lin, C.S. Vasam; *Coord. Chem. Rev.* **2007**, *251*, 642-670; (c) T.J. Siciliano, M.C. Deblock, K.M. Hindi, S. Durmus, M.J. Panzner, C.A. Tessier, W.J. Youngs; *J. Organomet. Chem.* **2011**, *696*, 1066-1071.

[131] (a) S.A. Mcluckey, D. Cameron, R.G. Cooks; *J. Am. Chem. Soc.* **1981**, *103*, 1313-1317; (b) S.A. Mcluckey, A.E. Schoen, R.G. Cooks; *J. Am. Chem. Soc.* **1982**, *104*, 848-850; (c) R.G. Cooks, P.S.H. Wong; *Acc. Chem. Res.* **1998**, *31*, 379-386.

[132] J.M. Hayes, M. Viciano, E. Peris, G. Ujaque, A. Lledos; *Organometallics* **2007**, *26*, 6170-6183.

[133] C. Hemmert, A. Fabie, A. Fabre, F. Benoit-Vical, H. Gornitzka; *Eur. J. Med. Chem.* **2013**, *60*, 64-75.

[134] (a) J.W. Steed, J.L. Atwood *Supramolecular chemistry*; 2nd ed.; Wiley: Chichester, UK, p.44, **2009**; (b) E.C. Dreaden, A.M. Alkilany, X.H. Huang, C.J. Murphy, M.A. El-Sayed; *Chem. Soc. Rev.* **2012**,

41, 2740-2779; (c) M. Guo, P. Liu, B. Huang, Y. Qiu, Y. Wei, Y. Ma; *Appl. Surf. Sci.* **2019**, 476, 1072-1078.

[135] (a) R. Uson, A. Laguna, M. Laguna, D.A. Briggs, H.H. Murray, J.P. Fackler; *Inorg. Syn.* **1989**, 26, 85-91; (b) I.J.B. Lin, C.S. Vasam; *Can. J. Chem.* **2005**, 83, 812-825; (c) P.C. Kunz, C. Wetzels, S. Kogel, M.U. Kassack, B. Spingler; *Dalton Trans.* **2011**, 40, 35-37.